THERMAL AND MECHANICAL DEVELOPMENT OF THE EAST AFRICAN RIFT SYSTEM

by

Cynthia J. Ebinger

B.S. Geology, Duke University
(1982)

S.M. Geophysics, Massachusetts Institute of Technology
(1986)

Submitted to the Department of
Earth, Atmospheric, & Planetary Sciences
In Partial Fulfillment of the Requirements for the Degree of

Doctor of Philosophy

at the

Massachusetts Institute of Technology

and the

Woods Hole Oceanographic Institution

May, 1988

Signature of Author:_____
MIT/WHOI Joint Program in Oceanography
Department of Earth,Atmospheric,
& Planetary Sciences, MIT

Certified by: _____
Leigh H. Royden,
Thesis Supervisor

Accepted by: ___
Marcia K. McNutt, Chairman

'Twas brillig, and the slithy toves,
Did gyre and gymbol in the wabe.
All mimsy were the borogroves,
And the momeraths outgrabe.

Beware the Jabberwock, my son,
The claws that catch, the jaws that bite.
Beware the Jub-Jub bird and shun
The frumious Bandersnatch.

He took his vorpal sword in hand,
Long time the maxome foe he sought,
And rested he by a tum-tum tree,
And stood a while in thought.

And as an offish thought he stood,
The Jabberwock, with eyes aflame,
Came whiffling through the tulgy wood.
It burbled as it came.

One-two, one-two, and through and through,
The vorpal blade went snicker-snack.
He left it dead, and with its head,
He went gallumphing back.

And hast thou slain the Jabberwock?
Come into my arms my beamish boy.
Oh frabjous day, Calloo-callay.
He chortled in his joy.

'Twas brillig and the slithy toves
Did gyre and gymbol in the wabe.
All mimsy were the borogroves,
And the momeraths outgrabe.

Lewis Carroll, Jabberwocky
(in *Through the Looking Glass*)

THERMAL AND MECHANICAL DEVELOPMENT OF THE EAST AFRICAN RIFT SYSTEM

by

CYNTHIA J. EBINGER

Submitted to the Departmert of Earth, Atmospheric, and Planetary Sciences
May 5, 1988, in partial fulfillment of the requirements for the Degree of
Doctor of Philosophy in Oceanography

ABSTRACT

The deep basins, uplifted flanks, and volcanoes of the Western and Kenya rift systems have developed along the western and eastern margins of the 1300 km-wide East African plateau. Structural patterns deduced from field, Landsat, and geophysical studies in the Western rift reveal a series of asymmetric basins bounded by approximately 100 km-long segments of the border fault system. These basins are linked by oblique-slip and strike-slip faults cross-cutting the rift valley. Faults bounding the Kenya and Western rift valleys delineate two north-south-trending, 40-75 km wide zones of crustal extension, and little or no crustal thinning has occurred beneath the uplifted flanks or the central plateau. In the Western rift, volcanism in Late Miocene time began prior to or concurrent with basinal subsidence, followed by rift flank uplift. Individual extensional basins developed diachronously, and basinal propagation may give rise to the along-axis segmentation of the rift valley. The coherence between gravity and topography data indicates that the mechanical lithosphere beneath the two rift valleys has been weakened relative to the central plateau and adjacent cratonic regions. Gravity and topography data at wavelengths corresponding to the overcompensated East African plateau can be explained by density variations within the upper mantle that are dynamically maintained .

Thesis Supervisor: Dr. Leigh H. Royden
Associate Professor of Geology and Geophysics

ACKNOWLEDGEMENTS

Permission to conduct the field studies were granted by the Malawi Geolgoical Survey Department, UTAFITI (Tanzanian National Scientific Research Council), Departement de l'Energie et des Mines (Burundi), Ministère de l'Energie, des Mines, et de l'Artisanats (Rwanda), and Institut de la Récherche Scientifique (Zaïre). Without the logistical and scientific support of Chuo Kikuu Dar es Salaam, Japhet and Priscilla Nanyaro, Karel Theunissen, Jean Klerckx, Luc Tack, A.N. Tesha, Mike Daly, Pascale Eeckelers, Jodi Scott, Shelley Wagner, Paul O'Bryan, the Crow family, the Aswathanarayana family, the IRS in Lwiro, Zaïre, and many Peace Corps volunteers the African field work would have been impossible. Asante sana to the Tukuyu Wazee: John Knight for his guide service to the Elton Plateau, Lawrence Willey and the Foraky team for rescuing the Landrover; to Sarah Townsend for the use of the piki-piki in Mwakaleli district; to l'Abbe Ignace and the mission at Mibirizi, Rwanda; and to Bujumburans Luc Tack and Shelley Wagner for help in locating the missing rock (rubber) samples. The assistance of Tim Bechtel in applying the coherence technique to gravity data from East Africa is greatly appreciated. Al Deino and Bob Drake of the Berkeley Geochronology Laboratory instructed me in the arts of K/Ar geochronology, and provided the 'seed' results for the volcanic stratigraphy project in Rungwe, funded by Mobil Exploration Production Services and encouraged by Bob Pauken. I thank Andy Cohen, Luc Tack, Dick Grove, Dan Livingstone, Mike Daly, Karel Theunissen, Jean Klerckx, Jean Chorowicz for helpful discussions, and Max Fernandez-Alonso for advice in preparing the Kivu study.

Mavis Driscoll, Paul Scharr, Matthew and Alexandra provided support and entertainment in Boston for which I am grateful. I appreciate the advice and humor offered along the way by Mary Hubbard, Barb Sheffels, Liz Schermer, Peter Wilcock, Larry McKenna, Vincent Salter, Clark Burchfiel, Joann Stock, Kip Hodges, Donna Blackman, Sarah Little, Karen Fischer, Sarah Townsend, Sarah Bennett, Jack Jemsek, Tom Trull, Dave Dubois, John Collins, Mireille Polvé, David Reynolds, Mark Kurz, Mark Murray, Mike McCartney, Sarah Kruse, Niall Slowey, Laura Kong, Peter Schweitzer, Matt Cordery, Carolyn Ruppel, Dick Von Herzen, Marty Jeglinski, Nancy Dallaire, Josh Hoyt, Jim Knapp, Peter Tilke, and Dave Dinter. I thank Liz Schermer for introducing me to the Women's Rugby team, and Anne Judge for helping me escape Boston for the White Mountains and fresh air. Wendy Smith and Tina Vlad kindly accommodated the late-night lapses. I appreciate the assistance of Abbie Jackson, Jake Peirson, Mary Athanis and the rest of the MIT/WHOI Education Office. My parents and siblings Lisa, Carl, Eric, David, and Ed did their best to keep me smiling and help me maintain perspective, as did the music of Rachmaninoff, George Winston, M'bilia Bel; the Livingstone Mountains, Nkhata Bay, Kitazungurwa, Murago, Karema, Hotel Tanganyika, isombe, marakuja, ugali na samaki, chambo, and doses of konyagi, Primus, and chloroquine along the way. The temperamental service of Angelique, the ancient Landrover, will be remembered long after her demise, pole sana.

Finally, I thank my thesis committee of Don Forsyth, Kip Hodges, Marcia McNutt, Carl Bowin, and my thesis Chairman, Sean Solomon for many suggestions for improvement, and for giving me the time to resolve problems. My thesis advisor, Wiki Royden, provided the freedom, opportunity, and support to complete this thesis and to start the field and gravity studies, and her comments greatly improved this manuscript.

This thesis is dedicated to my independent grandmother, Mary R. Ebinger, who died as I completed Chapter 5, and my strong little niece, Kirsten Elizabeth Hjelm, who entered the world with Chapter 3.

TABLE OF CONTENTS

Introduction

Sedimentary sequences within basins bordered by the escarpments and volcanoes of the East African rift system record man's early history, and the flanking rift mountains and volcanic cones now form an impressive backdrop for the wildlife of East Africa. The East African rift system consists of two narrow rift valleys flanked by uplifted shoulders that are superimposed on a topographic plateau that spans nearly half the continent. The geologist J.W. Gregory (1896) first described the volcanically active valley along the eastern side of the East African plateau, and the Kenya rift valley often is referred to by his name. Later exploration within the uplifted interior of Africa led to the identification of a western branch of the rift system, the Western rift valley. The fault-bounded basins filled by deep lakes marking the sinuous outline of the Western rift valley originally were interpreted as compressional features (e.g. Willis, 1936), and the 1-4 km high uplifted flanks were believed to be isostatically compensated by crustal thickening (Bullard, 1936). Gregory (1896) interpreted the long rift valleys as tensional cracks that serve as conduits for magma, and Vening-Meinesz (1950) proposed an alternative isostatic compensation mechanism consistent with an extensional origin for the rift valleys. More recently proposed causal mechanisms for the broad uplift and associated negative Bouguer gravity anomaly, and in the Western and Kenya rift valleys, elevated heat flow, Miocene to Recent volcanism, crustal extension, basinal subsidence, and rift flank uplift generally invoke thermal processes within the mantle, with differences related to the temporal sequences of volcanism, uplift, and faulting predicted (e.g. Ramberg and Morgan, 1982).

Prior to 1981 little was known of the magnitude, timing, and spatial extent of Tertiary faulting within the lake basins of Tanganyika and Malawi and other parts of the Western rift. Unlike geological reports from the better known Kenya rift valley, Late Cenozoic fault patterns in parts of the Western rift valley were rarely mentioned in reconnaissance reports written during the colonial period, when the focus of geological studies was primarily mineral resource evaluations. In 1981, seismic reflection surveys designed to locate deep drill sites for paleoclimatic studies revealed a series of thickly-sedimented asymmetric basins beneath Lakes Malawi and Tanganyika (Rosendahl and Livingstone, 1983). Since that time, thousands of kilometers of multi-channel seismic reflection data have been added to these single-channel data, and a number of sedimentological, geophysical, and industrial studies have provided new information on structural and stratigraphic patterns within the Western and Kenya rift valleys (e.g. Kaufulu et al., 1981; Ilunga, 1984; Shudofsky, 1985; KRISP, 1987; Peirce and Lipkov, in press; D. Stone, pers. comm.). Recently completed radiometric age determinations of a suite of volcanic rocks from a Western rift volcanic province, the South Kivu province indicate that

rifting in the Western rift began later than initial rifting in the Kenya rift system to the east (e.g. Pasteels et al., in press), but no age constraints were available from the southernmost volcanic province in the East African rift system, the Rungwe volcanic province, prior to this study.

The preliminary results of the geophysical surveys in Lakes Malawi and Tanganyika in the Western rift are reported in Chapters 1 and 2. In these two chapters seismic reflection data and existing heat flow, gravity, magnetic, and geological information are integrated to delineate fault patterns within the sedimentary basins of the Malawi rift, which has developed along the southwestern margin of the uplifted East African plateau (Figure 1). Chapter 2 describes a three-dimensional rift basin model, developed in collaboration with David Reynolds and Bruce Rosendahl at Duke University, that is based on repetitive patterns in the sense of basinal asymmetry and topographic relief noted in studies of Malawi and Tanganyika basins. A comparison of structural and stratigraphic patterns observed within the Malawi rift to those within the Tanganyika rift reveals that the cross-sectional morphology of these asymmetrical extensional basins depends on the geometrical arrangement along the length of the Western rift valley of distinct segments of the border fault system.

Chapters 1 and 2 and previous studies in the Western rift system summarize the important geometric elements of Tanganyika and Malawi rift basins, and show that structural and stratigraphic patterns in the youthful Western rift system are similar to those of other continental rift systems. However, the spatial extent of Neogene faults and the detailed relationship between the timing of crustal movements along the length of the Western rift system with respect to the Kenya rift system and the regional uplift of the East African plateau were poorly constrained by existing data. Specifically, the structural linkage of half-graben tilted in opposite directions along the length of the rift valley, the extent of faulting along the uplifted flanks of rift basins, and the timing of basinal subsidence and rift flank uplift were needed in order to estimate crustal extension within the broad East African plateau region. In 1986 and 1987, I conducted detailed field studies designed to address these problems within and along the flanks of several representative rift basins, and in interbasinal accommodation zones and volcanic provinces of the Western rift valley. The results of these field studies within the South Kivu and Rungwe volcanic provinces of the Western rift valley are summarized in Chapter 3. I also report radiometric (K/Ar) age determinations of samples from the Rungwe and South Kivu volcanic provinces, analyses done in collaboration with Robert Drake and Alan Deino at the Berkeley Geochronology Laboratory (Institute for Human Origins).

In Chapter 4 structural interpretations made from these field studies and analyses of high resolution Landsat imagery, integrated with existing reports and seismic reflection data from lake basins, are used to develop a model for the evolution of the western limb of the East African rift system. I have used the tectonic framework provided by the detailed field studies within representative Western rift basins (Chapter 3) and synthesis of new and existing data to compare Western rift basins to those of the Kenya rift system, and to evaluate proposed mechanical models for the segmentation of continental rift valleys. Chapter 4 also summarizes geometric and kinematic aspects of the youthful Western rift system that are characteristic of many other continental rift systems.

The similarities between the Kenya and Western rift systems in the chronology of basinal development and volcanism, and the geometry of rift basins indicates that parallel processes have led to the formation of these narrow zones of crustal extension. However, previous interpretations of geophysical data from East Africa have focused on parts of the Kenya rift system that may not be representative, and no direct comparison of gravity data from the entire dome region using a single data base had been undertaken. Therefore, with respect to upper mantle processes beneath the seismically and volcanically active East African rift system, there remain important unresolved questions: 1) Are the Kenya and Western rift systems underlain by mechanically thinned and/or heated lithosphere, or has the entire uplifted East African plateau region been affected by rifting processes during the Tertiary?, and 2) By what process is the broad East African plateau compensated?

Previous studies of isostatic compensation for the topography of the East African plateau and the tectonically similar Afar plateau to the north using both Airy (Bullard, 1936; Girdler and Sowerbutts, 1970; Fairhead, 1976; Banks and Swain, 1978) and regional, or flexural compensation models (Vening-Meinesz, 1950; Forsyth, 1985; Bechtel et al., 1987) have been restricted to sections of the two plateaus that may not be representative of the average lithospheric structure beneath the two plateaus. These regions also were too small to examine the compensation for the longest wavelength topographic elements of the East African and Afar plateau topography. In Chapter 5, we examine data from central and eastern Africa using a consistent data base provided by Carl Bowin in order to estimate the flexural rigidity of the African plate and its variability between and along the length of the Afar, Kenya, and Western Branch rift systems. The coherence between gravity and topography was used to estimate the effective elastic plate thickness beneath many smaller regions of the rift system and the stable cratonic regions to the west and northwest of the East African and Afar plateaus using a spectral technique developed by Donald Forsyth and

Timothy Bechtel (e.g. Forsyth, 1985; Bechtel et al., 1987), who co-authored Chapter 5. Estimates of effective elastic plate thickness beneath regions of the East African plateau that encompass the fault-bounded rift valleys (22-55 km) are significantly less than estimates beneath the stable cratonic regions (65-180). We attribute this weakening to a combination of thermal and faulting processes and suggest that the lithosphere beneath the rift valleys behaves as a broken plate. Nevertheless, much of the topographic relief of the broad plateaus occurs at wavelengths longer than the flexural wavelength of the lithosphere beneath the plateaus, indicating that the uplift is supported by density variations beneath the elastic plate. In a concluding discussion, we compare the transfer function between gravity and topography at long wavelengths to transfer functions predicted by convection within a fluid layer overlain by a cold elastic plate. Our results indicate that the gravity field and topographic relief of the East African plateau can be explained by convective processes within the uppermost mantle and some conductive heating of the mechanical lithosphere. This dynamic mechanism is consistent with the chronology of rift movements and the limited spatial extent of crustal extension within the uplifted plateau region.

References

Banks, R.J. and C. Swain, The isostatic compensation of East Africa, *Proc. R. astr. Soc., Ser. A, 364,* 331-352, 1978.

Bechtel, T., D. Forsyth, and C. Swain, Mechanisms of isostatic compensation in the vicinity of the East African rift, Kenya,*Geophys. J. R. astr. Soc., 90,* 445-465, 1987.

Bullard, E., Gravity measurements in East Africa,*Proc. Roy astr. Soc., 235,* 445-531, 1936.

Crough, S.T., Thermal origin of mid-plate hotspot swells, *Geophys. J. Roy. astr. Soc., 55,* 451-469, 1978.

Fairhead, J., Structure of the lithosphere beneath the Eastern rift, East Africa, deduced from gravity studies, *Tectonophysics, 30,* 269-298, 1976.

Forsyth, D.W., Subsurface loading and estimates of the flexural rigidity of the continental lithosphere. *J. Geophys. Res., 90,* 12,623-12,632, 1985.

Girdler, R., and Sowerbutts, W.T.C., Some recent geophysical studies of the rift system in E. Africa, *Jour. Geomag. Geoelectr., 22,* 153-163, 1970.

Gregory, J., *The Great Rift Valley,* London, John Murray, 405p., 1896.

Ilunga, L.K., Le quaternaire de la plaine de la Ruzizi, [Thèse doctorat]: Bruxelles, Belgium, University Bruxelles, 340p., 1984.

Kaufulu, Z., E. Vrba, and T. White, Age of the Chiwondo beds, northern Malawi, *Ann. Transv. Mus., 33,* 1-8, 1981.

KRISP, Working Group, Kenya Rift International Scientific Project: Preliminary results, *Nature, 325,* 239-242, 1987.

Pasteels, P., P. DePaepe, M. Villeneuve, and J. Klerkx, Age of the volcanism of the southern Kivu area, *Earth Planet. Sci.Letts.*, in press.

Peirce, J., and L. Lipkov, Structural interpretation of the Rukwa rift, Tanzania, *Geophysics,* in press.

Ramberg, I. and P. Morgan, Physical characteristics and evolutionary trends of continental rifts, *Proc. 27th Int. Geol. Congr., 7,* 165-216, 1982.

Rosendahl, B., and D. Livingstone, The rift lakes of East Africa,*Episodes, 1983,* 14-19,1983.

Shudofsky, G.N., Source mechanisms and focal depths of East African earthquakes using Rayleigh wave dispersion and body-wave modeling, *Geophys. J. R. astr. Soc., 83,* 563-614, 1985.

Vening-Meinesz, F.A., Les 'grabens' est-africains: résultat de compression ou de tension dans la croûte terrestre?, *K. Belg. Kol. Inst. Bull., 21,* 539-552, 1950.

Willis, B., East African plateaus and rift valleys, Carnegie Inst.Washington Pub. 470, Washington, D.C., 1936.

Chapter 1

STRUCTURAL EVOLUTION OF LAKE MALAWI, AFRICA

C.J. Ebinger — M.I.T./Woods Hole Joint Program in Oceanography
Dept. of Earth, Atmospheric, & Planetary Sciences, M.I.T.
Cambridge, MA 02139

M.J. Crow — Institute of Geological Sciences, Keyworth
Nottingham, U.K. NG12 5GG

B.R. Rosendahl
D.A. Livingstone — Duke University
Durham, N.C. 27706

J. LeFournier — Société Nationale Elf Aquitaine
Boussens, France

Published in *Nature*, v. 308, p. 627-629, 1984.

Structural evolution of Lake Malawi, Africa

C. J. Ebinger*, M. J. Crow†, B. R. Rosendahl‡, D. A. Livingstone‡ & J. LeFournier§*

Woods Hole Oceanographic Institute, Woods Hole, Massachusetts 02543, USA
† Institute of Geological Sciences, Keyworth, Nottingham NG12 5GG, UK
‡ Duke University, Durham, North Carolina 27708, USA
§ Société Nationale Elf Aquitaine (Production), Boussens, France

Over 2,000 km of seismic reflection profiles have been collected in Lake Malawi (Nyasa), the southernmost of the East African Rift Lakes. These studies, reported here, reveal a severely faulted lake floor bounded by rift structures of Pliocene or greater age. Faults that penetrate the uppermost sedimentary units and numerous earthquakes[1] attest to continuing activity in the rift. Inter-basinal differences in fault spacing, orientation and sedimentary thicknesses have led to a subdivision of Lake Malawi into four discrete structural provinces. These provinces only now are linked by faults attributed to the most recent episodes of extension. An evolutionary sequence of: (1) initial block faulting and subsidence, (2) fragmentation of fault blocks, (3) uplift and (4) renewed subsidence and rotation of fault blocks is proposed for the central part of the Malawi Rift.

Single-channel reflection surveys were conducted as part of a programme to evaluate sites for a proposed deep-drilling project (CEGAL) in the East African Rift Lakes[2]. Profiles were obtained using an airgun sound source (40 cubic inches) occasionally supplemented by an 800 J sparker, and radar navigation provided the principal means of trackline control. A single 13-m-long piston core was collected from the southern part of the lake (Fig. 1).

With a length of 560 km and an average width of 50 km, Lake Malawi fills the central valley of the Malawi Rift (Fig. 1). The lake floor reaches a maximum depth of 700 m, or 225 m below sea level[3]. Structural patterns[4] and geophysical data[5] indicate that the Malawi Rift is tectonically connected to the western branch of the East African Rift system. Agreement on the age of initiation of the Malawi Rift has been hampered by the paucity of reliable field data and rock dating. Earlier researchers believed rifting began in the Jurassic–Cretaceous[6,7], but recent workers have suggested a much younger Pliocene age[4]. Faunas from the earliest known lacustrine sediments exposed onshore, the Chiwondo Beds, have been dated at 2.5–5 Myr[8] and are separated from the overlying Chitimwe Beds by an erosional event of unknown duration[9].

The surface geology to the west of Lake Malawi has been reported previously[10], but little information is available as to the age of faulting on the eastern shores (Tanzania and Mozambique). The results of a recent research programme along the Tanzanian shores of Lake Malawi indicate that the large vertical offset along the Livingstone Fault (Fig. 1) is accompanied by an even greater amount of horizontal displacement (J. LeFournier, personal communication). Before our seismic survey, knowledge of the lake floor had been derived from a reconnaissance heat flow survey[11], a few echograms from the south-west arm of the lake[3] and a theoretical study of lake bed topography[12]. Sediment distribution was poorly known, but sand, mud, diatomite and iron precipitates were found in the uppermost layers[13].

Set within the roughly north–south boundary fault system shown in Fig. 1, the Malawi Rift transects Precambrian metamorphic basement and north-east-trending Mesozoic (Karroo) fault troughs. Some reactivation of pre-existing zones of weakness has been described onshore[4], and our seismic records show that submerged segments of the Maniamba and Ruhuhu Karroo fault troughs have been reactivated. The segmented character of the boundary fault system and inter-basinal differences in seismic stratigraphy lead to a division of the rift into four discrete structural provinces. Each province has a distinct fault pattern, and few faults extend between provinces; therefore, principal stress orientations are inferred to shift at province boundaries (Fig. 1). The provinces are typically 60 km long and 50 km wide, with the cross-sectional forms of half-graben. The main graben are composed of many closely spaced, usually tilted, fault blocks. Faults penetrate to all levels of the sedimentary column and diapiric features occur along some faults (Figs 2, 3).

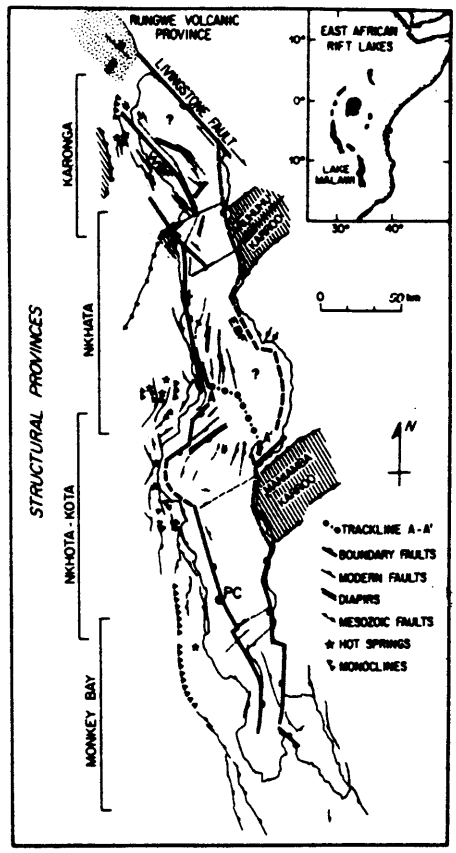

Fig. 1 Tectonic map of Lake Malawi region (lakeshore shaded for clarity) showing the principal structural provinces that comprise the lake basin. Faults with large offsets roughly defining the sedimentary basins are designated as Eastern Boundary Fault (EBF) and Western Boundary Fault (WBF). Note that these occur within the monoclines bounding the Malawi Rift Valley. PC denotes location of the 13-m piston core. Symbols: diagonal line pattern, Mesozoic sediment troughs; random dashes, Rungwe volcanics.

The four provinces (Fig. 1) reflect different stages of rift evolution, with the youngest, the Monkey Bay Province, showing the least amount of subsidence and fragmentation of major fault blocks. Maximum subsidence has occurred along the Western Boundary Fault in the Nkhata Province where sediment thicknesses are also greatest. A structural interpretation of the southern Nkhata Province is shown in the block diagram of Fig. 2. Up to 2.0 km of subsidence is observed in the seismic records, but the actual amount could be much greater as basement was often obscured by the bottom multiple (Fig. 3). Steeply dipping synthetic and antithetic normal faults trend roughly north–south within this province. Shallow earthquakes of $m_b \geq 3$ correlate well with mapped structures and appear to be related to movements along the Western Boundary Fault and a mid-lake basement high (Fig. 2).

The southern part of the Nkhata Province contains many north-east-trending faults (Fig. 2) with little or no vertical offset. These are interpreted as strike-slip faults that link this part of

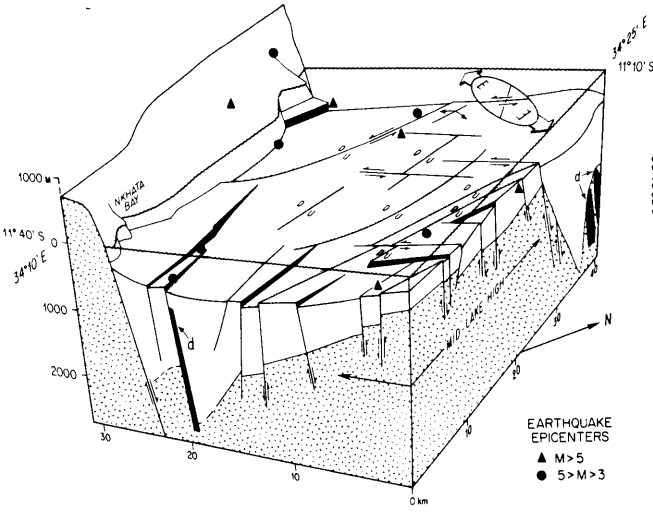

Fig. 2 Schematic block diagram depicting the major structural elements of the southern Nkhata Province. (Interpretation based on seismic reflection profiles shown in inset to Fig. 3.) The strain ellipse superimposed on the lake surface indicates approximate orientation of principal strain axes inferred from fault geometries. Faults with a north-east trend correspond to planes of high shear strain, and north–south-trending faults lie along planes normal to the principal extension direction. Epicentres of earthquakes of $m_b \geq 3$ (1966–77) are shown in their approximate locations. Symbols: random Vs, crystalline basement; d, diapirs; blank, lake sediments.

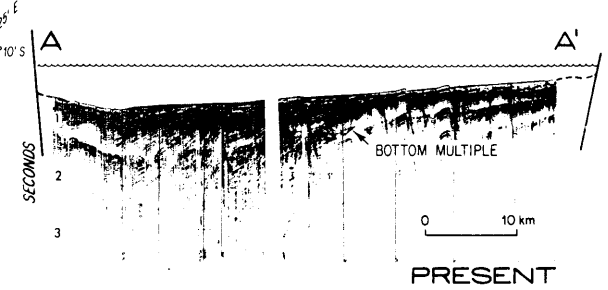

Fig. 3 Seismic reflection profile A–A' (see Fig. 1 for location) referred to in Fig. 4. Vertical scale in seconds two-way travel time. Horizontal extent ~70 km.

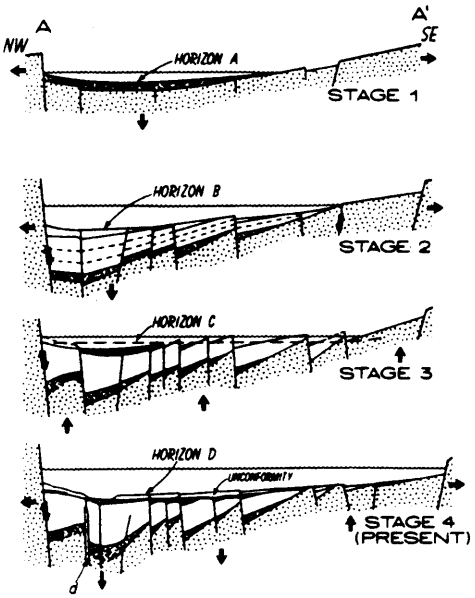

Fig. 4 Four-stage evolutionary sequence envisioned for trackline A–A' (see Fig. 3). Horizons A–D refer to seismic horizons used as datum in the reconstructions. Arrows denote relative movements within the lake. Symbols as in Fig. 2.

the Nkhata Province to the Nkhota-kota Province near the bend in the lake. A zone of transcurrent movement mapped onshore in this area[14] supports a strike-slip interpretation. In Lake Malawi the propensity towards half-graben morphologies could be related to oblique extension across the lake or between individual segments, as basin asymmetry alternates between provinces. Where rift segments are offset along strike this oblique extension would introduce a strong component of horizontal shear into the regional tensional regime. A similar alternating pattern of basinal asymmetry and transcurrent faults has been observed in the Rio Grande Rift[15].

Diapiric features observed along some faults in this area (Figs 2, 3) could be related to the period of uplift which created or enhanced a mid-lake high. Although no rift-related igneous activity has been described onshore in the Nkhata region, the Rungwe volcanic zone to the north[16] (Fig. 1) has been active since the Pliocene. These diapirs could be Rungwe-related igneous intrusive bodies or the lake bed equivalent of hydrothermal springs that occur along the Western Boundary Fault (Fig. 1).

Many of the previously described features and relations are observed in a seismic line across the southern part of the Nkhata Province near the bend in Lake Malawi (Fig. 3). The nearly cross-sectional seismic section shown in Fig. 3 serves as the basis for the evolutionary sequence depicted in Fig. 4. To remove non-diastrophic effects from the lake bottom morphology, reconstructions were made to acoustic horizons that are presumed to be time-stratigraphic. Information from nearby seismic lines was also used in the reconstructions. The Western Boundary Fault serves as a fixed point of reference for all four stages to illustrate the relative amount of extension that has occurred along this transect.

Little is known of the pre-rift terrains of central Africa. Therefore, stage 1 depicts depositional pulses in an already faulted basin (horizon A). Reconstruction to the top of acoustic (presumably crystalline) basement indicates that the graben developed on the western margin of a broad dome. The north–south elongate rift apparently interrupted a west-to-east drainage pattern, capturing detritus derived predominantly from the west. The discontinuous, fuzzy reflectors of the lowermost acoustic unit are interpreted as the earliest Malawi Rift sediments, probably sands shed from the uplifted rift flanks. These sediments could be the equivalent of the shallow lake and alluvial plain deposits of the exposed Chiwondo Beds[9,10]. The wedge-shaped geometry of this basal unit suggests that a few faults in the central valley were active during the initial infill stages.

The period between stages 1 and 2 was one of extension and rapid subsidence as rift-flank drainage patterns became more extensive. At the time corresponding to stage 2, the boundary faults were well established and the rift had achieved most of its present width. Subsidence along the western fault proceeded much more rapidly than its eastern counterpart, and this asymmetry was enhanced by clastic input largely from the west. The parallel-banded reflectors in this middle unit are indicative of deep-water deposition of muds (via turbidity currents?) and biogenic oozes, with lake conditions presumed to be similar to those prevailing today. The geometry of acoustic laminations shows deposition on an uneven lake floor concomitant with rotation of fault blocks.

Stage 3 is a reconstruction to the top of a strongly reflective, nearly horizontal layer (horizon C) that appears to truncate the uplifted corners of rotated fault blocks. As deposition on continuously tilting fault blocks can account for only part of the reflector inclinations at this level, an erosional unconformity is proposed. Further evidence for a period of relative uplift is seen in the central lake area where a structural basement high developed (Fig. 2). The intertonguing bed pattern in the adjacent

central graben indicates sediments derived not only from the west but from a shallow or subaerially exposed mid-lake high. An apparently short-lived period of uplift in segments of Lake Malawi may be analogous to the mid-Jurassic doming episode observed in the central North Sea area[17], and to doming in the central basin of Lake Tanganyika[2]. Two major erosional events described for central Africa[18] could be related to drier periods and lowstands of the lake, but too little is known of the timing, duration or extent of these events in the region surrounding Lake Malawi to make any well-constrained correlations at this time.

Stage 4 is an interpretation of the present-day structural and stratigraphic relations in the Nkhata Basin of Lake Malawi. Extension, rotation and continued fragmentation of fault blocks dominated the latest rift episode. Substantial movements along the border fault system led to general subsidence, while the lake refilled to its present level. The unconformity surface in the Nkhata Province was overlain by a 60-m thick, acoustically 'transparent' unit. Core studies of the upper 13 m show this to be a diatomite with minor clays and organic debris. In the extensional periods between stages 1 and 2 the border faults became more diffuse. The more rapid subsidence between stages 3 and 4 was largely restricted to a 20-km wide central graben and was achieved by vertical and rotational movements along a few major faults. A similar narrowing of the zone of maximum subsidence has also been observed in the South Kenya Rift[19].

An extrapolation of the chronological history of the Nkhata Province to the remaining lake provinces indicates that Lake Malawi has grown through the coalescence of structural basins during successive episodes of regional extension, uplift and subsidence. Half-graben morphologies and fault patterns with strike-slip geometries (north-east-trending faults) indicate that the Malawi Rift is opening obliquely to the axis of the rift (north–south). This is most apparent in the region surrounding the bend in the lake, which could evolve into a transform zone if the Malawi Rift becomes a true spreading system.

The areal dimensions of the four structural provinces (60 km × 50 km) are remarkably similar within Lake Malawi, the East African Rift System and many other continental rifts. Fault patterns within the rift are influenced by pre-existing structural grains, but the dimensions of basins in the Malawi Rift remain fairly constant. Rosendahl and Livingstone[2] have suggested that the recurrence of these dimensions reflects a fundamental response of the lithosphere to the process of rifting that is only secondarily affected by pre-existing structural grains. Further studies in the rift lakes of East Africa, where it may be possible to observe continental separation in its juvenile stages, are needed to define the vertical and horizontal extent of basement structures within the extensional basins, and to relate the observed repeatability of dimensions to crustal, lithospheric or asthenospheric properties.

This paper was made possible by the Government of Malawi and the Malawi Geological Survey Department. We thank J. Turner, J. Barrett; the scientific crew of R. Dunseath, J. Nelson, M. Patterson, F. Spy-Anderson, K. Haberyan and C. Stager; M. Connor for the artwork; J. Karson for critical comments; and E. Uchupi for reviewing the paper. The work was supported by NSF grant BNS 7926762, Société Nationale Elf Aquitaine (Production), and Mobil Oil Corporation.

Received 12 September 1983; accepted 5 January 1984.

1. Fairhead, J. *20th a. Rep. res. Inst. Afr. Geol. Univ. Leeds*, 42–46 (Leeds Univ., 1976).
2. Rosendahl, B. & Livingstone, D. *Episodes 1983*, 14–19 (1983).
3. Eccles, D. *Limnol. Oceanogr.* **19**, 730–742 (1974).
4. Crossley, R. & Crow, M. *Geodyn. Evol. Afro-Arab. Rift Syst.*, 77–87 (Accad. Nazion. dei Lincei, 1980).
5. Girdler, R. & Sowerbutts, W. J. *Geomag. Geoelect.* **22**, 153–162 (1970).
6. Dixey, F. Q. *Jl geol. Soc. Lond.* **83**, 75–108 (1929).
7. Bloomfield, K. & Garson, M. *Bull. geol. Surv. Malawi* **17** (1965).
8. Kaufulu, Z., Vrba, E. & White, T. *Ann. Transv. Mus.* **33**, 1–8 (1980).
9. Crossley, R. *Paleoecol. Afr.* **15**, 139–144 (1982).
10. Carter, G. & Bennett, J. *Bull. geol. Surv. Malawi* **6** (1973).
11. Von Herzen, R. & Vacquier, V. *Geophys. Res.* **72**, 4221–4226 (1967).
12. Yairi, K. *2nd Prelim. Rep. Afr. Stud. Nagoya Univ.*, 51–69 (Nagoya Univ., 1977).
13. Muller, G. & Forstner, U. *Miner. Deposita* **8**, 278–290 (1973).
14. Bloomfield, K. *Nature* **211**, 612–614 (1966).
15. Cape, C., McGeary, S. & Thompson, B. *Geol. Soc. Am.* **94**, 3–14 (1983).
16. Harkin, D. *Mem. Geol. Tanganyika* **2** (1960).
17. Ziegler, P. *Nature* **304**, 561 (1983).
18. Lister, L. *Rec. geol. Surv. Malawi* **7**, 15–28 (1967).
19. Baker, B., Crossley, R. & Goles, G. *Petrology and Geochemistry of Continental Rifts* (eds Neumann, E. & Ramberg, I.) 62–78 (Reidel, Dordrecht, 1978).

Chapter 2

TECTONIC MODEL OF THE MALAWI RIFT, AFRICA

C.J. Ebinger — M.I.T./Woods Hole Joint Program in Oceanography
Dept. of Earth, Atmospheric, & Planetary Sciences, M.I.T.
Cambridge, MA 02139

B.R. Rosendahl — Project PROBE
Duke University
Durham, N.C. 27706

D.J. Reynolds — Exxon Co., USA
Oklahoma City, OK 73106

Published in *Tectonophysics*, v. 141, p. 215-235, 1987

Tectonophysics, 141 (1987) 215–235
Elsevier Science Publishers B.V., Amsterdam – Printed in The Netherlands

Tectonic model of the Malawi rift, Africa

C.J. EBINGER [1], B.R. ROSENDAHL [2] and D.J. REYNOLDS [3]

[1] *Massachusetts Institute of Technology / Woods Hole Oceanographic Institution Joint Program in Oceanography, Woods Hole, MA 02543 (U.S.A.)*
[2] *Project PROBE, Department of Geology, Duke University, Durham, NC 27706 (U.S.A.)*
[3] *Exxon Company, Oklahoma City, OK 73106 (U.S.A.)*

(Received December 23, 1985; accepted June 25, 1986)

Abstract

Ebinger, C.J., Rosendahl, B.R. and Reynolds, D.J., 1987. Tectonic model of the Malawi rift, Africa. In: Z. Ben-Avraham (Editor), Sedimentary Basins within the Dead Sea and Other Rift Zones. *Tectonophysics*, 141: 215–235.

In the seismically active Malawi rift (Africa), uplifted segments of the border fault system flank basins with different acoustic stratigraphies, sediment thicknesses, and styles of faulting. Regionally curvilinear border fault segments bound sigmoidal-shaped basins linked along the length of the rift in accommodation zones. Accommodation zones that trend oblique to the approximately N–S trend of the rift system occur within the rift valley bounded by border fault segments, suggesting little thinning occurs beneath the elevated rift flanks. Cross-sectional morphologies and fault patterns within Malawi rift basins depend on the geometrical arrangement of border fault segments, and these patterns are similar to those observed in the Tanganyika rift. Border fault segments locally may reactivate or have an orientation sub-parallel to Proterozoic–Mesozoic structures, but the border fault segmentation and alternating asymmetries of rift basins show no consistent relationship with pre-existing faults and lithologic contacts. The central parts of border fault segments, where maximum vertical displacements have been observed, are separated from any adjacent segment by 50–90 km in both the Malawi and Tanganyika rifts. The uniform separation of border fault segments in both the Malawi and Tanganyika rifts, despite their differences in age and geologic setting, suggests stress concentrations with an average spatial wavelength of 70 km occur along the length of the Tanganyika and Malawi rifts.

Introduction

Continental rift zones generally are characterized by deep sedimentary basins bordered by steep escarpments, high seismicity, alkaline volcanism, and are regions underlain by thin crust and elevated lithospheric geotherms. Recent studies have revealed that the systems of normal faults forming the rift escarpments (border fault systems) are segmented along their length (Crossley and Crow, 1980; Zorin, 1981; Cape et al., 1983; Baldridge et al., 1984; Ebinger et al., 1984; Reynolds and Rosendahl, 1984; Smith and Bruhn, 1984; Bosworth, 1985; Rosendahl et al., 1986). Because of this segmentation, rift valleys comprise a series of discrete structural basins (Rosendahl et al., 1982).

Typically, continental rift basins are bordered along one side by one or more normal faults showing large vertical displacements, which we define as a border fault segment. Structural relations in rifts indicate that the high-angle border faults become low-angle detachment faults or shear zones at depth (e.g., Wernicke and Burchfiel, 1982), and rheological considerations of extended continental crustal materials support these observations (e.g., Kligfield et al., 1984). It is generally agreed that extension occurs along these normal-slip detachments, hence the original location and orientation of border fault segments influences

0040-1951/87/$03.50

later stages of rifting and passive margin development. The opposite side of the rift is bordered by a monocline, outward-tilted step faults with minor vertical offsets, or a flexure, producing a half-graben basinal morphology. This structural asymmetry appears to be a ubiquitous feature of extended continental crust; asymmetric sedimentary basins typify active and ancient continental rifts (Bally, 1982; Reynolds, 1984; Reynolds and Rosendahl, 1984), and conjugate passive continental margins generally reflect a structural asymmetry (Lister et al., 1986). Significant variations in cross-sectional profile also occur along the length of continental rifts (Ziegler, 1978; Anderson et al., 1983; Reynolds, 1984; Bosworth, 1985). The side of the rift bounded by a steep border fault segment (rift mountains) often alternates to the opposite side of rift valleys at approximately 100 km intervals, or from basin to basin (Chenet and Letouzey, 1983; Reynolds, 1984; Bosworth, 1985; Aldrich, 1986; Rosendahl et al., 1986).

Several three-dimensional models have been proposed to explain the segmented border faults and alternating asymmetries of rift basins observed along the length of continental rifts and passive continental margins. Differences between the various tectonic models largely stem from the geometry of border fault segments and cross-fault

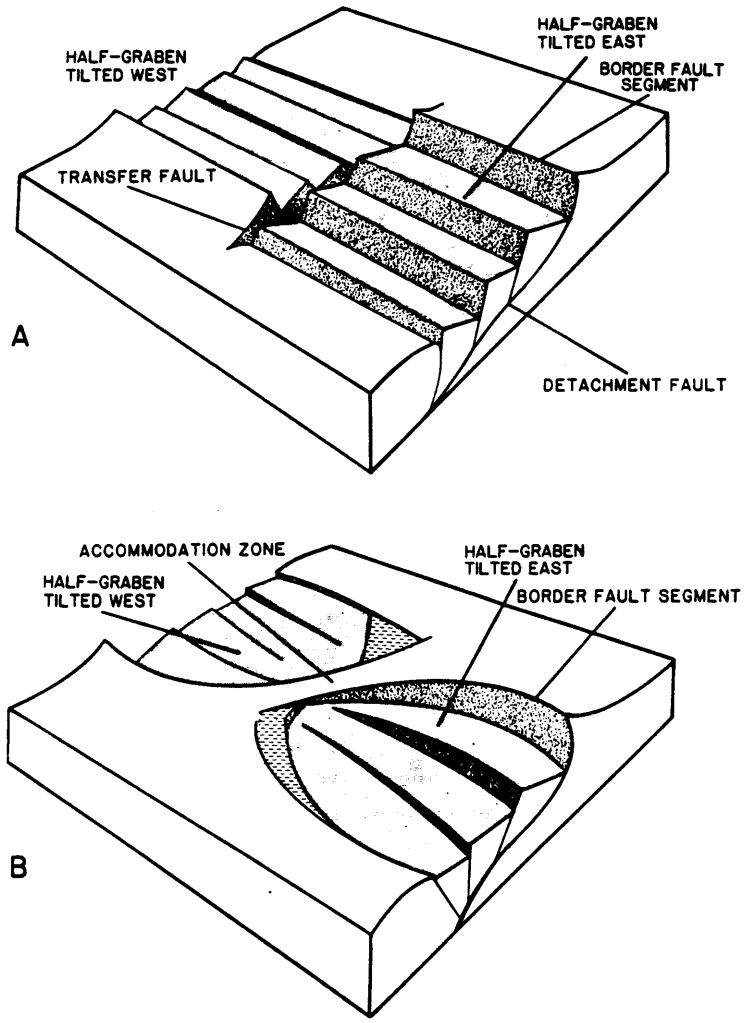

Fig. 1. Three-dimensional models of continental rift systems. A. Orthogonal system of border faults and transfer fault systems (Bally, 1982; Lister et al., 1986). B. Curvilinear border fault segments, with linkage occurring in accommodation zones between border fault segments (after Reynolds, 1984). Both models make use of high-angle border fault systems that become low-angle detachments at mid-crustal levels.

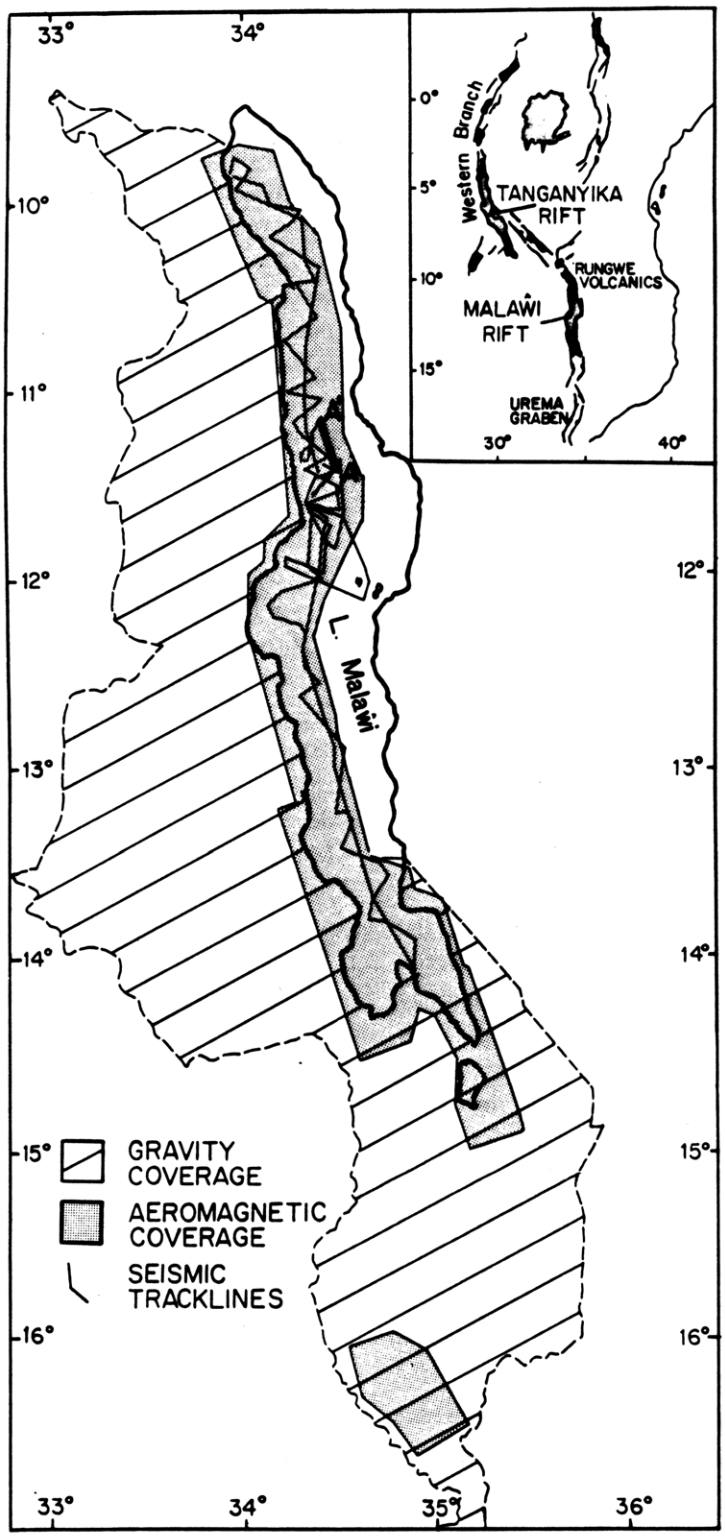

Fig. 2. Location of Malawi and Tanganyika rifts within the East African rift system (inset) and geophysical data base used in tectonic interpretation of the Malawi Rift. Gravity data from Andrew (1974). Reproductions of aeromagnetic data were made available through the Malawi Government. Seismic line A–A' designates the location of seismic profile shown in Fig. 4.

systems (Aydin and Reches, 1982; Gibbs, 1984; Reynolds and Rosendahl, 1984) that accommodate differential movements between extensional fault segments. Bally (1982) and Gibbs (1984) describe a series of linear (in plan view) border fault segments separated by transfer faults (Gibbs, 1984) that trend orthogonal to border fault segments (Fig. 1A). The tilt direction of fault blocks within rectangular basins bounded by border fault segments also reverses from basin to basin. Alternatively, tectonic models of the Gulf of Suez (Chenet and Letouzey, 1983), the Tanganyika rift (Reynolds, 1984), and the Keewenawan and Kenya rifts (Bosworth, 1985) employ a series of spoon-shaped border faults that are curvilinear in plan view (Fig. 1B). Curvilinear border fault segments are linked within the Tanganyika rift in accommodation zones (Reynolds and Rosendahl, 1984; Rosendahl et al., in press) that are similar to those described by Bosworth (1985).

The purpose of this report is to describe systematic variations in the geometry of border fault systems along the length of the Malawi rift system (Fig. 2), to illustrate the relationship between basinal morphology and the linkage of border fault segments, and to present possible explanations for the observed along-axis segmentation. In this geometrical classification of structural patterns, the location of border fault systems, their spatial arrangement, and the cross-sectional morphology of basins are used to interpret structural patterns in the Malawi rift (Fig. 2). We use existing seismic reflection data from Lake Malawi to interpret recently acquired aeromagnetic data, to correct heat flow values measured in a previous study for sedimentation effects (Von Herzen and Vacquier, 1967), and to synthesize these data to update and expand earlier interpretations of Malawi rift structures (Yairi, 1977; Crossley and Crow, 1980; Ebinger et al., 1984). This discussion of the Malawi rift focuses on the surface geometry of major faults involving crystalline basement; the current data base from the Malawi rift is inadequate to address the questions of border fault geometry at deeper crustal levels.

Several explanations for the observed structural segmentation of the Western Branch rift system have been proposed. Previous researchers noted a correlation between Precambrian to Mesozoic structural trends and the outline of the Malawi rift, and they suggested that Neogene faults reactivated ancient zones of weakness (Dixey, 1956; Bloomfield and Garson, 1965; McConnell, 1972). In their studies of structural patterns in the Basin and Range province of the U.S., Smith and Bruhn (1984) suggest that the location of transfer zones corresponds to major structural and lithological boundaries between regions with variable crustal thicknesses. This interpretation would imply that the segmentation of border fault systems and the development of sedimentary basins have been controlled by lateral heterogeneities in the continental crust.

Alternatively, the repetitive length scales and spatial arrangement of border fault systems in the Tanganyika rift and other continental rifts (e.g., Reynolds, 1984) may reflect variations in amounts of lithospheric extension along the length of the rift system, or an along-axis propagation of rifting. We use the tectonic model of the Malawi rift discussed below to examine the relationship between Precambrian to Mesozoic structures and the development of border fault systems bounding the Malawi rift. In a concluding section, we compare patterns in the spatial arrangement of border fault segments to observations along oceanic spreading ridges, and discuss possible mechanisms for the regular segmentation.

Tectonic setting

The Malawi rift extends over 900 km from the Rungwe volcanic province in the north to the Urema graben in Mozambique. The rift is situated at the southern margin of the c. 1000 m high Tanganyika plateau. The rift valley floor maintains a fairly constant elevation of 400 m south to the Urema graben where the rift valley floor descends from the dome to a height of 100 m (Fig. 3). Continuity in topographic, free-air gravity (Bowin et al., 1982) and seismicity trends (Fairhead and Stuart, 1982; Bungum and Nnko, 1984) indicate that the seismically active Malawi rift is a southern extension of the Western Branch rift system (Fig. 2). Seismic (Nolet and Mueller, 1982) and gravity data (Fairhead and Reeves, 1977; Brown

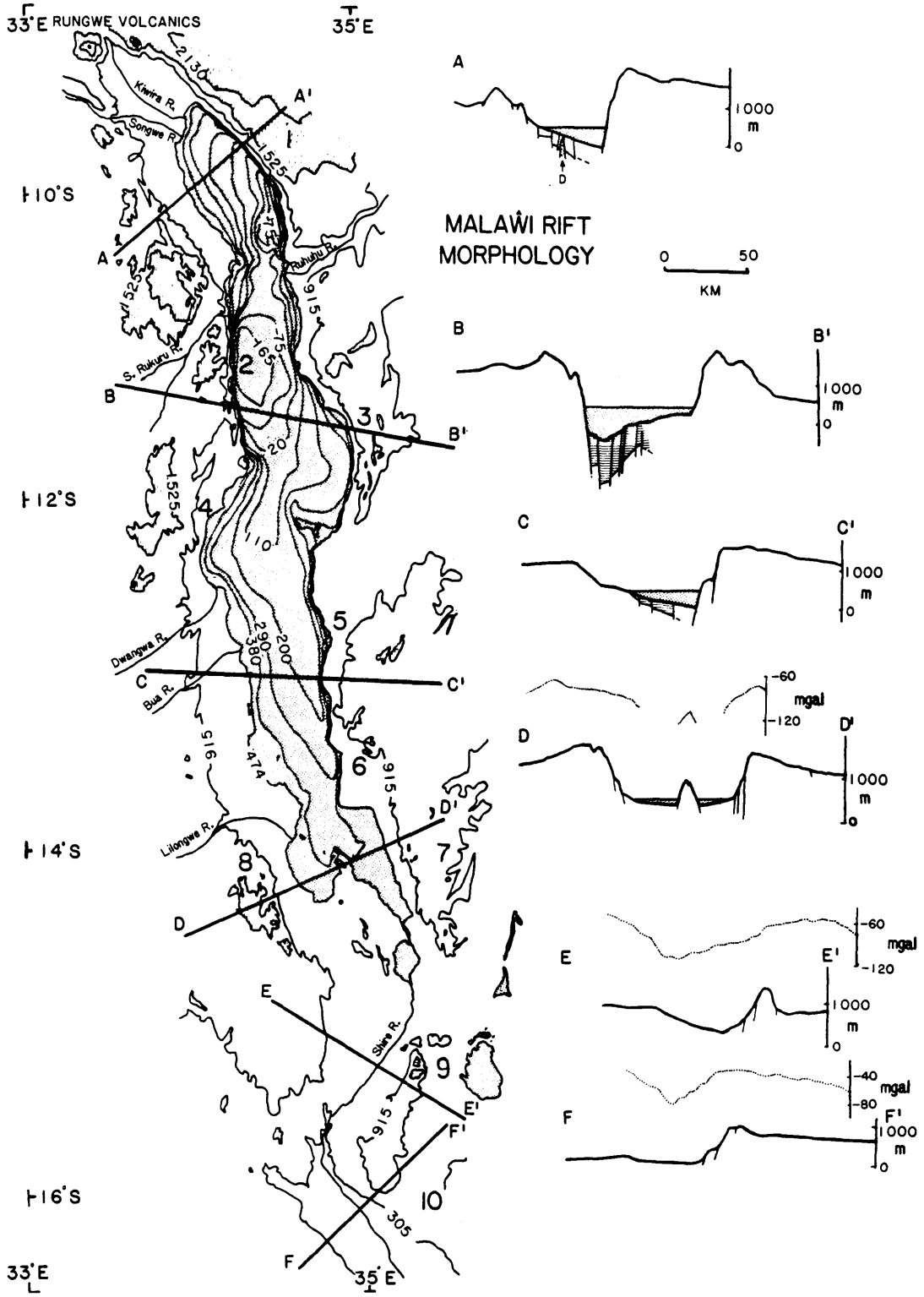

Fig. 3. Lake Malawi bathymetry and elevation of surrounding region, in meters above and below sealevel. Cross-sectional profiles illustrate the alternating patterns of basinal asymmetries along the length of the Malawi rift. Horizontal line pattern shows sediment thickness beneath Lake Malawi, where known. Bouguer gravity data (mGal) along southern transects from Andrew (1974). Major rivers entering and leaving Lake Malawi are also indicated. *D* = diapir.

and Girdler, 1980) indicate that the crust and/or lithosphere beneath the Western Branch has been thinned. In contrast to the extensive magmatism characteristic of the Kenya rift system to the east, volcanism in the Malawi Rift is restricted to alkalic volcanics at the northern end of the lake (Harkin, 1960).

Malawi rift structures are assumed to be younger than the late Miocene for several reasons, although no direct evidence is available to date the initiation of rifting in this part of the rift system. The oldest known sediments associated with recent rifting in Malawi are mid-Pliocene sediments found in the northern portion of the rift (Kaufulu et al., 1981). These sediments are intercalated with Plio-Pleistocene volcanics from the Rungwe center (Harkin, 1960). Using a linear extrapolation of present-day sedimentation rates within the lake (Von Herzen and Vacquier, 1967), sediment thicknesses in excess of 1.8 km observed in seismic records from the Malawi rift (corrected for sediment compaction), represent a minimum age of 2.0 Ma. In support of a post-mid-Miocene age assignment, fault scarps bounding the rift valley displace a regional mid-Miocene erosional surface (Lister, 1967). Exposed lakebeds, abandoned shorelines, and drowned river valleys along border fault systems are evidence for recent vertical movements (Stockley, 1948; Crossley and Crow, 1980). Spurs are facetted along the shores of the lake and there has been little or no modification of fault scarps by waves (Dixey, 1956; Crossley and Crow, 1980), also indicating recent activity.

The elevated flanks of the rift outside the border fault system rise 900–2500 m above sealevel, or 400–2000 m above the level of the lake (Fig. 3). Using the mid-Miocene erosional surface as a horizontal datum (Lister, 1967), the flanks of the rift are uplifted (Fig. 3) and are tilted away from the rift valley (Dixey, 1937; Carter and Bennett, 1973). Source mechanisms for earthquakes occurring in the Western Branch are of normal faulting type, and tensional axes are perpendicular to surface faults (Shudofsky, 1985). Epicentral depths within the Western Branch are less than 20 km, and average 12–15 km depth (Wohlenberg, 1968; Fairhead and Stuart, 1982; Shudofsky, 1985).

Seismic reflection data from within the Malawi rift reveal faults often separated by less than a kilometer penetrating both sediments and basement, and few faults extend from one province into the adjoining basin (Ebinger et al., 1984). The seismic reflection profile shown in Fig. 4 was collected parallel to border faults in the Nkhata basin (Fig. 2), and illustrates the extent of along-strike variations occurring within the Malawi rift. Along-strike variations in depositional sequences and fault patterns suggest that segments of the Malawi rift have developed diachronously (Ebinger et al., 1984). For the purpose of discussion, these differences have been used to divide the rift into five structural provinces. These provinces will be referred to as the Karonga, Nkhata, Nkhotakota, Monkey Bay, and Shire regions (Fig. 5).

Earlier interpretations of Malawi rift structures primarily have been based on observations from the western (Malawi) side of the rift where seismic reflection, magnetic, and gravity data have been collected (Fig. 2). In this study, we have compiled geological information on faults bounding the rift, recently acquired aeromagnetic data (Malawi Geologic Survey, 1985 report), and seismic reflection data to delineate border fault segments and basinal morphologies within the Malawi rift. A comparison to geometrical associations between border fault systems and cross-sectional profiles apparent in the model of the Tanganyika rift (Rosendahl et al., 1986) provides additional insights into the structural architecture of the Malawi rift.

Malawi rift border fault segments

Faults mapped onshore that displace the mid-Miocene erosional surface and faults beneath Lake Malawi have been compiled and used to delineate border fault segments in the Malawi rift (Fig. 5). Based on a correlation of seismic reflection and magnetic data, nearly all lineated magnetic anomalies are associated with faults identified in the seismic records. We have used aeromagnetic data from the western and southern portions of the rift (Fig. 2) to constrain the orientations of faults observed in seismic profiles and in the Shire province south of the lake (Fig. 5). Aeromagnetic anomaly patterns are highly varia-

ble along the length of the Malawi rift (Malawi Geological Survey, 1985), but the axial zone of lineated highs and lows associated with magmatic intrusions in other continental rifts (e.g., Ramberg and Morgan, 1984) is not apparent in data from the Malawi rift.

Gravity profiles of the Malawi rift zone are characterized by a long wavelength (~ 100 km) Bouguer gravity low (Brown and Girdler, 1980). Shorter wavelength Bouguer anomalies superimposed on the broad gravity low (Andrew, 1974) provide additional constraints on the geometry of faults within the southern basins of the Shire province (Fig. 5). These data were used to determine the sense of asymmetry within the rift basins to the south of Lake Malawi, where little information on subsurface structures is available. In our tectonic analysis of Malawi rift border fault

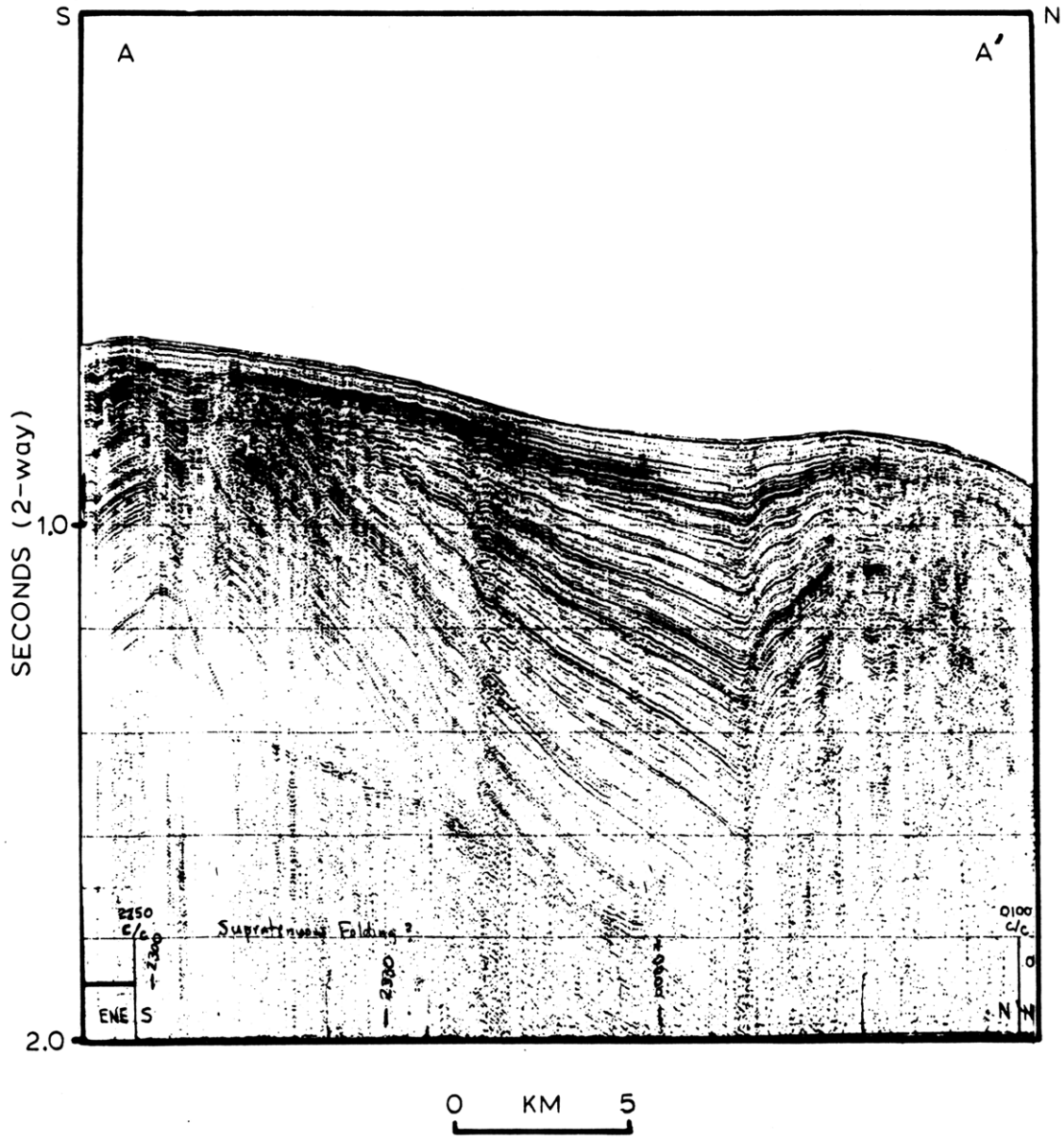

Fig. 4. Single-channel seismic reflection profile illustrating structural variations occurring along the length of the Nkhata Basin. (Location of profile A–A' shown in Fig. 2). Disturbed region near end of profile interpreted as a positive flower structure. Vertical exaggeration ~ 16 : 1.

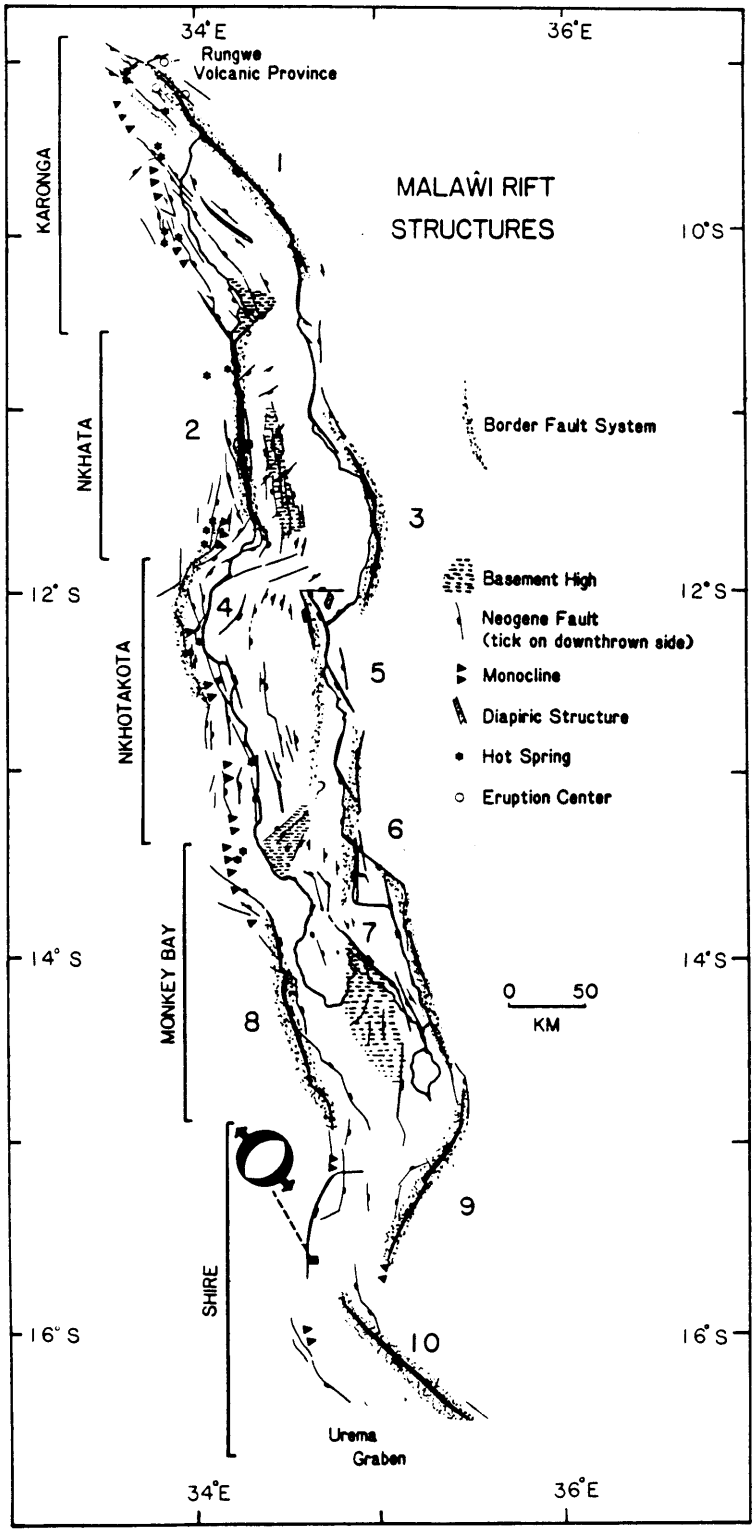

Fig. 5. Compilation of Malawi rift structures showing locations of structural provinces referred to in text. Fault patterns mapped onshore from Stockley (1948), McKinlay (1954), James (1956), Quennell et al. (1956), Harkin (1960), Wooley and Garson (1970), Carter and Bennett (1973), Afonso (1976), and Crossley and Crow (1980). Lake bed structures from Ebinger et al. (1984) and interpretations of gravity and magnetic data. Heavier line weights denote faults with larger vertical displacements. Numbers refer to border fault segments described in the text. Focal mechanism solution of 6 May, 1966 earthquake (m_b = 5.3) from Shudofsky (1985). Location of hot springs from Kirkpatrick (1969).

systems, detailed (2 fm contour interval) bathymetric charts (Yairi, 1977), topographic relief along the rift flanks, and previously mapped faults (McKinlay, 1954; James, 1956; Harkin, 1960; Quennell et al., 1956; Afonso, 1976) were the principal data base used along the eastern side of the rift. A Landsat-5 Thematic Mapper image was used to extend observations into the rugged region between Lake Malawi and the Rungwe volcanic province at the northernmost part of the rift (Fig. 2).

The location of monoclines dipping into the rift valley and step faults is also important in the identification of border fault segments, as these structures generally are found opposite major border fault systems in the Tanganyika rift (Reynolds, 1984; Burgess, 1985). Because of the low topographic relief on the monoclinal side, the presence of rivers with extensive drainage basins and lacustrine deltas also have been used to identify the flexural or shoaling side of a basin (cf. Rosendahl et al., 1986).

In the following section, we provide a brief description of the ten border fault segments (BFS) comprising the Malawi rift, referred to as BFS 1–10, and structural patterns commonly associated with border faults or that modify the geometry of border fault segments. In this analysis border fault segments are defined as sections of the Malawi rift border fault system that show large vertical displacements, high topographic relief, and bound asymmetric basins tilted toward the border faults. Patterns in the geometry of border fault and rift basin linkage will be discussed in a later section.

In the northernmost part of the rift, vertical movements along several closely-spaced faults down-dropped to the west form an escarpment (Livingstone Mountains) that rises nearly 2000 m from the surface of Lake Malawi (Stockley, 1948; Harkin, 1960). The trace of BFS 1 north of the lake is clearly marked by triangular fault scarps in high resolution (< 30 m) satellite imagery. To the south where the lake follows a N–S trend, BFS 1 extends onshore with an orientation approximately N30° W (McKinlay, 1954). A deep, lenticular basin at the base of BFS 1 has the cross-sectional form of a half-graben tilted to the east (*A–A'*, Fig. 3). NNW-oriented monoclines and step faults bound the western side of this rift segment, and several small deltas have formed on the shallow western side (Crossley and Crow, 1980). A linear diapiric structure noted in seismic data that extends from the Karonga province to the Rungwe center, and an associated positive magnetic anomaly, suggest that an igneous dike has intruded sediments beneath the Karonga province (Figs. 3 and 5).

The border fault system immediately to the south, BFS 2, is found on the western side, creating a half-graben that deepens to the west (*B–B'*, Fig. 3). The deepest basin within Lake Malawi occurs adjacent to BFS 2. Assuming an average seismic velocity of 2 km/s, sediment thicknesses beneath the lakefloor are at least 1.8 km. A fault-bounded basement high was mapped in a detailed survey of the Nkhata region, and the N–S oriented ridge is down-faulted to the north by SW-trending faults (Fig. 5). On the opposite side of the lake, eastward-tilted step fault blocks have been mapped onshore (McKinlay, 1954; James, 1956). Lower topography on the northeastern side of the rift is indicated by the entrance of the Ruhuhu River, and bathymetric data suggest that a small fan has formed at the mouth of the river (Fig. 3). There is little evidence for magmatic activity in this province; magnetic anomalies associated with severely deformed sediments observed in seismic profiles from the northern part of the Nkhata basin (e.g. Fig. 4) are small and slightly negative. The complicated sedimentary structure shown in Fig. 4 is similar to "flower" structures described by Harding and Lowell (1979), hence we interpret the lineated structural pattern observed here and in the southern part of the lake as evidence for transcurrent or wrench faulting.

Although little information is available from the eastern side of the rift in the Nkhata region, we interpret a major border fault system (BFS 3) lying southeast of BFS 2. Based on fault patterns in this area described by Quennell et al. (1956) and Crossley and Crow (1980), BFS 3 appears to be a single fault that curves from NW to a N–S orientation near the widest part of the lake. However, the magnitude of vertical displacement along this fault system onshore is less than along either

BFS 1 or 2 (Fig. 3). The basement ridge in the central part of the Nkhata basin separates a narrow basin on the eastern side from the westward-tilted half-graben bounded by BFS 2. Because of the differences in vertical displacements along BFS 2 and BFS 3, the arrangement of these two half-graben produces a generally asymmetric cross-sectional profile in the Nkhata province (B–B', Fig. 3).

BFS 4 occurs on the western side of the rift south of BFS 2 and contributes to the bend, or kink, in the rift outline. Faults with several orientations occur within this region, but both gravity data onshore and magnetic data (Malaŵi Geologic Survey, 1985) reveal a well-defined set of structures with a SSW trend both on and offshore (Fig. 5). The lineated magnetic pattern correlates to closely-spaced faults with minor vertical displacements in seismic records, and flower structures occur within the sedimentary sequences in the northern part of the basin. We interpret structures with a WSW trend within the rift valley as strike-slip faults in an accommodation zone between the Nkhata and northern Nkhotakota extensional segments, but the sense and amount of any horizontal displacement is unconstrained by existing data. Crossley and Crow (1980) report no evidence onshore for recent displacement along WSW-trending shear zones bounding granulitic rocks to the west of the rift (Haslam et al., 1980); hence extension appears to be restricted to the rift valley bounded by the border fault segments.

BFS 5 is found on the eastern side of the rift and bounds a half-graben tilted down to the east. This part of the rift is dominated by N–S oriented structures that also are apparent in aeromagnetic data from the Nkhotakota region (Malaŵi Geologic Survey, 1985). Fault-bounded rift mountains on the eastern shore rise approximately 1100 m above the lake (Afonso, 1976). In comparison to BFS 1–4, the lower relief along the northern part of BFS 5 may be related to the pre-rift topography and composition of rocks the border fault segment cuts across. An unknown thickness of Permo-Triassic sediments deposited in a fault-bounded trough have been eroded in a narrow strip along the eastern side of the lake (see Fig. 8); both the original trough and erodability of the Permo-Triassic sediments contribute to the low relief along the northern part of BFS 5. Monoclines occur along the length of the western side (Fig. 5), and several deltas have formed at the mouths of the Bua and Dwangwa rivers (Fig. 3). Faults in the Nkhotakota province are more widely-spaced across the rift than in the northern two provinces (Fig. 5), and limited seismic data reveal over 1 km of sediments in the northern part of this eastward-tilted basin.

South of BFS 5, water depths are shallower, and the half-graben morphology characteristic of the northern basins is less evident. These observations suggest that the Nkhotakota and Monkey Bay provinces (Fig. 5) may be younger than the Karonga and Nkhata segments. In contrast to the fairly smooth, elongate magnetic anomalies observed in the two northern provinces, isolated, shorter wavelength anomaly patterns are found in this region (Malaŵi Geologic Survey, 1985). These patterns may indicate that crystalline basement is shallower in the southern basins, or that basement has a different magnetic character. Along the shores of the lake south of BFS 5, faults with NW and N–S trends (30°–45° to one another) form a zig-zag border fault system (Fig. 5) that contrasts with the more curvilinear outline of BFS 1–5. Based on changes in sediment thickness, differences in the geometry of faults bordering the lake, and a structural high that extends beneath the lake, we interpret a second border fault segment, BFS 6, south of BFS 5. The narrow, eastward-tilted basin defined by this border fault segment continues to the narrowest part of the lake separating the Nkhotakota from the Monkey Bay region.

In the Monkey Bay province, a fault system with a N–S orientation on the eastern arm of Lake Malawi forms BFS 7, which defines a shallow narrow basin. BFS 8 is a NNW-trending fault system on the western side of a fault-bounded peninsula. The southwestern portion of BFS 8 is a single scarp that rises nearly 1000 m above sediments on the lakeshore plain, and there is a progressive decrease in elevation of this segment both to the north and south (Walter, 1967; Thatcher, 1968). A 10 km-wide shelf, back-tilted to the west, occurs immediately to the east of BFS 8. A

NNW-trending fault-bounded ridge separates these two rift basins (D–D', Fig. 3) and structurally is similar to the mid-lake high in the Nkhata basin (B–B').

Two additional border fault segments occur south of Lake Malawi. A SSW-oriented escarpment, BFS 9, on the southeastern side of the rift contributes to the sinuous outline of the southern Malawi rift, and a faulted monocline is found opposite BFS 9. Metamorphic basement is exposed along the southern part of the rift valley bordered by BFS 9 which reveals a gentle basinal tilt to the southeast (E–E', Fig. 3). The asymmetry in the projected gravity anomaly profile may be related to Jurassic volcanic plutons on the southeastern escarpment (see Fig. 8). The focal plane of an earthquake that occurred along the flexural side of the basin bounded by BFS 10, indicates the axis of least compressive stress is N40° E, or parallel to the Zomba escarpment (Fig. 5). Over 1000 m of vertical displacement have occurred along BFS 10 (Crossley and Crow, 1980), and gravity data (F–F', Fig. 3) indicate that the half-graben bounded by BFS 10 tilts to the northeast. A 2–12 km wide platform tilted to the east is found at its base (Dixey, 1937). Malawi rift movements have warped a Mesozoic (Karroo) basin opposite BFS 10 into a NE-dipping monocline or a low scarp (Wooley and Garson, 1970).

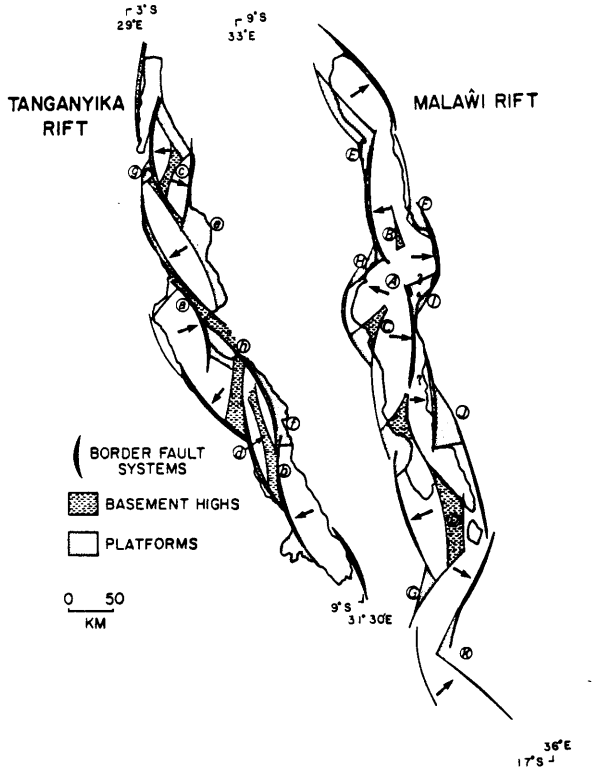

Fig. 6. Stylized tectonic models of the Malawi rift and the Tanganyika rift (after Rosendahl et al., 1986). Circled letters designate specific geometric relations described in the text. Arrows within basins point to down-dropped side of basins. "?" refer to unsurveyed regions beneath the lake.

Tectonic model

The observed geometry of border fault systems and variations in structural patterns within the Malawi rift have been used to construct the stylized tectonic model shown in Fig. 6. We compare border fault geometries and spacings of Malawi rift basins to a tectonic model of the Tanganyika rift (Rosendahl et al., 1986) in order to evaluate possible explanations for the observed segmentation.

From the structural analysis of border fault segments in the Malawi rift, discrete changes in the orientations of faults comprising each border fault system result in a regionally curvilinear border fault segment. Similar curvilinear "master" fault systems and half-graben rift morphologies have been produced in clay model experiments of extension (Stewart, 1971; Elmohandes, 1981). Vertical displacements along border fault segments are usually greatest near the central part of these systems. For example, in the Karonga and Nkhata regions of the Malawi rift, prominent rift mountains border deep lozenge-shaped sedimentary basins (Fig. 7). The spatial arrangement of these curvilinear border fault systems produces the sinuous rift valley shown in Fig. 7.

In the southern part of Lake Malawi (Dixey, 1956) and in other rifts (Freund, 1982), criss-crossing faults form rhomb-shaped fault blocks and a zig-zag border fault system (Fig. 5). If the border fault segments in the southern part of the rift are more youthful than those in the Nkhata and Karonga provinces, zig-zag border fault systems may evolve to curvilinear border fault segments, such as BFS 1 and BFS 2 in the Malawi rift and in the Tanganyika rift, during successive episodes of rifting.

Border fault linkage

The alternation of border fault segments along the rift and associated "flip-flopping" of basinal asymmetries produces complicated fault patterns where border fault segments abut or overlap. However, several consistent patterns emerge from this synthesis of data from the Malawi rift and comparison to patterns observed within the Tanganyika rift. These results provide a framework to distinguish between tectonic models of continental rift systems. Examples of specific geometries discussed in the text are referred to by upper case (Malawi rift) and lower case (Tanganyika rift) letters in Fig. 6.

The geometry of border fault linkage illustrated in Fig. 1B occurs where border fault segments with opposite senses of concavity abut one another to form an S-shaped geometry. In Lake Malawi, this geometry occurs where BFS 2 and BFS 5 extend beneath the lake and are linked end-to-end (*A*). Segments 2 and 5 are sub-parallel with opposite senses of concavity, producing a sigmoidal rift valley and alternating basinal asymmetries. In the Tanganyika rift basement ridges are observed where border fault systems have a similar geometry (*a*, *b*). The abutting half-graben geometry is analogous to the San Luis and Espanola basins in the Rio Grande rift where two half-graben with opposing asymmetries are linked by the Jemez volcanic lineament (Aldrich, 1986).

Two border fault systems with opposite concavities that face one another (across the rift) produce the archetypal rift profile of a full-graben, a morphology that is exceptional in the Malawi and Tanganyika rifts (*B–B'*, *D–D'*, Fig. 5). This basinal morphology is produced by the juxtaposition across the rift of two half-graben with opposite senses of asymmetry (Rosendahl et al., 1986). Elevated basement ridges or buried axial antiforms trending parallel to the border fault systems are usually associated with full-graben cross-sectional morphologies. For example, a NNW-oriented ridge occurs in the central part of Lake

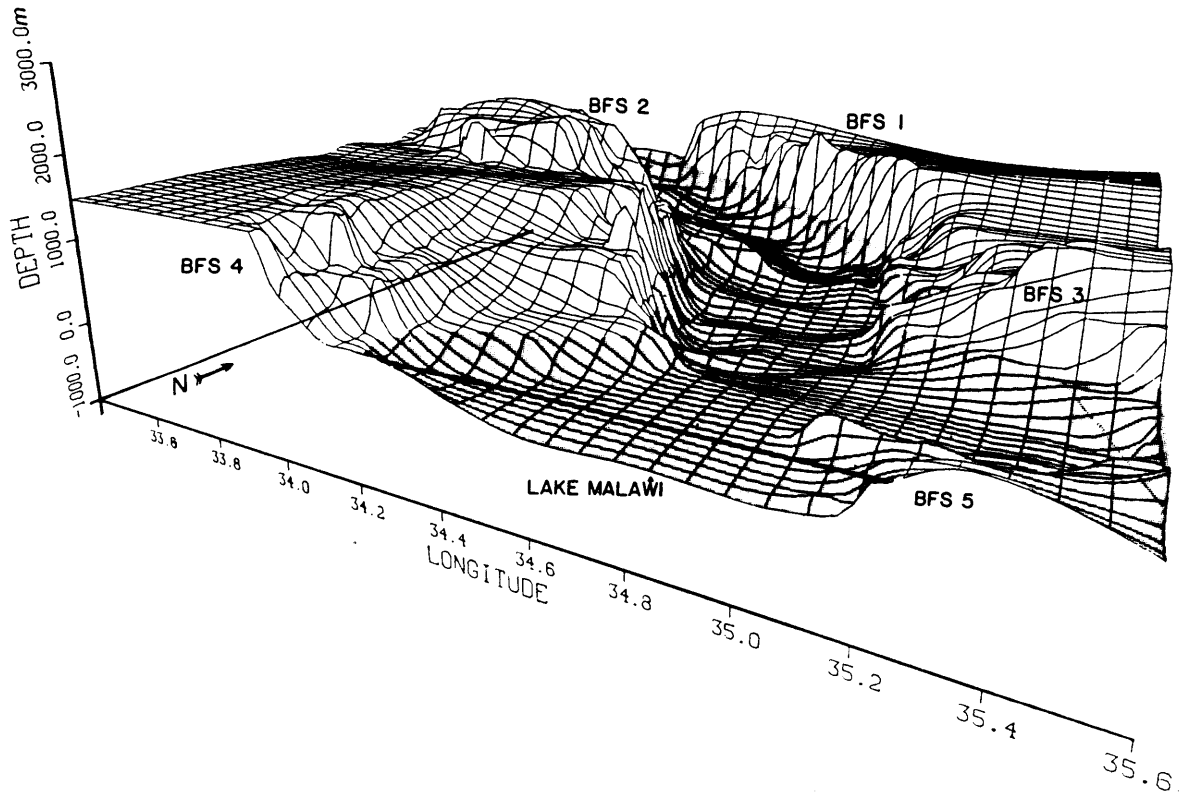

Fig. 7. Three-dimensional diagram of border fault segments 1–5 (12°S to 9°12'S; block rotated ~ 60° C clockwise from north). Region filled by Lake Malawi is shaded. Elevation in meters above and below sealevel. Vertical exaggeration ~ 35 : 1.

Malawi where BFS 2 and BFS 3 face one another across the rift (*B*). Similarly, full-graben with axial ridges occur in the central (*C*) and southern parts of the Malawi rift (*D*) and at locations (*c*) and (*d*) in the Tanganyika rift. In both rifts, the structural high separating the two facing half-graben appears to function as a hinge for subsidence in the half-graben on either side. This type of geometry prompted Rosendahl et al. (in press) to describe these features as "hinged highs".

The geometry of later-stage faults within the sedimentary sequences of rift units, such as the mid-lake high in the Nkhata basin, indicates that continued movements may produce structural reorientations and local uplift. For example, depositional patterns within the Nkhata region (*B*) indicate the central horst was once part of the sedimentary basin bounded by BFS 2, and that this ridge has only recently been uplifted relative to the Nkhata basin.

Shallow platforms, or back-tilted fault blocks, within the rift valley and adjacent to border faults are found at the junctions of border fault systems and monoclines (*E*, *F*, *G*), or where the tips of two border fault segments are linked on the same side of the rift (*H*, *I*, *J*, *K*). Similar relations are observed in the Tanganyika rift at locations (*e*, *f*) and (*g*, *h*). In both the Malawi and Tanganyika rifts, platforms are generally triangular in plan view. Back-tilted platforms are fault blocks pinned where border fault systems and flexural boundaries intersect (see Fig. 1B).

The along-axis segmentation within the Malawi rift explains observations of extensional and strike-slip structures within a regionally extensional environment. These movements are related both to differential motions or strain accommodations between rift segments and, more locally, along the zig-zag border fault systems (Fig. 5). With continued extension, interbasinal regions could become sites of large transcurrent movements. Depositional and rotational patterns of fault blocks interpreted from sedimentary sequences and reconstructions of basement faults (e.g., Gibbs, 1984) provide indirect evidence that these major border fault segments are listric, but there is no direct evidence to constrain the geometry of border faults within the crust.

Influence of pre-existing structural trends

We have summarized the tectonic history of this region in order to examine the role of ancient structural trends on the development of Malawi rift basins (Fig. 8). Faults attributed to the Malawi rift have formed in Proterozoic to Precambrian mobile belts between Archaean cratons. During the Ubendian orogeny (1800–2250 Ma) deformation occurred in a belt of tightly-folded rocks with NW-trending fold axes (Fitches, 1970). Along the northeastern side of the Karonga region, a discontinuous lineament of basic and ultrabasic rocks, in thrust fault contact with underlying Ubendian rocks (Stockley, 1948), is interpreted as a suture zone that closed during the Kibaran orogeny (1300 Ma). Basement rocks on the western central margin of the Malawi rift (Irumidian) were folded along NE–SW axes during the same period (Carter and Bennett, 1973). On the eastern margin of the Malawi rift, rocks with N–S oriented grains were deformed during the Mozambiquian orogeny (400–700 Ma; Cannon et al., 1969). Foliation directions indicate parts of the Ubendian and Kibaran orogenic belts were overprinted during the Mozambiquian orogeny, and widespread outcrops of granulites and migmatites occur within this belt (Carter and Bennett, 1973).

Several fault-bounded sedimentary basins containing Permo-Triassic (Karroo) sediments and volcanics occur near or within the boundaries of the rift system (Fig. 8). In the northern Nkhata region, the subdued character and SW-trend of magnetic anomalies, and a change from highly reverberant acoustic basement to fuzzy, discontinuous reflectors in seismic profiles indicate that Permo-Triassic Karroo sediments exposed onshore in the Ruhuhu trough may extend beneath the lake. In the Shire province, a NE-trending lineament of alkaline plutons and dikes within a narrow graben was emplaced during a Jurassic–Cretaceous phase of rifting (Wooley and Garson, 1970; Carter and Bennett, 1973).

When viewed in a regional framework, both the Malawi and Tanganyika rifts have formed in mobile belts and tend to avoid the rocks of the Tanganyika craton (Cahen and Snelling, 1984), which may indicate that the Western Branch fol-

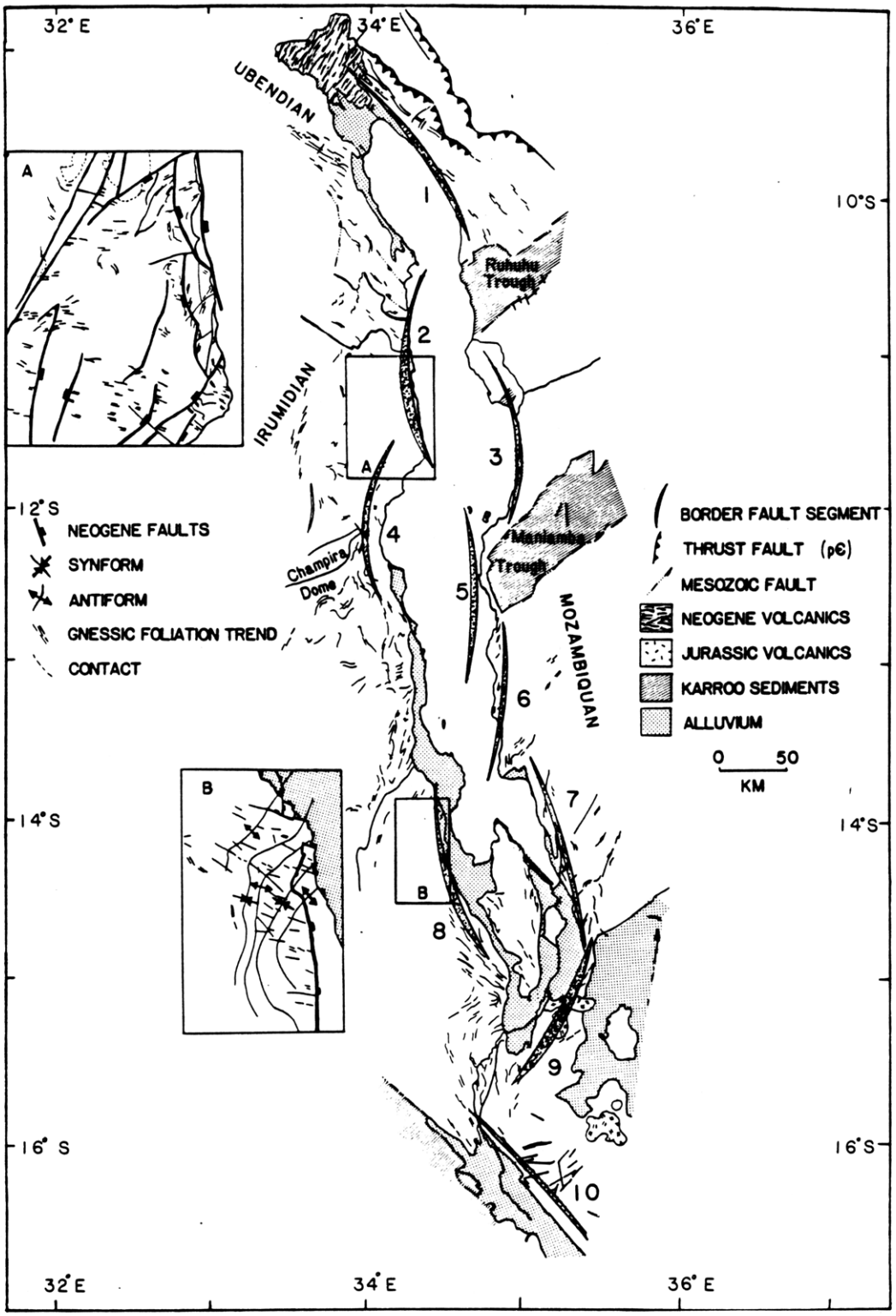

Fig. 8. Regional geology of the Malawi rift zone showing relationship between numbered border fault segments and Precambrian–Mesozoic structures. Geologic information from: Afonso (1976); Carter and Bennett (1973); Harkin (1960); James (1956); Quennell et al. (1956); Stockley (1948); Wooley and Garson (1970). Ubendian, Irumidian, and Mozambiquan refer to tectonic provinces associated with Proterozoic to Precambrian orogenies that affected this region. Details of structures within regions *A* and *B* are from Hopkins (1975) and Thatcher (1968), respectively.

lows a large-scale zone of weakness in the lithosphere. In our analysis of Malawi rift structures, we have described border fault segmentations that occur with repetitive length scales of 100 km, hence we will assess the influence of pre-existing structures at this same length scale. Pre-existing structures are defined as faults, folds, dikes, and gneissic foliation planes in the metamorphic rocks adjacent to the rift that are attributed to these earlier orogenies. In a previous study of faults along the western flanks of the Malawi rift, Crossley and Crow (1980) noted little correlation between Neogene and ancient faults. We have concentrated on regional structural patterns along the northeastern, western, and southern parts of the Malawi rift to examine the influence of Precambrian to Mesozoic structures on the development of border fault segments described above.

By superimposing the traces of Malawi rift border fault segments on the regional tectonic framework (Fig. 8), several consistent relationships between the location and orientation of border fault segments can be observed. Few (if any) border fault segments follow lithologic or tectonic contacts, and the trace of border fault segments may continue from one tectonic province to another with little change in orientation (e.g. BFS 2). Where the trend of pre-existing structures is approximately parallel to the regional N–S trend of the Malawi rift, some parts of border fault systems follow the trends of older structures, but rarely reactivate ancient faults (Crossley and Crow, 1980). For example, BFS 1 on the northeastern side of the Karonga basin is sub-parallel to Precambrian thrust faults and elongate belts of Proterozoic rocks, but there is little evidence in Landsat imagery or field data (Stockley, 1948) for reactivation of Precambrian thrust faults just to the northeast of BFS 1. It is interesting to note that the basement structure in the northern part of the Malawi rift is similar to that found in the Basin and Range province, where some Mesozoic and Tertiary thrust faults have been reactivated as detachments for low-angle normal faults (Wernicke and Burchfiel, 1982; Smith and Bruhn, 1984).

The central parts of border fault systems, where the greatest vertical displacements occur, have orientations that are often oblique to pre-existing structures. For example, BFS 2 is oriented nearly orthogonal to NNW-trending Ubendian structures, BFS 5 cuts across a Karroo trough, and BFS 8 is oriented approximately 60° to the trend of metamorphic fabric in basement rocks. Along BFS 8, open folds and shear zones with axial traces oriented WNW are displaced by Malawi rift faults (inset B, Fig. 8). Jurassic–Cretaceous plutons have been truncated by BFS 9, and BFS 10 cross-cuts granophyre dikes in the southern part of the rift.

In several locations within the Malawi rift, faults located within the border fault systems have orientations parallel to joints or nearly vertical axial planes of gneissic foliations in rocks exposed on the rift flanks. For example, WSW-oriented faults between BFS 2 and BFS 4 parallel shear zones bounding the Champira dome (Fig. 8), although there is little evidence onshore that the faults in this region have been rejuvenated by recent rifting (Crossley and Crow, 1980). In the southern part of Lake Malawi, where BFS 8 crosses high-grade metamorphic rocks in the southern part of the rift, some faults follow joints and foliation planes in the short segments, forming a rectilinear or "zig-zag" pattern (inset B, Fig. 8). Regionally, the longer faults with a NNW trend do not follow synforms and antiforms or lithologic contacts (Thatcher, 1968).

Summarizing these observations, the terminations of major boundary fault systems show no consistent correlation with pre-existing structures, and border fault segments do not appear to alternate sides of the rift to "avoid" stronger rock units. The terminations of border fault segments and reversals of basinal asymmetries at regular intervals along the length of the Malawi and Tanganyika rifts rarely occur at lithologic contacts or at the boundary between tectonic units. An exception may occur between BFS 2 and BFS 4 at the bend in Lake Malawi, as the offset coincides with high-grade metamorphic rocks in the Champira dome (Fig. 8). In interbasinal regions, or accommodation zones, reactivation is more commonly observed where ancient structures have an orientation subparallel to the regional N–S trend of the Malawi rift valley, or at the tips of border fault segments where vertical movements

are distributed along a system of closely-spaced faults with minor offsets.

Locally, individual faults comprising the border fault segment may follow joints or foliation planes, particularly where existing structures trend roughly N–S, or parallel to the general trend of the rift. From laboratory tests of pre-strained rocks, rejuvenation of pre-existing fractures may occur where differences between principal stress orientations in successive episodes are small, depending upon the material properties of the rocks (Handin, 1969). With differences in principal stress directions less than 25°, rejuvenation is often observed in metamorphic rocks (Handin, 1969). These results may explain the similarity between Neogene faults and ancient structural trends near BFS 1, where pre-existing structures in the Ubendian belt are oriented approximately 25° to the N–S trend of the Malaŵi rift.

Estimates of extension

Seismic reflection profiles from the western side of Lake Malaŵi were used to correct measured heat flow values (Von Herzen and Vacquier, 1967) for thermal blanketing effects, which tend to depress the measured heat flux from the rift. Core samples from the thermally stratified anoxic lake reveal the upper 13 m of sediments are composed of diatomites and muds, and sedimentation rates range from 1 to 5 mm/yr (Von Herzen and Vacquier, 1967; Muller and Forstner, 1973; Ebinger et al., 1984). Estimates of sedimentation corrections were obtained using a nomogram presented by Hutchison (1985) that relates the variation of heat flux through time for deposition of shales or deep-water marine sediments. The various corrections assume both a constant sedimentation rate and sediment grain conductivity, pore water advection, and changing bulk conductivity with depth due to sediment compaction (Hutchison, 1985). In unsurveyed parts of the lake, a 1.2 km sediment thickness was assumed. Seismic profiles from the Nkhata Province reveal several measurements were made in disturbed sediments interpreted as massive slumps, and these extremely low values were not considered in the re-interpretation (Fig. 9). We anticipate that the extremely low (< 25 mW/m^2) values at the base of BFS 1 have been affected similarly, and we have not included these measurements in the compilation.

Based on this graphical comparison, the present heat flow from the Malaŵi rift has been reduced by 10–30% by the rapid deposition of sediments. The average corrected heat flow value of 75.3 mW/m^2 is higher th .n the uncorrected mean value of 52.4 mW/m^2, and is above the African continental mean of 49.8 mW/m^2 (Sclater et al., 1980). These data have a large standard deviation (± 35 mW/m^2), but both the mean values and variability within the rift are typical of observations within other continental rift systems (e.g. Ramberg and Morgan, 1984).

Much of the scatter in these data is eliminated when the corrected values are grouped with respect to the structural provinces described above (Figs. 3 and 7). As shown in Fig. 9, there is a large difference in mean values between basins bounded by separate border fault systems. Where seismic reflection data are available, there is no correlation between extreme values and local basement highs or faults, suggesting that the high values are not caused by pore water expulsion along faults or heat refraction through basement highs (Green et al., 1981). The along-axis variations may be affected by hydrothermal circulation patterns within the rift; numerous hot springs occur along faults bordering the Malaŵi rift (Fig. 9), and iron-rich compounds (nontronite) recovered in shallow cores from Lake Malaŵi suggest that hydrothermally active areas occur beneath the lake (Muller and Forstner, 1973). However, the length scales of basinal groupings in the Malaŵi rift are much greater than the 5–10 km wavelengths of hydrothermal cells reported in oceanic crust (Green et al., 1981).

We have estimated lithospheric extension by graphically comparing heat flow and subsidence within the Malaŵi rift to values predicted in a one-dimensional, two-layer stretching model presented by Royden (1986). A deep-water sediment factor (Crough, 1983) was used to correct basement depths for sediment loading, and vertical movements have been referenced to a mid-Miocene erosional surface (Lister, 1967). Because the number of values within each of the four extensional

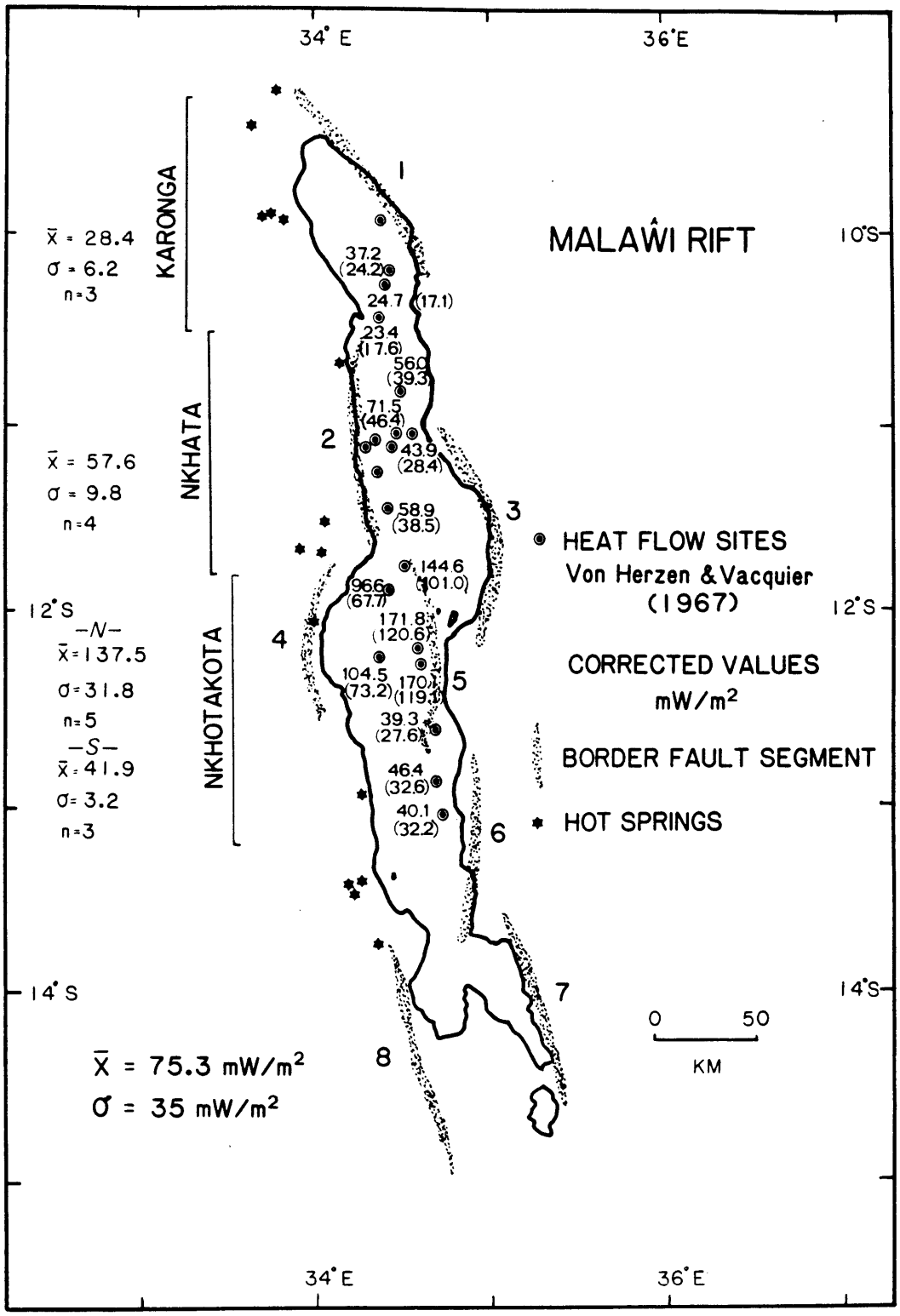

Fig. 9. Measured heat flow values (in parentheses) and values corrected for sedimentation effects within the Malawi rift. Measurements at unlabelled sites were made in disturbed sediments and were omitted. Mean values and standard deviations of corrected values within sedimentary basins bounded by border fault segments are indicated to the left of figure.

segments is small, we have used the mean heat flow value for the entire rift (75 mW/m^2) to estimate extension. The average heat flow and subsidence indicates that both the crust and subcrustal lithosphere have been thinned by approximately 50%. The 5–10 km of crustal extension obtained from reconstructions of fault geometries in the Nkhata basin is much less than the 25 km predicted using the mean value from the rift. However, this value is in good agreement with the 5–20% extension predicted using the basinal heat mean for the Nkhata extensional segment (Fig. 9).

Discussion

These studies indicate that the major structural components of the Malawi rift are regionally curvilinear border fault segments that are 60–120 km long. Border fault segments bound sigmoidal-shaped basins linked along the length of the rift by accommodation zones. In the Malawi and Tanganyika rifts, differential movements in accommodation zones between extensional basins occur along fault systems with minor vertical offsets. Accommodation zones trend oblique to border fault segments, supporting the tectonic model shown in Fig. 1B. In many parts of both rifts, the tips of border fault segments serve to accommodate these movements, producing the sinuous rift outline characteristic of many continental rift systems. Translational movements between rift segments within the Malawi rift occur within the border fault systems, but there is little evidence that these strike-slip fault zones continue across the rift flanks and into the adjoining regions. Crustal extension largely appears to be restricted to the rift valley, which suggests that little thinning occurs beneath the rift flanks.

The similarity between patterns observed in the Malawi and Tanganyika rifts indicate that the location of uplifted shoulders on the deep side of asymmetric basins marks the initial position of crustal detachments. With continued extension, these alternating border fault segments or detachment faults may coalesce and the accommodation zones become sites of large transcurrent motions. Initial faulting in the Tanganyika rift is believed to have commenced in the Miocene (Bellon and Pouclet, 1980), or 5–10 Ma prior to rifting in the Malawi region. The similarity between structural and morphological patterns within the Malawi and Tanganyika rifts, which have formed at different times and in different basement rocks (e.g. Cahen and Snelling, 1984), indicate that these geometric relations can be used as predictive tools in other rift systems. We hope this type of basinal classification will be adopted by others to facilitate comparisons between rift systems. Because the three-dimensional model presented in this report does not consider the injection of new material, the geometries we have described may not be directly applicable to rifts characterized by extensive volcanic activity.

The lines of evidence used in this study suggest that the border fault segments are 100 km-scale fractures caused by extensional stress concentrations at discrete intervals along the length of the rift system. The inconsistent correlation between the trends of border fault segments and pre-existing structures, and the geometry of extensional segments indicates that the segmentation of the Malawi and Tanganyika rifts is not caused by variations in lithospheric structure along the length of the rift, but is a direct response of continental crust to extension. In this concluding section, we discuss two possible rifting mechanisms that are consistent with the observations of along-axis segmentations and alternating asymmetries within the Malawi and Tanganyika rifts.

The interbasinal differences in sediment thickness, heat flow, and structural style may be temporal, which suggests that the rift has propagated along-axis in a complex manner. With continued episodes of extension, the rift may propagate laterally, additional border fault segments form, and transfer fault systems develop to link extensional segments. For example, the locus of sedimentation within several Tanganyika rift basins has shifted through time, apparently in response to structural readjustments caused by the formation of additional border fault segments (Burgess, 1985). In support of this hypothesis, there is a similarity between the spatial arrangement and linkage of curvilinear border fault segments in the Malawi and Tanganyika rifts and the geometry of propagating oceanic ridge crest segments where

they overlap along the length of the rift (Pollard and Aydin, 1984; Sempère and MacDonald, 1986).

Alternatively, the observed segmentation may be initiated by a spatially periodic mantle anomaly along the length of the rift. Because many of the border fault systems overlap or oppose one another, we have used the distance between the central part of each border fault segment and the adjoining border fault segment to measure the spacing of border fault segments along the rift. The spacing between border fault segments are nearly identical in the Malaŵi (73 ± 14 km) and Tanganyika (69 ± 10 km) rifts (Fig. 6), despite their differences in geologic setting and age of rift initiation. These values may be biased on the high side, as subsurface coverage in both rifts is not complete and additional border fault segments may be found.

Indirect support for a three-dimensional rifting mechanism comes from a comparison to observations of segmentations along oceanic spreading ridges. The 70 km wavelength observed in the Malaŵi and Tanganyika rifts is close to the 50–60 km spacing of axial volcanism along the Red Sea rift, the Mid-Atlantic ridge, and the East Pacific rise (Bonatti, 1985; Schouten et al., 1985). With little information on the structure of the lithosphere beneath the Malaŵi and Tanganyika rifts, we can only speculate on rifting processes producing the spatial arrangement of regularly spaced border fault segments. In an experimental model proposed to explain along-axis variations in oceanic ridge magmatism and morphology, a sinusoidal pattern of diapirs developed from a linear gravitational instability of a less dense fluid beneath a more dense fluid (Whitehead et al., 1984). If the mantle beneath the East African rift system is hotter and less dense than the overlying lithosphere, a similar pattern of diapiric upwellings may have caused the regular segmentations observed within the Malaŵi and Tanganyika rifts. Tests of these hypotheses for the segmentation of continental rift zones awaits detailed field studies within active continental rifts.

Acknowledgements

The Malaŵi Geological Survey kindly provided aeromagnetic data used in this study. Seismic data were collected under NSF grant BNS 7926762, and grants from Société National Elf Aquitaine (Production), and Mobil Oil Corporation. We appreciate the assistance provided by Mobil in producing photographic images of Landsat data from the northern part of the rift. Reviews by T. Brocher, H. Dick, J. Jemsek, L. Royden, B. Tucholke, and R. Von Herzen greatly improved this report. Woods Hole Oceanographic Institution contribution number 6187.

References

Afonso, R., 1976. A geologia de Mocambique. Dir. Serv. Geol. Minas, Maputo, Mozambique, 142 pp.

Aldrich, M., 1986. Tectonics of the Jemez lineament in the Jemez Mountains and Rio Grande Rift. J. Geophys. Res., 91: 1753–1762.

Anderson, E., Zoback, M. and Thompson, G., 1983. Implications of selected subsurface data on the form and evolution of some basins in the northern Basin and Range Province, Nevada and Utah. Geol. Soc. Amer. Bull., 94: 1055–1072.

Andrew, E., 1974. Gravity survey of Malaŵi: fieldwork and processing. Rep. Inst. Geol. Sci., 74/15.

Aydin, A. and Reches, Z., 1982. Number and orientation of fault sets in the field and in experiments. Geology, 10: 107–112.

Baldridge, S., Olsen, K. and Callendar, J., 1984. Rio Grande Rift: problems and perspectives. New Mexico Geol. Soc. Guideb., 35th Annu. Conf., pp. 1–12.

Bally, W., 1982. Musings over sedimentary basin evolution. Philos. Trans. R. Soc. London, Ser. A, 305: 325–328.

Bellon, H. and Pouclet, A., 1980. Datation K-Ar de quelques laves du rift ouest de l'Afrique Centrale; implications sur l'evolution magmatique et structurale. Geol. Rundsch., 69: 59.

Bloomfield, K. and Garson, M., 1965. The geology of the Kirk Range–Lisungwe Valley area. Bull. Geol. Surv. Malaŵi, 17.

Bonatti, E., 1985. Punctiform initiation of seafloor spreading in the Red Sea during transition from a continental to an oceanic rift. Nature, 316: 33–37.

Bosworth, 1985. Geometry of propagating continental rifts. Nature, 316: 625–627.

Bowin, C., Warsi, W. and Milligan, J., 1982. Free-air gravity anomaly atlas of the world. Geol. Soc. Am., Map Chart Ser., MC-46.

Brown, C. and Girdler, R., 1980. Interpretation of African gravity and its implications for the break-up of the continents. J. Geophys. Res., 85: 6443–6455.

Bungum, H. and Nnko, A., 1984. Seismicity of Stiegler's Gorge Area, Tanzania. J. Geophys. Res., 89: 1874–1888.

Burgess, C., 1985. Structural and stratigraphic evolution of Tanganyika: a case study of continental rifting. M.S. Thesis, Duke Univ., Durham, N.C., 46 pp.

Cahen, L. and I. Snelling (Editors), 1984. The Geochronology and Evolution of Africa. Oxford Univ. Press., Oxford, 501 pp.

Cannon, R., Hopkins, D., Thatcher, E., Peters, E., Kemp, J., Gaskell, J. and Ray, G., 1969. Polyphase deformation in the Mozambique belt, northern Malawi. Geol. Soc. Am. Bull., 80: 2515–2677.

Cape, C., McGeary, S. and Thompson, G., 1983. Cenozoic normal faulting and the shallow structure of the Rio Grande rift near Socorro, New Mexico. Geol. Soc. Am. Bull., 94: 3–14.

Carter, G. and Bennett, J., 1973. The geology and mineral resources of Malaŵi. Bull. Geol. Surv. Malaŵi, 6: 62 pp.

Chenet, P.-Y. and Letouzey, J., 1983. Tectonique de la zone comprise entre Abu Durba et Gebel Mezzazat (Sinai, Egypte) dans le contexte de l'evolution du rift du Suez. Bull. Centres Rech. Explor.-Production Elf Aquitaine, 7: 201–215.

Crossley, R. and Crow, M., 1980. The Malaŵi Rift. In: Geodynamic Evolution of the Afro-Arabian Rift System. Accad. Naz. Lincei, 47: 77–87.

Crough, S.T., 1983. The correction for sediment loading on the seafloor. J. Geophys. Res., 88: 6449–6454.

Dixey, F., 1937. The early Cretaceous and Miocene peneplains of Nyasaland and their relation to the Rift Valley. Geol. Mag., 74: 46–67.

Dixey, F., 1956. Erosion and tectonics in the East African rift system. Q. J. Geol. Soc. London, 95: 75–108.

Ebinger, C., Crow, M., Rosendahl, B., Livingstone, D. and LeFournier, J., 1984. Structural evolution of Lake Malaŵi. Nature, 308: 627–629.

Eccles, D., 1974. An outline of the physical limnology of Lake Malaŵi. Limnol. Oceanogr., 19: 730–742.

Elmohandes, 1981. The central European graben system: rifting initiated by clay modelling. Tectonophysics, 73: 69–78.

Fairhead, J. and Reeves, C., 1977. Teleseismic delay times., Bouguer anomalies, and inferred thickness of the African lithosphere. Earth Planet. Sci. Lett., 36: 63–76.

Fairhead, J. and Stuart, G., 1982. The seismicity of the East African rift and comparison with other continental rifts. In: G. Pálmason (Editor), Continental and Oceanic Rifts. American Geophysical Union, Washington, D.C., pp. 41–61.

Fitches, W., 1970. A part of the Ubendian orogenic belt in northern Malaŵi. Geol. Rundsch., 59: 444–458.

Freund, R., 1982. The role of shear in rifting. In: G. Pálmason (Editor), Continental and Oceanic Rifts. American Geophysical Union, Washington, D.C., pp. 33–38.

Gibbs, A., 1984. Structural evolution of extensional basins. J. Geol. Soc. London, 141: 609–620.

Green, K., Von Herzen, R. and Williams, D., 1981. The Galapagos spreading center at 86° N: a detailed geothermal survey. J. Geophys. Res., 86: 979–986.

Handin, J., 1969. On the Coulomb-Mohr failure criterion. J. Geophys. Res., 74: 5343–5348.

Harding, T. and Lowell, J., 1969. Structural styles, their plate tectonic habitats, and hydrocarbon traps in petroleum provinces. Bull. Am. Assoc. Pet. Geol., 63: 1016–1059.

Harkin, D., 1960. The Rungwe volcanics at the northern end of Lake Nyasa. Geol. Surv. Tanganyika, Mem., II: 172 pp.

Haslam, H., Brewer, M., Davis, A. and Darbyshire, D., 1980. Anatexis and high-grade metamorphism in the Champira Dome, Malaŵi: petrological and Rb-Sr studies. Mineral. Mag., 43: 701–714.

Hopkins, D., 1975. The geology of the Rumphi–Nkhata Bay area. Bull. Geol. Surv. Malaŵi, 38/39.

Hutchison, I., 1985. The effects of sedimentation and compaction on oceanic heat flow. Geophys. J.R. Astron. Soc., 82: 439–459.

James, T., 1956. The nature of rift faulting in Tanganyika. Commission for Technical Cooperation in Africa south of the Sahara (CCTA), East-Central Reg. Comm. Geol., Proc. 1st Meet. pp. 81–94.

Kaufulu, Z., Vrba, E. and White, T., 1981. Age of the Chiwondo Beds, northern Malaŵi. Ann. Transvaal Mus., 33: 1–8.

Kirkpatrick, I., 1969. The thermal springs of Malaŵi. Int. Geol. Congr., 23rd, 19: 111–120.

Kligfield, R., Crespi, J., Naruk, S. and Davis, G., 1984. Displacement and strain patterns of extensional orogens. Tectonics, 3: 577–609.

Lister, G., Etheridge, M. and Symonds, P., 1986. Detachment faulting and the evolution of passive continental margins. Geology, 14: 246–250.

Lister, L., 1967. Erosion surfaces in Malaŵi. Rec. Geol. Surv. Malaŵi, 7: 15–28.

Malawi Geological Survey, 1985. Aeromagnetic map of Malaŵi. Malawi Geol. Surv., Zomba, Internal Rep.

McConnell, R., 1972. Geological development of the rift system of East Africa. Geol. Soc. Am. Bull., 83: 2549–2572.

McKenzie, D., 1978. Some remarks on the development of sedimentary basins. Earth Planet. Sci. Lett., 40: 25–32.

McKinlay, A., 1954. Geology of the Ketewaka–Mchuchuma Coalfield, Njombe District. Geol. Surv. Dep. Tanganyika, 21: 45 pp.

Muller, G. and Forstner, U., 1973. Recent iron ore formation in Lake Malaŵi, Africa. Mineral. Deposita, 8: 278–290.

Nolet, G. and Mueller, S., 1982. A model for the deep structure of the East African rift system from the simultaneous inversion of teleseismic data. Tectonophysics, 20: 283–293.

Pollard, D. and Aydin, A., 1984. Propagation and linkage of oceanic ridge segments. J. Geophys. Res., 89: 10,017–10,028.

Quennell, A., McKinlay, A. and Aitken, W., 1956. Summary of the Geology of Tanganyika, Part 1: Introduction and Stratigraphy, Mem. Geol. Surv. Tanganyika, I: 264 pp.

Ramberg, I. and Morgan, P., 1984. Physical characteristics and evolutionary trends of continental rifts. Proc. 27th Int. Geol. Conf., 7: 165–216.

Reynolds, D., 1984. Morphology and structural repetition in rifts. M.S. Thesis, Duke Univ., Durham, N.C.

Reynolds, D. and Rosendahl, B., 1984. Tectonic expressions of continental rifting. Eos, Trans. Am. Geophys. Union, 65: 1116.

Rosendahl, B., Patterson, M. and Ebinger, C., 1982. Structural styles during the early stages of continental fragmentation. Eos, Trans. Am. Geophys. Union, 63: 1117.

Rosendahl, B., Reynolds, D., Lorber, P., Burgess, C., McGill, J., Scott, D., Lambiase, J. and Derksen, S., 1986. In: L. Frostick (Editors), Sedimentation in the East African Rifts. Geol. Soc. London, Spec. Publ., 25: 29–43.

Royden, L., 1986. Simple method for analyzing subsidence and heat flow in extensional basins. In: J. Burrus (Editor), Thermal Modeling in Sedimentary Basins. Coll. Colloq. Seminaires, 44: 49–73.

Schouten, H., Klitgord, K., 1982. The memory of the accreting plate boundary and the continuity of fracture zones. Earth Planet. Sci. Lett., 59: 255–266.

Schouten, H., Klitgord, K. and Whitehead, J., 1985. Segmentation of mid-ocean ridges. Nature, 317: 225–229.

Sclater, J., Jaupart, C. and Galson, D., 1980. The heat loss through oceanic and continental crust and the heat loss of the earth. Rev. Space Planet. Phys. 18: 289–311.

Sempère, J.-C. and Macdonald, K., 1986. Overlapping spreading centers: Implications from crack growth simulation by the displacement discontinuity method. Tectonics, 5: 151–163.

Shudofsky, G., 1985. Source mechanisms and focal depths of East African earthquakes using Rayleigh wave inversion and body-wave modelling. Geophys. J.R. Astron. Soc., 83: 563–614.

Smith, R. and Bruhn, R., 1984. Intraplate extensional tectonics of the eastern Basin-Range: Inferences on structural style from seismic reflection data, regional tectonics, and thermal-mechanical models of brittle–ductile deformation. J. Geophys. Res., 89: 5733–5762.

Stewart, J., 1971. Basin and Range structure: A system of horsts and grabens produced by deep-seated extension. Geol. Soc. Am. Bull., 82: 1019–1044.

Stockley, G., 1948. Geology of North, West and Central Njombe District, Southern Highlands Province. Bull. Geol. Surv. Tanganyika, 18: 67 pp.

Thatcher, E., 1968. The geology of the Dedza Area. Bull. Geol. Surv. Malaŵi, 29: 161 pp.

Von Herzen, R. and Vacquier, V., 1967. Terrestrial heat flow in Lake Malaŵi Africa. J. Geophys. Res., 16: 4221–4226.

Walter, M., 1967. A brief account of the geology of the Lilongwe–Dowa–Salima Area of central Malaŵi. Annu. Rep. Res. Inst. Afr. St. Univ. Leeds, 11: 16–18.

Wernicke, B. and Burchfiel, C., 1982. Modes of extensional tectonics. J. Struct. Geol., 4: 105–115.

Whitehead, J., Dick, H. and Schouten, H., 1984. A mechanism for magmatic accretion under spreading centers. Nature, 312: 146–148.

Wohlenberg, J., 1968. Seismizität der ostafrikanischen Grabenzonen zwischen 4° N and 12° S sowie 23° E und 40° E. Veröff. Bayerischen Komm. Int. Erdmess., 43: 95 pp.

Wooley, A. and Garson, M., 1970. Petrochemical and tectonic relationship of the Malaŵi carbonatite-alkaline province and the Lupata–Limpopo volcanics. In: T. Clifford and I. Gass (Editors), African Magmatism and Tectonics. Hafner, New York, N.Y., pp. 237–262.

Yairi, K., 1977. Preliminary account of the lake-floor topography of Lake Malaŵi in relation to the formation of the Malaŵi Rift Valley. In: K. Suwa (Editor), 2nd Prel. Rep. Afr. Studies. Nagoya Univ., Nagoya, pp. 51–69.

Ziegler, P., 1978. North Sea rift and basin development. In: I. Ramberg and E-R. Neumann (Editors), Tectonics and Geophysics of Continental Rifts. Reidel, Dordrecht, pp. 249–277.

Zorin, Y., 1981. The Baikal rift: an example of the intrusion of asthenospheric material into the lithosphere as the cause of disruption of lithospheric plates. Tectonophysics, 73: 91–104.

CHAPTER 3

STRUCTURAL CONTROLS ON RIFT MAGMATISM IN THE WESTERN BRANCH OF THE EAST AFRICAN RIFT SYSTEM

C.J. Ebinger M.I.T./Woods Hole Oceanographic Institution Joint Program
Dept. Earth, Atmospheric, & Planetary Sciences
Massachusetts Institute of Technology
Cambridge, MA 02139

Introduction

The tectonically active continental rift system of East Africa consists of two limbs, the Kenya (Gregory) rift valley and the more remote Western rift valley, which is filled by deep lakes along much of its length (Figure 1). The results of recent studies in the great lakes of the Western rift valley and in the Kenya rift system show that the two rift valleys are segmented along their length into a series of extensional basins (e.g., King, 1978; Crossley and Crow, 1980; Chorowicz, 1983; Ebinger et al, 1984; Bosworth, 1985; Rosendahl et al, 1986; Baker, 1986). The predominantly half-graben basinal morphologies and alternating basinal asymmetries observed along the length of the Western rift system are similar to patterns of uplift and subsidence observed in the Kenya rift valley, and other continental rift systems (e.g., King, 1978; Chenet and Letouzey, 1983; Reynolds, 1984; Smith and Bruhn, 1984; Bosworth, 1985). However, the geometry, lateral extent, and continuity of Tertiary fault systems between basins and across the uplifted regions flanking the Western rift valley have been poorly understood in many parts of the Western rift system; existing geological maps from the western side of the rift valley are at a scale of 1:250,000 to 1:2,000,000.

Volcanic activity in the Western rift system is restricted to four isolated centers where less than 2500 km^3 of material has erupted, in contrast to the Kenya rift system where over 220,000 km^3 of volcanic material has accumulated during Tertiary time (Meyer, 1954; Pouclet, 1977; Baker, 1986). Nevertheless, significant variations in basaltic geochemistry with time within the volumetrically small Western volcanic provinces suggests a complex interplay between basinal development, crustal extension, and thermal processes within the mantle during the evolution of these volcanic provinces (Harkin, 1960; Kampunzu et al., 1983; Auchapt et al., 1987; Pasteels et al., in press). Previous petrological and radiometric analyses of Tertiary volcanic rocks provide information on the timing and evolution of the South Kivu volcanic provinces, but the relationship between volcanic centers and border fault systems was not addressed in these studies (Guibert, 1977; Bellon and Pouclet, 1980; De Paepe and Fernandez-Alonso, 1983; Pasteels et al., in press). A range of phonolitic to alkalic basalts has been described within the Rungwe volcanic province, but no age constraints previously were available to intepret these sequences.

The objectives of this study are to examine the three-dimensional geometry of Western border fault systems and to characterize structural patterns in fault zones linking half-graben that are tilted in opposite directions. Remote sensing and field studies were conducted in the South Kivu and Rungwe volcanic provinces, where Neogene basalts provide kinematic constraints on the timing of horizontal and vertical crustal movements

within extensional basins and along the uplifted flanks of the rift valley. I supplement field observations made during four months in 1986 and 1987 with new radiometric age determinations from alkalic rocks within the previously undated Rungwe volcanic province and in part of the South Kivu province, and with existing data from beneath lake basins to interpret the spatial and temporal development of several Western rift basins. These studies also were designed to determine the tectonic relationship between volcanic centers and fault systems bordering and linking basins, and their relationship with pre-existing basement structures.

Background

Both the Kenya and Western rift systems have been interpreted as zones of lithospheric thinning linking the East African rift system with the Afar-Red Sea-Gulf of Aden rifts to the north (e.g., Gregory, 1896; Fairhead and Girdler, 1969; Degens et al., 1971; Chorowicz, 1983). Within the Western rift valley, normal fault systems showing large vertical displacements (border faults) extend along one side of asymmetric basins, and the sense of basinal asymmetry often alternates along the length of the rift (Crossley and Crow, 1980; Ebinger et al., 1984; Rosendahl et al., 1986). Earthquake focal mechanisms from the Western rift system indicate that faults maintain dips of 40°-60° to depths of 17-29 km beneath rift basins (Shudofsky, 1985). The 150-200 km wide zones of uplift flanking both sides of Western rift basins rise 1-3 km above the surrounding topography of the East African dome, or nearly 5 km above sealevel (e.g., Chapter 4).

Previous estimates of crustal thickness beneath the Kivu and the northern Tanganyika rift are approximately 30 km, or slightly less than the 35-41 km thick crust found beneath the largely unfaulted region between the Western and Kenya rift valleys, based on the results of seismic refraction studies (Rykounov et al., 1972; Bram and Schmeling, 1975; Hebert and Langston, 1985). However, crustal thicknesses beneath individual rift basins may be less than 30 km because these seismic refraction profiles average crustal structure over distances of 200-800 km (e.g., Bram and Schmeling, 1975).

Chronologic constraints from the Western rift system indicate that crustal movements leading to the formation of individual rift basins began during Neogene time. Initial volcanism in the northern part of the Western rift valley commenced at approximately 12 Ma, or 10-12 My after initial volcanic activity within the Kenya rift system (e.g., Bellon and Pouclet, 1980; Baker, 1986). Tertiary volcanic activity within the Western rift system is limited to four isolated occurrences: at the northern end of Lake Edward (Toro-Ankole province); at the northern end of Lake Kivu (Virunga province); at the southern end of Lake Kivu (South Kivu province); and at the northern end of Lake Malawi (Rungwe province) (Figure 1). Basalts from the South Kivu province previously

dated as 40 Ma -Recent (e.g., Bellon and Pouclet, 1980) recently have been shown to be younger than 10 Ma (Pasteels et al., in press). These studies indicate that the more evolved tholeiitic basalts were erupted at 10-6 Ma, prior to the eruption of less evolved alkalic basalts at 8-4 Ma, and Late Pliocene to historic eruptions of tholeiitic rocks (Pasteels et al., in press; this study). A wide range of magmatic products have been erupted within a small region, although the chronological relationship between volcanic units of different composition in the Rungwe province was not known (Harkin, 1960). In the southern part of the Western rift valley, lacustrine sediments deposited at less than 5 Ma are found along the margins of northern Lake Malawi (Kaufulu et al., 1981).

Faults bounding the Western rift valley have developed within Proterozoic orogenic belts linking the Archaean cratons of central and eastern Africa (Figure 2). Much of the Western rift system is floored by the Ubendian/Rusizian system (~2100 Ma) that is characterized by northwest-southeast trending mylonites and shear zones (Cahen and Snelling, 1984). The Kibaran and Irumidian orogenic belts (1300 Ma) are made up of northeast-trending basement structures in the western and central part of the Western rift system (Reeves, 1960; Cahen and Snelling, 1984; Daly, 1986), and similarly-aged rocks have a northwest trend in the Burundian belt northeast of Lake Tanganyika (Theunissen, in press). Folds with east-west striking axes and northeast-striking thrust faults assigned to the Pan-African orogeny (900-600 Ma) are found in the Rungwe province (Ukingan orogeny). Parts of the South Kivu and Rungwe regions also were affected by episodes of rifting during the Permo-Triassic and Cretaceous, prior to the development of the East African rift system in Tertiary time. Within these two volcanic provinces, Permo-Triassic sediments (Karroo) are limited to the southwestern part of the Rungwe province where over 5 km of sediments have accumulated (Peirce and Lipkov, in press). An examination of Figures 1 and 2 suggests that the general location of the Western and Kenya rift valleys may follow inherited zones of weakness within the continental lithosphere and avoid the Archaean craton.

Structural Analyses

I illustrate the geometry of border fault systems, interbasinal fault zones (accommodation zones), and volcanic occurrences within the Western rift system with examples of structural patterns within the South Kivu volcanic province (Rusizi and Kivu basins), and the Rungwe volcanic province (Songwe, Usangu, Karonga basins) (Figure 1). High resolution color Landsat-5 Thematic Mapper (TM) and Multi-Spectral Scanner (MSS) imagery were used as a primary data base to examine fault patterns within, between, and along the uplifted flanks of these basins, as well as to compile existing data (see Appendix I). Within the South Kivu volcanic province, aerial photographs were used to

establish continuity of structures and to extend field observations. Exploratory multichannel seismic reflection data within the eastern part of the Rusizi basin and existing seismic reflection and core data from the Kivu rift provided subsurface information (Degens et al., 1973; Wong and Von Herzen, 1974; D. Stone, pers. comm.). The uplifted flanks of the northern and central parts of the remote Western rift system are thickly vegetated and exposure is limited to stream valleys and road cuts, hence, I used these imagery to identify areas for detailed field studies conducted during 1986 and 1987.

Where faults and lineaments had not been noted previously, the following criteria were used to differentiate Neogene faults from older structures: displacement of Neogene volcanic and sedimentary units, amount of topographic relief, appearance of fault scarps, occurrence of hot springs, and horizontal offsets of pre-rift basement faults and geologic contacts. The scale of topographic maps used was 1:50,000, except in regions to the west and east of Lake Kivu where 1:200,000 maps provided by Musée Royal de l'Afrique Centrale were used.

In this study of structural and stratigraphic relations within the Souht Kivu and Rungwe provinces, I define border fault segments as sections of fault systems bordering rift basins that are characterized by large vertical throws, uplifted rift flanks (high topographic relief), and that bound half-graben (e.g Ebinger et al., 1987). I also use the term interbasinal transfer fault zone, or accommodation zone, to describe fault patterns linking basins along the length of the rift (e.g., Burchfiel and Stewart, 1966; Bally, 1982; Gibbs, 1984; Bosworth, 1985; Rosendahl et al., 1986).

South Kivu Volcanic Province

From north to south, I delineate border fault segments along the northwestern margin of Lake Kivu (West Kivu basin), along the southeastern shores of Lake Kivu (East Kivu basin), and along the western margin of the Rusizi basin (Figure 3). Based on seismic reflection profiles from the Kivu and Rusizi basins, the basins bounded by these border fault segments have the cross-sectional form of a half-graben, with the sense of asymmetry at the central part of the ~100 km long border fault segment tilted toward the steep escarpments. The Rusizi basin is separated from the Kivu basins by a fault-bounded topographic high that transects the rift valley, and I refer to this interbasinal region as an accommodation zone. Flows from the mid-Miocene to Recent volcanism in the South Kivu province are located near the accommodation zone between the two basins. The three-dimensional diagram shown in Figure 4 illustrates the relationship between eruptive centers and the general morphology of the East and West Kivu basins, the Rusizi basin, and the accommodation zone linking basins with opposite sense of asymmetries.

The East Kivu border fault segment bounds the eastern side of Lake Kivu, and Idjwi Island marks the western extent of the East Kivu basin (Figure 3). To the north along the eastern margin of the Virunga volcanic province, the East Kivu border fault segment splays out in a diffuse zone of normal faults with minor topographic relief. A series of subparallel high-angle normal faults rise in a stair-step pattern to the elevation of the uplifted flank (~2500m).

At the base of the escarpment and within the basin, Miocene to Recent volcanics overlie metamorphic basement (Figures 3, 4). I was unable to establish a volcanic stratigraphy that was applicable over distances greater than 1 km within the South Kivu volcanic province, as individual flows are of limited areal extent and volcanic centers are difficult to locate due to pervasive alteration and thick soil profiles characteristic of the region. The following basinal stratigraphy is based on petrographical correlations with previously dated units and dated stratigraphic horizons beneath Lake Kivu (Degens et al., 1973; Stoffers and Hecky, 1978; Bellon and Pouclet, 1980; Pasteels et al., in press). Highly altered tholeiitic basalts (Tv1) similar to samples dated at 10-6 Ma overlie metamorphic basement at the base of the East Kivu border fault segment in the southern part of the basin (Figure 5). Within the southeastern and central part of the East Kivu basin, these tholeiitic basalts are overlain by alkalic basalts, basanites, and hawaiites (Tv2) similar to samples dated at 8.0-5.4 Ma (De Paepe and Fernandez-Alonso, 1981; Pasteels et al., in press; this study). Within both sequences (Tv1, Tv2) basalt flows are thin (<5m) and flows usually are separated by altered ash units and soil horizons, and depositional contacts are conformable or erosional. A less than 100m thick sequence of alkalic basalts and altered ash units continue at approximately the same elevation to the west across the gorge cut by the Rusizi River where basalts overlie basement and dip gently to the north. Predominantly varved biogenic sediments interbedded with pyrite and siderite-rich sandstone and siltstone layers (Ts) directly overlie metamorphic basement and basalts beneath Lake Kivu (Degens et al., 1973; Stoffers and Hecky, 1978). Within the northern and central part of the East Kivu basin, Wong and Von Herzen (1974) report the greatest sediment thicknesses (~500m) at the base of the central part of the East Kivu border fault segment.

Along the series of subparallel faults forming the East Kivu escarpment I found a previously unreported lacustrine sedimentary sequence of Neogene age, based on the presence of mammalian bones found within these sediments (Gisakura basin). The top of this sequence near the eastern margin of the basin is elevated approximately 600m above Lake Kivu, and similar lacustrine sediments are not exposed elsewhere in the East Kivu basin (Figure 6). Along the western margin of the basin, hollow basalt tubes filled with

sandstones derived from Precambrian basement are interbedded with rounded cobbles, possibly marking an ancient lake shoreline (Ts; Figure 5). These units are overlain by a <1m thick sequence of well-sorted siltstones (Ts, Qs), and two approximately 5m thick basalt flows (Qv), separated by a baked soil horizon and thin lenses of white sandstones. The upper, less altered basalt flow (Qv) has been dated at 342,000 BP using K/Ar dating methods (Table I). The sedimentary sequence thickens to the northwest, where basal conglomerates and reworked Proterozoic sediments derived from the south and southeast overlie metamorphic basement. Numerous low angle growth faults, drag folds, and debris flows in the well-laminated lacustrine sediments attest to syn-sedimentary deformation. The clastic and metalliferous sediments are interbedded with hyaloclastites and thin layers of olivine basalts, probably the basinal equivalent of the olivine basalts (Qv) found along the margin of the basin, and the sequence coarsens upward. Near the base of the escarpment, low-grade metamorphic rocks beneath the sediments are in fault contact with a small pyroclastic cone on the hanging wall. To the north, the contact of the Gisakura sequence with metamorphic basement is obscured by dense vegetation. Siderite- and pyrite-rich sediments reported beneath the eastern side of the Lake Kivu are similar to those found along the terrace (e.g., Stoffers and Hecky, 1978). Thus, the Gisakura basin sequence may have been contiguous with Lake Kivu sequences in the past.

The southern part of the East Kivu basin is characterized by 5-10 km wide tilted blocks that generally trend northwest and parallel the East Kivu border fault segment (Figure 3). Steeply-dipping faults (>45°) within the rift valley cut the early Miocene tholeiitic and alkalic basalts, and depositional contacts between units dip 10°- 25° (Figures 3, 6). I find no systematic decrease in dip to the top of the section that would indicate progressive rotation of fault blocks between volcanic episodes. Erosion has removed the thin cover of basalts from the upthrown footwall of many of these blocks, and marshy regions characterize the downthrown side of normal faults (Figures 3, 4). The orientation of slickensides along N60°E and less commonly N10°W fault planes indicate a component of oblique-slip movement in a left-lateral sense along faults in the southern part of the East Kivu basin near the accommodation zone.

The locations of eruptive centers within the East Kivu basin appear to have been controlled by border faults and intrabasinal faults throughout the history of the basin. For example, at the base of the East Kivu border fault segment, I found fissures and dikes striking N10°E and N30°E. Recent roadcuts expose a complex of pyroclastic cones along an east-dipping normal fault that is along strike with east-dipping faults bounding the eastern side of Idjwi Island to the northeast (e.g., Figures 3, 4). DePaepe and Fernandez-Alonso (1981) note a predominance of younger alkali basalts (Tv2) in the southwestern part

of the East Kivu basin near the accommodation zone, where I find explosive volcanic centers and fissures located along the margins of tilted blocks. Gisakura basin sequences are intruded by basaltic dikes that strike N20°E, parallel to the border faults.

The East Kivu basin is bounded to the west by Idjwi Island (Figure 3). In the geometrical arrangement of the West and East Kivu border fault segments, Idjwi Island separates the narrow sedimentary basins formed by the West Kivu and East Kivu border fault segments (Figure 4). Seismic reflection data from Lake Kivu indicate that the horst extends north of Idjwi Island to the northern end of Lake Kivu (Wong and Von Herzen, 1974). In these earlier lake studies, Wong and Von Herzen report that hydrothermal vents occur along the length of Idjwi Island, and earthquake epicenters are located along the margins of the block. Thus, this horst serves as a hinge for subsidence within two basins bounded by border fault segments on opposite sides of the rift valley (Figures 3, 4).

The western side of Lake Kivu is bounded by a steep escarpment that borders a basin filled with up to 500m of sediments and basalts derived from the Virunga province to the north (Wong and Von Herzen, 1974). The West Kivu escarpment comprises a series of subparallel, high-angle normal faults, and earthquake epicenters cluster along the base of the escarpment (Wohlenberg, 1968; Zana and Hamaguchi, 1978). Vertical displacements increase from the northern and southern tips of the basin toward the central part of the West Kivu border fault segment where the rift flanks reach an elevation of 3km above sealevel (Figure 3; inset). This fault zone extends north into the Virunga basin where normal faults displace 12,000 BP basalts of the Karisimbi volcano (Pouclet, 1977; De Mulder and Pasteels, 1986; this study). To the south, the border fault system widens and high-angle normal faults displace 10-5 Ma basalts (Pasteels et al., in press; Figure 3). Near the top of the escarpment, the footwalls of normal faults often are covered by marshes, attesting to recent faulting (e.g., Boutakoff, 1939; this study).

As in the East Kivu basin, individual flows are difficult to trace for more than 1 km, due to alteration and faulting post-dating volcanism, and the limited original extent of flows. A thin (<100m) sequence of predominantly alkalic basalts (Tv2) overlies metamorphic basement within the West Kivu basin (Figure 5). Flows mapped in these field studies are petrographically similar to alkalic basalts from the southwestern part of the West Kivu basin that have been dated at 8.0 -4.1 Ma by Pasteels et al (in press). Thickness variations of locally occurring units suggest that possible centers for fissure eruptions are north of Bukavu, and along faults bounding peninsulas along the western shores of Lake Kivu (Figure 3). Within the north central part of the basin (northern Lake Kivu) over 500m of predominantly biogenic sediments have accumulated along the footwalls of three approximately 5 km wide tilted fault blocks (Degens et al., 1973). Pleistocene flows (Qv)

from cones located along the crest of the West Kivu escarpment (Tshibinda, Tshibati, Leymera) flowed down the escarpment and fill pre-existing topographic depressions in the generally altered Late Miocene to early Pliocene basalts (Tv2) found at the base of the escarpment (Figure 5).

Fault patterns within the southern part of the West Kivu basin are characterized by approximately 5 km-wide tilted blocks bounded by normal faults oriented N10°-20°E, or, less often, normal faults oriented north-south to N10°W that dip to the northeast (Figure 3). Tilted fault blocks bounded by northeast-striking faults form peninsulas that project into Lake Kivu, and fault scarps bounding these blocks are triangular. A thin cover of altered alkali basalts and ash overlying metamorphic basement has been eroded from the footwall of many intrabasinal faults, and hot springs and travertine deposits are found along normal faults within the basin.

Within the West Kivu basin, eruptive centers identified in the field correlate with major fault systems. Along the southern section of the West Kivu border fault segment basaltic flows from a lineament of pyroclastic cones younger than 1.9 Ma cover the escarpment below the cones (Meyer and Burette, 1957; Guibert, 1977a; Bellon and Pouclet, 1980; this study). These 100-600m wide cones are located on both the hanging walls and foot walls of normal faults bounding the West Kivu basin. Along the uplifted rift flank flows directed away from the axis of the rift valley (northwestward) and these flows follow present-day topography, attesting to the youthfulness of faulting and volcanism in this area.

The cross-section of the South Kivu volcanic province shown in Figure 7 is based on observations made along a new road crossing the eastern half of the rift that provides excellent exposure, and on a transect across the West Kivu border fault segment in Zaïre where many road cuts are overgrown by rain forest (Figure 3). No subsurface structural information is available from the southern part of Lake Kivu. Further north within the central part of the rift, the two basins are separated by a horst (Idjwi Island). Based on an extrapolation of dips of contacts between volcanic units, the basalts sequences are probably less than 100m thick. Tholeiitic basalts (Tv1) are restricted to the East Kivu basin and the eastern part of the West Kivu basin (Idjwi Island).

A reconstruction of surface fault geometries shown in Figure 7 indicates that the crust beneath the Kivu region has been extended by approximately 15%. Within the eastern part of the Kivu basin, I found evidence for significant penetrative deformation internal to one of these 5 km wide tilted fault blocks (Figure 8). Geometrical relations between normal faults that dip 30-40° and displace Miocene basalts and ash layers that dip 30-35°within this tilted block indicate that crustal extension locally is on the order of 60-

80% (e.g., Wernicke and Burchfiel, 1982). Because these low-angle normal faults have been observed in few locations, crustal extension within the Kivu rift valley probably falls at the lower end of the range between these two estimates (15-80%).

Rusizi basin

Northeast-striking normal faults bounding the west side of the Rusizi basin curve southward to follow a nearly north-south strike. As along the Kivu escarpments, the Rusizi border fault segment consists of 3-4 sub-parallel normal faults, and the innermost scarp is the least facetted. Seismic reflection data from the central part of the Rusizi basin indicate that the inner fault bounding the western side of the basin remains steep (>45°) to depths of 5 km, measured from the top of the uplifted escarpment. Seismicity during the period 1958-1965 within the Rusizi basin clusters along the central part of the Rusizi border fault segment, and epicenters of aftershocks from a 1960 earthquake beneath the Rusizi border fault segment fall throughout the depth range 5 to 30 km (Wohlenberg, 1968; Zana and Hamaguchi, 1978). Sedimentary accumulations are greatest near the central part of the Rusizi border fault segment and decrease toward the tips, producing a spoon-shaped basin tilted to the west (Patterson, 1983). The eastern side of the Rusizi basin is bounded by north-south trending faults that form a stairstep pattern rising to the level of the uplifted flank (step faults) that dip 60-75° to the west, and slickensides are sub-vertical within these fault zones.

Tholeiitic (Tv1) and alkalic basalts (Tv2) with petrographical characteristics similar to those of 5-6.5 Ma basalts found 600m higher within the West Kivu basin directly overlie metamorphic basement at the northern end of the Rusizi basin (Figure 5; DePaepe and Fernandez-Alonso, 1981; Tack and De Paepe, 1983; Kampunzu et al., 1986; this study). At least two flows occur within the Rusizi basin and they are separated by a 50 cm thick paleosol (Figure 5). The maximum observed thickness of basalts is less than 20m, and thicknesses decrease southward into the Rusizi basin. Some basalt layers in the northern Rusizi basin show signs of sub-lacustrine alteration, but there is no evidence for sub-lacustrine volcanic flows within the Rusizi basin (Tack and DePaepe, 1983; this study). High amplitude magnetic anomalies (100 γ) similar to anomalies observed where basalts crop out in the northern Rusizi basin continue for approximately 10 km south of the southernmost exposure of basalts (D. Stone, pers. comm.). Plio-Pleistocene gravels, and lacustrine sandstones and siltstones are found along the inner Rusizi fault system and cover much of the plain north of Lake Tanganyika (Figure 5). Late Pleistocene alluvial cones and talus (Ps) extend onto the valley floor over lacustrine sediments along the eastern and western margins of the basins near major faults (Figures 3, 5).

The floor of the northern Rusizi basin has been faulted into a series of tilted blocks, and faults bounding blocks cut Miocene basalts (Tv1, Tv2) and the overlying sediments. The central part of the Rusizi basin is a narrow graben filled by the Rusizi River, and sediments exposed along the inner river terraces contain volcanic clasts. Hot springs are located along north-south and N10°W striking faults within the basin and along faults bounding the eastern margin of the basin. Seismic reflection data from the Rusizi plain and beneath Lake Tanganyika reveal over 1.5 km of displacement along many of the north-south oriented faults, although most faults have little surface expression (Patterson, 1983; D. Stone, pers. comm.).

A cross-sectional profile of the central part of the Rusizi basin shown in Figure 9 illustrates the half-graben morphology characteristic of Western Branch rift basins, with the western flank of the Rusizi basin at a higher elevation (3275m) than the eastern flank of the basin (2600m). Within the Rusizi basin, there is a predominance of faults synthetic to the border fault segment (Figure 9). Eastward-dipping faults are found near the eastern side of Lake Tanganyika, and faults penetrate to all stratigraphic levels in sedimentary sequences beneath Lake Tanganyika. A terrace of well-laminated lacustrine sediments covers the hanging wall of an eastward-tilted block along the eastern, or monoclinal, margin of the Rusizi basin, nearly 500m above Lake Tanganyika (Figure 3). This tectonic setting is similar to the terraces of lacustrine sediments noted along the East Kivu border fault segment.

Accommodation zone

Volcanic rocks of the South Kivu volcanic province cover an accommodation zone between the Kivu and Rusizi extensional basins where the two basins with alternating basinal asymmetries are linked (Figures 3, 4). The eastward shift of the rift valley axis from Lake Kivu to Lake Tanganyika is accompanied by a 650m drop from the elevation of Lake Kivu to the average elevation of the Rusizi basin (Figure 3; inset). The Rusizi River, which serves as the hydrographic connection between Lake Kivu at an elevation of 1420m and Lake Tanganyika at an elevation of 774m, developed during Holocene time when Lake Kivu was dammed in the north by volcanic flows from the Virunga province (Hecky and Degens, 1973). Below, I describe from north to south stratigraphic and structural relations within the accommodation zone between the Kivu and Rusizi basins.

The change in elevation between these two basins occurs across the northern tip of the Rusizi border fault segment and the southern continuation of normal faults bounding the East Kivu basin (Figures 3, 4). A narrow, north-south trending graben, the Bugarama graben, is bounded to the east by seismically active normal faults (e.g., Wohlenberg, 1968) that mark the southern tip of the East Kivu border fault segment and to the west by

normal faults of the Rusizi border fault segment. Metamorphic basement beneath the narrow Bugarama graben gradually rises to the north, and it is covered by both tholeiitic (Tv1) and alkalic basalts (Tv2) overlain by a thin cover of alluvium (Figure 5). Prior to faulting, basalt units in the Bugarama graben were probably once contiguous with petrographically similar basalts found 500m higher to the north in the Kivu basins, although much of the basalt cover has been eroded along the uplifted footwall of the western fault system (DePaepe and Fernandez-Alonzo, 1981; this study). Hot spring deposits occur along the base of the western fault system, but lacustrine sediments similar to those found in terraces along the East Kivu escarpment are absent in the Bugarama basin. These tufa and alluvium (Qs) are separated by calcrete horizons, indicating a depositional environment characteristic of the hotter, drier climate found at the lower elevation of the Rusizi basin (e.g., Ilunga, 1984). Peaty horizons within these faulted sediments contain Pleistocene mammal bones and gastropods typical of Lake Tanganyika assemblages (A. Cohen, pers. comm.; P. Williamson, pers. comm.).

At the northern end of the Bugarama graben, no structures are apparent in the field or in aerial photographs, and exposure is poor. Altered alkalic basalts dip 15° to the east along the eastern fault system bounding the graben. Fault zones on both sides of the basin are less than 5m wide and often mineralized, and slickensides are subvertical along fault planes. Triangular fault scarps, hot springs, and sag ponds at the base of the western fault system are evidence for recent activity along this fault system (Figure 3).

Northeast-trending lineaments on the western flank of the Rusizi basin where normal faults curve to the southwest correspond to narrow, steep-walled valleys characterized by brecciated and calcified fault zones. These fault zones have no apparent vertical offsets, but a component of left lateral movement is indicated by slickensides plunging 30° to N45°W in one of these fault zones. I interpret other lineaments parallel to this N45°E striking fault zone as oblique-slip or strike-slip faults.

Northeast-striking oblique-slip faults also are found at the southern end of the Bugarama graben. An approximately 2 km-wide rhomb-shaped fault block is bounded by normal faults that strike N10°E (Kivu trend) and N10°W (Rusizi trend). The plunge of slickenside surfaces along faults striking N10°E is 45°, and I interpret the northeast-trending faults as oblique-slip faults with a left lateral sense of movement. Numerous northeast-trending lineaments occur within the the northernmost part of the Rusizi basin, and segments of the youthful Rusizi River follow the northeast trend (Figure 3). Isolated exposures of lacustrine sediments and tholeiitic basalts atop this horst were probably continuous with a 7.6 My tholeiitic unit (Tv1) adjacent to the horst found at an elevation 300m lower (Tack and DePaepe, 1983; Figure 3). To the east of this block, basalts from

an explosive volcanic center that flowed to the east are now tilted down to the west, thus indicating post-6 My rotation of this westward-tilted block (Tack and DePaepe, 1983; this study). Within the northern Rusizi basin near the accommodation zone, synthetic and antithetic faults are numerous, and faults are difficult to trace between seismic reflection profiles that are separated by only 2-4 km (D. Stone, pers. comm.).

Timing of Crustal Movements

A structural control on volcanic occurrences is evident throughout the development of the Kivu and Rusizi basins, as volcanic centers within the Kivu basins have been active from mid-Miocene to Pleistocene, or possibly historic times (Figure 5). Throughout the Miocene-Recent development of these rift basins, recognizable centers for volcanic eruptions are along the margins of tilted intrabasinal fault blocks near the accommodation zone, and along the tips of the East and West Kivu border fault segments (Figures 3, 4). Pleistocene volcanism is localized to the southern tips of the East and West Kivu border fault segments and Idjwi Island, indicating that fault systems bounding both sides of the basin are active. This strong structural control on volcanism suggests that volcanic activity occurred concurrently with initial faulting that led to the formation of the Kivu and Rusizi basins.

The initial tholeiitic volcanism (10-6 Ma) is limited to the East Kivu basin and along the southern part of Idjwi Island (7.6 Ma), which suggests that the East Kivu border fault segment formed prior to the development of the West Kivu border fault segment (Figure 11). Basalts directly overlie metamorphic basement along the eroded footwall of normal faults within the West Kivu basin and no sediments have been found beneath or intercalated with basalts, indicating that subsidence in the West Kivu basin post-dates the Mid-Miocene to Early Pliocene magmatism within the South Kivu province. Centers for the later alkalic volcanism are found in both basins, and ages of alkalic sequences within the two basins indicate that the alkalic volcanism occurred in both basins during the same time period (8.5-4.1 Ma; Figure 5).

The occurrence of basalts along the northern flanks of the Rusizi border fault segment and directly overlying metamorphic basement beneath the Rusizi basin indicates that subsidence within the Rusizi basin post-dates the eruption of tholeiitic basalts (6 Ma), although fault systems may have developed to the south within the central Rusizi basin (Figure 11). Normal faults bounding both sides of the Bugarama basin displaced tholeiitic basalts of the East Kivu province into the northern part of the Rusizi basin and the Bugarama graben. The occurrence of basalts at elevations 600m higher than petrographically similar basalts within the Rusizi basin indicate that the Bugarama graben and the Rusizi basin developed after the Miocene volcanism (R3L; Table I). This

interpretation is supported by a comparison of sedimentary sequences found within the Rusizi and Kivu basins. Although few paleostratigraphic fauna are found within exploratory drill data, more than 1500m of clastic sediments that have accumulated within the Rusizi basin and that onlap basalts at the northern end of the basin are believed to be Pliocene or younger (D. Stone, pers. comm.). The inner fault-bounded terrace of the Rusizi River contains volcanic clasts not found elsewhere in the Rusizi basin, indicating that faults bounding the Rusizi River north of Lake Tanganyika are younger than the Rusizi River (~11,000 BP).

Northeast- to east-west-striking left slip faults at the northern end of the Rusizi basin link the Kivu and Rusizi basin within the accommodation zone (Figures 3, 4, 11). I find indirect evidence that the geometry of the accommodation zone has changed with time in the Kivu and Rusizi basins. Faults bounding the western side of the Kivu basin appear more youthful than along the eastern side, the western scarp is more active seismically, and a line of Pleistocene to historically active pyroclastic cones is found along the southwestern part of the escarpment (Wohlenberg, 1968; Guibert, 1977a). These observations suggest that the western border fault segment is more active than the eastern border fault segment, and that currently extension is occurring primarily along the western border fault segment of the Kivu basin. The opening of the Bugarama graben may have occurred later than initial subsidence within the Rusizi basin, as Plio-Pleistocene lacustrine sediments found in the Rusizi basin are absent in the narrow Bugarama graben.

Pleistocene tholeiites erupted from Tshibinda, Tshibati, and Leymera flowed down the West Kivu escarpment; vertical relief along the West Kivu border fault segment existed prior to 1.9 Ma. Wong and Von Herzen (1974) suggest that the northern part of the West Kivu basin formed less than 3 Ma, based on an extrapolation of present day biogenic sedimentation rates to the 500m of sediments found in the northern and eastern basins of Lake Kivu. Degens et al. (1973) note an absence of volcanogenic sediments in cores from beneath the southwestern arm of Lake Kivu, and suggest that subsidence in southern Lake Kivu commenced after volcanic activity (~ 4 Ma). This interpretation is consistent with structural and stratigraphic relations within the Kivu basin. Intrabasinal faults that displace Miocene-early Pliocene basalts with little change in dip through the section suggest that much of the extensional faulting occurred after volcanism, or during Plio-Pleistocene time.

Based on these kinematic and geometrical constraints within the Kivu and Rusizi basins, the Kivu-Rusizi accommodation zone is a pull-apart basin (Bugarama graben), with northeast-trending oblique-slip faults at the southern, and possibly northern, ends of the Bugarama graben accommodating translational movements between the two extensional basins. Prior to the development of the Rusizi border fault segment and the Bugarama

graben, the East Kivu border fault segment may have continued to the southwest, but it now is cut by north-south striking faults bounding the Bugarama graben (Figure 11). Structural and stratigraphic relations within these three basins indicate that the Rusizi border fault segment propagated northward during the Plio-Pleistocene, when normal faults bounding the western side of the Bugarama graben cut across the southernmost tip of the East Kivu border fault segment (Figure 11). During this period, the West Kivu border fault segment became the more active zone for crustal extension within the Kivu basin, and vertical offsets along the western margin of the basin led to the formation of the West Kivu basin. The geometrical arrangement shown in Figure 11 also requires northeast-striking oblique-slip faults along the southwestern margin of the West Kivu basin. Little geological information is available from this area, hence this interpretation is difficult to test.

Narrow terraces of Pleistocene lacustrine sediments along the East Kivu border fault segment and along the eastern (monoclinal) side of the Rusizi basin are elevated several hundred meters above similar, and probably correlative, units within lake basins (e.g., Stoffers and Hecky, 1978), indicating recent uplift. Pleistocene lacustrine sediments found along the East Kivu border fault segment are not found at the same or lower elevations along the shores of Lake Kivu, so that they probably represent local uplift of the rift flanks, rather than a lake level highstand. The terraces of Pleistocene lake sediments are tilted to the northwest and thicken away from border faults, or in the opposite sense expected if they had been deposited in a narrow trapped lake along the hanging wall of the border fault segment. Similarly, lacustrine sediments are found in faulted terraces along the eastern (monoclinal) side of the Rusizi basin (e.g., Figure 10). This Pleistocene uplift along the flanks of the rift narrows the zone of subsidence with time.

Significant vertical movements occurred along the West Kivu border fault segment during Holocene time. Shoreline deposits dated at 6000 BP were found at 300m water depth at the base of this escarpment; hyaloclastites on the western side of Idjwi Island interbedded with 12,000 BP diatomites now are elevated approximately 80m above the highest Kivu lake level (Degens et al., 1973; Guibert, 1977b). If Holocene lake levels have remained fairly constant, subsidence rates along the West Kivu border fault segment were 5 cm/yr during the past 6000 years, and Idjwi Island has been uplifted at a minimum rate of 0.8 cm/yr, assuming that the diatomites were deposited at a shallow depth of 20m.

Relationship between Neogene and pre-rift structures

High-angle normal faults of the East Kivu border fault segment striking N20°E cross-cut Proterozoic folds trending N30°-45°E (Figure 6). The eastern edge of the East Kivu escarpment is characterized by normal faults displacing pegmatites with minor offsets and narrow brecciated zones. Within the northwest-trending Precambrian folds of

sandstones, slates, and phyllites to the southeast of the border fault escarpment, I find no evidence for recent faulting, although Neogene uplift and erosion enhances lithologic contacts between basement structures apparent in the Landsat imagery. Within the West Kivu basin, I find that lineaments trending N30-50°W interpreted by Boutakoff (1939) as rift-related structures correspond to the orientations of joints in metamorphic basement flooring the Kivu valley, and are probably unrelated to Late Cenozoic strains within the Kivu basin.

A poor correlation between Neogene faults and metamorphic foliations and shear zones also is found within the accommodation zone between the two basins. Metamorphic basement exposed along the length of the 500m deep Rusizi River gorge has a dominant N30-50°W trend that is nearly orthogonal to Neogene normal and oblique-slip faults (Figure 3). These north-south and N10°E striking normal faults displace basement gneisses and phyllites that have a dominant metamorphic grain of N50°W.

Pre-rift faults and shear zones in Precambrian basement along the eastern margin of the Rusizi basin generally are oriented N20-N50°W, or nearly orthogonal to Neogene normal faults (Figure 10). The relationship between basement and intrabasinal faults is impossible to determine due to the obscuring cover of sediments, but basement structures and lineaments have a northwest strike on the western side of the Rusizi basin, indicating that basement with a northwest trend underlies the basin. In the northern basin near the accommodation zone, Neogene faults generally are oblique to pre-rift fabrics with a dominant N40°W trend. For example, normal and oblique-slip faults bounding the horst near the accommodation zone are oblique to N45°W strike of metamorphic basement (Figure 3). Elsewhere in the Rusizi basin, some Neogene faults are subparallel to north-south striking faults within Burundian basement, but these Precambrian shear zones show little evidence for reactivation (K. Theunissen, pers. comm.; this study).

Rungwe Volcanic Province

The Rungwe volcanic province is located at the intersection of three basins bounded by border fault systems with three different orientations: the eastward-tilted Songwe basin, the westward-tilted Usangu basin, and the eastward-tilted Karonga basin (Figure 10). As in the South Kivu province, volcanic units cover the accommodation zone between the three basins, as well as the uplifted flanks of basins (e.g., Figures 12, 13). The volcanically-constructed Poroto Mountains effectively form a physiographic barrier between Lake Rukwa to the north and Lake Malawi to the south, which lies over 300m lower than Lake Rukwa (Figure 12). Exposure in the much drier region to the north of the arcuate Poroto Mountain chain is good, whereas much of the volcanic province to the south of the mountains and north of Lake Malawi is covered by rain forest. Erosion and the

obscuring cover of ashes and tuffs from recent eruptions makes it difficult to identify volcanic centers within the earliest volcanic sequences erupted in the Rungwe province (Ot, Op, Ob). Katete and Ngozi were the probable centers for this initial volcanism, based on the much more extensive erosion that has occurred along the slopes of Katete and Ngozi in comparison to Rungwe and Kiejo (Figure 12).

Faults drawn in Figure 12 are based on interpretations of Landsat TM imagery calibrated by field studies, aeromagnetic data (A. Tesha, pers. comm.), gravity data, supplemented with my field observations and existing geological reports (Harkin, 1955; Grantham et al., 1958; Fick and Van der Heyde, 1959; Harkin, 1960; Teale et al., 1962; Harkin and Harpum, 1978). Volcanic rock descriptions were supplemented by observations made by A. Tesha (pers. comm.), and several samples were submitted for K/Ar age determinations described below and in Table I.

Songwe basin

The narrow Songwe basin is bounded on the eastern side by a 1200m escarpment that comprises a series of high-angle (60°-80°) *en echelon* faults that rise to the level of the uplifted flank (step faults). Subvertical slickenside striae commonly are found in gneisses and carbonatites exposed along the escarpment, and the base of the scarp is littered with 20m wide boulders of brecciated material. Vertical relief along the Songwe escarpment decreases to the north where this fault system displaces Cretaceous sediments of the Rukwa trough and Neogene lacustrine sediments (Spence, 1954; Grantham et al., 1958; this study). To the south along this border fault segment, basalts and phonolites cover the southern corner of the triangular-shaped plateau that has formed at the junction of the Songwe and the Usangu border fault segments. The west side of the basin is bounded by dissected Cretaceous sediments and Precambrian basement, and no clearly defined Late Cenozoic fault system has developed (Grantham et al., 1958; this study).

Within the basin, the Songwe River and its tributaries have deeply incised Neogene sediments, exposing underlying Cretaceous sediments dated on the basis of faunal remains (Grantham et al., 1958). Poorly-consolidated red Cretaceous sediments (K) dipping up to 20° to the northeast are unconformably overlain by Neogene white to tan sandstones and siltstones containing numerous basement clasts (Ns; Figure 14). A progressive decrease in the dip of sedimentary units is found within the Neogene sequences; the light-colored clastic sequences dip 15° to the northeast, whereas dips in the uppermost (~30m thick) section of lacustrine sediments within numerous rolled pumice fragments (Ns*), tuffs ($Sf_{1,2}$), and a thin cover of basalts (Po) dip 10° to the northeast, toward the border fault segment. An angular unconformity commonly separates the lacustrine sequence below from the predominantly volcaniclastic sequences above. A thin (< 5m thick) olivine basalt

flow (Po) covers the southwestern part of the basin and is overlain by melanonephelinites and trachytes (Pu; Figure 14). Olivine basalts and picrites that I refer to as Sb_1 are found in elongate lenses capping the footwalls of several step faults forming the Songwe border fault segment, and these flows may be correlative with petrographically similar units found 300m below within the rift valley (Figures 12, 14). Further south near the ridge separating the Songwe and Karonga basins, a thin cover (<10m) of olivine basalts (Po), brown sandstones with numerous rounded pumice clasts, and pink tuffs overlie metamorphic basement, and these sedimentary and volcanic sequences are tilted 25°-30° to the northeast (Figure 12).

Normal fault systems within the Songwe basin trend approximately parallel to the Songwe escarpment. For example, the northwest-southeast-trending Songwe River flows south at the base of a normal fault that dips to the southwest. Several hot springs are found along the eastern margin of the basin, where tufa and travertines accumulated (Grantham et al., 1958). Moving south from the Songwe basin into the accommodation zone between the Songwe and Karonga basins, one ascends a northeast-oriented ridge and the Poroto Mountain chain (Figure 12). Ascending the ridge from the Songwe basin, the spacing between normal faults that strike N50°W decreases and the dip of sedimentary and basalt units increases. Within the accommodation zone between the Songwe basin and the Usangu basin to the northeast, the floor of the basin also rises to the southeast.

Centers for volcanic eruptions within the Songwe basin occur in two settings: along step faults at the tip of the border fault segment, and along the footwalls and hanging walls of accommodation zone structures. Several small pyroclastic cones and fissures have formed along the *en echelon* step faults of the Songwe escarpment (Sb). Although few structures are apparent beneath the Poroto volcanoes, this volcanic lineament probably marks a buried fault system. Pyroclastic cones and numerous fissures and dikes mark *en echelon* normal faults within the rift valley in the region between the Songwe and Usangu border fault segments where alkali basalts are overlain by flat-lying lacustrine sediments (Figure 12).Volcanic centers for the olivine basalts and trachytes covering the accommodation zone structures were located nearby, as indicated by the numerous pyroclastic bombs and scoria contained in these units.

Usangu basin

The Usangu basin is bounded on its western side by a system of north-south oriented step faults, each of which is capped by basalts along the southern tip of the border fault segment (Figure 15a). Triangular scarps of the Usangu fault system continue to the north for approximately 100 km, where topographic relief decreases. Boulders of metamorphic basement and basalts fill steep gorges along this active fault scarp. At the

junction of the Songwe and Usangu border fault systems, northwest-striking normal faults truncate north-south trending faults (Figures 12,13). There is little evidence for faulting outside the rift valley along the western flank of the Usangu escarpment, and this uplifted flank is characterized by gentle topographic relief (Figure 15b). The southeastern margin of the Usangu basin is bounded by a severely dissected scarp whose western continuation is the Poroto Mountain chain (Teale et al., 1962; this study).

Late Miocene olivine basalts (Mbm) displaced by faults along the Usangu escarpment and Pliocene olivine basalts capping the Usangu flank are cut by faults exposing basement gneisses along the Usangu escarpment (Figure 14). Generally altered trachytes (Ot) dated at 2.2 Ma and olivine basalts (Po) dated at 600,000 BP are overlain by trachytes (Pt) and phonolites ($Pp_{1,2}$) in the southwestern part of the Usangu basin (Table I; Figure 14). These volcanic units are overlain by flat-lying lacustrine sediments and water-deposited pyroclastics (Ns*; Figure 14). Volcaniclastic sediment accumulations are greatest along the downthrown side of 1-5 km wide tilted fault blocks within the Usangu basin. Near the base of the escarpment, sandstones interbedded with coarse pumice dip 20°-30° to the northeast toward the Usangu scarp. These sediments are intruded and overlain by trachytes and phonolites extruded from small pyroclastic cones (Figure 12). Peirce and Lipkov (in press) suggest that metamorphic basement may be buried by 2 km of sediments and volcanics based on the interpretation of aeromagnetic data. However, the 1-2 km thick sequences of Mesozoic sediments exposed elsewhere in the Rungwe province are not observed at the surface in the Usangu basin, and basement underlies a less than 50m thick sequence in the southwestern part of the basin. Likewise, a comparison of gravity anomalies and basinal structures shows little evidence for a thick sedimentary sequence within the basin (C. Bowin. pers. comm.). The most negative Bouguer gravity anomalies correlate with Neogene volcanic centers to the west of the Usangu basin, and are elongate along the trend of the Karonga border fault segment. Thus, the gravity low in the accommodation zone is probably due to the presence of low-density magmatic material along accommodation zone structures. As in the accommodation zone between the Karonga and Songwe basins, the accommodation zone between the Usangu and Karonga basins is topographically higher than both the Usangu and Songwe basins. At the surface in this region, I find sub-vertical north-south striking faults with small (~6m) throws and east-dipping faults that strike N10°W (Karonga trend).

Olivine basalts covering the uplifted Usangu plateau flowed to the northwest away from the rift axis, and a youthful-appearing cone is located along a fault bounding the escarpment (Ub_1). Within the Usangu basin, numerous pyroclastic cones constructed if

trachytes and phonolites (Pp1,2) occur along the footwalls and hanging walls of normal faults in the southwestern part of the Usangu basin (e.g., Figures 12, 13).

Karonga basin

The Karonga basin is bounded along its eastern margin by the Livingstone escarpment that rises 1500m in a 4 km wide zone (Figure 12). Vertical displacements along the Livingstone escarpment increase to the south where the valley is filled by Lake Malawi and over 2 km of sediments (Ebinger et al., 1987). Spurs along the Livingstone escarpment are facetted, and the innermost fault zone is characterized by triangular scarps (Figure 12). The opposite side of the Karonga basin is bordered by a diffuse and dissected system of faults that cut Permo-Triassic and Cretaceous rift sediments and metamorphic basement (Stockley, 1948; Harkin and Harpum, 1978; this study). These Karroo sediments may once have been contiguous with sediments within the Luangwa Karroo basin to the southwest, with the Karroo sediments that originally covered the intervening region eroded during Neogene time probably due to uplift along the western flank of the Karonga basin (e.g., Figure 2).

A sequence of altered volcanic flows, tuffs, and scoria is repeated along the step faults rising to the level of the Elton plateau (2600m), although erosion has removed basalts along the footwall of the outermost fault (Figures 12, 14). The smooth topographic relief of the Elton plateau is covered by a thin sequence of phonolites, trachytes, and basalts (Harkin, 1960) that flowed away from the axis of the rift valley (Harkin, 1960; this study). A trachytic unit (Et) from the uplifted Elton plateau was dated at 7.2 Ma (Figure 14; Table I). Along the northwestern part of the Karonga basin, Ubendian basement is overlain by <1000m thick sequence of purplish upper Jurassic-Lower Cretaceous lacustrine sediments that dip 10-30° to the north (Dixey, 1928). These sequences are overlain by pink Cretaceous mudstones and sandstones that dip approximately 10° to the west (Dixey, 1928; Harkin, 1955). An erosional unconformity separates these Mesozoic sediments from basalts (Wb) that are overlain by olivine basalts dated at 2.8 Ma (To), phonolites (Tp), and trachytes (Kg, Rg) derived from Tukuyu, Kiego, and Rungwe and small pyroclastic cones within the rift valley, and Neogene lacustrine sediments. Dips between lacustrine sandstones and siltstones (Ns) increase to the south where these beige and white sediments and overlying tuffs from Rungwe or Tukuyu dip at 25°-30° (Figure 12, 14).

Within the Karonga basin, normal faults cutting Neogene sediments and volcanics generally strike N25°W. South of Tukuyu the spacing between faults decreases, and faults displace surface sediments (Ns) and capping basalts (To) and trachytic phonolites (Tp). Drag folds commonly occur along east-west striking normal faults in sediments north of Lake Malawi (Figure 12). To the south of the Songwe-Karonga accommodation zone

within the Karonga basin, a normal fault system with a N40°W strike that is oblique to normal faults of the Livingstone escarpment accommodates the 300m elevation difference from the Songwe and Usangu basins down into the Karonga basin (Mbaka fault zone). The fault surface is calcified and slickensides on the N60°W striking fault plunge 70°, indicating a minor component of oblique-slip (right-slip) movement along the fault. The Mbaka fault exposes metamorphic basement and displaces basalts from Kiejo (Kb) dated at 2.4 Ma (Table I). Eroded centers for the Pliocene volcanic activity form lineaments subparallel to the Mbaka escarpment, indicating that the fault system existed in Pliocene time. The Mbaka fault displaces Quaternary ankaramites and picrites (Kb1) that flowed down an existing escarpment, as well as undated flows from the western side of Rungwe (Ro, Rf, Rg), down to the southwest (Figure 14). Pleistocene flows from cones located along the the footwall of the Mbaka fault (Kb_1) have been displaced down to the southwest by at least 10m during more recent movements (Figure 16).

Volcanic centers within the Karonga basin coincide with the margins of tilted fault blocks within basins near accommodation zones, and are found along the tips of border fault segments. Lineaments of pyroclastic cones and shield volcanoes also may mark oblique-slip and/or strike-slip faults that have little surface expression (e.g., Poroto Mountains).Within the northernmost part of the basin, 10-30 km long chains of pyroclastic cones are found along both the hanging and footwall sides of tilted fault blocks, as in the Usangu basin.

Timing of Crustal Movements

Radiometric analyses of the volcanic sequences within the Rungwe province are in progress, and I summarize interim results below. The occurrence of volcanic units that flowed away from the present rift axis along the uplifted flanks of the Usangu and Karonga basins and petrologically similar basalts within these basins indicates that vertical displacements along the Usangu and Livingstone escarpments post-date the flows. Basalts covering the uplifted flanks and step faults of the Usangu escarpment (Mbm) and that are found near the base of the Usangu scarp were erupted at 3.5- 8 Ma concurrent with or prior to faulting along the Usangu border fault segment. A topographic depression within the Usangu basin existed at the time of eruption of the olivine basalts (Po; 600,000 BP) derived from cones to the south of the basin (Poroto Mountains). Therefore, initial faulting occurred sometime between the eruption of Mbm and Po. Olivine basalts (Mb1) derived from a youthful pyroclastic cone constructed along the footwall of the outermost border fault flow ~100m to the northwest along the flank of the rift, which indicates that the eastward-tilted rift flank existed prior to the construction of the cone. Along the uplifted flanks of the Kronga basin at Chaluhangi, the highest point along the plateau (2930 m)

trachytes petrologically similar to those found in the Katete region 400m below have been dated at 7.2 Ma (Et; Table I), suggesting that initial faulting along the Karonga border fault segment post-dates this flow. The oldest lacustrine sediments exposed along the western shore of the Karonga basin were deposited 5-2.5 Ma (Figure 14). Tukuyu basalts dated at 2.6 Ma overlie lacustrine sediments along the western margin of the basin, and these basalts were erupted at approximately the same time as trachytes along the northern Porotos (Et) and basalts (Kb) and trachytes (Ot) in the eastern part of the Karonga basin. Therefore, deposition within the northern Karonga basin began during the period between 7.2 and 2.5 Ma. Centers for the mid-Pliocene eruptions are located in linear belts or along hanging walls and footwalls of normal and oblique-slip faults within the Karonga basin, suggesting that faulting and subsidence occurred during this time period.

The Karonga basin is 300m lower than Lake Rukwa to the north, but faunal evidence argues against a hydrographic connection between Lake Rukwa and Lake Malawi (Grove, 1983). Lacustrine sequences now found several hundred meters above the present Rukwa lake level indicate that Lake Rukwa was much more extensive during Holocene time. Based on the geometries of the Karonga, Songwe, and Rukwa basins and structural patterns within the volcanic chain, I suggest that subsidence in the Malawi trough post-dates the construction of the Poroto volcanic chain separating Lake Rukwa from the Malawi rift (Figure 10). Within the accommodation zone between the Karonga and Songwe basins, volcanic centers along the Mbaka fault zone have been active during the period 2.4 Ma (Kb) to 0.5 Ma (Kb1), and these units have been offset by more recent faulting (Figures 14, 16).

Relationship between Late Cenozoic and pre-rift structures

Unlike border fault segments within the South Kivu province, Neogene normal faults of the Songwe escarpment may have been influenced by pre-existing zones of weakness within metamorphic basement, but many Mesozoic faults that parallel younger structures have not been reactivated. Along the Songwe scarp, Neogene faults have an orientation that is subparallel to Ubendian metamorphic foliation (Grantham et al., 1958). Recent faulting has exhumed an elongate Cretaceous carbonatite that was probably intruded along normal faults during the Cretaceous rifting episode (Fick and Van der Heyde, 1959; Brown, 1964). Facetted fault scarps marking a southern projection of the Lupa fault cut the uplifted flank of the Songwe escarpment to the north of Mbeya. However, the active Songwe border fault segment is located 10-20 km to the west of the fault system for the Mesozoic basin (Lupa fault zone). Topographic relief along the Lupa fault system is less than 100m, and the morphology of this older, apparently inactive fault system contrasts with the triangular scarps and uplifted flanks of the Neogene Songwe border fault segment, and Neogene lacustrine sediments cover the dissected footwall of the Lupa fault. However,

there is little evidence for reactivation of Mesozoic normal faults within the Songwe basin. Normal faults within the Karroo sediments at the northeastern margin of the basin strike N20-30°E and N50°W, whereas Neogene normal faults that displace surface sediments at the surface strike N20°W, or less commonly, nearly east-west (Spence, 1954).

Metamorphic foliations in Ubendian and Archaean rocks along the Usangu scarp trend approximately east-west, or nearly orthogonal to the orientation of Neogene normal faults bounding the Usangu basin. At the southern tip of the Usangu border fault segment, faults that strike N60°E cut highly sheared Ubendian basement with N45°-60°E metamorphic foliation. Uplift and extensive erosion along the southern margin of the basin (Chimala scarp) has enhanced east-west trending Pan-African structures, but there is little evidence for rejuvenation of these older faults (Teale et al., 1962). Metamorphic basement beneath at least the southwestern part of the Usangu basin is Pan-African (Buanji) that has a dominant east-west structural trend (Stockley, 1948; this study). Clasts of Buanji sediments are found near explosive centers in the Usangu basin, indicating that Pan-African basement with an east-west structural trend floors the basin, whereas intrabasinal faults are oriented north-south or N10°E. Mylonites and shear zones within Ubendian basement are oriented sub-parallel to normal faults bounding the Karonga escarpment. However, along the uplifted flank of the Karonga border fault segment, there is no evidence for Neogene reactivation of Pan-African structures. It is difficult to determine if normal fault zones coincide with Ubendian shear zones or Permo-Triassic and Cretaceous normal faults within the basin due to the obscuring cover of sediments and basalts. Along the western margin of the Karonga basin, Triassic normal faults within the Karroo and Cretaceous sequences strike approximately north-south and N40°E, which differs from the orientations of Neogene faults in this part of the Karonga basin by 20-30°.

Summary of Observations and Interpretations

Observations

Summarizing observations of border fault and accommodation zone geometries found within the Kivu, Rusizi, Songwe, Usangu, and Karonga basins and illustrated in Figures 4 and 13:

1) These Western rift basins generally have the cross-sectional form of half-graben. High-angle (45°-75°) normal faults occur in a 10-15 km wide zone along one side of basins, and the opposite side of basins largely is unfaulted and regionally has the form of a monocline. Along the faulted margin of basins, *en echelon* border faults are separated by approximately 1km , and narrow fault zones (~5m) are brecciated and mineralized. Significant vertical displacements occur along these border fault systems (1-6 km), and faults remain steep to depths of 6 km or more. The geometrical arrangement of normal and

oblique-slip faults along the length of basins produces segments of the border fault system that are curvilinear in plan view. Vertical displacements are greatest near the central part of basins at the base of the escarpment, and decrease toward the northern and southern tips of approximately 100 km long basins. Thus, sedimentary basins are spoon-shaped, although magnitudes of subsidence vary significantly from basin to basin. Less commonly, border fault segments occur along both sides of extensional basins (full graben), requiring a more complicated geometry than the spoon-shaped fault systems described above.

2) Normal and strike-slip faults at the tips of border fault segments accommodate differential vertical and minor horizontal displacements between basins. Oblique-slip faults also accommodate regional variations in topographic relief related to domal uplift of East Africa (e.g., Chapter 4). Near these interbasinal accommodations zones, faults are more closely-spaced than within basins and sedimentary and volcanic units commonly have been rotated 20-30°.

3) Volcanic sequences of the South Kivu and Rungwe regions coincide with interbasinal accommodation zones. Prior to basinal subsidence these regions were originally topographic highs, as initial flows were directed away from the present rift valley. Volcanic centers within these two provinces are found along the margins of tilted intrabasinal fault blocks near accommodation zones, between *en echelon* border faults at the tips of border fault segments, and along transverse structures cross-cutting the rift valley within interbasinal accommodation zones. Within the rift valley, pyroclastic cones and craters occur along oblique-slip faults with orientations that are oblique to the regional trend of border faults. The general occurrence of volcanic centers along the tips of border fault segments and along steep oblique-slip faults linking basins suggests that these faults remain steep to greater depths than do the central parts of border fault segments.

4) Three structural relations consistently observed within the Kivu and Rungwe regions suggest that zones of crustal thinning are limited to rift basins bounded by approximately 100 km long border fault segments. First, few faults occur on the uplifted flanks outside inward-facing normal faults bounding the rift valley. Second, along the length of the Western Branch rift system oblique-slip faults linking basins do not appear to extend outside the rift valley across the uplifted rift flanks. Third, the location of volcanic centers with respect to rift basin structures reflects a lack of faulting along the rift flanks. Although initial flows that preceded major fault movements covered a wider region than the present-day rift basins, eruptive centers within the volcanic provinces are restricted to rift basins within the inward-facing normal faults bordering basins.

5) The Western rift system generally follows older orogenic belts and avoids the central craton. At the length scale of border fault segments, however, the orientations of

Neogene faults show little correlation with metamorphic lineations or pre-Neogene faults (e.g., Figures 3, 6, 10, 12). In most instances, Neogene faults extend across older contacts between tectonic units or cross-cut structures in metamorphic basement. Mesozoic normal faults rarely are rejuvenated in the Neogene rifting, and no youthful volcanic centers have been found along Mesozoic fault systems within the Songwe and Usangu basins. An exception is the Songwe escarpment which follows a Cretaceous fault zone. Where the orientations of the pre-rift faults and metamorphic fabrics trend approximately north-south, or sub-parallel to Neogene faults, I find little evidence for reactivation of older structures. Differential erosion of the uplifted flanks of the rift commonly emphasizes lithologic contacts. Where these lithologic contacts coincide with older structures, I find little evidence for reactivation.

6) Faults within accommodation zones are operative throughout the evolution of basins, although the geometry of accommodation zones may change with time and continued extension within basins. For example, lineaments of volcanic centers marking accommodation zone structures formed early in basinal development, and historically active centers are found along their length (e.g., Mbaka fault zone, Poroto Mountains). Because amounts of subsidence, rift flank uplift, and possibly crustal extension vary from basin to basin along the length of the rift valley, in part due to differences in age, fault systems between basins accommodate both vertical and horizontal displacements. For example, the southern margin of the Usangu basin is the uplifted flank of the Karonga basin, and normal faults on the southeastern side of the Usangu basin accommodate uplift along the flanks of the Karonga basin, rather than subsidence and extension within the Usangu basin.

7) Consistently observed patterns in the development of these five basins are summarized in Figure 17. During the Mid-Miocene, basalts in both the South Kivu and Rungwe province erupted along fissures onto gentle topography and flowed away from the present axis of the rift valley. Faulting and subsidence within basins created topographic depressions that filled with sediments and volcanics, and volcanic centers localized to rift basins within the inner facing border faults. Vertical movements along the escarpments displaced the originally flat-lying basalts, producing the terraces of volcanics along the step fault systems bounding rift basins.

Interpretations

1) I find little evidence that the general orientations of border fault segments change between successive episodes of rifting, although activity along border fault segments may propagate along the length of the rift, and the geometry of accommodation zones may change. For example, the full-graben morphology of the Kivu basin that is atypical of the

Western rift may be caused by temporal variations in border fault development. During the initial stages of rifting, the East Kivu border fault segment may have served as the detachment for crustal extension, but during later episodes of rifting, the West Kivu border fault segment developed and only minor discplacements occurred along the East Kivu border fault segment. This interpretation alleviates the complicated detachment fault geometries at depth beneath the rift valley required by simultaneously active structures on both sides of the rift valley (e.g., Mohr, 1987).

2) Stratigraphic relations within rift basins indicate that the zone of subsidence has narrowed with time. Terraces of Pleistocene lacustrine sediments along the rift valley escarpments commonly are elevated from lakelevel highstands. Likewise, the morphology of step faults along border fault segments indicates that the innermost fault is active, while higher scarps are deeply dissected. This narrowing appears to be synchronous with uplift occurring along both sides of rift basins. Narrow terraces of lacustrine sediments are found near the central parts of asymmetric basins where maximum amplitudes of subsidence occur, and as lenses along faults with minor displacements on the monoclinal side of basins. The spatial occurrence of lacustrine sediments indicates that the terraces were uplifted along normal fault systems relative to the subsiding basin.

Acknowledgements

Permission to conduct field research was granted by the Ministère de l'Energie, des Mines, et des Artisanats, Rwanda; Dept. de l'Energie et des Mines, Burundi; UTAFITI (Tanzanian National Scientific Research Council), and Institut de la Recherche Scientifique (Zaïre). J.Nanyaro (University of Dar es Salaam), K. Theunissen and J. Klerkx (Musée Royal de l'Afrique Centrale), L. Tack, (University of Bujumbura), A. Tesha, J. Knight, L. Willey, S. Townsend, P. Tilke, M. Daly, S. Wagner, P. Eeckelers, and many Peace Corps volunteers provided invaluable assistance in field areas. Revisions suggested by L. Royden and K. Hodges greatly improved the text. I thank J. Klerkx, K. Theunissen, L. Tack, and B. Rosendahl for use of unpublished information, and M. Daly, P. Williamson, A. Cohen, D. Livingstone, and D. Grove for helpful discussions. A. Tesha provided an interpretation of aeromagnetic data; photos were contributed by P. Eeckelers, K. Theunissen, and P.Tilke. I gratefully acknowledge Mobil Oil Exploration Production for photographic reproduction of Thematic Mapper imagery, B. Drake and A. Deino at Berkeley Geochronology Laboratory for assistance in sample preparation, and Amoco Production for making available proprietary data used in basinal analyses. This project was funded by an NSF Presidential Young Investigator Award granted to L. Royden; Geological Society of America Research grant 3754-87, Sea Grant NA84-AA-D-00033, R/G-11; and NSF grant EAR-84-18120.

Appendix I

Landsat-5 Multi-Spectral Scanner (MSS) and Thematic Mapper (TM) images used in this study cover 170 km by 185 km regions. Standard radiometric and geometric corrections were made at the EROS processing center, and images are displayed using a space oblique Mercator projection that preserves length and angular relations. False-color composite images corresponding to Scenes 1 and 2 were generated from reflectance data in bands 2 (0.5-0.6 μm), 4 (0.6-0.7 μm) and 5 (0.8-1.1 μm), displayed as blue, green and red, respectively. Digital data from TM scene 2 (Figure 1) were processed to enhance faults, lineaments and to distinguish volcanic units using a variety of filtering, color ratioing, and contrast stretching techniques. MSS image 1 shown in Figure 1 is E-50870-07370; TM image is Y-50850-07204. Quality of data is excellent; cloud cover was less than 10% in both scenes.

References

Auchapt, A., C. Dupuy, J. Dostal, and M. Kanika, 1987, Geochemistry and petrogenesis of rift-related volcanic rocks from South Kivu (Zaïre): J. Volc. Geotherm. Res., v. 31, p. 33-46.

Bagdasaryan, G.P., V.I. Gerasimovskiy, A.I Polyakov, R.Kh. Gukasyan, 1973, Age of volcanic rocks in the rift zones of East Africa: Geochem. Internat., v. 1973, p. 66-71.

Baker, B.H., 1986, Tectonics and volcanism of the southern Kenya Rift Valley and its influence on rift sedimentation: *in* L.E. Frostick, et al., eds.: *Sedimentation in the East African Rifts*, Geol. Soc. London Spec. Pub. 25, p. 45-57.

Bally, W., 1982, Musings over sedimentary basin evolution: Roy. Soc. London Phil. Trans., v. A305, p. 325-328.

Bellon, H., and A. Pouclet, 1980, Datations K-Ar de quelques laves du Rift-ouest de l'Afrique Centrale; Implications sur l'évolution magmatique et structurale: Geol. Rund., v. 69, p. 49-62.

Bosworth, W., 1985, Geometry of propagating continental rifts: Nature, v. 316, p. 625-627.

Boutakoff, N., 1939, Géologie des territoires situés a l'Ouest et au Nord-Ouest du fossé tectonique du Kivu: Mem. Inst. Geol. Univ. Louvain, t .IX, p. 23-161.

Bram, K., and B.D Schmeling, 1975, Structure of crust and upper mantle beneath the Western Rift of East Africa, derived from investigations of near earthquakes: *in* A.Pilger and A. Rosler, eds., Afar Between Continental and Oceanic Rifting, Schweizerbart, Stuttgart, p. 138-142.

Brown, P., 1964, The Songwe scarp carbonatite and associated feldspatization in the Mbeya range, Tanganyika: Q. J. Geol. Soc. London, v. 120, p. 223-240.

Brun, J.P., and P. Choukroune, 1983, Normal faulting, block tilting, and décollement in a stretched crust: Tectonics, v. 2, 345-356.

Burchfiel, B.C., and J.Stewart, 1966, The "pull-apart" origin of Death Valley, California: Geol. Soc. Amer. Bull., v. 77, 439-442.

Cahen, L., and I. Snelling, 1984, The geochronology and evolution of Africa: Clarendon Press, Oxford, 591p.

Capart, A., 1949, Sondages et carte bathymetrique: *in* Exploration Hydrobiologique du lac Tanganyika (1946-1947): Brussels: Inst. R. Sci. Nat. Belg., p. 1-16.

Chenet, P-Y., and J. Letouzey, 1983, Tectonique de la zone comprise entre Abu Durba et Gebel Mezzazat (Sinai, Egypte) dans le contexte de l'évolution du rift du Suez: Bull. Centres Rech. Explor. Prod. Elf-Aquitaine, v. 7, p. 201-215.

Chorowicz, J., 1983, Le rift est-africain: début de l'ouverture d'un ocean?, Bull. Centres Rech. Explor. Prod. Elf-Aquitaine: v. 7, p. 155-162.

Chorowicz, J., and C. Thouin, 1980, Failles synsedimentaires et structure de la plaine de la Rusizi (Nord Tanganyika): C.R. Acad Sci. Paris, t. 301, p. 835-841.

Crossley, R., 1982, Late Cenozoic stratigraphy of the Karonga area in the Malawi rift, *in* : J.A. Coetzee and E.M. van Zinderen Bakker: Paleoecology of Africa, v. 15, p. 139-144.

Crossley, R. and M.J. Crow, , 1980The Malawi rift, *in* : Geodynamic Evolution of the Afro-Arabian rift system, Rome, p. 77-87.

Daly, M.C., 1986, Crustal shear zones and thrust belts: Their geometry and continuity in Central Africa: Phil Trans. Roy. Soc. Lond., A317, p. 111-128.

De Mulder, M., and P. Pasteels, 1986, K-Ar geochronology of the Karisimbi volcano (Virunga, Rwanda-Zaire): Jour. African Earth Sci., v. 5, p. 575-579.

De Paepe, P., and M. Fernandez-Alonso, 1981, Contribution à la connaissance du volcanisme du Sud-Kivu : La region de Cyangugu-Bugarama (Rwanda): Rapp. ann. Mus. roy. Afrique Centrale, v. 1980, p. 111-126.

Degens, E.T., R.P. Von Herzen, and H-K. Wong, 1971, Lake Tanganyika: Water chemistry, sediments, and geological structure: Naturwissenschaften, v. 58, p. 229-241.

Degens, E.T., Von Herzen, R.P., Wong, H.K., Deuser, W.G., and Jannasch, H.W., 1973, Lake Kivu: Structure, chemistry, and biology of an East African rift lake: Geol. Rund., v. 62, p. 245-277.

Dixey, F., 1928, The Dinosaur beds of Lake Nyasa, Trans. Roy. Soc. S. Africa, v. 16, p. 54-67.

Ebinger, C.J., M.J. Crow, B.R. Rosendahl, D.L. Livingstone, and J. LeFournier, 1984, Structural evolution of Lake Malawi, Africa: Nature, v. 308, p. 627-629.

Ebinger, C., B. Rosendahl, and D. Reynolds, 1987, Tectonic model of the Malawi rift, Africa: *in* Z. Ben-Avraham, ed., Sedimentary Basins within the Dead Sea and Other Rift Zones, Tectonophysics, v. 141, p. 215-235.

Fairhead, J. and R.W. Girdler, 1969, How far does the rift system extend through Africa?, Nature, v. 221, p. 1018-1020.

Fick, L.J., and C. Van der Heyde, 1959, Additional data on the geology of the Mbeya carbonatite: Economic Geology, v. 54, p. 842-872.

Gibbs, A.D., 1984, Structural evolution of extensional basin margins: J. geol. Soc. London, v. 141, p. 609-620.

Grantham, D.R., E.O. Teale, A.M. Spurr, D.A. Harkin, and P.E. Brown, 1958, Geological Survey Tanganyika Quarter Degree Sheet 224 (Mbeya).

Gregory, J., 1896, The Great Rift Valley: London, John Murray, 405p.

Grove, A.T., 1983, Evolution of the physical geography of the East African rift valley region, *in* R.W. Sims, J.H. Price, and P.E.S. Whalley, eds., *Evolution, Time, and Space: The Emergence of the Biosphere*, London: Academic Press, p. 115-155.

Guibert, Ph., 1977a, Contribution a l'étude du volcanisme du Sud-Kivu (Zaïre): I: La chaîne volcanique Tshibinda-Kalehe: Archive Science Genève, v. 30, p. 15-27.

Guibert, Ph., 1977b, Contribution a l'étude du volcanisme du Sud-Kivu (Zaïre): II: Les épanchements basaltiques anciens et recents de l'île Idjwi: Archive Science Genève, v.30, p. 29-43.

Harkin, D.A., 1955, The geology of the Songwe-Kiwira coalfield, Rungwe District: Tanganyika Geol. Surv. Bull. 27, 33p.

Harkin, D.A., 1960, The Rungwe volcanics at the northern end of Lake Nyasa: Geological Survey Tanganyika Mem. II, 172p.

Harkin, D.A., and J.R. Harpum, 1978, Quarter Degree Sheet 78 (Tukuyu): Geol. Surv. Tanganyika .

Hebert, L., and C. Langston, 1985, Crustal thickness estimate at AAE (Addis-Ababa, Ethiopia) and NAI (Nairobi, Kenya) using teleseismic P-wave conversions: Tectonophysics, v. 111, p. 299-327.

Hecky, R.E. and E.T. Degens, 1973, Late Pleistocene-Holocene chemical stratigraphy and paleolimnology of the rift valley lakes of central Africa: Tech. Rept. WHOI 73-28, Woods Hole Oceanographic Inst., 93pp.

Holmes, A., 1940, The basaltic lavas of South Kivu, Belgian Congo: Geol. Mag., v. 77, p. 89-101.

Ilunga, L.K., 1984, Le quaternaire de la plaine de la Ruzizi, [Thèse doctorat]: Bruxelles, Belgium, University Bruxelles, 340p.

Kampunzu, A.B., J-P. Caron, and R.T. Luabala, 1986, The East African rift, magma genesis and astheno-lithospheric dynamics: Episodes, v. 9, p. 211-216.

Kaufulu, Z., E. Vrba, and T. White, 1981, Age of the Chiwondo beds, northern Malawi: Ann. Transv. Mus., v. 33, p. 1-8.

King, B.C., 1978, Structural and volcanic evolution of the Gregory rift valley, *in* W.W. Bishop, ed.: *Geologic Background to Fossil Man*, Edinburgh: Scottish Academic Press, p. 29-54.

Lepersonne, J., 1977, Carte géologique du Zaïre, Rep. Zaïre: Musée Royal Afrique Centrale, Tervuren, Belgium (1:2,000,000).

Lavreau, J., V. Patricec, and A. Waleffe, 1981, Carte lithologique du Rwanda (1:250,000): Musée Royal de l'Afrique Centrale, Tervuren, Belgium.

Lister, G., M. Etheridge, and P. Symonds, 1986, Detachment faulting and the evolution of passive continental margins: Geology, v. 14, p. 246-250.

McConnell, R.B., 1972, Geological development of the rift system of eastern Africa, Geological Society of America Bulletin, v. 83, p. 2549-2572.

Meyer, A., 1954, Notes volcaniques, les basaltes du Kivu meridional: Mèm. Serv. Géol. Congo Belge: 2, 25-52.

Meyer, A., and H. Burette, 1957, Nouveaux phenomènes volcaniques au sud Kivu (Congo-Belge): Serv. Geol. Congo-Belge, Bull. 7, 1-17.

Moeyersons, J., 1979, Surfaces d'aplanissement, anciens bassins hydrographiques et mouvements tectoniques post-précambriens au Rwanda: Bull. Soc. belge de Geologie: T. 88, p. 87-96.

Mohr, P.A., 1987, Structural style of continental rifting in Ethiopia: Reverse décollements: Eos, Trans. Amer. Geophys. Un., v. 68, p. 721-729.

Pasteels, P., P. De Paepe, M. Villeneuve, and J. Klerkx, 1987, Age of the volcanism of the southern Kivu area (Western Rift: Burundi, Rwanda, Zaire): Earth Planet. Sci. Letters, in press.

Patterson, M.B., 1983, Structure and acoustic stratigraphy of the Lake Tanganyika rift valley, [M.S. Thesis], Duke University, Durham, North Carolina, 89p.

Peirce, J., and L. Lipkov, Structural interpretation of the Rukwa rift, Tanzania, Geophysics, in press.

Pentel'kov, V., and S. Veronovskiy, 1979, Radiometric age of the Mbalizi carbonatite, Tanzania, and correlation with other carbonatites of the Rukwa-Malawi zone: Dokl. Akad. Nauk SSR, v. 235, p. 1136-1139.

Pouclet, A., 1977, Contribution a l'étude structurale de l'aïre volcanique des Virunga, rift de l'Afrique centrale: Rev. Géogr. Phys. Géol. Dynam, v. XIX, p. 115-124.

Quennell, A.M., A.C.M. McKinlay, W.G. Aitken, 1956, Summary of the geology of Tanganyika: Memoirs Geological Survey Tanganyika, 264p.

Reeves, W., 1960, Geologic map of Northern Rhodesia, Geological Survey Department Rhodesia, 1: 1,000,000.

Reynolds, D.J., 1984, Structural and dimensional repetition in continental rifts, [M.S. Thesis], Duke University, Durham, N.C., 158p.

Rosendahl, B., Reynolds, D., Lorber, P., D. Scott, J. McGill, J. Lambiase, 1986, in L.E. Frostick, et al., eds., Sedimentation in the East African Rifts: Geol. Soc. London Spec. Pub. 25, p. 29-34.

Shudofsky, G.N., 1985, Source mechanisms and focal depths of East African earthquakes using Rayleigh wave dispersion and body-wave modelling: Geophys. Jour. Roy. astr. Soc. , v. 83, p. 563-614.

Smith, R. and R.L. Bruhn, 1984, Intraplate extensional tectonics of the eastern Basin-Range: Inferences on structural style from seismic reflection data, regional tectonics, thermal mechanical models of brittle-ductile behavior: J. Geophys. Res., v. 89, 5733-5762.

Spence, J., 1954, The geology of the Galula Coalfield, Mbeya district: Geol. Surv. Tanganyika, v. 25 , 34p.

Stockley, G., 1948, Geology of north, west, and central Njombe district, southern highlands province: Geol. Surv. Dept. Tanganyika, 68p.

Stoffers, P., and Hecky, R.E., 1978, Late Pleistocene-Holocene evolution of the Kivu-Tanganyika basin: Spec. Pub. int. Ass. Sediment., v. 2, p. 43-55.

Tack, L., and DePaepe, P., 1983, Le volcanisme du Sud-Kivu dans le nord de la plaine de la Rusizi au Burundi et ses relations avec les formations géologiques avoisinantes: Rapp. Ann. Mus. roy. Afr. centr., v. 1981-1982, p. 137-145.

Teale, E.O., Eades, N.W., Harkin, D.A., Harpum, J.R., and Horne, R.G., 1962, Geological Survey Department Tanganyika, Quarter Degree Sheet, 245 (Irambo).

Theunissen, K., Carte géologique de Burundi, Feuille Cibitoke, Min. Trav. Publ. Ener. Mines, Burundi, in press.

Theunissen, K., Carte géologique du Burundi, Feuille Bujumbura, Min. Trav. Publ. Ener. Mines, Burundi, in press.

Wernicke, B., and Burchfiel, B.C., 1982, Modes of extensional tectonics, Journal of Structural Geology, p. 105-113.

Wohlenberg, J., 1968, Seismizitat der ostafrikanischen Grabenzonen zwischen 4°N und 2°S sowie 23°E und 40°E: Veroffentlichung der Bayerischen Kommission fur die Internationale Erdmessung, v.43, 95p.

Wong, H-K, and Von Herzen, R.P., 1974, A geophysical study of Lake Kivu, East Africa: Geophys. J. R. astr. Soc., v. 37, p. 371-389.

Zana, N., and N. Hamaguchi, 1978, Some characteristics of aftershock sequences in the Western rift valley of Africa: Sci. Rep. Tôhoku Univ., Ser. 5, Geophysics, 25: 55-72.

Table I

Kivu Volcanic Province						
ID#	**Map Unit**	**Location**	**Lat (S)**	**Long(E)**	**%K+**	**Age**
R5N	Qv; Ol-basalt	E. Kivu b.	2.476°	29.113°	1%	**0.342**

Rungwe Volcanic Province							
ID#	**Map Unit**	**Location**	**Lat.**	**Long.**	**%K+**	**Age**	**(Ma)**
T4D	Mbp; Ol-basalt	Usangu plateau	8.818°	33.500°	1%	**3.5**	±.4
T5F	Mbm; Ol-basalt	Usangu scarp	8.866°	33.528°	2%	**8.0**	±.8
T5K	Po; Ol-basalt	Usangu b.	8.833°	33.674°	1%	**0.60**	±.006
T7A	Ot; Trachyte	N. Porotos	8.979°	33.618°	4.7%	**2.2**	±.2
T8D	To; Ol-basalt	W.Karonga b.	9.356°	33.596°	2%	**2.6**	±.2
T11A	Ot; Trachyte	Katete	9.131°	33.765°	2.5%	**2.8**	±.3
T13F	Et; Trachte	Chaluhangi	9.084°	33.888°	4.7%	**7.2**	±.7
T14B	Kb1; Ol-basalt	Mbaka f.z.	9.357°	33.815°	2%	**0.50**	±.005
T15A	Kb; Ankaramite	Mbaka f.z.	9.340	33.787°	2%	**2.4**	±.2

Selected samples of volcanic rocks collected in 1986 and 1987 prepared at M.I.T.by C.E. and dated using K/Ar methods at Berkeley Geochronology Laboratory (BGCL) by B. Drake and A. Deino. All samples were examined for alteration in thin section; olivine phenocrysts are fresh or show only slight alteration to iddingsite in sample R5N, and secondary minerals are rare in all samples analysed. In preparation for standard whole rock K/Ar analyses at BGCL, samples of basalts and trachytes were crushed and sieved to retain the 30-60 mesh size fraction. Phenocrysts of olivine from R5N, 14B, 15A, and 8D were removed prior to analyses. All samples were bathed in 5% HCL solution (to remove secondary minerals), a 5% HF solution, and washed in warm water in an ultrasonic cleaner. Potassium concentrations were determined at the U.S.G.S. in Menlo Park using flame photometry techniques.

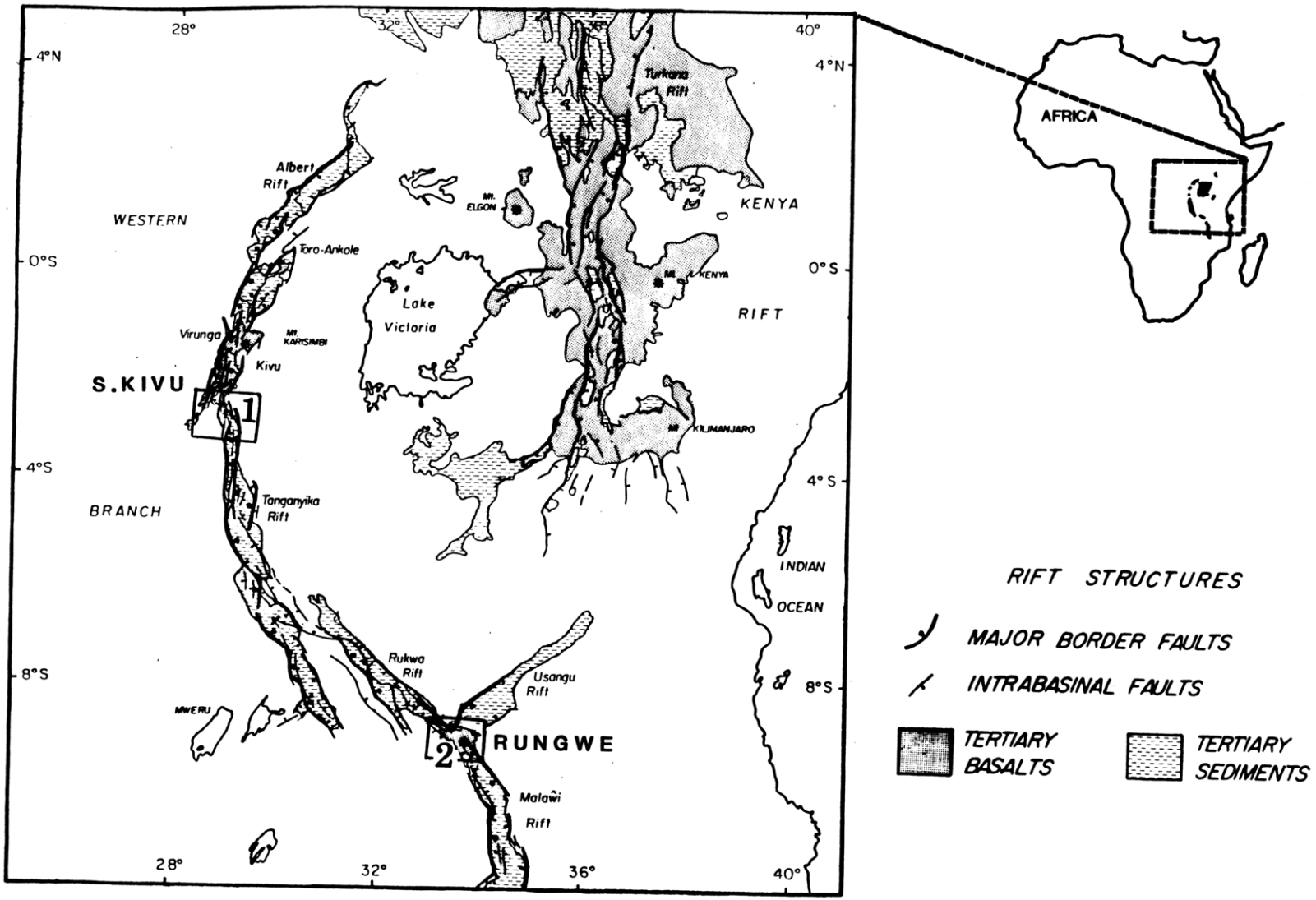

Figure 1. Major border fault systems, volcanic provinces, and rift basins of the Tertiary East African rift system showing location of South Kivu and Rungwe volcanic provinces in Western rift system. Boxes enclose regions of Landsat-5 coverage used in studies within South Kivu and Rungwe volcanic provinces (Scenes 1, 2).

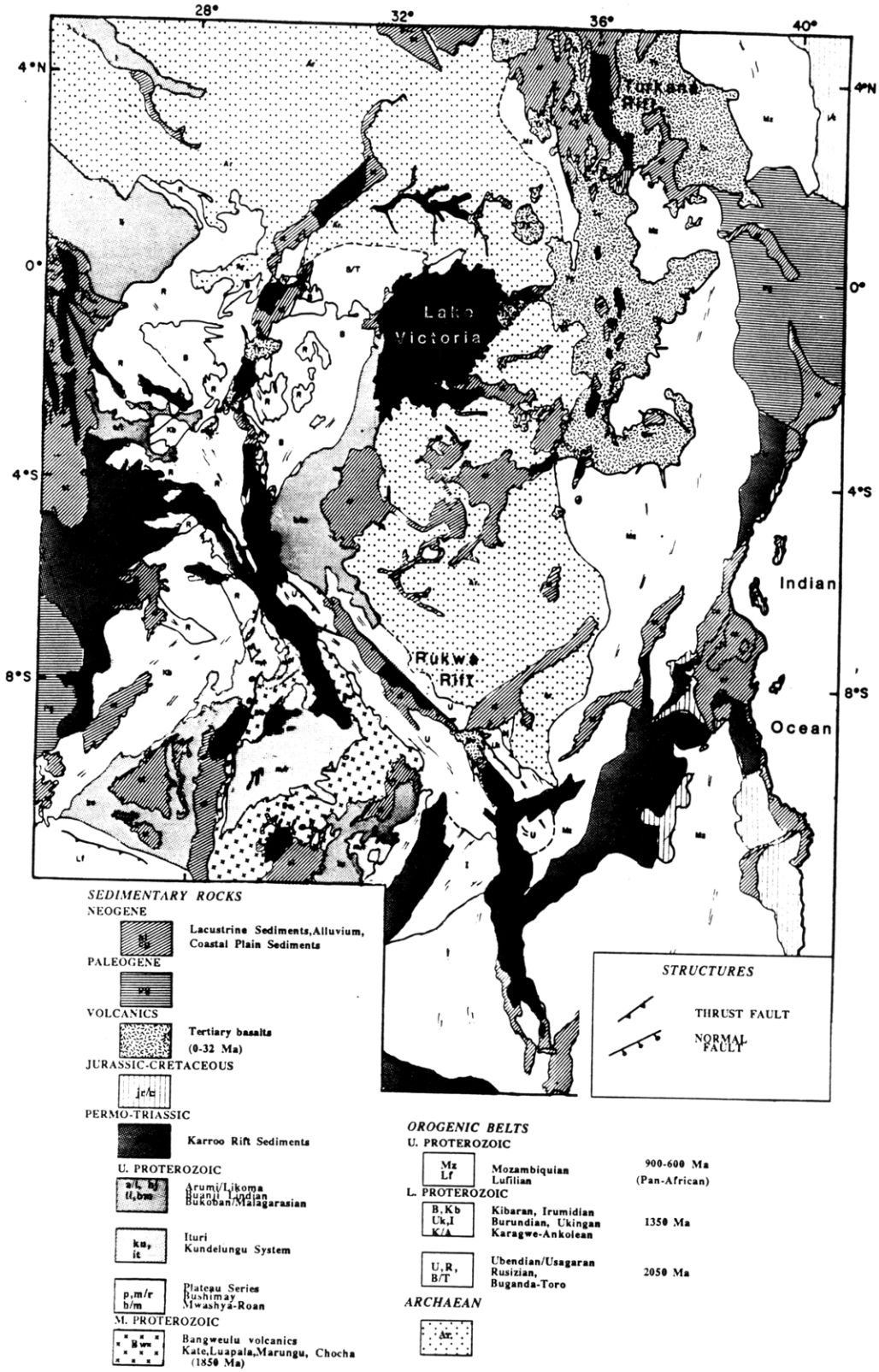

Figure 2. Summary of East African geology showing major pre-rift faults and regional metamorphic trends within Precambrian orogenic belts. Geological information from: Baker (1986); Cahen and Snelling (1984); Carter and Bennett (1973); Kent et al. (1971); Lepersonne (1977); Quennell et al (1956); Reeves (1960).

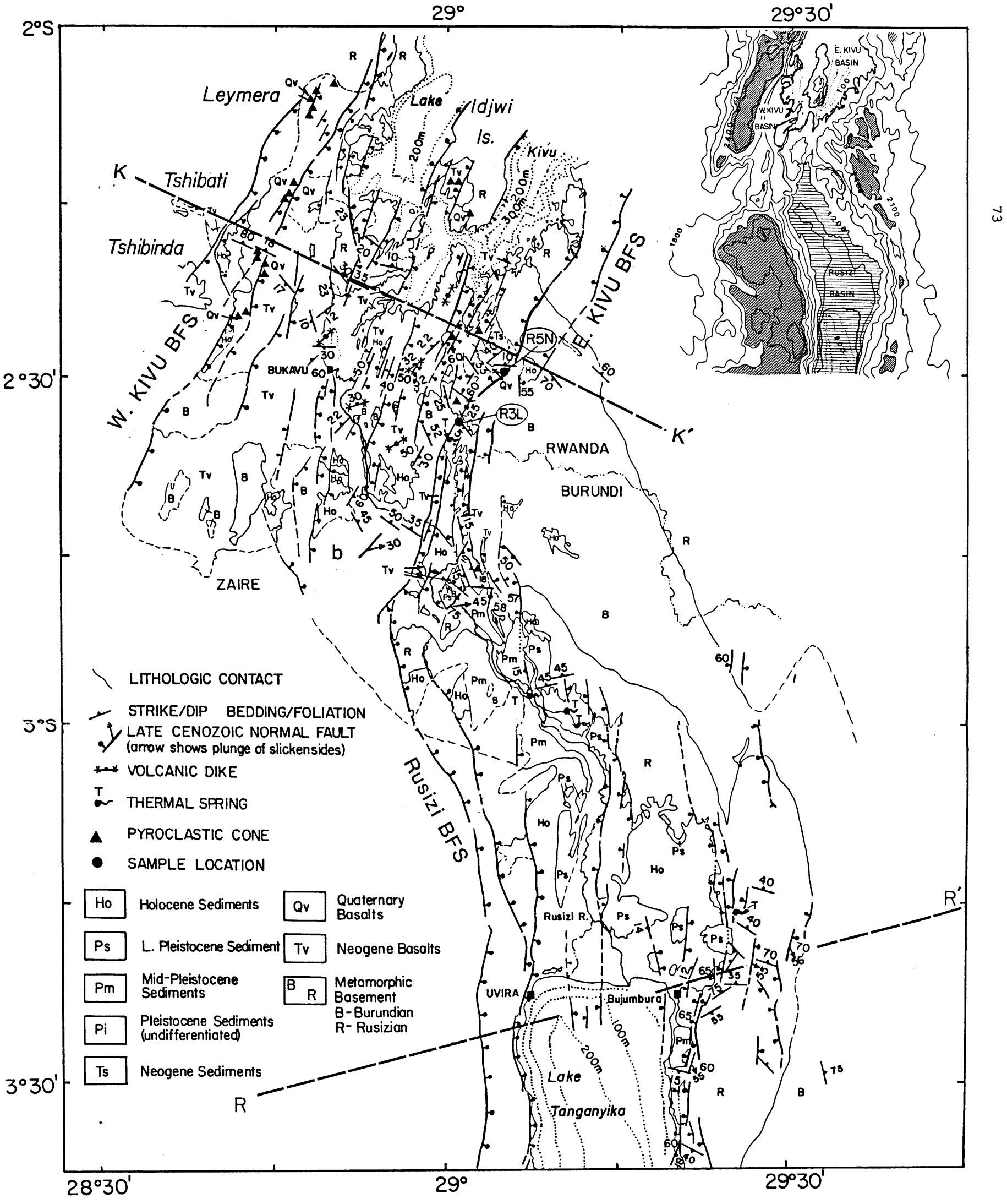

Figure 3. Structural interpretation of Landsat MSS image from South Kivu province calibrated by detailed field studies. Lithologic contacts and faults dashed where uncertain. Plio-Pleistocene and Holocene sediments within the Rusizi basin described and mapped by Ilunga (1984) and Theunissen (1986; in press). Approximate limits of basement units from Theunissen (in press) and Lepersonne (1977b). Inset shows elevations (above sealevel) within study region. K-K', R-R' indicate locations of cross-sectional profiles shown in Figures 7 and 9, respectively.

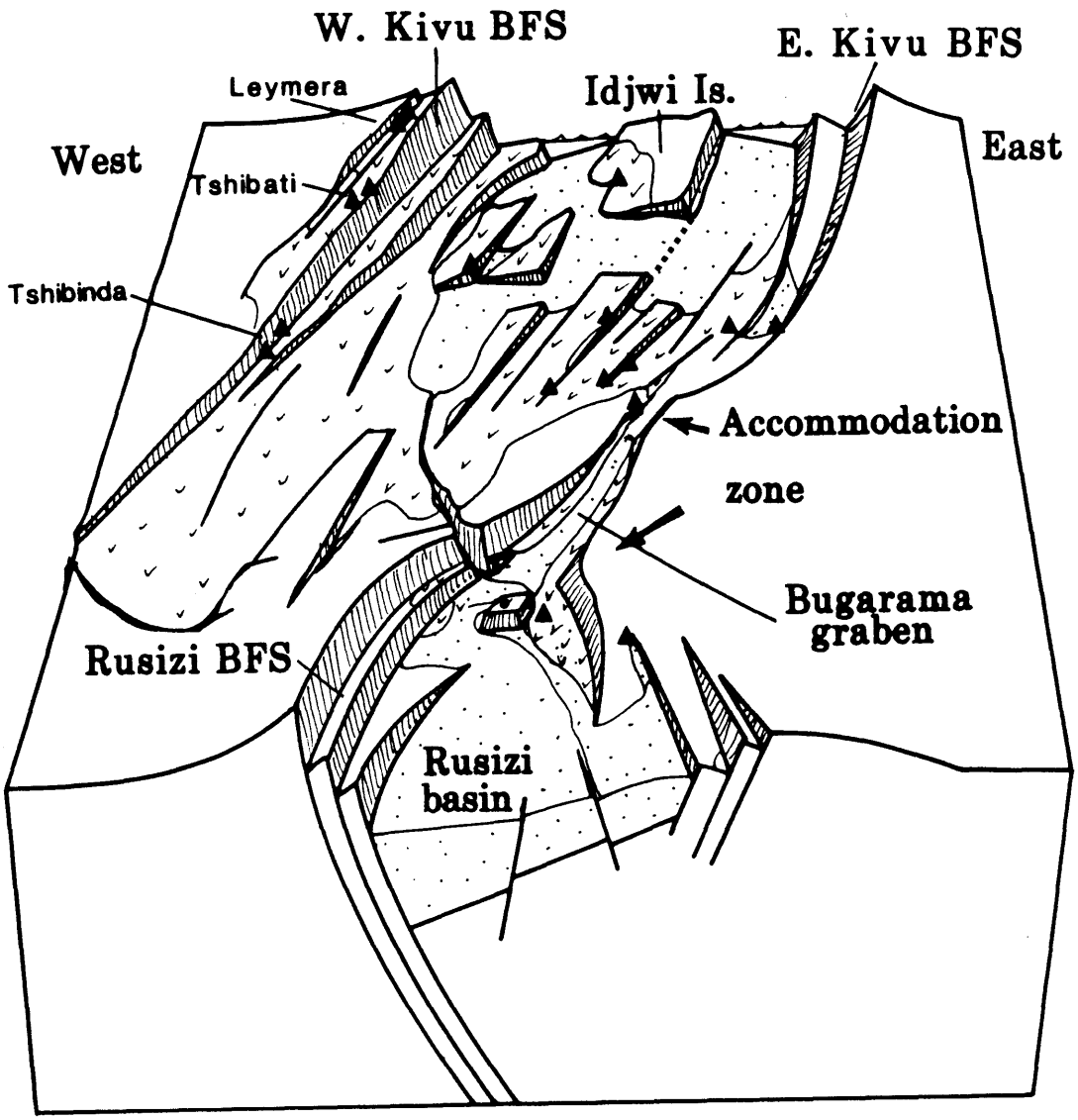

Figure 4. Three-dimensional diagram of basins and accommodation zone. Three-dimensional model of two spoon-shaped rift basins and accommodation zone separating basins. Border fault segments are regionally curvilinear in plan view, and the zone of maximum subsidence is at the base of the central part of approximately 100 km long border fault segments. With respect to major rift basin structures, volcanic centers generally are located along the margins of tilted intrabasinal fault blocks, between *en echelon* border faults,and along transverse structures cross-cutting the rift valley marking interbasinal accommodation zones.Stippling indicates lacustrine sediments and alluvium; random vees Tertiary volcanics.

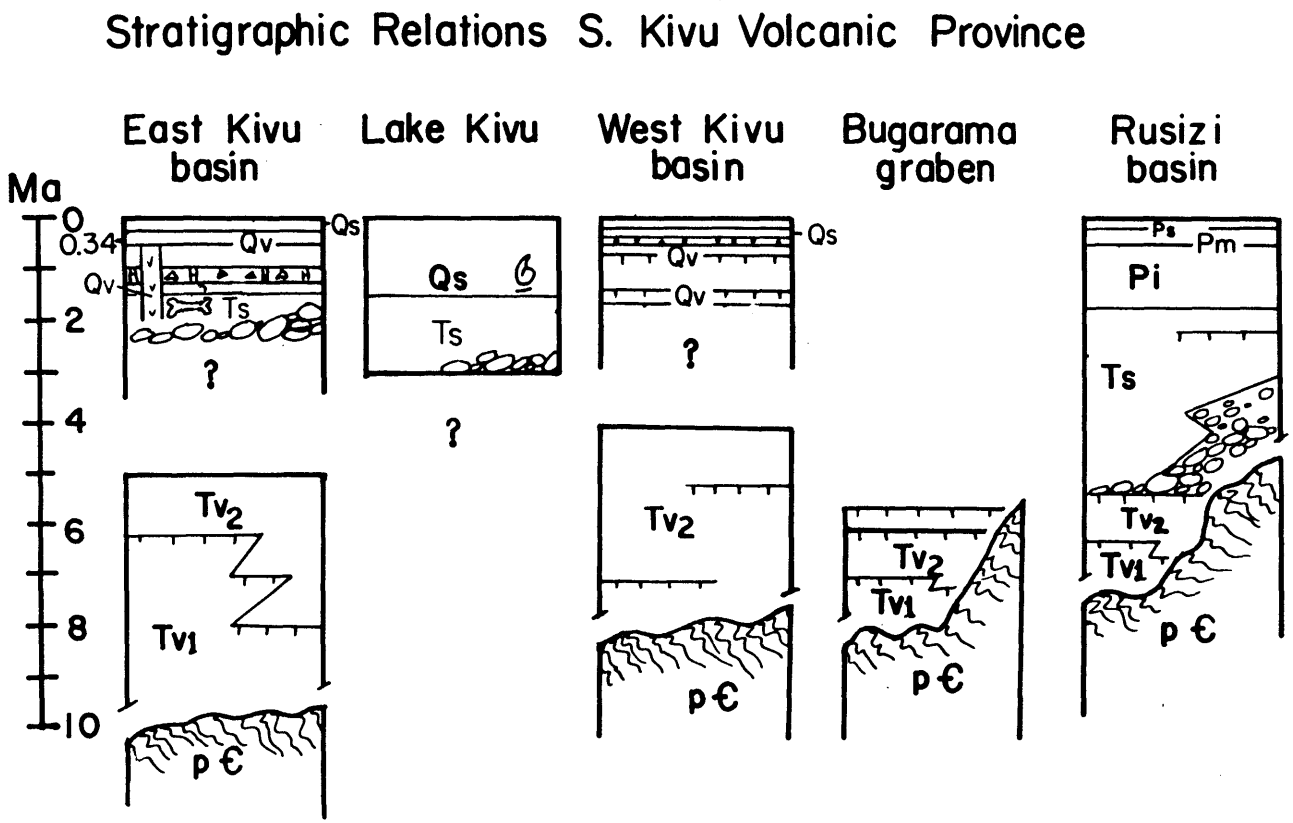

Figure 5. Summary of stratigraphic relations within the East Kivu, West Kivu, and Rusizi basins, and the Bugarama graben. Vertical scale is units of time; thickness of units not drawn to scale. Units Tv1 (tholeiites), Tv2 (alkali basalts) and Qv (olbasalts, West Kivu basin) based on range of ages determined in K/Ar analyses made by Pasteels et al. (in press). Age of olivine basalt unit Qv in Gisakura sequence (342,000 BP) from K/Ar analysis of sample R5N (Figure 3) collected in 1986 (Table I). Ash units in stippled pattern. Sedimentary units beneath Lake Kivu from Stoffers and Hecky (1978) and above basalts in Rusizi basin from Ilunga (1984); D. Stone (pers. comm.).

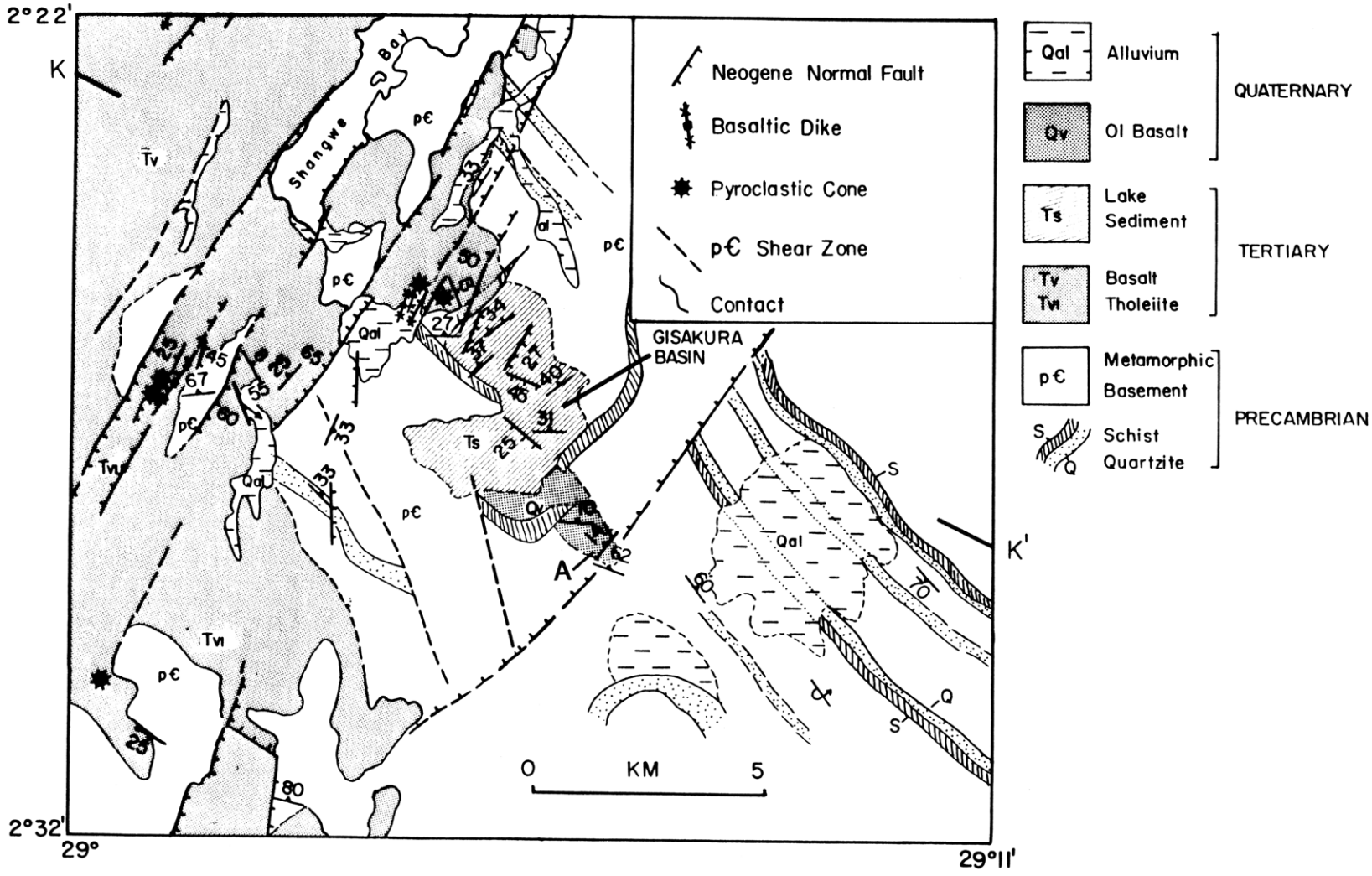

Figure 6. Relationship between Precambrian structures and Neogene faults along the East Kivu border fault segment. Basement structures from K. Theunissen (pers. comm.). Lacustrine sedimentary sequence labelled Gisakura basin described in text. Location of olivine basalt flow dated at 342,000 BP indicated by letter A.

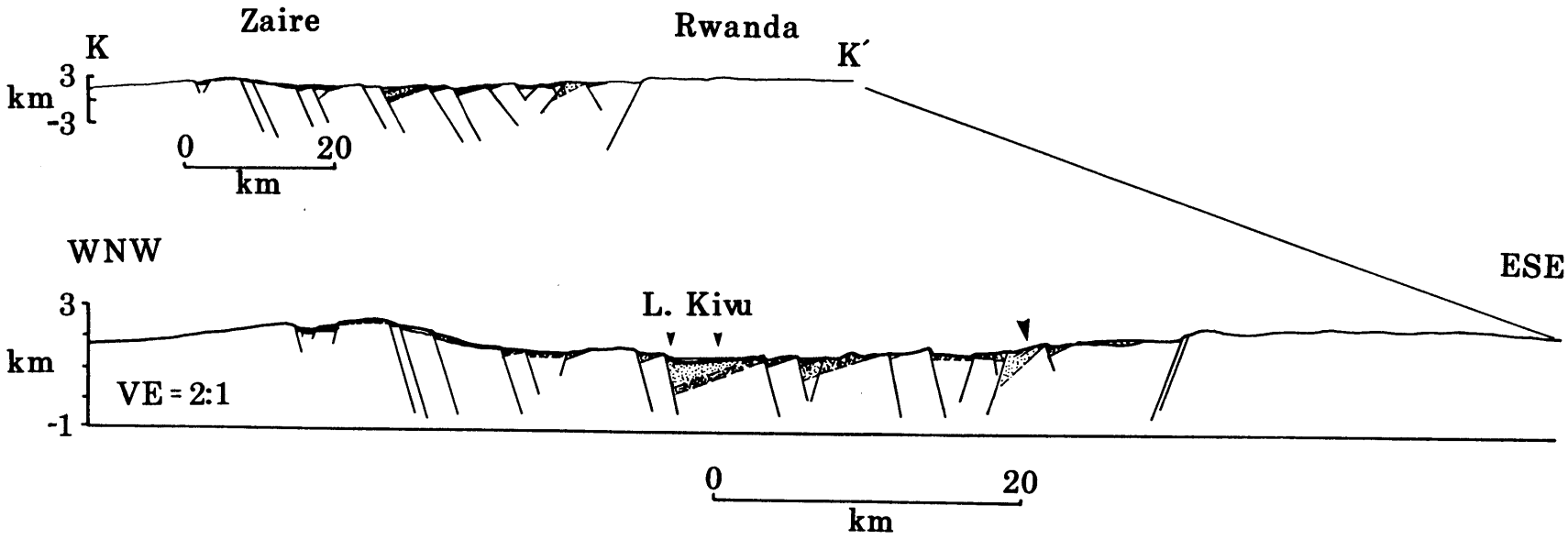

Figure 7. Cross-section of the West and East Kivu basins along profile K-K' north of accommodation zone (Figure 3). Vertically exaggerated section drawn to illustrate stratigraphic relations. Note: central part of West and East Kivu basins located to north, where two basins separated by horst (Idjwi Island).

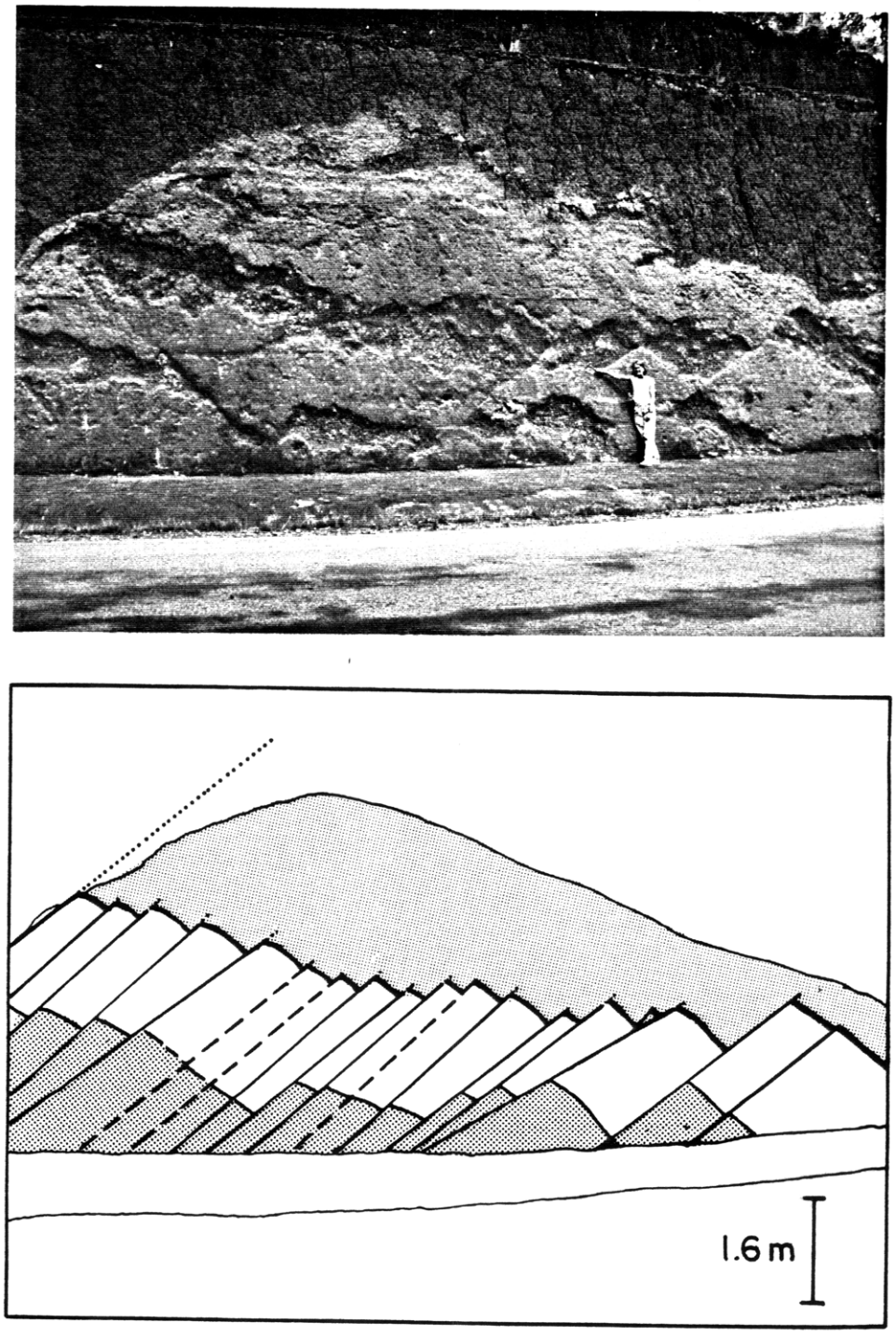

Figure 8. Photo and interpretation from East Kivu basin showing rotated, *en echelon* normal faults displacing basalts (shaded), altered ash layers, and baked soil horizons (see Figure 3 for location). Dip of faults 30-40° (photo taken slightly obliquely to strike of faults). Faults separated by approximately 1m within the 10m wide tilted fault block. Estimate of crustal extension 60-80%.

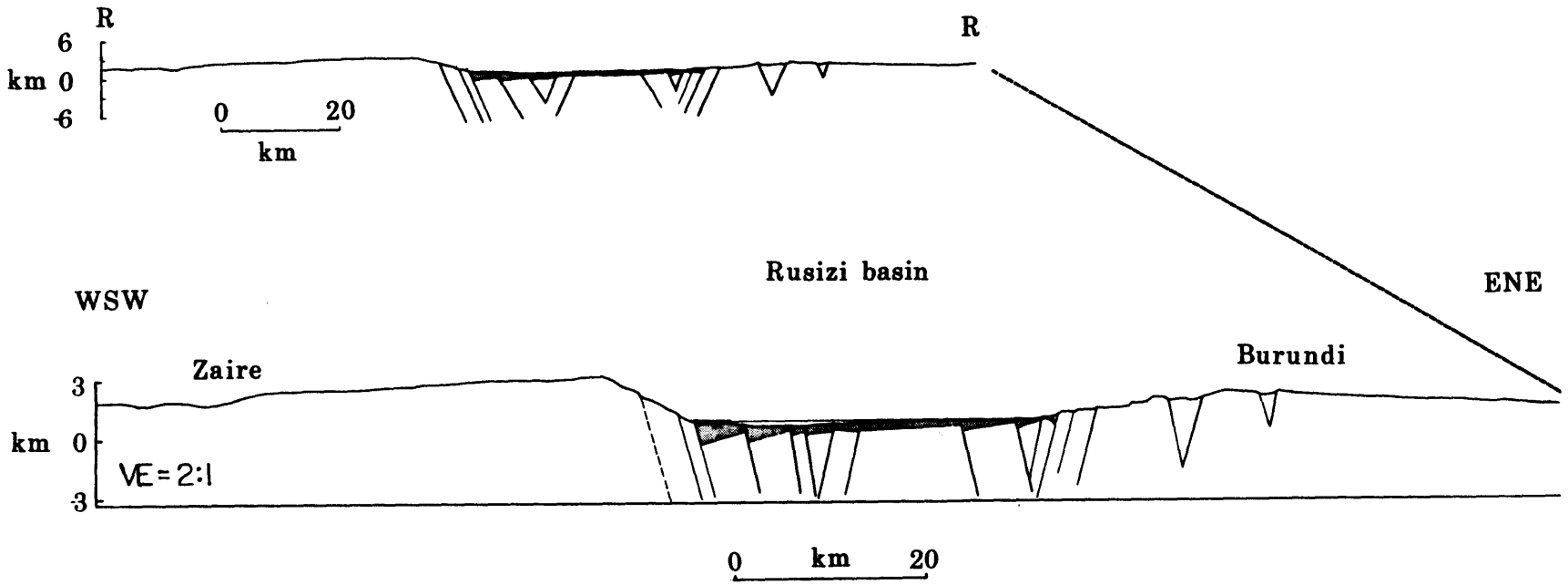

Figure 9. Rusizi cross-section R-R' (Figure 3). Structural patterns beneath Lake Tanganyika interpreted from Figure 8, in Patterson (1983).

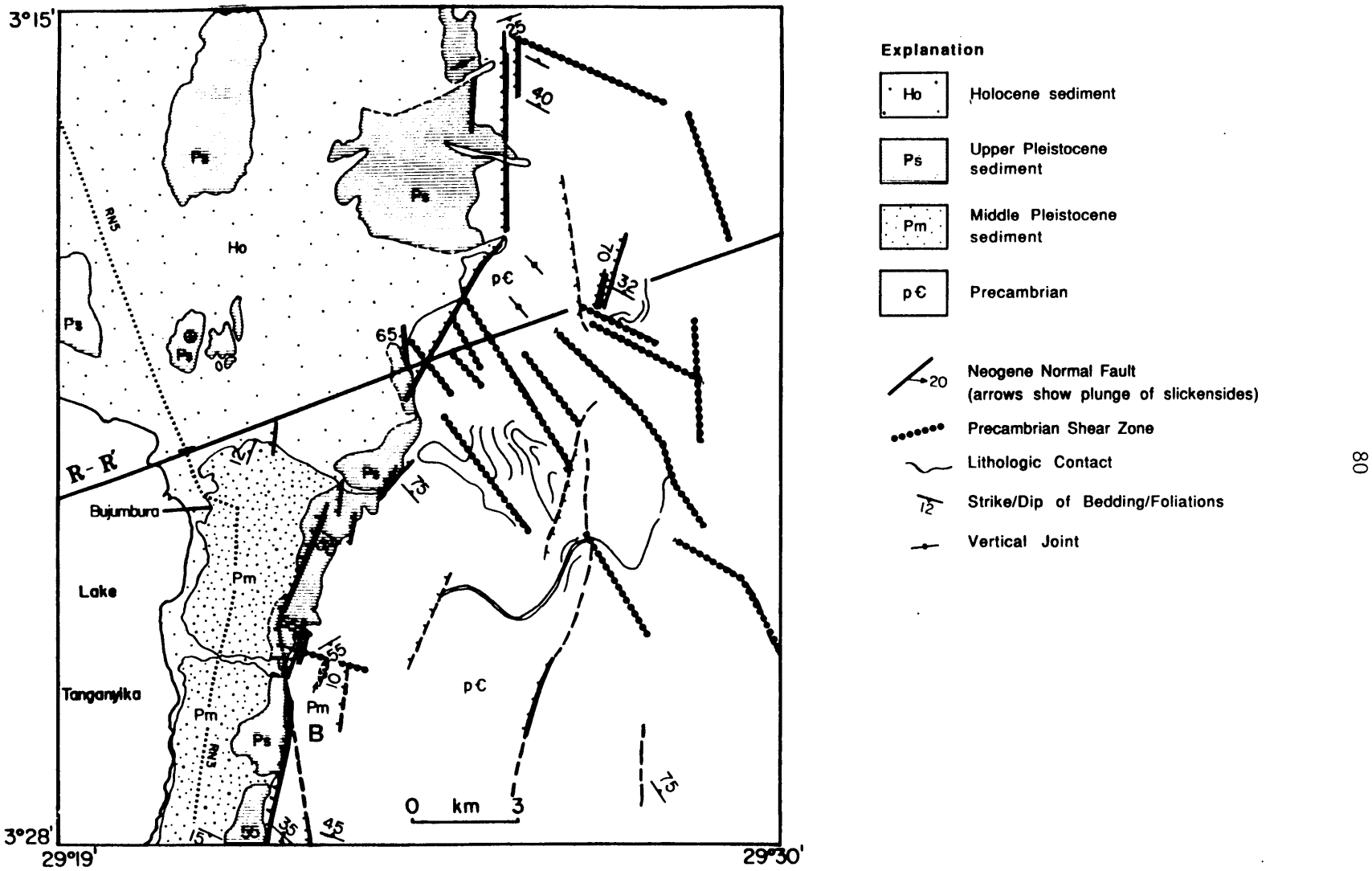

Figure 10. Relationship between Precambrian structures and Neogene faults along the eastern margin of R-R' across the Rusizi basin. Basement structures from Theunissen et al. (in press); this study. Note predominantly N40°W trend of faults in Precambrian basement and terrace of lacustrine sediments indicated by letter B.

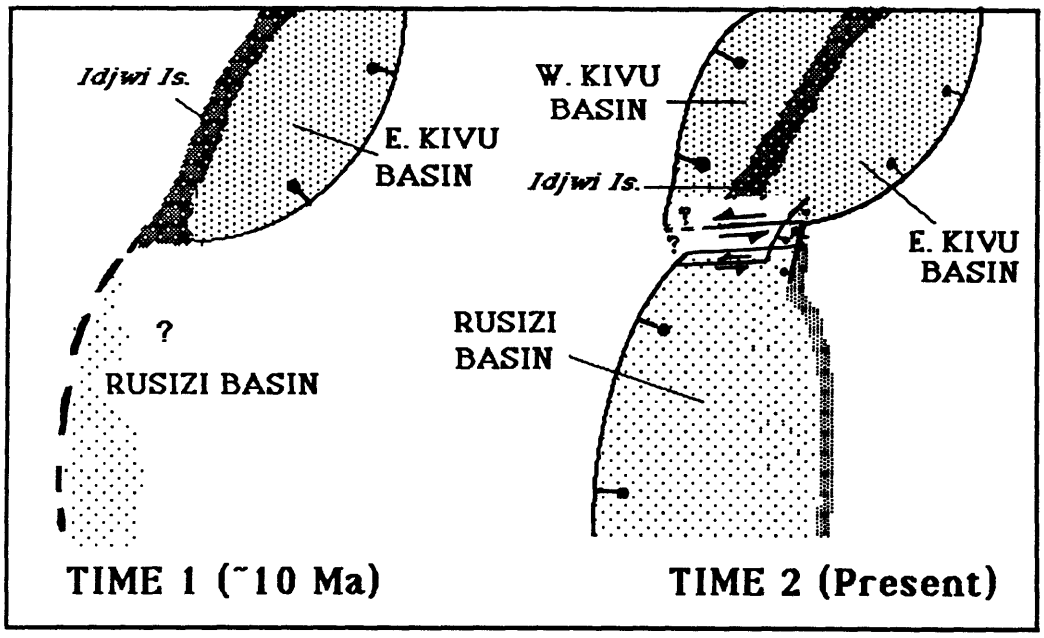

Figure 11. Tentative chronology of basinal development within the Kivu and Rusizi basins. Tholeiitic volcanism within East Kivu basin during Stage 1; Rusizi basin may have formed by this time, but no connection between the two basins existed until Holocene time.

Figure 12. The Rungwe volcanic province is located at the intersection of three basins bounded by border fault segments: the Songwe basin, the Usangu basin, and the Karonga basin. Faults are based on interpretations of Landsat TM imagery calibrated by field studies, aeromagnetic data, supplemented by the lithologic mapping reported by Grantham et al. (1958), Harkin (1960), Teale et al. (1962), Harkin and Harpum (1978).Inset shows elevations (above sealevel) within Rungwe region.

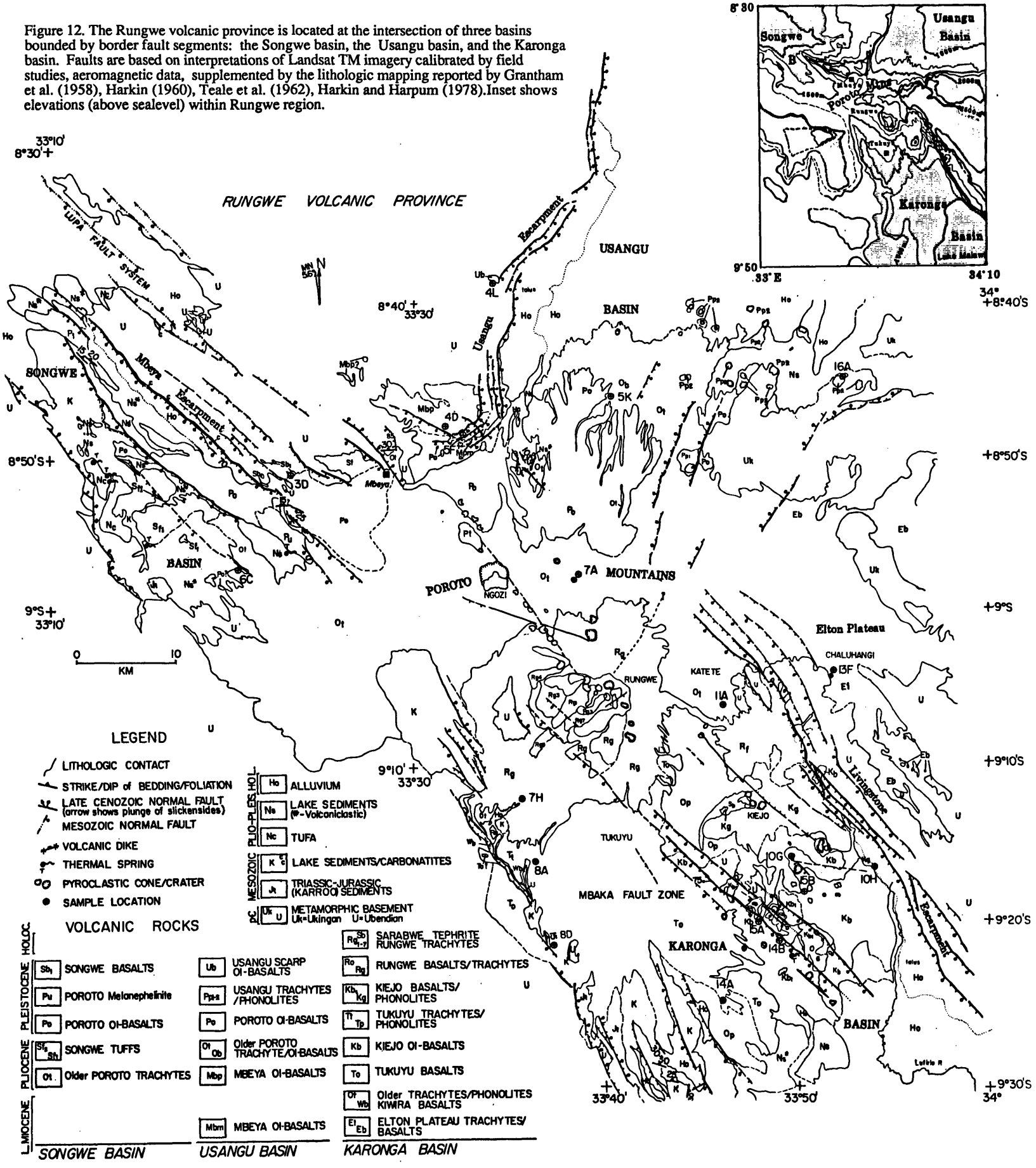

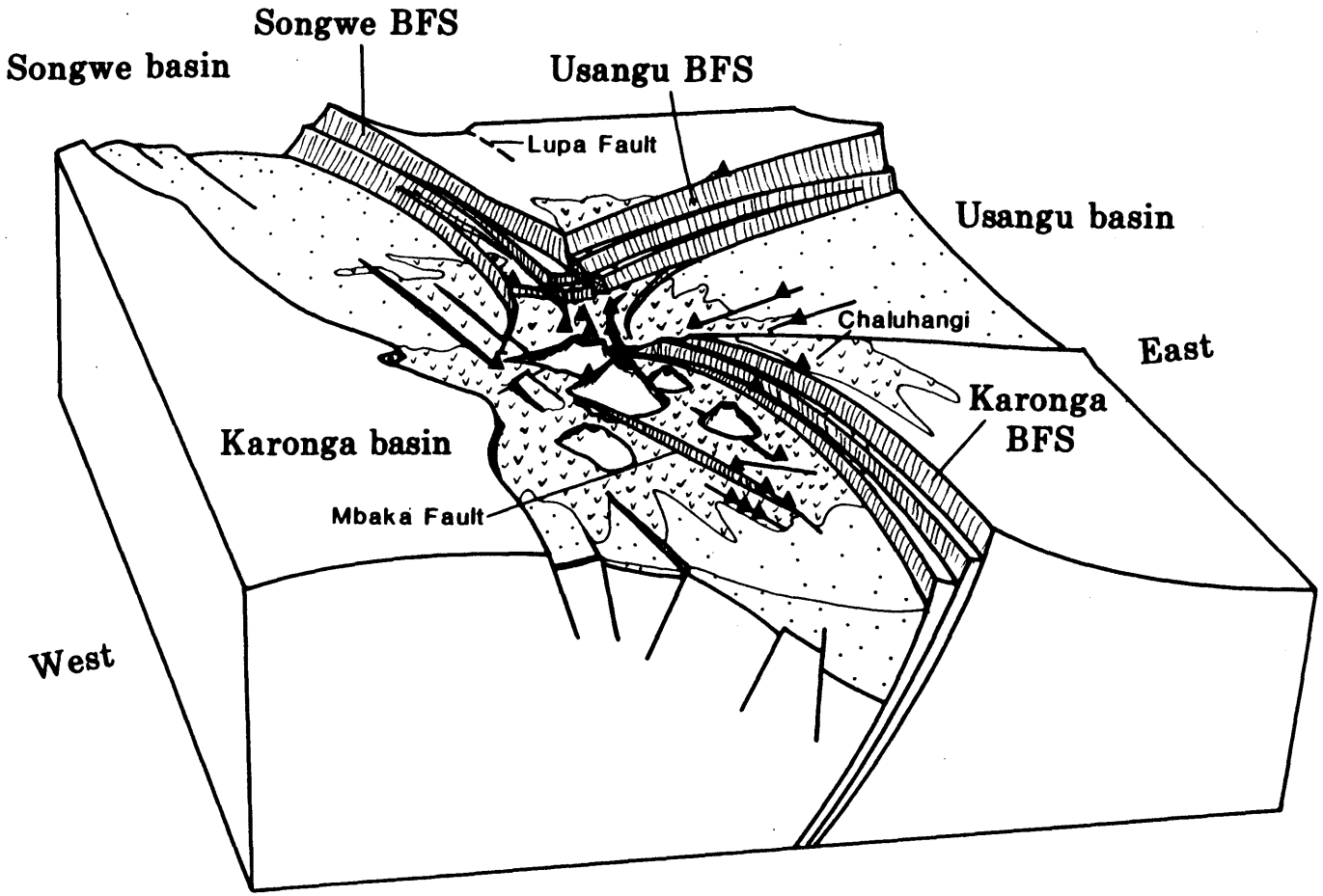

Figure 13. Three-dimensional diagram of Rungwe volcanic province with respect to major structures bounding the Songwe, Usangu, and Karonga basins. Neogene-Holocene volcanics cover accommodation zones between the three extensional basins, and eruptive centers are located along major fault systems bounding basins and along the margins of tilted intrabasinal faults. Stippling indicates lacustrine sediments and alluvium; random vees Tertiary volcanics.

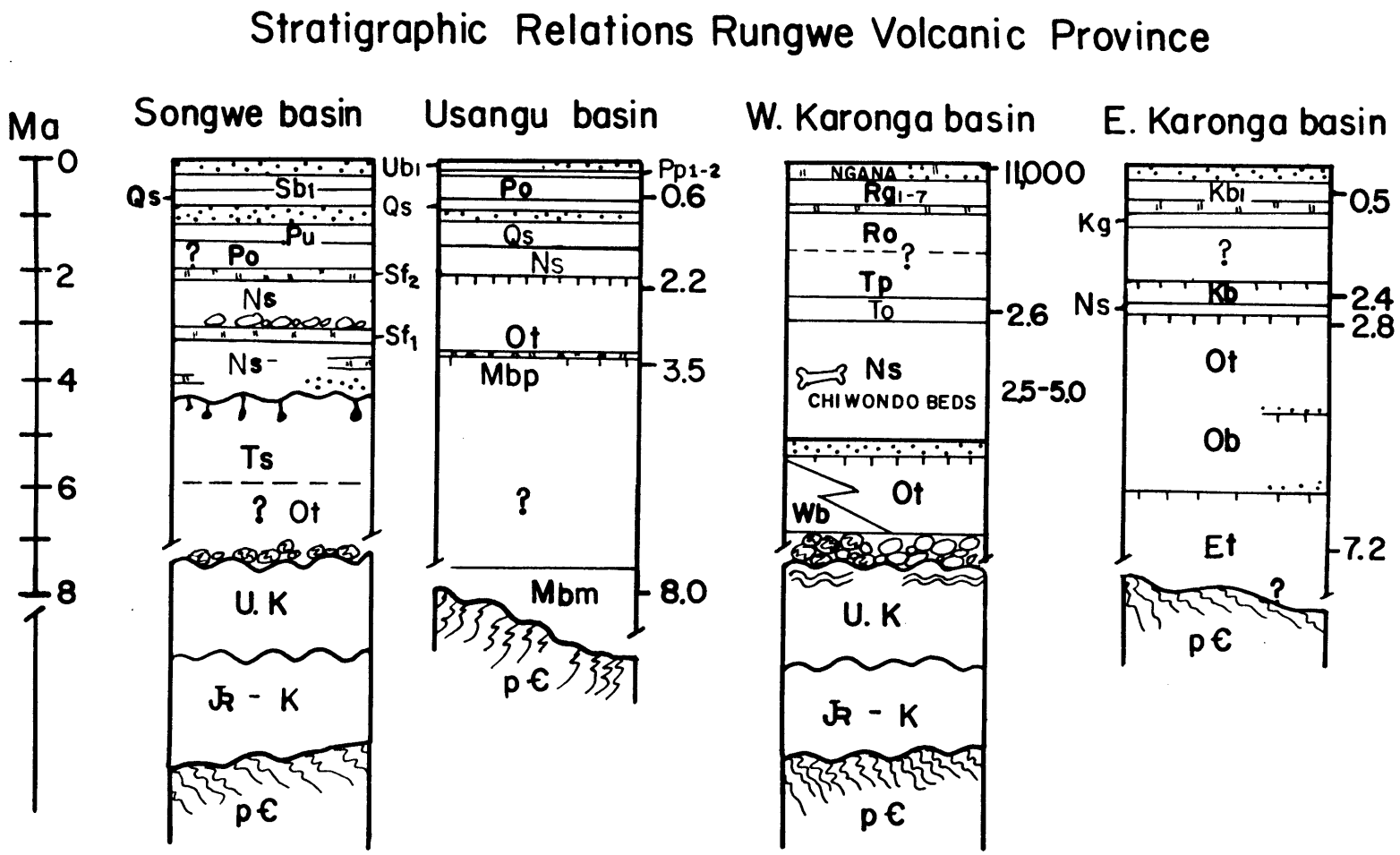

Figure 14. Generalized stratigraphic sections within the Songwe, Usangu, and western and eastern parts of the Karonga basin. Vertical scale is units of time; thickness of lithologic units not drawn to scale. Units described in Harkin (1960); Sb_1 and Mb_1, this study. Age constraints based on K/Ar age determinations of samples listed in Table I. Radiocarbon date of wood within Ngana pyroclastic unit from Crossley, 1982. Ash units between flows indicated by stippled pattern. In West Karonga basin, maximum age of Chiwondo beds (Ts) constrained to 5-2.5 Ma based on faunal remains (Kaufulu et al., 1981).

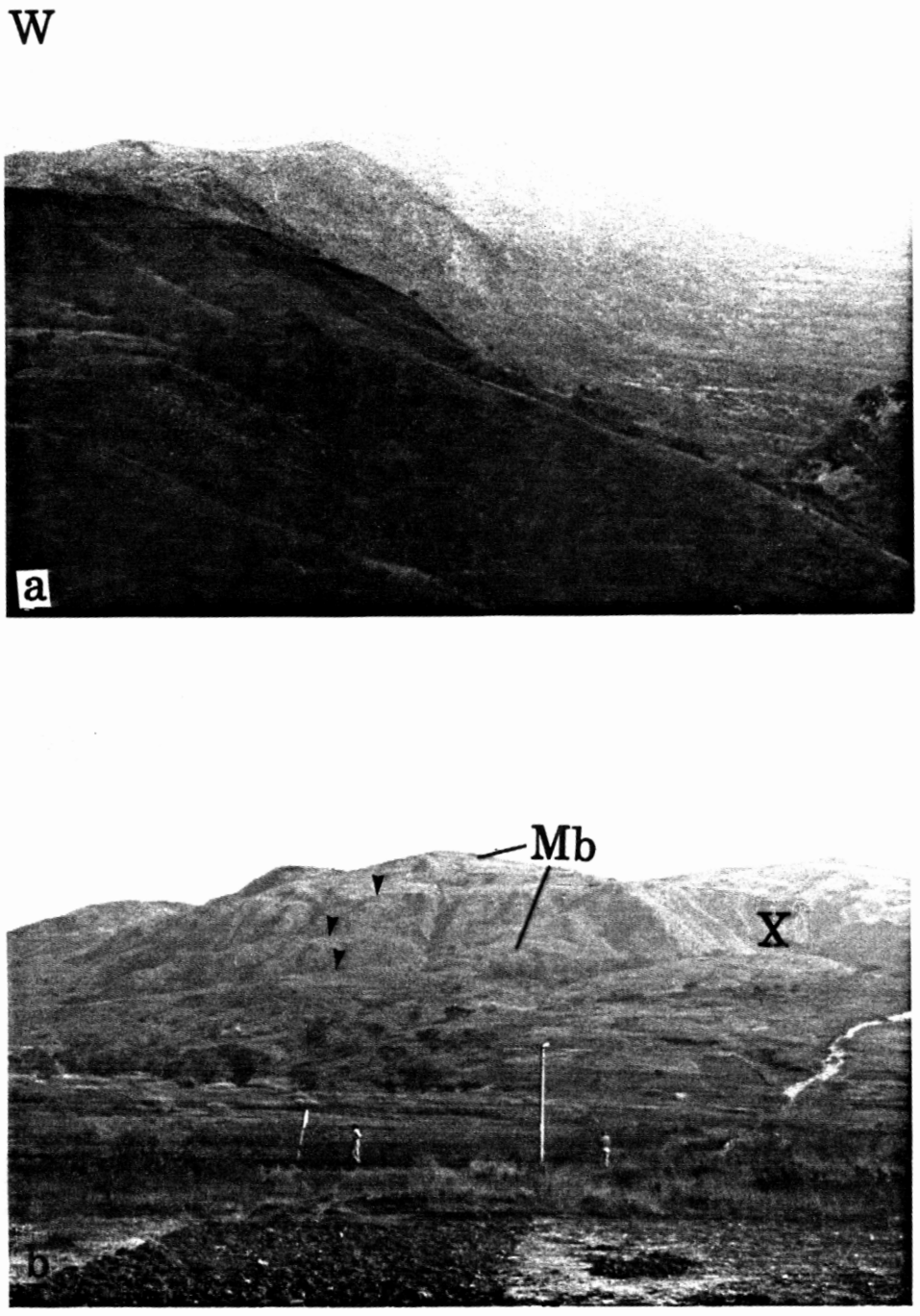

Figure 15. a) The Usangu border fault segment comprises a series of active *en echelon* step faults that displace Neogene basalt flows 800 above petrologically similar sequences covering the rift valley floor. Metamorphic (**M**) basement underlying basalts exposed along scarps (arrowheads). b) Active fault scarp along Usangu border fault segment, illustrating typical morphology of unfaulted rift flank that is gently tilted away from rift valley. Photo taken along strike of approximately north-south trending fault system.

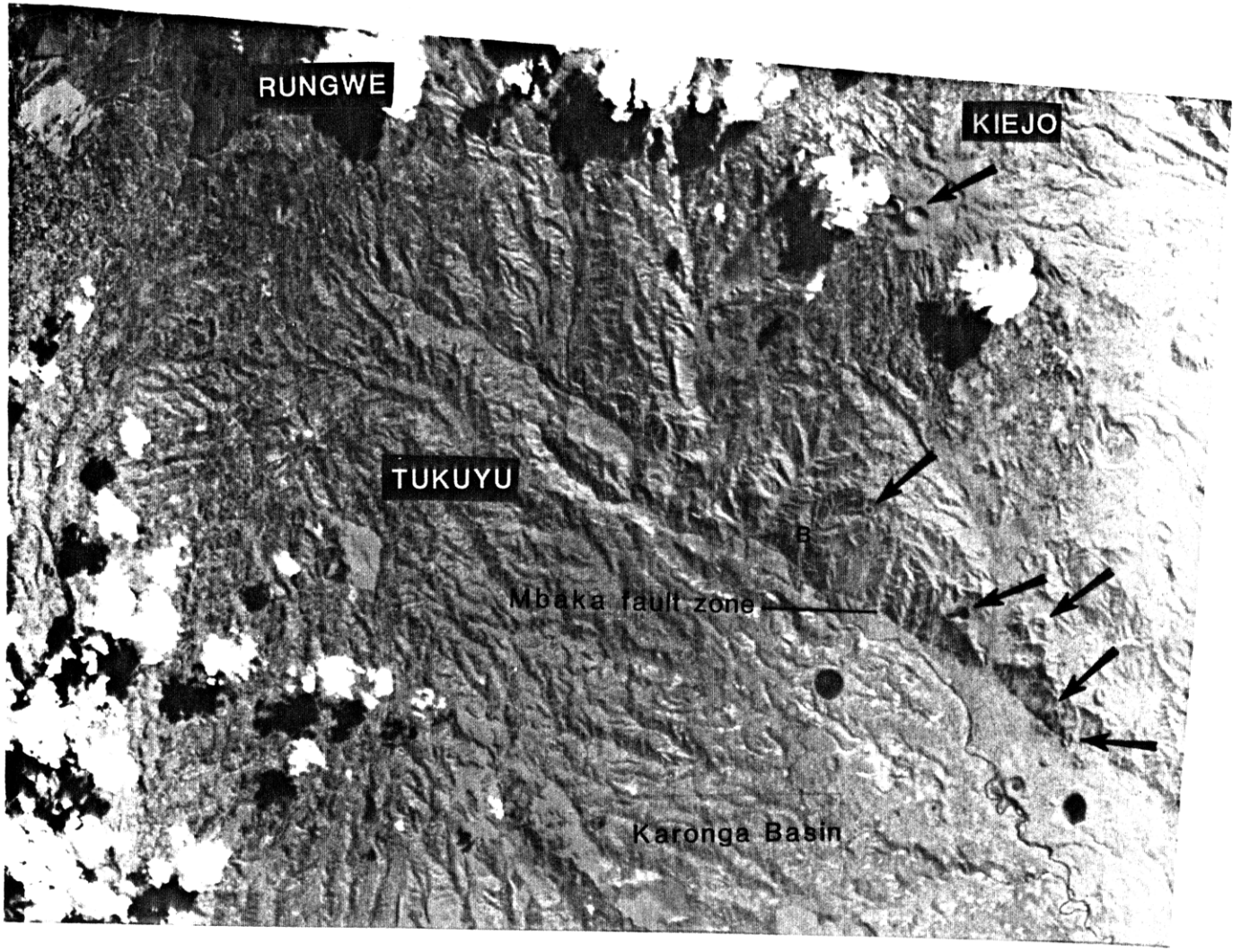

Figure 16. Portion of Landsat-5 Thematic Mapper image from the Rungwe volcanic province (see Figure 1) illustrating active fault scarps that displace Neogene-Quaternary flows and pyroclastic cones. Tukuyu, Rungwe, and Kiejo are shield volcanoes; water-filled craters appear black in image. Arrows point to smaller (~100m wide) pyroclastic cones. **B** denotes metamorphic basement exposed along fault scarp. Note triangular scarps along Mbaka fault.

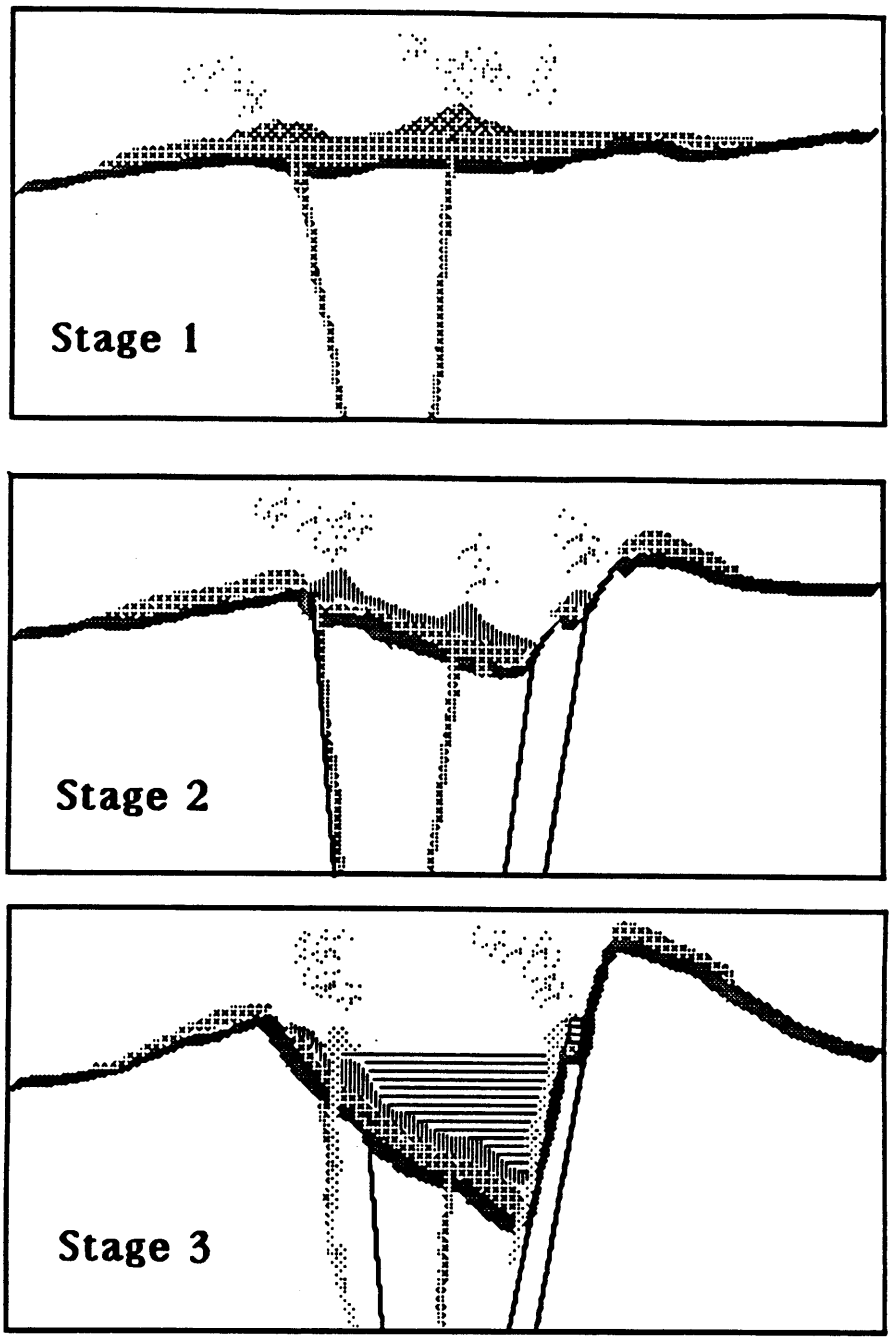

Figure 17. Generalized sketch of subsidence patterns within rift basins. Stage 1: Basalts erupt from fissures onto gentle topography and flow away from present-day rift valley. Stage 2: Subsidence commences along en echelon faults that form a stairstep pattern rising to the level of the uplifted plateau (border fault system), and volcanic centers localize to intrabasinal faults. Stage 3: Continued subsidence and faulting displaces originally flat-lying basalts, and basins fill with sediments. Uplift along the flanks of the rift effectively narrows the basin and elevates sediments in narrow terraces along the uplifted border fault segment.

Chapter 4

TECTONIC DEVELOPMENT OF THE WESTERN BRANCH OF THE EAST AFRICAN RIFT SYSTEM

C.J. Ebinger M.I.T./Woods Hole Oceanographic Institution Joint Program
Dept. Earth, Atmospheric, & Planetary Sciences
Massachusetts Institute of Technology
Cambridge, MA 02139

Abstract

The Western rift, the western branch of the East African rift system, comprises a series of discrete half-graben that are bounded along one side by an approximately 100 km long segment of the border fault system. Border fault segments are made up of normal and strike-slip faults and are curvilinear in plan view. Along the length of the Western rift, the zone of crustal extension is confined to the narrow rift valley, and little evidence is found for faulting along the uplifted rift flanks. The individual half-graben are linked along the the length of the rift valley by accommodation faults within interbasinal transfer zones. Oblique-slip and normal faults between basins accommodate both horizontal and vertical offsets between adjacent half-graben. Neither these accommodation zone faults nor border fault segments show any consistent correlation with pre-rift faults or tectonic contacts. Sedimentary basins of the Western rift valley have developed mainly in Late Miocene to Quaternary time. Uplift in the regions flanking Western rift sedimentary basins has been concurrent with or post-dates the initial subsidence within basins, and the zone of subsidence within individual basins has narrowed with time. Volcanic activity, which began at approximately 12 Ma in the northern part of the Western rift system and at 8 Ma in the southern part of the rift, appears to pre-date initial subsidence within basins. The timing of both rifting and volcanism appears to have progressed from north to south within the Western rift valley, and rift basin propagation may have given rise to the along-axis segmentation of the Western rift valley. Basinal geometries and patterns of basinal development are similar to those of the Kenya rift system, the eastern branch of the East African rift system, although volcanic activity has been more widespread and of longer duration in the Kenya rift system.

Introduction

The tectonically active East African rift system lies atop a broad intracontinental swell, the East African plateau, and consists of two branches, the Western and Kenya (Gregory) rift valleys (Figure 1). Both the Kenya and Western rift systems have been interpreted as incipient plate boundaries linked to the Afar -Red Sea-Gulf of Aden rift systems to the northeast, with one or both limbs of the rift system interpreted as failed continental rifts (e.g., Gregory, 1896; Fairhead and Girdler, 1969; Degens et al., 1971; McConnell, 1972; Chorowicz, 1983; Courtillot et al., 1987). The results of recent studies in the great lakes of the Western rift valley and in the Kenya rift system show that the two rift valleys are segmented along their length into a series of extensional basins (e.g., King, 1978; Crossley and Crow, 1980; Chorowicz, 1983; Bosworth, 1985; Rosendahl et al., 1986; Baker, 1986; Ebinger et al., 1987). However, the geometry, lateral extent, and continuity of Tertiary border fault systems between basins and across the uplifted regions flanking the Western rift valley have been poorly understood in many parts of the Western rift system. Earlier compilations of East African rift structures often have included inactive structures now shown to be pre-Tertiary in age. A detailed chronology of basinal subsidence, rift flank uplift, domal uplift, and volcanism is needed for all parts of the rift system and the associated topographic dome to establish a tectonic framework for the East African rift system.

The objectives of this study are 1) to delineate Tertiary border fault systems along the length of the lesser known Western rift valley, and to use structural and stratigraphic relations within individual basins and along the uplifted rift flanks to constrain the timing of vertical and horizontal movements along the length of the Western rift system; and 2) to compare results from the Western rift system to existing data from the Kenya rift system and the uplifted East African plateau in order to establish to the relationship between faulting, volcanism, and the timing of uplift and subsidence within the East African plateau region. Within this tectonic framework, I examine the spatial and temporal development of Western sedimentary basins, and summarize consistent geometric and kinematic relations within and between basins. Observations made during the course of two field mapping seasons and during geophysical surveys of Lakes Malawi and Tanganyika supplement structural interpretations of high resolution Landsat imagery from the Western rift system and previous reports and geologic maps from the Western region. These studies also were designed to enhance and check existing structural and stratigraphic interpretations used in this compilation of Western rift basins.

Background

The East African plateau is separated from the Afar plateau to the north by a topographic depression, and the region between the two uplifted plateaus is aseismic (Fairhead and Stuart, 1982). Geophysical evidence for crustal thinning across the 1300 km wide East African plateau is restricted to zones beneath the 40-75 km wide Western and Kenya rift valleys (Rykounov et al., 1972; Bram and Schmeling, 1975; Maguire and Long, 1976; Hebert and Langston, 1985; KRISP, 1987). There is seismic evidence for minor amounts of crustal thinning beneath the northern part of the Western rift system. Crustal thickness estimates from the Edward-Kivu rift systems and the Kivu-Tanganyika rifts are approximately 30 km, or 5-11 km less than those found beneath the flanks of the Kenya rift and the central plateau (Bram and Schmeling, 1975; Maguire and Long, 1976; Hebert and Langston, 1985). However, because seismic refraction profiles from the Western rift average crustal structure over distances of 200-800 km, crustal thicknesses beneath individual rift basins may be less. Numerous earthquakes with tensional focal mechanisms occur in an approximately 100 km wide zone along the length of the Western rift system, which is more active than the Kenya rift valley to the east (Wohlenberg, 1968; Rodrigues, 1970; Brown and Girdler, 1980; Fairhead and Stuart, 1982; Shudofsky, 1985).

Chronologic constraints from the Western rift system indicate that crustal movements leading to the formation of individual rift basins began during Neogene time (Table I). Faults bordering the Western rift valley displace Miocene basalts overlying metamorphic basement, a regionally-occurring mid-Miocene erosional surface, and a late Miocene to Pliocene erosional surface in the Malawi rift region (Dixey, 1956; Pulfrey, 1960; Saggerson and Baker, 1965; Lister, 1967). The earliest Mobutu basin sediments were deposited at 5 Ma, although Mid-Miocene age fauna found in fluvial sequences of the Mobutu (Albert) basin previously had been cited as evidence for initial faulting during the early Miocene (Figure 1; Hopwood and Lepersonne, 1953; Pickford, 1987). In the southern part of the Western rift system, the oldest reported lacustrine sediments are Pliocene in age (Kaufulu et al., 1981).

The earliest volcanism in the East African plateau region occurred at 23 Ma in the central plateau region and near the future site of the Kenya rift system (e.g., Baker, 1986). Initial uplift of at least the eastern part of the plateau began in early Miocene time, corresponding to a period of rapid sedimentation within the marine basin (Somali basin) to the east (Saggerson and Baker, 1965; Shackleton, 1978; King, 1978; Coffin and Rabinowitz, 1983). Initial volcanism within the Western rift valley commenced at approximately 12 Ma in the northern part of the Western rift system (Virunga province), and volcanic activity within the Western rift valley (Toro-Ankole, Virunga, South Kivu,

and Rungwe provinces) continues to historic time (Harkin, 1960; Bagdasaryan et al., 1973; Bellon and Pouclet, 1980; Pasteels et al., in press).

The Western and Kenya rift systems have formed largely within Proterozoic orogenic belts surrounding the Archaean cratons of central and eastern Africa, although the southern part of the Tanganyika rift fractures an undeformed Proterozoic volcanic sequence (Figure 2). In a regional sense, the location of the two rift valleys follows Proterozoic orogenic belts and avoids the central cratonic region, possibly reflecting differences in strength across the uplifted plateau. Much of the Western rift system is floored by metamorphic rocks assigned to the Ubendian system (~2100 Ma) which are made up of northwest-southeast trending mylonites and shear zones (Cahen and Snelling, 1984). Within the uplifted region, the Kibaran and Irumidian orogenies (1300 Ma) are represented by northeast-trending basement structures (Reeves, 1960; Cahen and Snelling, 1984; Daly, 1986), and similarly-aged rocks have a northwest trend in the Burundian belt (Theunissen, in press). The Mozambiquian (Pan-African) orogeny (600-900 Ma) produced north-south trending folds and metamorphic fabrics in the eastern part of the region, and these north-south trends often overprint Ubendian rocks (Cahen and Snelling, 1984).

Several fault-bounded sedimentary basins containing Permian to Jurassic sediments (Karroo) crop out near the shores of Lakes Tanganyika and Malawi, and in the southern part of the Malawi rift (Figure 2). Cretaceous rift sediments unconformably overlie Karroo rift sediments (Permo-Triassic) in parts of the Rukwa and Malawi region, and in the Turkana rift region between the Kenya rift and Ethiopian rifts (Arambourg, 1933; Spence, 1954; Dixey, 1956; Williamson and Savage, 1986). Late Jurassic/Early Cretaceous carbonatites are found along northwest-southeast trending faults that extend northwest of Lake Rukwa to the eastern shore of Lake Tanganyika (Pentel'kov and Veronovskiy, 1979; Brown, 1964; Coetzee, 1964). Largely undeformed Late Proterozoic to Holocene continental sequences have been eroded within the uplifted regions of the central plateau and are now restricted to topographic depressions (Figure 2).

Western rift basins

Repetitive patterns in the three-dimensional geometry of individual basins and the fault systems bounding these basins have been noted in recent studies of Lakes Malawi and Tanganyika (Rosendahl et al., 1986; Ebinger et al., 1987). It appears that the Western rift valley comprises a series of deep asymmetric sedimentary basins (half-graben) separated by horsts or shallow sills, and the sense of basinal asymmetry commonly alternates along the length of the rift valley (Crossley and Crow, 1980; Ebinger et al., 1984; Rosendahl et al., 1986; Burgess et al., in press; Peirce and Lipkov, in press). However, the geological data base on which these results are based is sparse in many parts of the rift system. For

example, existing geological maps are at a scale of 1:250,000 to 1:2,000,000 in the western regions of the Western rift system. More detailed reports generally have focused on mineral resources and Precambrian structures; Neogene structures largely were ignored or unreported.

I have used high resolution color Landsat-5 Thematic Mapper (TM) and Multi-Spectral Scanner (MSS) imagery as a primary data base to examine fault patterns between discrete rift basins and along the uplifted rift flanks and to integrate existing maps from the region (see Appendix I; Figure 1). In order to extend these structural interpretations between the specific study locales shown in Figure 1, a collage of 1:1,000,000 MSS imagery provided by Musée Royale de l'Afrique Centrale was assembled. I used these imagery to identify key areas for detailed field studies along the uplifted flanks of the the northern and central parts of the remote Western rift system (Chapter 3). During five months of field work during 1986 and 1987, I made transects of over 14 of the major normal fault systems that bound the Western rift system. Where faults and lineaments had not been noted previously, the following criteria were used to differentiate Neogene faults from older structures: amount of topographic relief, appearance of fault scarps, occurrence of hot springs, and horizontal offsets of pre-rift basement faults and geologic contacts. The scale of topographic maps used was generally 1:50,000.

Sediment thicknesses, intrabasinal fault patterns, and the sense of asymmetry within rift basins are derived from interpretations of single and multi-channel seismic reflection and magnetic data from Lake Tanganyika (Degens et al., 1971; Patterson, 1984; Lorber, 1984; Rosendahl et al., 1986; Burgess et al., in press), Lake Kivu (Degens et al., 1973), the Rusizi basin (D. Stone, pers. comm.), and the Malawi rift (Ebinger et al., 1987). In the Rukwa rift, recent gravity and aeromagnetic surveys calibrated by exploratory drilling have been used to interpret subsurface structures (Peirce and Lipkov, in press; D. Stone, pers. comm.).

Generalized 3-Dimensional Geometry of Western basins

A detailed description of the geometry of individual faults bounding several Western basins and in the accommodation zones between several basins is presented in Chapter 3. I draw upon the results of these detailed field studies to interpret similar patterns occurring along the length of the Western rift system. In this section, I illustrate the three-dimensional geometry of Western rift basins with specific examples from the Tanganyika rift, the Moba and Marungu basins (Figure 4).

I use the term border fault segment to describe sections of fault systems bordering the Western rift valley that have large vertical displacements and uplifted footwalls that form the rift flanks with high topographic relief. The asymmetric rift basins that are

bounded by the border fault segment are tilted down toward the border fault segment (Ebinger et al., 1987). I also use the term interbasinal transfer fault zone, or accommodation zone, to describe closely-spaced normal and strike-slip faults at the tips of border fault segments that are related to differential vertical and minor horizontal displacements between extensional basins (e.g., Burchfiel and Stewart, 1966; Bally, 1982; Bosworth, 1985; Rosendahl et al., 1986).

Two border segments along the southwestern shore of Lake Tanganyika can be identified from topographic relief and seismic reflection data within the Moba and Marungu basins (Rosendahl et al., 1986; Figure 4). High-angle (45°-75°) normal faults occur in a 10-15 km wide zone along the western margins of the Moba and Marungu basins, and these faults appear as prominent lineaments in Landsat Scene 1 (Figure 5). Faults bounding the Moba basin trend northwest; those bounding the Marungu basin trend approximately north-south, and hot water and salt water springs are found along several faults (Figure 5, 6). Seismic reflection data from Lake Tanganyika indicate that faults bounding the western side of the basins remain steep to depths of 5 km or more,(Figure 7a,b; Rosendahl et al., 1986). The approximately 2000m high plateau on the western side of the Moba and Marungu basins dips gently to the west away from the rift valley, and no evidence for faulting is found outside the inner facing normal faults along the uplifted western flanks of the basins (Figures 5, 6). The eastern margins of both basins are structural monoclines, and metamorphic basement dips gently to the west beneath sedimentary sequences contained in these two basins (Figure 7). Thus, sedimentary basins bounded by these 100 km long, 10-15 km wide border fault segments have the characteristic cross-sectional form of half-graben (Figure 7).

The arrangement of generally linear faults along the margins of the two basins produces a curvilinear basinal geometry in plan view (Figure 8). For example, along the Marungu border fault segment, lineaments apparent in Landsat imagery and aerial photographs strike approximately north-south and N30°W. North-south striking lineaments often show 100m or more vertical relief, and fault scarps are triangular along the shores of the lake (e.g., Capart, 1949); I interpret N-S striking lineaments along the Marungu border fault segment as normal faults. The northwest-trending lineaments are interpreted as oblique-slip faults, and subhorizontal striations have been reported along northwest-trending faults in this region (Figures 5, 6; Chorowicz, 1983). Faults striking northwest and north-south bound the western margin of the Moba basin. In contrast to the Marungu basin, the northwest striking faults show significant topographic relief and spurs commonly are facetted. Thus, the Moba and Marungu border fault segments regionally are curvilinear, and normal and oblique-slip faults intersect at the tips of the two border fault

segments, or within the interbasinal accommodation zone (Figures 5, 6, 8).

The Moba basin is characterized by 5-10 km wide tilted blocks that generally trend northwest, parallel to the normal faults bounding the Moba basin. Faults within the Marungu basin generally are oriented north-south parallel to Marungu border faults (Figure 6). Syn-sedimentary faults penetrate to all stratigraphic levels of the sedimentary sequence (Figure 7). Sedimentary accumulations are greatest near the central part of these border fault segments and decrease toward the tips, producing spoon-shaped basinal morphologies, although the magnitude of subsidence is greater in the Marungu basin than in the Moba basin (Figures 6, 7).

At the southern end of the Moba basin and the northern end of the Marungu basin (accommodation zone), a basement ridge separates the two basins (e.g., Rosendahl et al., 1986), but subsurface information is insufficient to constrain the geometry of faults linking the two extensional basins beneath the lake. In the region between the two basins on the eastern side of the rift, normal faults striking N20°W and N10°E, and strike-slip faults striking east-west characterized by subhorizontal slickensides displace augen gneisses of the Ubendian system (Figures 8b, 9). However, the orientations of these two sets of faults show no correlation with metamorphic foliations and mylonites (Figure 8b). No lithologic or structural indicators were found to document the sense and amount of displacement along these faults. The plunge of slickendside surfaces along oblique-slip faults suggest that the sense of movement is dextral along strike-slip faults within this accommodation zone (Figure 8b).

Basinal descriptions

Regional tectonic maps of rift basins bounded by Border Fault Segments (BFS) 1-23 shown in Figures 3 and 4 and briefly described below from north to south represent a summary of similar analyses of topography, surface and subsurface structures, and analogy to border fault geometries illustrated above. Structural patterns within accommodation zones are complex, and require detailed analyses on a case by case basis to interpret the linkage of individual basins (e.g., Chapter 3). Because existing seismic coverage and structural maps from the the Western rift system are too sparse to document detailed structural relations within most parts of the Western rift system, I only summarize commonly occurring morphologic patterns in regions linking Western rift basins. The general strike of border fault segments, the sense of asymmetry within basins, and constraints on the timing of subsidence, uplift, and volcanism are listed in Table II. For comparative purposes, amounts of subsidence within basins are listed as present elevations of the rift valley or lake floor, because depth to pre-rift basement is not known in many basins. Seismic studies within Western lake basins show that the greatest depths to pre-rift

basement generally are found beneath the deepest part of basins (e.g., Wong and Von Herzen, 1974; Ebinger et al., 1984; Rosendahl et al., 1986).

Mobutu basin (BFS1)

The northwestern margin of the Mobutu (Albert) basin is bounded by BFS1 (Figure 3a). At its central part, the escarpment formed by this border fault segment rises 1300m above the surrounding region and vertical separations decrease toward the north and south (Figure 3b). Faults comprising this system are seismically active, and hot salt water springs and oil seeps have been reported along the base of the escarpment (Davies, 1951; Rodrigues, 1970). The fault plane mechanism determined by Shudofsky (1985) for an earthquake at 10 km depth along the Mobutu basin border fault segment indicates pure normal faulting along a north-south striking fault plane (Figure 3a). The eastward-tilted surface of westward-dipping faults form a stair-step pattern (step faults) rising to the elevation of the uplifted East African plateau on the eastern side of the Mobutu basin (Davies, 1951). Lacustrine sequences (Kaiso beds) began to accumulate in a fault-bounded basin at approximately 5 Ma, and borehole data indicate that at least 1250m of sediments have accumulated (Davies, 1951; Pickford, 1987).

Semliki basin (BFS2)

The Semliki basin is bounded by a series of normal faults dipping 60-80°W along the western side of the 5000m high Ruwenzori mountains (Figure 3a, b). A faulted monocline forms the northwestern side of the basin. The fault planes inferred from focal mechanisms of earthquakes that occurred at depths of 7-29 km within the Semliki basin strike N20°E (Shudofsky, 1985), or parallel to orientations of normal faults bounding the Semliki basin (Figure 3a). At the northern end of the Semliki basin, Plio-Pleistocene sediments stratigraphically equivalent to those found in the Mobutu basin crop out along the nose formed by the intersection of the monocline and BFS2 (Wayland, 1934; Holmes, 1951). Numerous hot springs are found along the escarpment, and hanging valleys and shelves attest to Holocene vertical movements in this part of the rift valley (Davies, 1951).

Lake George basin (BFS 3)

The fault system on the eastern margin of the Ruwenzori mountains (BFS3) extends to the northeast and bounds the western side of Lake George (Figure 3a). Based on the focal mechanism from an earthquake at approximately 29 km depth beneath the eastern margin of the basin (Shudofsky, 1985), extension is perpendicular to the strike of BFS3 (Figure 3a). Subdued topographic relief characterizes the eastern margin of the Lake George basin, the monoclinal side of the basin (Figure 3b). Pleistocene alkalic basalts of the Toro-Ankole province are found along the northern part of BFS3, and isolated vents and craters mark the margins of tilted fault blocks at the southern end of the Lake George

basin (Figure 3a; Combe, 1943; Bagdasaryan et al., 1973). Plio-Pleistocene sedimentary sequences in these basins are similar to those found in the Mobutu basin (Wayland, 1934).

Lake Edward basin (BFS4)

The northwestern (monoclinal) side of the Semliki basin becomes faulted to the south, and vertical offsets along BFS4 are greatest near the north central part of Lake Edward (Figure 3a). *En echelon* faults with minor vertical displacements border the southeastern side of the Edward basin (Hopwood, 1970). Faunal remains within the lacustrine Kaiso sequence, the earliest rift sediments, have been correlated to Pliocene stratigraphic sequences in the northern part of the Kenya rift system (Table II). Periods of basinal desiccation correlated with major faunal radiations at 4 and between 2-3 Ma may be related to crustal movements in the Edward basin (P. Williamson, pers. comm.).

Rutshuru basin (BFS5)

The eastward-tilted Rutshuru basin is bounded by a north-south trending border fault segment (BFS5) with an escarpment that rises 1200m above the rift valley floor (Figure 3b). An unknown thickness of Plio-Pleistocene lacustrine sediments floors part of the Rutshuru valley, which has been covered by basalts from the Virunga province to the south. Terraces of these sediments now are found at 1225m, 1300m, 1400m, 1450m, and 1600m above the Rutshuru valley floor and at least 500m above the highest reported lake level (de la Vallee Poussin, 1933; Pouclet, 1977).

Virunga basin (BFS6)

The northeast-trending Tongo escarpment (BFS6) rises 1000-1500m above the western margin of the Virunga basin (Figure 3b), which is floored by Neogene basalts of the Virunga and Bufumbira volcanoes (Bellon and Pouclet, 1980). Structural and stratigraphic relations within the Virunga basin indicate that volcanism preceded faulting and basinal subsidence (Bellon and Pouclet, 1980). Within the southern part of the Virunga basin northwest-trending active fissures and shield volcanoes cross-cut the rift valley (Figure 3). Terraces of Plio-Pleistocene lacustrine sediments at elevations of 1450m, 1500m, 1650m, 2000m, and 2050m cover high-angle (50-70°), east-dipping faults, and the highest terrace is now 800 above the ancient lakelevel highstand (Pouclet, 1975). During Pleistocene time the zone of subsidence localized to a narrow trough at the base of the Tongo escarpment and Holocene basalts from Karisimbi volcano have been uplifted on the monoclinal side of the basin (Pouclet, 1975; De Mulder and Pasteels, 1986).

Kivu basins (BFS7, 8)

The western side of Lake Kivu is bounded by a steep escarpment (BFS7) that borders a basin filled with up to 500m of sediments, and with basalts from the Virunga province to the north (Figure 3b; Wong and Von Herzen, 1974). The trace of this fault

extends north into the Virunga basin where it displaces 12,000 BP basalts of the Karisimbi volcano (Pouclet, 1977; De Mulder and Pasteels, 1986; this study). To the south, BFS7 displaces 10-5 Ma basalts of the South Kivu and Mwenga-Kamituga provinces (Pasteels et al., in press; Figure 3a). A lineament of much younger (<1.9 Ma) pyroclastic cones has formed along the central section of this escarpment, and these 100-600m wide cones (Tshibinda, Tshibati, and Leymera) are located within the inner facing normal faults bounding the rift valley (Guibert, 1977a; Bellon and Pouclet, 1980; this study). Observations made during 1986 indicate that basalts from these eruptive centers flowed down an escarpment, hence vertical movements along BFS7 occurred prior to 1.9 Ma. Wong and Von Herzen (1974) suggest that the central part of the Kivu basin is 3 Ma, based on an extrapolation of Holocene sedimentation rates to the observed 500m of sediments. Significant vertical movements occurred along BFS7 during the Holocene: shoreline deposits dated at 6000 BP were found at 300m water depth at the base of BFS7; 12,000 BP hyaloclastites on the western side of Idjwi Island are now elevated approximately 80m above the highest Kivu lake level (Degens et al., 1973; Guibert, 1977b).

A second border fault segment, the East Kivu border fault segment (BFS8), bounds the opposite side of the rift (Figure 3a). In this geometrical arrangement a horst (Idjwi Island) separates the narrow sedimentary basins formed by BFS7 and BFS8, and the horst serves as a hinge for vertical movements in the two basins (Figure 3a). A terrace of lacustrine sediments similar to sediments found beneath Lake Kivu (e.g., Stoffers and Hecky, 1978) are interbedded with Late Pleistocene basalts, and these sequences have been uplifted approximately 500m from the highest lakestand in the Kivu basin (Chapter 3). An estimate of crustal extension across the Kivu basin based on a reconstruction of surface fault geometries is less than 10%, although crustal extension locally is on the order of 60-80% (Chapter 3).

Rusizi basin (BFS9)

The Rusizi border fault segment follows the western margin of the westward-tilted Rusizi basin (Figures 4, 10). Seismicity during the period 1958-1965 within the Rusizi basin clusters along the central part of the Rusizi border fault segment, and epicentral depths throughout the range 0-30 km have been reported within the Rusizi basin (Wohlenberg, 1968; Zana and Hamaguchi, 1978). The eastern side of the Rusizi basin is bounded by facetted step faults that dip 60-75° to the west, and fault surfaces there often exhibit subvertical slickensides (Figure 11). Basalts with similar petrological characteristics as those of the South Kivu province and dated at 5-6.5 Ma have been faulted into a series of tilted blocks at the northeastern tip of the Rusizi basin, and Plio-Pleistocene lacustrine sediments onlap the late Miocene basalts (Tack and De Paepe, 1983; Ilunga,

1984; Chorowicz and Thouin, 1985; Theunissen, 1986; Theunissen, in press; Pasteels et al., in press; Chapter 3). These sediments thicken to over 1500m in the central part of the basin beneath Lake Tanganyika (D. Stone, pers. comm.). Structural and stratigraphic relations indicate that faults within the accommodation zone between the Rusizi basin and Kivu basins post-date approximately 6 Ma, and that subsidence has been much more rapid along BFS9 than along BFS8 (Chapter 3). Lacustrine sediments found in thin lenses between eastward-tilted fault blocks are elevated nearly 500m above Lake Tanganyika (Location **a**, Figure 10; Table I).

Rumonge basin (BFS10)

The sense of asymmetry within the Rumonge basin is down-to-the east, opposite to the sense of asymmetry within the Rusizi basin (Figure 4a; Figure 10). The southern tip of the Rumonge border fault segment extends beneath Lake Tanganyika where normal faults striking N10°E continue to the southwest of the Ubwari peninsula (Figure 10). The western side of the Rumonge basin is the southern tip of the Rusizi border fault segment. As along the Kivu fault systems, there is no evidence for Neogene faults along the uplifted flanks outside the rift valley, where topographic relief is gentle (Figure 4b).

Nyanza-lac basins (BFS11, 12)

The eastern side of the Ubwari peninsula is bounded by a border fault segment defining a narrow basin that is tilted to the west (Figures 10, 11). An intrabasinal horst separates the West Nyanza-lac basin bounded by BFS11 from the East Nyanza-lac basin bounded by BFS12, a half-graben tilted to the east. This geometry is similar to that of the Kivu basin. A thin sedimentary sequence overlies metamorphic basement in the northern part of the East Nyanza-lac basin, but sediment thicknesses increase to over 2.5 km to the south where the East Nyanza-lac basin is tilted to the east (Table II). Topographic relief dips gently to the east on the rift flank outside BFS12, and I find no evidence for recent faulting outside the inner-facing faults bordering the rift valley (Figures 11, 12). Based on a reconstruction of fault geometries determined from seismic profiles and field studies along the eastern side of the lake, I estimate crustal extension to be less than 20%. A balanced cross-section of this profile indicates that the depth to detachment for faults within the Nyanza-lac basin is 10-15 km, assuming plane strain (e.g., Gibbs, 1984).

Kigoma basin (BFS13)

A shallow NW-SE trending ridge separates the Nyanza-lac basin from the Kigoma basin, which is tilted to the west (Figure 4b). BFS13 extends along the western side of the rift, and nearly 4 km of sediments have accumulated at the base of this steep escarpment (Rosendahl et al., 1986). The southern end of the Kigoma basin border fault segment curves to the east and bounds a shallow ridge separating the Kigoma and Kalemie basins

(Figure 4a).

Kalemie basin (BFS14)

The northern continuation of BFS14 bounding the Kalemie basin curves to the west to become the southern border of the shallow basement ridge (Rosendahl et al., 1986). The S-shaped geometry of BFS13 and BFS14 serves to accommodate greater subsidence within the Kigoma basin than within the Kalemie basin, and a component of strike-slip displacement has been suggested along NW striking faults bounding the ridge between the two basins (Lorber, 1984). Tilted fault blocks within the Kalemie basin trend north-south (Burgess et al., in press). Along the eastern flank of BFS14 outside the rift valley, an eastward-dipping fault reactivates normal faults bounding a Mesozoic rift basin (Figure 4a; A).

Karema basin (BFS15)

A border fault segment with a northwest trend bounds the Karema basin (BFS15), and an earthquake at 12 km depth with a SW-NE tensional axis (Shudofsky, 1985), or perpendicular to the strike of BFS15, occurred along this escarpment (Figure 4a). The northeastern part of the basin is a flat shelf that lying at an elevation just above the present level of Lake Tanganyika (Figure 4). Fault patterns within the Karema basin are complicated by structures bounding the Mesozoic Rukwa rift system, and older (pre-Cretaceous) faults may have been reactivated by Tertiary movements in the accommodation zone between the Kalemie and Karema basins (Figure 4a).

Moba basin (BFS16)

The Moba basin, described in an earlier section, is bounded along the its western side by a northwest-striking border fault segment. A shallow horst separates the deeper Moba basin, described in an earlier section (Figure 4), from the Kalemie basin to the north, and a horst separates the Moba basin from the Karema basin to the northeast (e.g., Rosendahl et al., 1986). Faults bounding the Moba and Marungu basins cut undeformed and homogeneous rocks of the Precambrian Bangweulu volcanic sequence and should represent Late Cenozoic strains (Figures 2, 6). The northern part of the Moba border fault segment extends across a tectonic contact between the Bangweulu unit and an older (Archaean?) tectonic unit southwest of Moba with no change in fault orientation (x; Figure 6). On the monoclinal (eastern) side of the Moba basin, normal and strike-slip faults cut older faults. Occasionally, Late Cenozoic movements may reactivate Mesozoic normal faults, but reactivation is not commonly observed (Figure 7a).

Marungu basin (BFS17)

Faults bordering the western margin of the rift shift to a more north-south strike along the border of the Marungu basin (BFS17), described in an earlier section. The

northern projection of BFS17 beneath the lake bounds the southern margin of a basement ridge separating the Marungu and Moba basins (Figure 4a). Rapid vertical movements within the Marungu basin in Quaternary time are indicated by V-shaped valleys of present day rivers at the base of the Marungu BFS that are found at over 500m water depth (Capart, 1949).

Mpulungu basin (BFS18)

Fault systems bounding the rift valley splay at the southern end of the Mpulungu basin: faults with a southwest trend bound a narrow graben along the southwestern margin of the lake, and less than 300m of sediment have accumulated in the eastward-tilted Mpulungu basin that is bounded to the east by BFS19 (Chorowicz, 1983; Rosendahl et al., 1986). Along the uplifted eastern rift flank of the Mpulungu basin, the mid-Miocene erosional surface has been uplifted relative to the East African plateau to the east, and Pleistocene lacustrine sediments now cropping out 300m above Lake Tanganyika attest to recent movements (Grantham et al., 1958; Haldemann, 1969).

Rukwa basin (BFS19)

The Rukwa region has experienced several episodes of rifting since the Permo-Triassic, and recent exploratory drilling in the Rukwa basin reveals 200m of Neogene sediments unconformably overlying 5 km of Mesozoic sediments (Spence, 1954; Brown, 1964; D. Stone, pers. comm.). The normal fault system that bounded the eastward-tilted Mesozoic trough is located along the northeastern side of the basin, but less than 100m of displacement have occurred along this reactivated escarpment during the latest period of rifting (Peirce and Lipkov, in press). The sense of asymmetry has been down-to-the-west for the Late Cenozoic rifting episodes (Table I). Normal faults that displace Holocene lacustrine sediments of the Rukwa trough have a north-south trend that is oblique to the northwest trending Mesozoic normal faults bounding the eastern side of the Rukwa trough (Fick and Van der Heyde, 1959; Peirce and Lipkov, in press; this study). Thus, faults along the western side of the Rukwa basin that trend approximately north-south serve as the border fault system in recent rifting episodes, and the border fault for the Mesozoic basin shows only minor offsets during Tertiary rifting.

Msangano basin (BFS20)

The orientation of Neogene-Quaternary faults trend approximately north-south along the western margin of the narrow Msangano basin (BFS21), where a thin cover of sediments overlies metamorphic basement (Peirce and Lipkov, in press). Normal faults forming the border fault escarpment largely are uneroded and triangular, in comparison to the deeply dissected fault system bounding the eastern margin of the Msangano basin, (Mbozi block). Neogene lacustrine sediments similar to those found at higher elevations

within the Rukwa trough and the Songwe basin to the east suggest recent movement along these faults (Brock, 1962).

Songwe basin (BFS21)

The narrow Songwe basin is bounded on its northwestern side by a 1200m escarpment (BFS21) that comprises a series of high-angle (60-80°) step faults. This fault system is located 10-20 km to the west of an inactive border fault bounding a part of the Mesozoic Rukwa trough (Peirce and Lipkov, in press; D. Stone, pers. comm.; Chapter 3). However, a linear Jurassic-Cretaceous carbonatite body has been exhumed by recent faulting, suggesting that the Songwe border fault segment has reactivated a Mesozoic shear zone intruded by a Jurassic carbonatite, possibly an intrabasinal fault within the Mesozoic basin (Fick and Van der Heyde, 1959; Brown, 1964). Neogene basalts are found in elongate lenses along the *en echelon* eastward-tilted faults of BFS21, and 300-800m above stratigraphically equivalent units within the rift valley. The 200-300m thick sequence of Neogene lacustrine and volcaniclastic sediments overlying unconsolidated Cretaceous sediments become progressively faulted and tilted in the southern part of the basin toward the accommodation zone between the Songwe and Karonga basins (Chapter 3).

Usangu basin (BFS22)

The Usangu basin is separated from the Kenya rift system to the east by over 600 km. The Usangu basin is bounded on the western side by a system of north-south oriented normal faults that form a stair-step pattern rising to the level of the uplifted Usangu flank. I find no evidence for faulting outside the rift valley along the western flank of BFS22. The southeastern margin of the Usangu basin is bounded by a severely dissected scarp (Teale et al., 1962; this study). Several 1-5 km wide tilted blocks bounded by normal faults strike N30-40°E within the Usangu basin. Based on an interpretation of aeromagnetic data, Peirce and Lipkov (in press) suggest that metamorphic basement may be buried by 2 km of sediments and volcanics. However, Mesozoic sediments exposed elsewhere in the Rungwe province are not found in or adjacent to the Usangu basin, and basement underlies a less than 50m thick volcaniclastic sequence in the southwestern part of the basin. Likewise, a comparison of gravity anomalies (C. Bowin, pers. comm.) and basinal structures shows little evidence for a thick sedimentary sequence within the basin. The most negative Bouguer gravity anomalies correlate with Late Miocene to Recent volcanic centers to the west of the Usangu basin, and anomalies are elongate in a northwest direction, possibly marking faults within the accommodation zone between the Usangu and Karonga basins. As in the Songwe basin, the locations of volcanic centers appear to be controlled by fault patterns within in the Usangu basin (e.g., Figure 10, Chapter 3). For example, lineaments of youthful-appearing pyroclastic cones mark the footwalls and

hanging walls of northeast-oriented normal faults in the southwestern part of the Usangu basin (Figure 4).

Karonga basin (BFS23)

The Karonga basin is bounded along the northeastern side by the Livingstone escarpment, and the top of the escarpment rises 2400m above the valley floor. Vertical displacements along the Livingstone escarpment (BFS23) are greatest near the central part of the basin where the rift valley is filled by Lake Malawi (Figure 4). There is little topographic relief along the uplifted flank of the Karonga basin which dips gently to the northeast (Figure 13). The opposite side of the Karonga basin is bordered by a regional monocline of highly dissected Mesozoic sediments and metamorphic basement (Stockley, 1948; Harkin and Harpum, 1978; Crossley, 1982; this study). Within the central part of the northern Karonga basin, 10-30 km long chains of pyroclastic cones are found along both the hanging and footwall sides of tilted blocks that are bounded by approximately N30°W trending normal and oblique slip faults (Chapter 3).

Volcanic activity began approximately 8 Ma in the Rungwe province prior to or concurrent with faulting along the Usangu and Karonga border fault segments, and continues through Quaternary time (Table I; Chapter 3). The oldest known sediments in the Karonga basin were deposited at 4-5 Ma in a shallow lacustrine environment (Kaufulu et al., 1981). The Karonga basin is 300m lower than Lake Rukwa to the north, but faunal evidence argues against a hydrographic connection between Lake Rukwa and Lake Malawi (Grove, 1983). Because Rukwa lake levels were much higher in the past, drainage patterns indicate that subsidence in the Malawi trough post-dates the construction of the Poroto volcanic chain now blocking drainage from Lake Rukwa into Lake Malawi.

Malawi rift basins

The Malawi rift continues to the south of the uplifted East African plateau, and consists of 11 border fault segments that have been delineated using these same criteria (Chapter 2). Seismic stratigraphies in Malawi rift basins vary along the length of the rift, suggesting that rift segments have developed diachronously (Chapter 1). Vertical displacements along Malawi rift border fault segments vary from over 4 km in the Karonga and Nkhata Bay basins to less than 1km in the Shire basin at the southern end of the Malawi rift.

Extensional Basin Geometry

The asymmetric sedimentary basins of the Western rift valley form a narrow, discontinuous belt along the western margin of the uplifted East African plateau (Figure 14). The Western rift system, including the Malawi rift, comprises at least 32 basins bounded by approximately 100 km long systems of normal and oblique-slip faults (border

fault segments). The typical cross-sectional profile of rift basins is half-graben, although amounts of basinal subsidence vary along the length of the rift valley (Table II). The flanks of the rift outside the rift valley are uplifted 1-4 km above the elevation of the East African plateau, and the magnitude of uplift is generally greater along the border fault segment side of the basin. The excellent correlation between directions of extension predicted by earthquake focal mechanisms occurring along the length of the rift and the orientations of border fault segments indicates that Western border faults form in response to present-day extensional stresses (Figures 3,4).

These half-graben typically are separated along the length of the Western rift by fault-bounded structural highs, and a rift valley axis is poorly defined in these zones. Strike-slip and oblique-slip faults that cross-cut the rift valley commonly are found within these densely faulted interbasinal accommodation zones. Kinematically, accommodation zone faults serve to link extension along border fault segments on opposite sides of the rift, although the geometry of accommodation zone faults appears to depend upon the arrangement of border fault systems and shifts in the axis of the rift valley. These oblique-slip and normal faults also accommodate regional variations in topographic relief related to the much broader scale uplift of the East African plateau. For example, the 700m elevation drop in elevation from the Kivu basin to the Rusizi basin is accommodated by the northern tip of the Rusizi border fault segment and a southern continuation of normal faults bounding the East Kivu basin. Faults within several accommodation zones have been operative throughout the evolution of basins, although the geometry of accommodation zones may have changed with time and continued extension within basins (e.g., Karonga basin; Chapter 3).

The location of volcanic provinces and volcanic centers within these provinces shows several consistent correlations with rift basin structures. In a regional sense, the Toro-Ankole, Virunga, South Kivu, and Rungwe volcanic provinces coincide with these interbasinal accommodation zones (Figures 3, 4; Table II). Within these volcanic provinces, volcanic centers occur along the tips of border fault segments and along oblique-slip faults linking basins. These volcanic lineaments often cross-cut the rift valley, as in the Virunga province (Pouclet, 1975). Eruptive centers within the volcanic provinces are restricted to rift basins within inner facing faults, although in some instances basalts from young pyroclastic cones located along border faults have flowed down outward-tilted margins flanking the rift valley and away from the rift valley. The general occurrence of volcanic centers along the tips of border fault segments and along oblique-slip faults linking basins suggests that these faults remain steep to greater depths than do the central parts of border fault segments. Faults within accommodation zones appear to control volcanism

throughout the history of basins; the Poroto Mountains form an east-west lineament separating the northern Karonga basin from the Songwe basin, and this active volcanic chain formed early in the development of the these basins.

Three structural relations consistently observed along the length of the Western rift valley strongly suggest that zones of crustal thinning are limited to rift basins bounded by approximately 100 km long border fault segments and do not extend outside the basins. First, few faults occur on the uplifted flanks outside inner-facing normal faults bounding the rift valley. Secondly, along the length of the Western rift system oblique-slip faults linking basins do not appear to extend outside the rift valley across the rift flanks. Thirdly, the location of volcanic centers with respect to rift basin structures reflects a lack of faulting along the rift flanks: volcanic centers are restricted to within fault bounded rift basins.

Balanced cross-sections indicate that less than 20% crustal extension (5-10 km) has occurred across several Western rift basins, assuming that faults are planar at mid-crustal levels. Depth to detachment calculations within several rift basins indicate that normal faults extend to depths of 12-15 km (Figure 12; Chapter 3). If deformation internal to fault blocks noted within the Kivu basin is common, then these estimates of crustal extension represent minumum estimates, and the low-angle fault geometries would tend to decrease the calculated depth to detachment as well.

Mechanical models proposed to explain alternating basinal asymmetries assume that border fault segments serve as detachments for crustal and/or lithospheric extension; differences among the models are related to the location of zones of subcrustal lithospheric thinning (Bally, 1982; Gibbs, 1984; Wernicke, 1985; Bosworth, 1987). No direct observations of border fault detachments at depth beneath the Western rift valley have been made, but earthquake epicentral depths throughout the range of 20-30 km (e.g., Zana and Hamaguchi, 1978; Shudofsky, 1985) suggest that border fault systems penetrate the crust. This interpretation is consistent with border faults that are linked by steeply-dipping strike-slip and oblique fault zones, leading to a spoon-shaped basinal morphology (e.g., Chenet and Letouzey, 1983; Rosendahl et al., 1986; Ebinger et al., 1987). Bosworth (1987) suggested that subcrustal lithospheric-scale detachments beneath the rift flanks opposite to the sense of border faults accommodate shifts in the axis of the Kenya rift valley. However, there is no evidence for faulting or volcanic activity along the flanks of Western rift basins, and approximately symmetric zones of uplift are found along the length of the Western rift system (e.g., Figure 1).

The occurrence of border fault segments along both sides of extensional basins (full graben) requires a more complicated geometry than the spoon-shaped fault systems described above, if both border fault segments are active synchronously (e.g., Mohr,

1987). Observations within the Kivu basin suggest that the West Kivu border fault segment accommodates crustal extension, and that the West Kivu border fault segment has been abandoned. The East Kivu border fault segment may have formed prior to the West Kivu border fault segment, followed by the development of the Rusizi basin to the south and the West Kivu border fault segment (e.g., Chapter 3). Faults bounding the western side of the Kivu basin appear more youthful than along the eastern side, the western scarp is more active seismically, and a line of Pleistocene to historically active pyroclastic cones is found along the southwestern part of the escarpment (Wohlenberg, 1968; Guibert, 1977a). These observations suggest that the eastern border fault segment now may be inactive, and that extension is occurring along the western border fault segment of the Kivu basin.

The geometrical relations noted above are not unique to the Western rift system, as similar patterns of alternating basinal asymmetries, border fault segmentations, and geometries of border fault linkage have been described along the length of the Kenya rift system (King, 1978; Bosworth, 1985; Baker, 1986). Seismic data from the Kenya rift valley also indicate that crustal thinning is restricted to the rift valley regions, and that high-velocity regions beneath the rift valley interpreted as magmatic intrusions do not extend beneath the rift flanks (Maguire and Long, 1976; Long and Backhouse, 1976; Bram and Schmeling, 1978; Hebert and Langston, 1985; Savage and Long, 1985; KRISP, 1987). However, the occurrence of volcanic centers within the Western rift system differs from the location of volcanic centers within the Turkana rift, part of the Kenya rift system, where Dunkelman et al. (1988) report a correlation between volcanic centers and the central part of rift basins.

Timing of Crustal Movements in East Africa

Due to the along-axis variations in elevation and possible fluctuation of lake levels in the Western rift valley, it is difficult to establish a horizontal datum for vertical movements during the development of individual basins. However, several indirect lines of evidence indicate that uplift of the rift flanks superimposed on the plateau topography was concurrent with or post-dated initial basinal subsidence along the length of both the Western and Kenya rift systems. The oldest known Western sedimentary sequences are mid-Pliocene (5 Ma); changes in drainage patterns across the plateau indicate that rift flank uplift was most rapid during Late Pliocene or Pleistocene time (Bishop and Posnansky, 1960; Holmes, 1978; Grove, 1983; Baker, 1986). During late Pliocene or Pleistocene time, rates of uplift along the northeastern flanks of the Western rift system exceeded rates of downcutting along several rivers that previously had flowed north into the Nile drainage basin, and rivers that originally flowed west into the Congo basin were diverted by uplift along the eastern flanks of the rift (Bishop and Posnansky, 1960; Holmes, 1978; Grove,

1983; Baker, 1986). These rivers are now ponded in shallow lakes in the central part of the uplifted plateau between the Western and Kenya rift systems (Figure 14). Late Pleistocene uplift along the eastern margin of the Kivu and northern Tanganyika rift basins produced eastward-tilted strand lines along the western margin of Lake Victoria (Bishop and Posnansky, 1960).

Stratigraphic relations within rift basins indicate that the zone of subsidence has narrowed with time, and terraces of lacustrine sediments along the rift valley escarpments commonly are elevated from lake level highstands by up to 800m (Table II). These narrow terraces are found near the central parts of asymmetric basins where maximum amplitudes of subsidence occur, and as lenses along faults with minor displacements on the monoclinal side of basins. Lacustrine sediments, if exposed, are found at elevations below these terraces at the ends of the spoon-shaped basins. Thus, in order to maintain a water-filled basin, the terraces were uplifted with the rift flanks relative to the subsiding basin. The morphology of step faults along border fault segments indicates that the innermost triangular fault is active, as higher scarps are deeply dissected, and basin margins beneath the lake are steep (>45°). This narrowing of the basins appears to be synchronous with uplift along both sides of rift basins (e.g., Chapter 3). In the Kenya rift system, a similar narrowing of the central graben has been noted, and lateritized Late Pliocene-Pleistocene basalts found along uplifted flanks formed at much lower elevations than present-day (King, 1978; Crossley, 1982).

Initial volcanic activity preceded faulting in the Western rift system, and this early Miocene volcanism occurred in isolated centers across the central part of the uplifted region prior to faulting and basinal subsidence (Baker et al., 1971). Major differences between the Kenya and Western rift systems primarily are related to the volume, timing, and areal extent of magmatic activity. Volcanic activity in the northern and middle part of the Kenya rift valley commenced 11-5 My prior to volcanic activity in the Western rift system (Figure 15). During the past 10 My, magmatic activity has localized to the fault bounded basins of the present-day Western and Kenya rift valleys where active volcanoes are located along faults and fissures (Baker, 1986). Vertical movements along high-angle step faults comprising border fault escarpments displace initial flows now capping the uplifted flanks from stratigraphically equivalent units in the rift valley, often by over 1 km. Considering the temporal development of propagating rift basins in East Africa, Pliocene-Holocene shield volcanoes along the flanks of the Kenya rift (Mts. Kenya and Kilimanjaro) may mark incipient zones of crustal extension. However, the tectonic relationship between accommodation zones and volcanic provinces in the Western rift system is not found in the Kenya rift system (e.g., Dunkelman et al., 1988). Considering the much longer history of

volcanism within the Kenya rift and that the earliest centers are obscured by later flows in the Kenya rift, most of the differences between the two rift systems can be interpreted as differences in stage of development.

Along-axis segmentation

One proposed mechanism for the along-axis segmentation of continental rift zones and the shifts in basinal asymmetry along the length of the rift valley and orientation of normal and strike-slip faults in transfer fault zones is that these faults reactivate pre-rift structures or pre-existing crustal shear zones (Dixey, 1956; McConnell, 1972; Villeneuve, 1978; Peirce and Lipkov, in press). The general outline of the Western rift system follows the surface expression of Precambrian orogenic belts and avoids the cratonic areas within the East African plateau region. This pattern may indicate that the continental lithosphere is weaker beneath the orogenic belts (see Figure 2). Perhaps the initial location of volcanic centers within the 1300 km wide East African plateau were controlled by pre-existing weaknesses within the continental lithosphere, but Neogene volcanic centers rarely, if ever, are found along Mesozoic fault systems (e.g., Songwe basin).

At a shorter length scale, a comparison of individual faults comprising Western rift border fault segments to pre-rift structures reveals a poor correlation between pre-rift metamorphic fabrics and recent fault orientations (Figures 6, 7, 10, 12). In most instances, faults extend across contacts between tectonic units (e.g., Moba basin) or cross-cut structures in metamorphic basement (Hopwood, 1970; Haldemann, 1969; Crossley and Crow, 1980; Ebinger et al., 1987). Mesozoic normal faults rarely are rejuvenated in the Late Cenozoic rifting episodes, and no young volcanic centers have been found along Mesozoic fault systems within the Songwe and Usangu basins. For example, lineaments of eruptive centers within the Usangu basin strike northeast and show no correlation with east-west and northwest-oriented basement faults. Exceptions to this generalization are normal faults along the flanks of the Kalemie border fault segment (BFS14) and the Songwe border fault segment (BFS21). In part of the Western rift where basement faults and metamorphic foliations have a dominant north-south trend, or subparallel to the regional orientation of the Western rift system, there is little evidence for reactivation of pre-rift shear zones (e.g., Chapter 3). Thus, the Western and Kenya rift segmentation and basinal morphologies generally represent the mechanical response of the continental lithosphere to Neogene-Quaternary rifting processes. Similarly, faults bounding Kenya rift basins show little correlation with the orientations of pre-rift structures (King, 1978; Chapter 3).

A second proposed mechanism for the sinuous outline of border fault systems bounding the Western rift valley is changing stress orientations during discrete episodes of

rifting. Although the timing of faulting in many parts of the Western rift system is poorly constrained, I find little evidence in the field that the orientations of border fault segments change betwen successive episodes of rifting. For example, the strike of fault systems that displace Miocene volcanic units are subparallel to active fault systems (see Chapter 3). However, the geometry of accommodation zones may change with continued extension and subsidence within rift basins. Because amounts of subsidence and possibly crustal extension vary from basin to basin along the length of the rift valley, in part due to differences in age, fault systems between basins accommodate both vertical and horizontal displacements. The geometry of this linkage contributes to the sinuous outline of the rift valley.

Some authors have suggested that rift segmentation is a fundamental feature of propagating rift systems, both continental and oceanic (Ebinger et al., 1984; Bosworth, 1985; Bonatti, 1985; Rosendahl et al., 1986). A north-south age progression in volcanic activity has been recognized in the Kenya rift, and a similar north-south propagation of rifting has been suggested based on geomorphological evidence in the Western rift system (Capart, 1949; Haldemann, 1969; Shackleton, 1978; Crossley and Crow, 1980; Williams and Chapman, 1986; Bosworth, 1987). Volcanic activity within the Western rift system also supports a north-south age progression (e.g., Table I; Chapter 3). Existing data from Western sedimentary sequences are insufficient to document a systematic age progression in sedimentary sequences, but I suggest that the basinal segmentation of the Western rift valley border fault system likewise is a product of this diachronous development of individual sedimentary basins.

A rift propagation model for the observed segmentation of the Western rift valley is supported by studies of oceanic spreading centers. The geometrical arrangement of border fault segments and fault patterns linking basins in the Western rift system, which generally are independent of older structures, are similar to morphologic patterns observed along propagating oceanic spreading centers and in theoretical models of crack propagation (e.g., Pollard and Aydin, 1984; Sempère and MacDonald, 1986). This interpretation suggests that the rift valley segmentation is not merely a feature of oceanic crust and lithosphere, but that it is a more fundamental tectonic process. However, further studies are needed to extend these results to the more rheologically complicated continental lithosphere.

Conclusions

The discontinuous Western rift valley is bounded by a series of border fault segments, or detachment faults, that border one or both sides of approximately 100 km long sedimentary basins that often are linked along the length of the rift system by oblique-slip and strike-slip faults. Border fault segments with 1-6 km of vertical displacement are

regionally curvilinear in map view, although the border fault segments comprise normal and oblique-slip faults that generally are linear. Western rift volcanic provinces cover interbasinal regions along the length of the rift valley, and eruptive centers are largely controlled by fault patterns within and between basins. The spatial distribution of fault systems and volcanic centers indicate that the zone of extension is restricted to rift basins bounded by border fault segments. Thus, extensional provinces within the 1300 km wide, 1250m high East African plateau region are restricted to the 40-75 km wide Western and Kenya rift valleys.

Volcanic activity commenced at 12 Ma in the northern part of the Western rift system and at 8 Ma in the southern part of the rift (Rungwe province), and many sedimentary basins formed during late Miocene and Pliocene times. Much of the uplift in 150-200 km wide regions flanking the Western rift valley superimposed on the East African plateau post-dates initial volcanism and basinal subsidence. These patterns in the spatial and temporal development of the Western rift valley are similar to those observed in the Kenya rift system on the eastern margin of the uplifted plateau, although volcanism and faulting commenced 12 My prior to volcanism in the Western rift system.

The poor correlation between the orientations of faults comprising border fault segments and pre-rift structures and metamorphic fabrics indicates that border fault geometry is not inherited from previous episodes of crustal deformation, although segments of faults bounding Mesozoic sedimentary basins locally may be reactivated along the uplifted rift flanks. Rift basins within the Western rift system have developed diachronously, and a north to south propagation of surface faulting may have caused the observed segmentation of the Western rift valley. The geometry of rift basin linkage in the Western rift system is similar to that of oceanic propagating rift segments, although extensional basins in East Africa are underlain by rheologically more complicated continental lithosphere.

Acknowledgements

Permission to conduct field research was granted by the Ministère de l'Energie, des Mines, et des Artisanats, Rwanda; Dept. de l'Energie et des Mines, Burundi; UTAFITI (Tanzanian National Scientific Research Council), and Institut de la Rècherche Scientifique (Zaïre). J.Nanyaro (University of Dar es Salaam), K. Theunissen and J. Klerkx (Musée Royal de l'Afrique Centrale), L. Tack, (University of Bujumbura), A. Tesha, J. Knight, L. Willey, S. Townsend, P. Tilke, P. Eeckelers, and many Peace Corps volunteers provided invaluable assistance in field areas. Revisions suggested by L. Royden, K. Hodges, M. Daly greatly improved the text. I thank J. Klerkx, K. Theunissen, L. Tack, and B. Rosendahl for use of unpublished information, and P. Williamson, A. Cohen, D. Livingstone, and D. Grove for helpful discussions. I gratefully acknowledge Mobil Oil Exploration Production for photographic reproduction of Thematic Mapper imagery, and Amoco Production for making available proprietary data used in basinal analyses. This project was funded by an NSF Presidential Young Investigator Award granted to L. Royden; Geological Society of America Research grant 3754-87, Sea Grant NA84-AA-D-00033, R/G-11; and NSF grant EAR-84-18120.

Appendix

Landsat-5 Multi-Spectral Scanner (MSS) and Thematic Mapper (TM) images used in this study cover 170 km by 185 km regions. Standard radiometric and geometric corrections were made at the EROS processing center, and images are displayed using a space oblique Mercator projection that preserves length and angular relations. False-color composite images corresponding to Scenes 1, 2,3, and 4 were generated from reflectance data in bands 2 (0.5-0.6 μm), 4 (0.6-0.7 μm) and 5 (0.8-1.1 μm), displayed as blue, green and red, respectively. Digital data from TM scene 4 (Figure 1) were processed to enhance faults, lineaments and to distinguish volcanic units using a variety of filtering, color ratioing, and contrast stretching techniques. MSS images 1-4 shown in Figure 1 are E-50870-07370, E-50143-07380, and E-50143-07382; TM image is Y-50850-07204. Quality of data is excellent; cloud cover was less than 20% in Scene 2, and less than 10% in Scenes 1, 3, 4, and 5.

References

Afonso, A., 1976, A geologia de Moçambique: Dir. Serv. Geol. Minas, Maputo, Mozambique, 142pp.

Arambourg, C., 1933, Les formations pré-tertiaires de la bordure occidentale du Lac Rodolphe (Afrique Orientale): Comptes Rendus Academie Science Paris, v. 197, p. 1663-1665.

Bagdasaryan, G.P., Gerasimovskiy, V.I., Polyakov, A.I. , and Gukasyan, R.Kh., 1973, Age of volcanic rocks in the rift zones of East Africa: Geochemistry International, v. 1973, p. 66-71.

Baker, B.H., 1986, Tectonics and volcanism of the southern Kenya Rift Valley and its influence on rift sedimentation: *in* L.E. Frostick, et al., eds., *Sedimentation in the East African Rifts*, Geological Society London Special Publication 25, p. 45-57.

Baker, B.H., Williams, L.A.J., Miller, J.A., and Fitch, F.J. , 1971, Sequence and geochronology of the Kenya rift volcanics: Tectonophysics, v. 11, p. 191-215.

Bally, W., 1982, Musings over sedimentary basin evolution: Royal Society London Philosphical Transactions, A305, p. 325-328.

Bellieni, G., Justin-Visentin, E., Zannetin, B., Piccirillo, E.M., Radicati, D.I., Brozolo, F., Rita, F., 1983, Oligocene transitional tholeiitic magmatism in northern Turkana (Kenya): comparison with coeval Ethiopian volcanism: Bulletin Volcanology, v. 44, p. 411-427.

Bellon, H., and A. Pouclet, 1980, Datations K-Ar de quelques laves du Rift-ouest de l'Afrique Centrale; Implications sur l'évolution magmatique et structurale: Geologische Rundschau, v. 69, p. 49-62.

Bishop, W.W. and M. Posnansky, 1960, Pleistocene environments and early man in Uganda: Uganda Journal, v. 24, p. 44-61.

Bosworth, W., 1985, Geometry of propagating continental rifts: Nature, v. 316, p. 625-627.

Bosworth, W., 1987, Off-axis volcanism in the Gregory rift, East Africa: Implications for models of continental rifting: Geology, v. 15, p. 397-400.

Boutakoff, N., 1939, Géologie des territoires situés a l'Ouest et au Nord-Ouest du fossé tèctonique du Kivu: Memoirs Institut Géologie University Louvain, t .IX, p. 23-161.

Bram, K., and Schmeling, B.D., 1975, Structure of crust and upper mantle beneath the Western Rift of East Africa, derived from investigations of near earthquakes: *in* A.Pilger and A. Rosler, eds., *Afar Between Continental and Oceanic Rifting*, Schweizerbart, Stuttgart, p. 138-142.

Brock, P.W.G., 1962, Tundumu rift valley: Univ. Leeds 6th Annual Report, Leeds, p. 31.

Brown, C., and Girdler, R.W., 1980, Interpretation of East African gravity data and its implications for the breakup of the continents: Journal Geophysical Research, v. 85, p. 6443-6455.

Brown, P., 1964, The Songwe scarp carbonatite and associated feldspatization in the Mbeya range, Tanganyika: Quarterly Journal Geological Society London, v. 120, p. 223-240.

Burchfiel, B.C., and J.Stewart, 1966, The "pull-apart" origin of Death Valley, California: Geological Society America Bulletin, v. 77, p. 439-442.

Burgess, C., Rosendahl, B.R., Sander, S., Burgess, C.A., Lambiase, J., Derksen, S., and Meader, N., in press, The structural and stratigraphic evolution of Lake Tanganyika: A case study of continental rifting: *in The Triassic System of the Eastern United States*, American Association Petroleum Geologists Special Publication

Cahen, L., and I. Snelling, 1984, The geochronology and evolution of Africa: Clarendon Press, Oxford, 591p.

Capart, A., 1949, Sondages et carte bathymetrique: *in Exploration Hydrobiologique du lac Tanganyika (1946-1947)* : Brussels, Institut Royal Sciences Naturelles Belge, p. 1-16.

Carter, G., and J. Bennett, 1973, The geology and mineral resources of Malawi: Bull. Geological Survey Department Malawi, v. 6, 62p.

Chenet, P-Y., and J. Letouzey, 1983, Tèctonique de la zone comprise entre Abu Durba et Gebel Mezzazat (Sinai, Egypte) dans le contexte de l'évolution du rift du Suez, Bulletin Centres Recherches Exploration Production Elf-Aquitaine, v. 7, p. 201-215.

Chorowicz, J., 1983, Le rift est-africain: debut de l'ouverture d'un ocean?: Bulletin Centres Récherches Exploration Production Elf-Aquitaine, v. 7, p. 155-162.

Chorowicz, J., and C. Thouin, Failles synsedimentaires et structure de la plaine de la Rusizi (Nord Tanganyika), Comptes Rendus Royal Academie Science Paris, t. 301, 835-841, 1980.

Coetzee, G., 1964, Carbonatites of the Karema depression, western Tanganyika: Transactions Geological Society S. Africa, 64, p. 283-340.

Coffin, M., and P. Rabinowitz, P., 1983, East African continental margin transect, in: A.W. Bally, ed., *Structural Styles,* American Association Petroleum Geology Studies in Geology, #2, 2.3.3-22.

Combe, A.D., 1943, The geology of the southern part of Ruwenzori: Annual Report Geological Survey Uganda for 1943, p. 4-15.

Courtillot, V., R. Armijo, P. Tapponnier, 1987, The Sinai triple junction revisited: Tectonophysics, v. 141, p. 181-190.

Crossley, R., 1982, Late Cenozoic stratigraphy of the Karonga area in the Malawi rift: *in* J.A. Coetzee and E.M. van Zinderen Bakker: *Paleoecology of Africa*, Rome, v. 15, p. 139-144.

Crossley, R. and M.J. Crow, 1980, The Malawi rift, *in* Geodynamic Evolution of the Afro-Arabian rift system, Rome, p. 77-87.

Crossley, R., and R. M. Knight, 1981, Volcanism in the western part of the rift valley in southern Kenya: Bulletin Volcanology, v. 44-2, p. 117-128.

Daly, M.C., 1986, Crustal shear zones and thrust belts: Their geometry and continuity in Central Africa: Phil. Trans. Roy. Society Lond., A317, p. 111-128.

Davies, K.A., 1951, The Uganda section of the Western Rift: Geology Magazine, v. 88, p. 377-385.

De Mulder, M., and Pasteels, P., 1986, K-Ar geochronology of the Karisimbi volcano (Virunga, Rwanda-Zaire): Journal African Earth Sciences, v. 5, p. 575-579.

Degens, E.T., Von Herzen, R.P., and H-K. Wong, 1971, Lake Tanganyika: Water chemistry, sediments, and geological structure: Naturwissenschaften, v. 58, p. 229-241.

Degens, E.T., Von Herzen, R.P., Wong, H.K., Deuser, W.G., and Jannasch, H.W., 1973, Lake Kivu: Structure, chemistry, and biology of an East African rift lake: Geologische Rundschau, v. 62, p. 245-277.

de la vallee Poussin, M., Quelques faits nouveaux apropos du graben central africain: Bulletin Société Belge Geologique, v. 43.

Dixey, F., 1956, The East African rift system, Colonial Geological Mineral Resources, No. 1.

Dunkelman, T.J., Karson, J.A., and Rosendahl, B.R., 1988, Structural style of the Turkana rift Kenya: Geology, v. 16, 258-261.

Ebinger, C.J., M.J. Crow, B.R. Rosendahl, D.L. Livingstone, and J. LeFournier, 1984, Structural evolution of Lake Malawi, Africa: Nature, v. 308, p. 627-629.

Ebinger, C., Rosendahl, B. and Reynolds, D., 1987, Tectonic model of the Malawi rift, Africa: *in* Z. Ben-Avraham, ed., *Sedimentary Basins within the Dead Sea and Other Rift Zones*, Tectonophysics, v. 141, p. 215-235.

Fairhead, J. and R.W. Girdler, 1969, How far does the rift system extend through Africa?: Nature, v. 221, p. 1018-1020.

Fairhead, J., and Stuart, G., 1982, The seismicity of the East African rift system and comparison with other continental rifts, *in* G. Palmason, ed., *Continental and Oceanic Rifts*, American Geophysical Union: Washington, D.C., p.41-61.

Fick, L.J., and C. Van der Heyde, 1959, Additional data on the geology of the Mbeya carbonatite: Economic Geology, v. 54, p. 842-872.

Gibbs, A.D., 1984, Structural evolution of extensional basin margins, Journal Geological Society London, v. 141, p. 609-620.

Grantham, D.R., Teale, E.O., Spurr, A.M., Harkin, D.A., and Brown, P.E., 1958, Geological Survey Tanganyika Quarter Degree Sheet 224 (Mbeya).

Gregory, J., 1896, *The Great Rift Valley*: London, John Murray, 405p.

Grove, A.T., 1983, Evolution of the physical geography of the East African rift valley region, *in* R.W. Sims, J.H. Price, and P.E.S. Whalley, eds., *Evolution, Time, and Space: The Emergence of the Biosphere*, London: Academic Press, p. 115-155.

Guibert, Ph., 1977a, Contribution a l'étude du volcanisme du Sud-Kivu (Zaïre): I: La chaine volcanique Tshibinda-Kalehe: Archive Science Genève, v. 30, p. 15-27.

Guibert, Ph., 1977b, Contribution a l'étude du volcanisme du Sud-Kivu (Zaïre): II: Les épanchements basaltiques anciens et recents de l'île Idjwi: Archive Science Genève, v. 30, p. 29-43.

Haldemann, E.G., 1969, Geological and physiographical setting of the Kalambo Falls prehistoric site, in: J. D. Clark, ed., *Kalambo Falls Prehistoric Site*, Cambridge: Univ. Press, p. 20-45.

Harkin, D.A., 1960, The Rungwe volcanics at the northern end of Lake Nyasa: Geological Survey Tanganyika Mem. II, 172p.

Harkin, D.A., and J.R. Harpum, 1978, Quarter Degree Sheet 78 (Tukuyu): Geol. Surv. Tanganyika .

Hebert, L., and C. Langston, 1985, Crustal thickness estimate at AAE (Addis-Ababa, Ethiopia) and NAI (Nairobi, Kenya) using teleseismic P-wave conversions: Tectonophysics, v. 111, p. 299-327.

Holmes, A., 1978, *Holmes Principles of Physical Geology*, New York: John Wiley and Sons, p. 647-657.

Holmes, A., 1951, Evidence of lava formation *in situ*, south-west Uganda, Geological Magazine, v. 88, p. 73-87.

Hopwood, A.M., 1970, Structural reorientation as evidence of basement warping associated with rift faulting in Uganda: Geological Society of America Bulletin, v. 81, p. 3473-3480.

Hopwood, A., and Lepersonne, J., 1953, Presence de formations d'age miocene inferieur dans le fossé tèctonique du lac Albert, Annals Société Géologique Belge, t. 77, p. 83-113.

Ilunga, L.K., 1984, Le quaternaire de la plaine de la Ruzizi, [Thèse doctorat]: Bruxelles, Belgium, University Bruxelles, 340p.

Kaufulu, Z., E. Vrba, and T. White, 1981, Age of the Chiwondo beds, northern Malawi, Annals Transvaal Museum, v. 33, p. 1-8.

Kent, P.E., J.A. Hunt, and D.W. Johnstone, 1971, The geology and geophysics of coastal Tanzania: Institute Geological Sciences, Geophysical Paper 6, 101p.

King, B.C., 1978, Structural and volcanic evolution of the Gregory rift valley, *in* W.W. Bishop, ed., *Geologic Background to Fossil Man*, Edinburgh: Scottish Academic Press, p. 29-54.

KRISP, 1987, Working Group, Kenya Rift International Scientific Project: Preliminary results: Nature, v. 325, p. 239-242.

Lepersonne, J., 1977, Carte géologique du Zaïre, Rep. Zaïre: Musée Royal de l'Afrique Centrale, Tervuren, Belgium (1:2,000,000).

Lavreau, J., V. Patricec, and Waleffe, A., 1981, Carte lithologique du Rwanda (1:250,000): Musée Royal de l'Afrique Centrale, Tervuren, Belgium.

Lister, L., 1967, Erosional surfaces in Malawi: Records Geological Survey Malawi, No. 7, p. 15-28.

Long, R. and Backhouse, R., 1976, The structure of the western flank of the Gregory Rift (Kenya). Part II: The mantle: Geophysical Journal Royal Astronomical Society, 44, p. 677-688.

Lorber, P.M., 1984, The Kigoma basin of Lake Tanganyika: Acoustic stratigraphy and structure of an active continental rift, [M.S. Thesis], Duke Univ., Durham, North Carolina, 76p.

Maguire, P., and Long, R., 1976, The structure of the western flank of the Gregory Rift (Kenya), Part I: The crust: Geophysical Journal Royal Astronomical Society, v. 44, p. 661-675.

McConnell, R.B., 1972, Geological development of the rift system of eastern Africa, Geological Society of America Bulletin, v. 83, p. 2549-2572.

Mohr, P.A., 1987, Structural style of continental rifting in Ethiopia: Reverse décollements: EOS, Transactions American Geophysical Union, v. 68, p. 721-729.

Pasteels, P., P. De Paepe, M. Villeneuve, and J. Klerkx, in press, Age of the volcanism of the southern Kivu area (Western Rift: Burundi, Rwanda, Zaire), Earth and Planetary Science Letters.

Patterson, M.B., 1983, Structure and acoustic stratigraphy of the Lake Tanganyika rift valley, [M.S. Thesis], Duke University, Durham, North Carolina, 89p.

Peirce, J., and L. Lipkov, in press, Structural interpretation of the Rukwa rift, Tanzania: Geophysics.

Pentel'kov, V., and S. Veronovskiy, 1979, Radiometric age of the Mbalizi carbonatite, Tanzania, and correlation with other carbonatites of the Rukwa-Malawi zone: Dokl. Akad. Nauk SSR, v. 235, p. 1136-1139.

Pickford, M., 1987, Implications of the Albertine (Uganda) fossil mollusc sequence, Comptes Rendus Academie Science Paris, t.305, p. 317-322.

Pollard, D.D., and A. Aydin, 1984, Propagation and linkage of oceanic ridge segments: Journal Geophysical Research, v. 89, p. 10,017-10,028.

Pouclet, A., 1977, Contribution a l'étude structurale de l'aïre volcanique des Virunga, rift de l'Afrique centrale: Revues Géographie Physique Géologie Dynamique, v. XIX, p. 115-124.

Pouclet, A., 1975, Histoire des grands lacs de l'Afrique centrale: Mise au point des connaissances actuelles: Revues Géographie Physique Géologie Dynamique, v. XVII, p. 475-482.

Pulfrey, W., 1960, Shape of the sub-Miocene erosion bevel in Kenya: Bulletin Geological Society Kenya, v. 3.

Quennell, A.M., A.C.M. McKinlay, W.G. Aitken, 1956, Summary of the geology of Tanganyika: Memoirs Geological Survey Tanganyika, 264p.

Reeves, W., 1960, Geologic map of Northern Rhodesia, Geological Survey Department Rhodesia, 1: 1,000,000.

Rodrigues, E.B., 1970, Seismological studies of the East African rift system, [Ph.D. Dissertation], Nairobi, Kenya: University of East Africa, 187p.

Rosendahl, B., Reynolds, D., Lorber, P., D. Scott, J. McGill, J. Lambiase, 1986, in L.E. Frostick, et al., eds., *Sedimentation in the East African Rifts*: Geological Society London Special Publication No. 25, p. 29-34.

Rykounov, L.N., Sedov,V.V., Savrina, L.A. , and Bourmin, V.J., 1972, Study of microearthquakes in the rift zones of East Africa: *in* R.W. Girdler, ed., *East African rifts*, Tectonophysics, v. 15, p. 123-130.

Saggerson, E.P., and B.H. Baker, 1965, Post-Jurassic erosion surfaces in eastern Kenya and their deformation in relation to rift structure: Quarterly Journal Geological Society London, v. 121, p. 5-72.

Savage, J.E.G., and R.E. Long, 1985, Lithospheric structure beneath the Kenya Dome: Geophysical Journal Royal Astronomical Society, v. 82, p. 461-477.

Sempère, J.-C., and K. MacDonald, 1986, Overlapping spreading centers: Implications from crack growth simulation by displacement continuity method: Tectonics, v. 5, p. 151-163.

Shackleton, R.M., 1978, Structural development of the East African rift system, *in* W.W.Bishop, ed., *Geologic Background to Fossil Man*, p. 20-28.

Shudofsky, G.N., 1985, Source mechanisms and focal depths of East African earthquakes using Rayleigh wave dispersion and body-wave modelling: Geophysical Journal Royal Astronomical Society , v. 83, p. 563-614.

Spence, J., 1954, The geology of the Galula Coalfield, Mbeya district: Geological Survey Tanganyika, v. 25 , 34p.

Stockley, G., 1948, Geology of north, west, and central Njombe district, southern highlands province, Geological Survey Department Tanganyika, 68p.

Stoffers, P., and Hecky, R.E., 1978, Late Pleistocene-Holocene evolution of the Kivu-Tanganyika basin, Special Publication International Association of Sedimentologists, v. 2, p. 43-55.

Tack, L., and DePaepe, P., 1983, Le volcanisme du Sud-Kivu dans le nord de la plaine de la Rusizi au Burundi et ses rélations avec les formations géologiques avoisinantes, Rapport Annuel Musée Royal de l'Afrique Centrale, v. 1981-1982, p. 137-145.

Teale, E.O., Eades, N.W., Harkin, D.A., Harpum, J.R., and Horne, R.G., 1962, Geological Survey Department Tanganyika, Quarter Degree Sheet, 245 (Irambo).

Theunissen, K., Carte géologique de Burundi, Feuille Rumonge, Ministère Travaux Publiques, Energie, Mines, Burundi, 1986.

Theunissen, K., Carte géologique de Burundi, Feuille Cibitoke, Ministère Travaux Publiques Energie Mines, Burundi, in press.

Theunissen, K., Carte géologique du Burundi, Feuille Bujumbura, Ministère Travaux Publiques Energie Mines, Burundi, in press.

Tshimanga, K., and Kabengele, M., 1981, Quelques données structurales sur la region des Marungu, Shaba (Zaïre): Cahiers Géologiques University Paris, v. 98, p. 456-463.

Villeneuve, M., 1983, Les sillons tectoniques du precambrien superieur dans l'est du Zaïre; comparaisons avec les directions du rift Est-Africain, Bulletin Centres Récherches Exploration Production Elf-Aquitaine, v. 7, p. 163-174.

Wayland, E.J., 1934, Peneplains and some other erosional platforms: Geological Survey Uganda, Annual Report 1933, p. 77-79.

Wernicke, B., 1985, Uniform-sense normal simple shear of the continental lithosphere, Canadian Journal of Earth Sciences, v. 22, p. 108-125.

Williams, L.A.J., and Chapman, G.R., 1986, Relationships between major structures, salic volcanism and sedimentation in the Kenya rift from the equator north to Lake Turkana: *in* L.E. Frostick, et al., eds., *Sedimentation in the East African Rifts*, Geological Society London Special Publication 25, p. 59-74.

Williamson, P., and R.J. Savage, 1986, Early rift sedimentation in the Turkana basin, northern Kenya: *in* L.E. Frostick, et al., eds., *Sedimentation in the East African Rifts,* Geological Society London Special Publication 25, p. 267-284 .

Wohlenberg, J., 1968, Seismizitat der ostafrikanischen Grabenzonen zwischen 4°N und 2°S sowie 23°E und 40°E: Veroffentlichung der Bayerischen Kommission fur die Internationale Erdmessung, v.43, 95p.

Wong, H-K, and Von Herzen, R.P., 1974, A geophysical study of Lake Kivu, East Africa: Geophysical Journal Royal Astronomical Society, v. 37, p. 371-389.

Zana, N., and N. Hamaguchi, 1978, Some characteristics of aftershock sequences in the Western rift valley of Africa: Sci. Rep. Tôhoku Univ., Ser. 5, Geophysics, 25: 55-72.

Table I

Chronologic Constraints on East African Rift Movements			
Site	Description	Age (Ma)	Reference
A	N. Turkana basalts	31.5±1.6	Bellieni et al., 1981
B	Samburu basalts, K/Ar	23.0±0.2	Baker et al., 1971
C	Mt. Elgon nephelinite, K/Ar	22.0±0.2	"
D	Rusinga Island tuff, K/Ar	21.7	"
E	Koro carbonatite tuff, K/Ar	19.9±0.6	"
F	Rangwa uncompahgrite, K/Ar	19.3±0.3	Bagdasaryan et al., 1973
G	Kishalduga nephelinite, K/Ar	15.1	Crossley and Knight, 1981
H	Upper Turkana basalts, K/Ar	14.0±1.2	Baker et al., 1971
I	Elgeyo phonolites K/Ar	13.6±0.6	Baker et al., 1971
J	Kapiti phonolite, K/Ar	13.1±0.5	Baker et al., 1971
K	Mushebele alkali basalt, K/Ar	12.6±0.7	Bellon and Pouclet, 1980
L	S. Kivu basalt, K/Ar	10.0±2.0	Pasteels et al., 1976
M	Rungwe Ol-basalt, K/Ar	8.0±0.8	B. Drake, pers. comm.
N	Mobutu basin, fauna	5.0±0.5	Pickford, 1987
O	Mwenga-Kamituga basalt, K/Ar	5.0	Kampunzu et al., 1986
P	Rusizi basin sediments	<5.0	D. Stone (pers. comm.)
Q	Chiwondo beds, fauna	4-5	Kaufulu et al., 1980
R	Mt. Sodiman nephelinite, K/Ar	4.5±0.4	Bagdasaryan et al., 1973
S	Edward basin sediments	4.1	Williamson, pers. comm.
T	Picritic basalt, K/Ar	3.8±0.2	Bagdasaryan et al., 1973
U	Ngorongoro basalt, K/Ar	3.7±0.8	"
V	Mt. Kenya syenite, K/Ar	3.1	Baker et al, 1971
W	Kilimanjaro nephelinite, K/Ar	2.3±0.4	Bagdasaryan et al., 1973
X	Tshibinda alkali basalt, K/Ar	1.9±0.1	Bellon and Pouclet, 1980
Y	Mt Hanang nephelinite, K/Ar	0.5±0.3	Bagdasaryan et al., 1973
Z	Kiyambogo (Uganda) mafurite, K/Ar	0.45±.15	"

Table II.

Summary of Western Rift Basins

BFS	Basin	Strike/Asymmetry	Flank(m)/ Subsidence(m)	Age Constraints	Reference
1	Mobutu	N30°E/ Northwest	2500/ 570	Lake sediments <5 Ma	(a)
2	Semliki	N20°E/ Southeast ?	5100/ 760	Lake sediments < 4.1 Ma	(b)
3	L.George	N20E°/ Northwest ?	5100/ 760		
Toro-Ankole volcanic province				Basalts<1 Ma	(c)
4	L. Edward	N10°E/ Northwest	3090/ 900		
5	Rutshuru	N10°E/ Southeast ?	2080/1120	Pleistocene terraces	(d)
6	Virunga	N10°E/ Northwest ?	2500/1100	Pleistocene terraces	(d)
Virunga volcanic province				Basalts <12 Ma	(e)
7	West Kivu	N20°E/ Northwest	3300/ 960	<10 Ma	
8	East Kivu	N20°E/ Southeast	2950/1060	<10 Ma; Pleistocene terraces	(f)
South Kivu volcanic province				<10 Ma	(g)
9	Rusizi	N10°W/Southwest	3300/ 400	<6 Ma; Pleist. terraces	(f)
10	Rumonge	N-S/ East	2600/ 250		
11	W. Nyanza-lac	N-S/ West	1620/ -250		
12	E. Nyanza-lac	N-S/ East	1920/ -480		
13	Kigoma	N20°W/Southwest	2750/ -540		
14	Kalemie	N-S/ East	2460/ -120		
15	East Moba	N30°W/ Northeast	1940/ 20		
16	West Moba	N30°W/ Southwest	2340/ 0		
17	Marungu	N-S/ West	2430/ -630		
18	Mpulungu	N20°W/ Northeast	2200/ 20		
19	Rukwa	N30°W/ Southwest	2660/ 790	Plio-Pleistocene	(h)
20	Msangano	N20°W/ West ?	2200/ 900		
21	Songwe	N30°W/ Northeast	2820/ 900	< 8 Ma	(f)
Rungwe volcanic province				Ol-basalts < 8 Ma	(f)
22	Usangu	N20°E/ Northwest ?	2300/ 950	< 8 Ma	(f)
Rungwe volcanic province				Ol-basalts < 8 Ma	(f)
23	Karonga	N30°W/ Northeast	2930/ -80	Lake sediments < 5 Ma	(i)
24	West Nkhata	N-S/ West	2360/ -165		
25	East Nkhata	N-S/ East	1980/ 200		
26	Likoma	N20°E/Northwest	1930/ 110		
27	N. Nkhotakota	N-S/ West	1820/ 150		
28	S. Nkhotakota	N-S/ East	1820/ 200		
29	E. Monkey Bay	N10°W / Northeast ?	1825/ 370		
30	W. Monkey Bay	N10°W/ Northeast ?	2180/ 370		
31	Shire	N25°E/ Southeast	2070/ 470		
32	Urema	N40°W/ Northeast	1445/ 68		

(a) Pickford (1986)
(b) Williamson (pers. comm.)
(c) Bagdasaryan et al. (1973)
(d) Pouclet (1975)
(e) Bellon and Pouclet (1980)
(f) Ebinger (Chapter 3)
(g) Pasteels et al, in press
(h) D. Stone, pers. comm.
(i) Kaufulu et al. (1981)

Table II. Summary of border fault geometries, sense of asymmetry within basins, and chronologic constraints from Western rift basins. Elevation of rift flanks and basins referenced to sealevel. Amounts of subsidence within basins are listed as present elevations of the rift valley or lake floor, as depth to pre-rift basement is not known in many basins. See Rosendahl (1988) for total sediment thicknesses beneath Tanganyika lake basins; Wong and Von Herzen (1974) for sediment thicknesses beneath Lake Kivu. Where depth to basement unknown, regional tilt of basins indicated with (?).

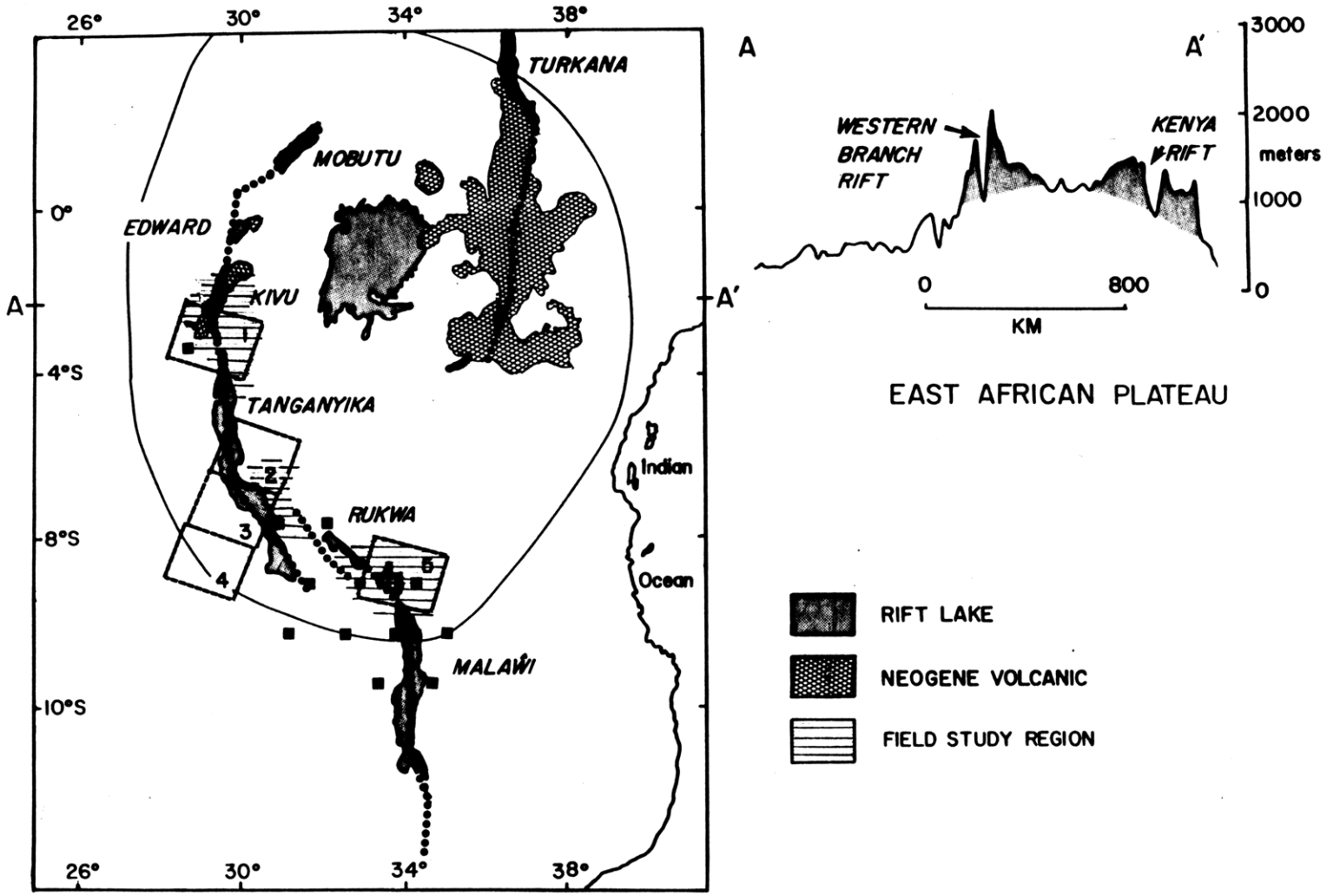

Figure 1. Tertiary volcanic provinces of East African rift system and lakes filling Western rift valley. Boxes show coverage provided by high-resolution Thematic Mapper (5) and Multi-Spectral Scanner (1-4) images; small squares show approximate centers of black and white MSS imagery used in analysis. Light lines enclose elevations greater than 800m corresponding to uplifted East African plateau. Bold dotted line indicates the approximate position of the axis of the Western and Kenya rift valleys. Inset: Profile A-A' across East African plateau. Shading emphasizes approximately 400 km wide zone of uplift flanking rift valley.

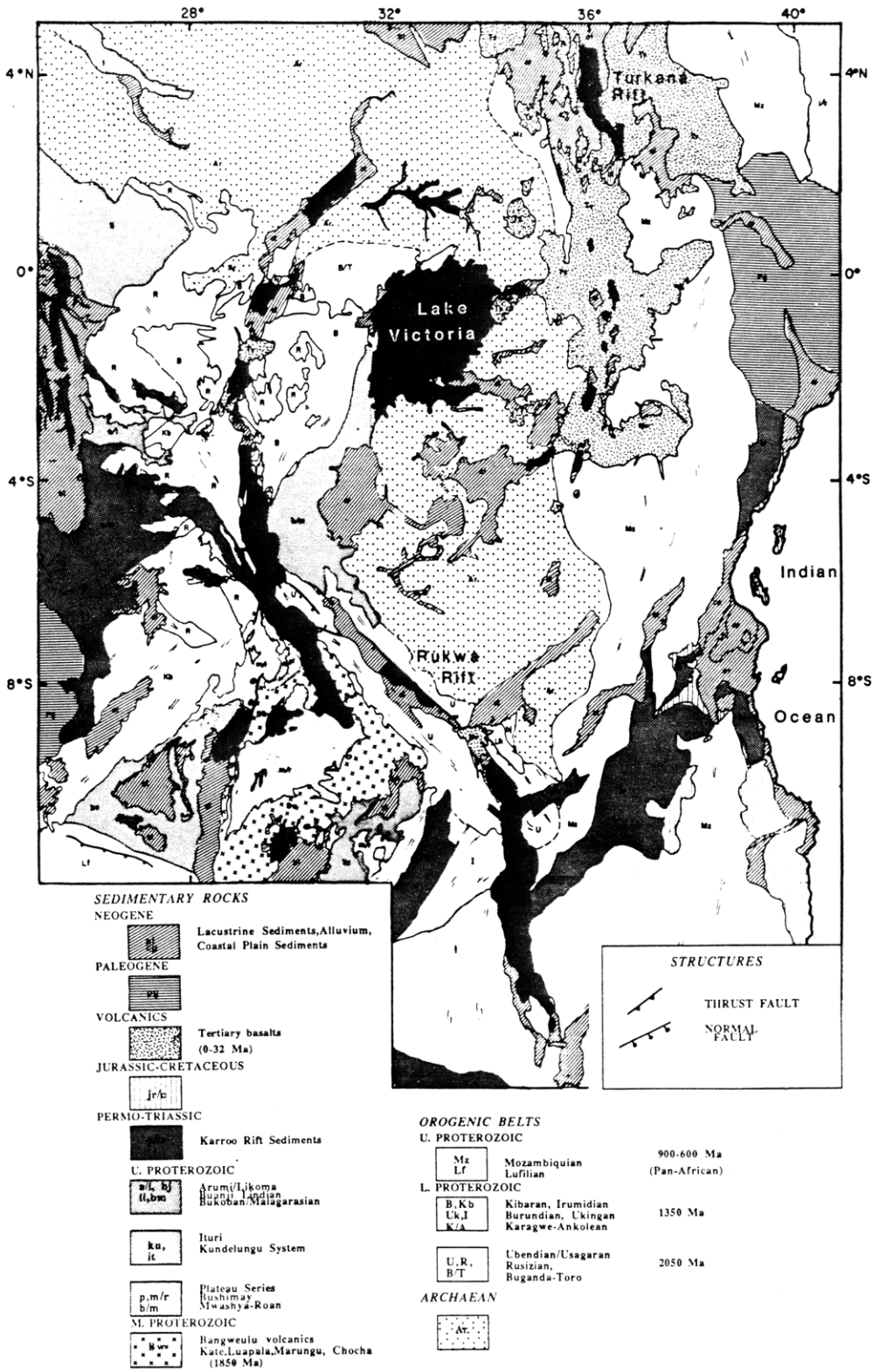

Figure 2. Summary of East African geology showing major pre-rift faults and regional metamorphic trends within Precambrian orogenic belts. Geological information from: Afonso (1976); Baker (1986); Cahen and Snelling (1984); Carter and Bennett (1973); Kent et al. (1971); Lepersonne (1977); Quennell et al (1956); Reeves (1960).

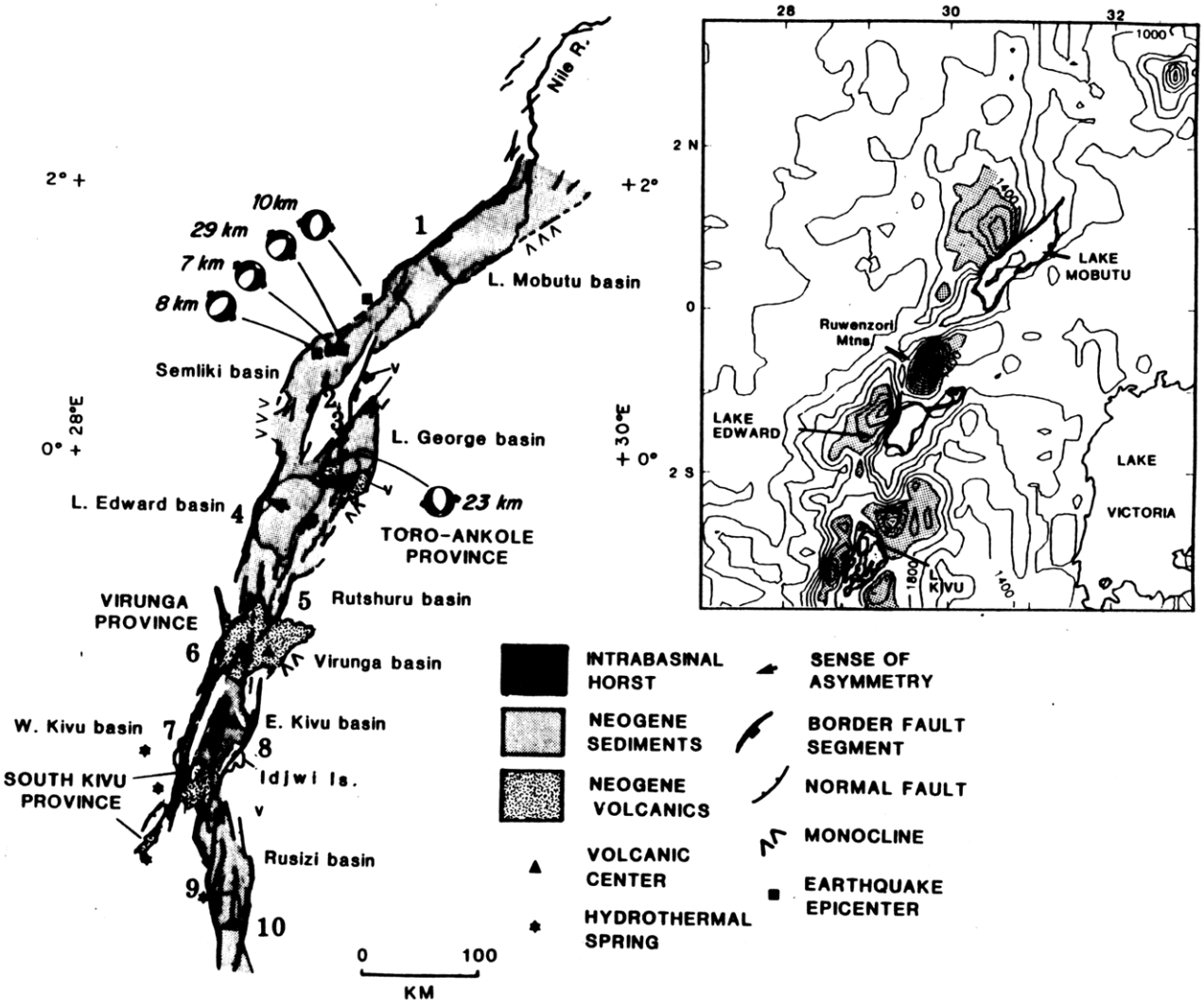

Figure 3. a) Tectonic interpretation of rift basins bounded by border fault segments (BFS) 1-10 described in text. Focal mechanism solutions of earthquakes with epicentral locations denoted by squares shown as lower hemisphere projections Western events; hypocentral depths as indicated (from Shudofsky, 1985). Structural interpretations from Holmes (1951); Davies (1951); Pouclet (1977); Degens et al (1973); b) Smoothed contours of topographic relief along northern part of Western rift valley. Contour interval 200m; elevations above 1400m shown shaded. Basinal regions indicated by line pattern.

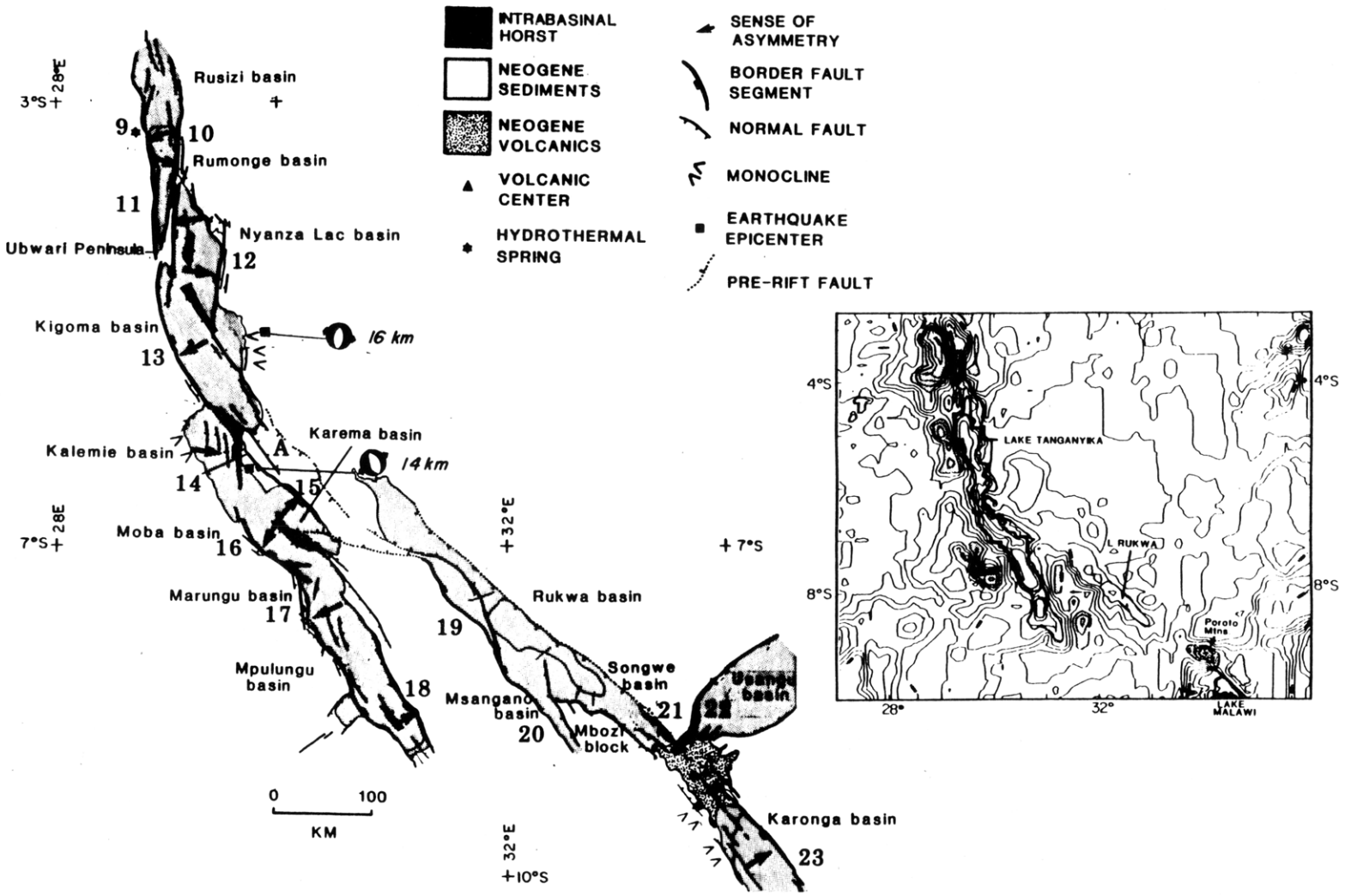

Figure 4. a) Tectonic interpretation of rift basins bounded by border fault segments (BFS) 11-12 described in text. Focal mechanism solutions of earthquakes with epicentral locations denoted by squares shown as lower hemisphere projections Western events; hypocentral depths as indicated (from Shudofsky, 1985). Structural patterns from Harkin (1960); Chorowicz (1983); Rosendahl et al (1986); Ebinger et al (1987); Peirce and Lipkov (in press); this study. b) Topographic relief along central part of Western rift valley. Contour interval 200m; elevations above 1400m shown shaded. Basinal regions indicated by line pattern. A indicates segment of Mesozoic fault system reactivated in Tertiary rifting.

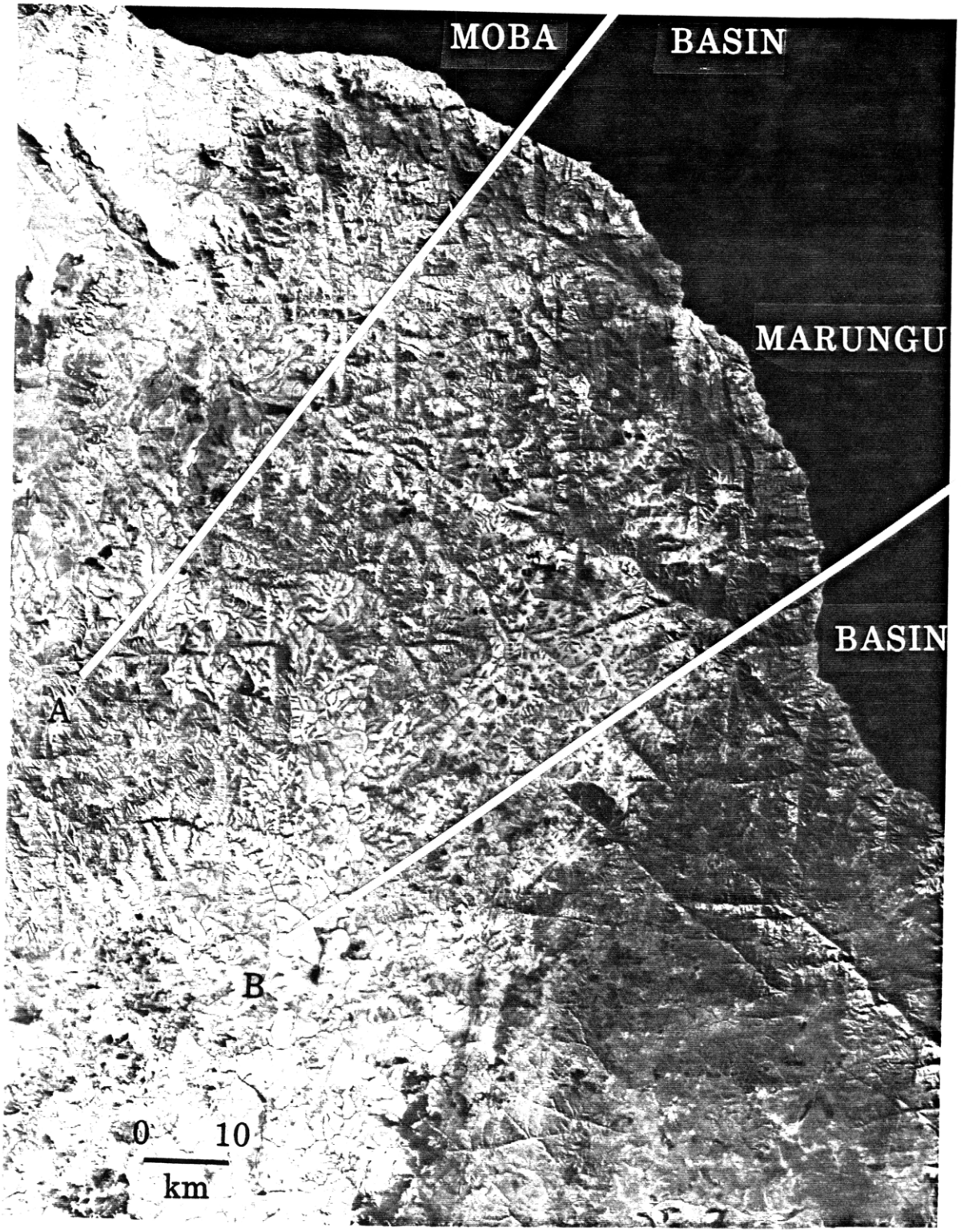

Figure 5. Portion of Landsat MSS image 3 (Figure 1) covering the southwestern part of the Tanganyika rift (Moba and Marungu basins).

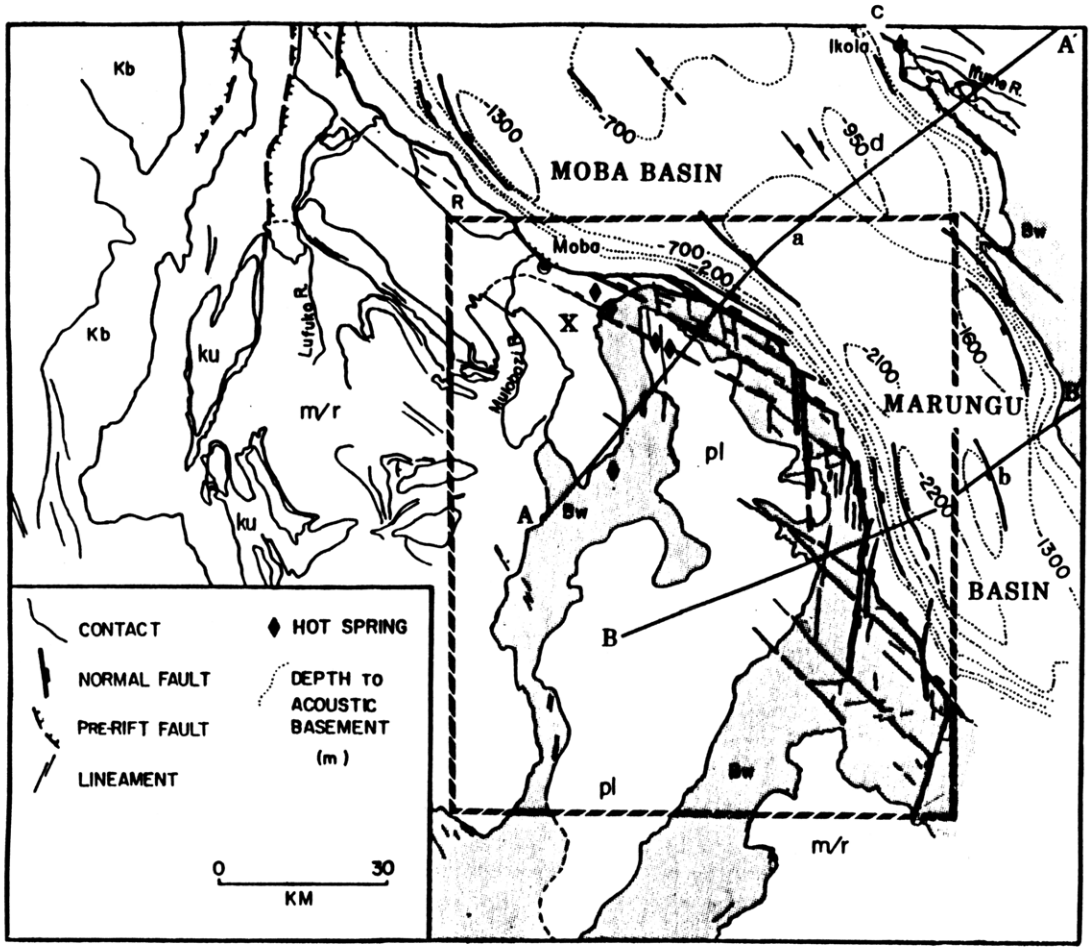

Figure 6. Interpretation of lineaments observed in part of MSS image shown in Figure 5. Faults have formed in undeformed Proterozoic volcanic sequence (stippled pattern); flat-lying sediments (pl) along the uplifted flank roughly correspond to highest elevations. Geologic legend same as Figure 2. x denotes tectonic contact between Archaean (?) and Proterozoic sequence referred to in text. Box encloses region shown in Figure 5b; fault patterns in upper right corner shown in Figure 8b. A-a-A', B-b-B' refer to cross-sectional profiles shown in Figures 7a, 7b. Location of hydrothermal springs from Tshimanga and Kabengele (1981); lithologic units and basement structures from Lepersonne (1977a) and McConnell (1950). Depths to basement corrected for sediment loading calculated from sediment isopach maps (Burgess et al, in press) using sediment loading correction described in Crough (1983); assumes sediment loads are locally compensated.

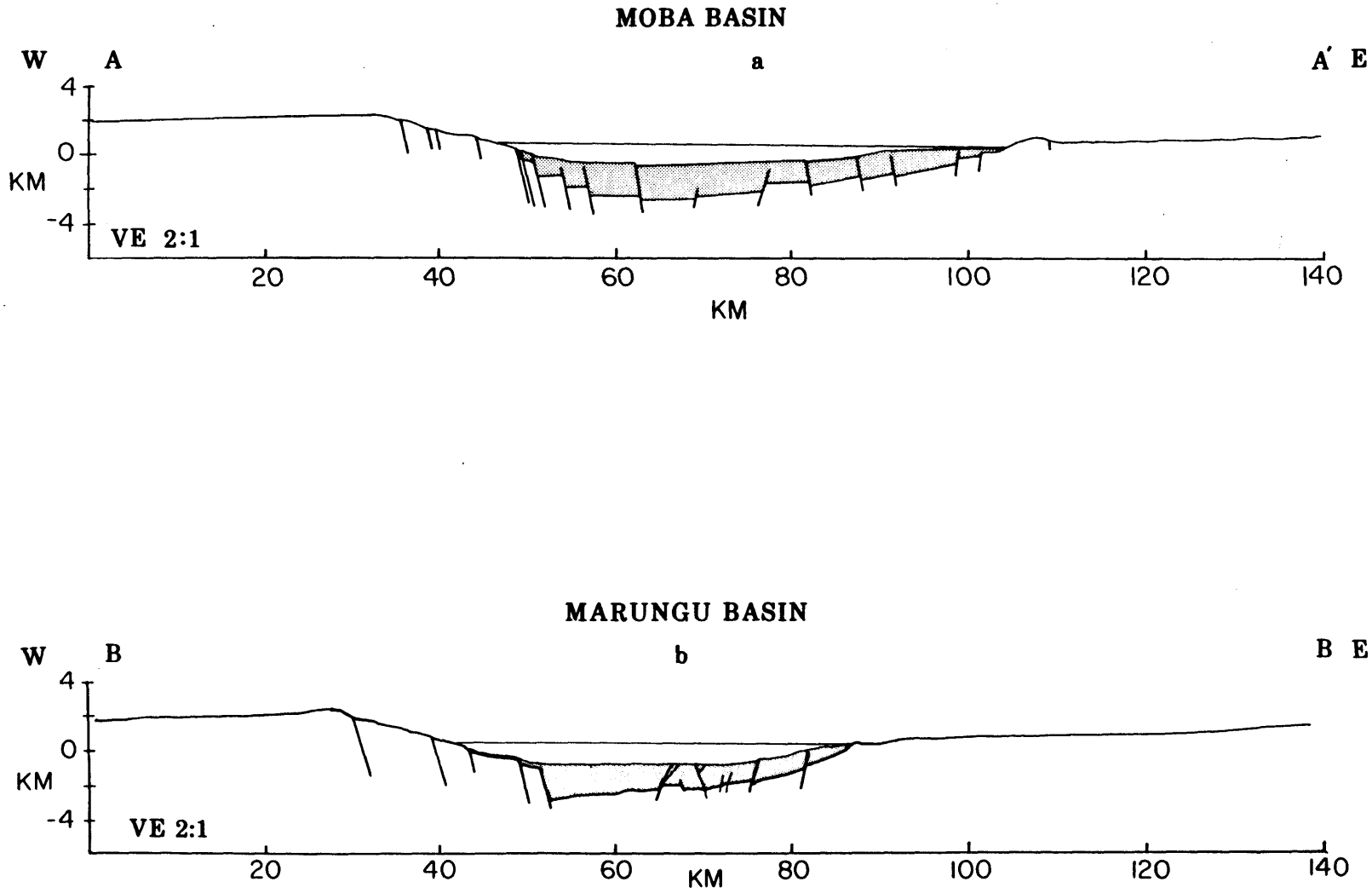

Figure 7. Cross-sectional profiles of Moba and Marungu basins vertically-exaggerated (VE=2:1) to illustrate uplifted flanks and basinal morphology a) Cross-sectional profile of Moba basin along line A-a-A' (figures 5, 6) b) Cross-sectional profile of Moba basin along line B-b-B'(Figures 5, 6). Structural patterns beneath lake from interpretation of seismic profiles 90, 220, respectively, from Rosendahl et al., 1986.

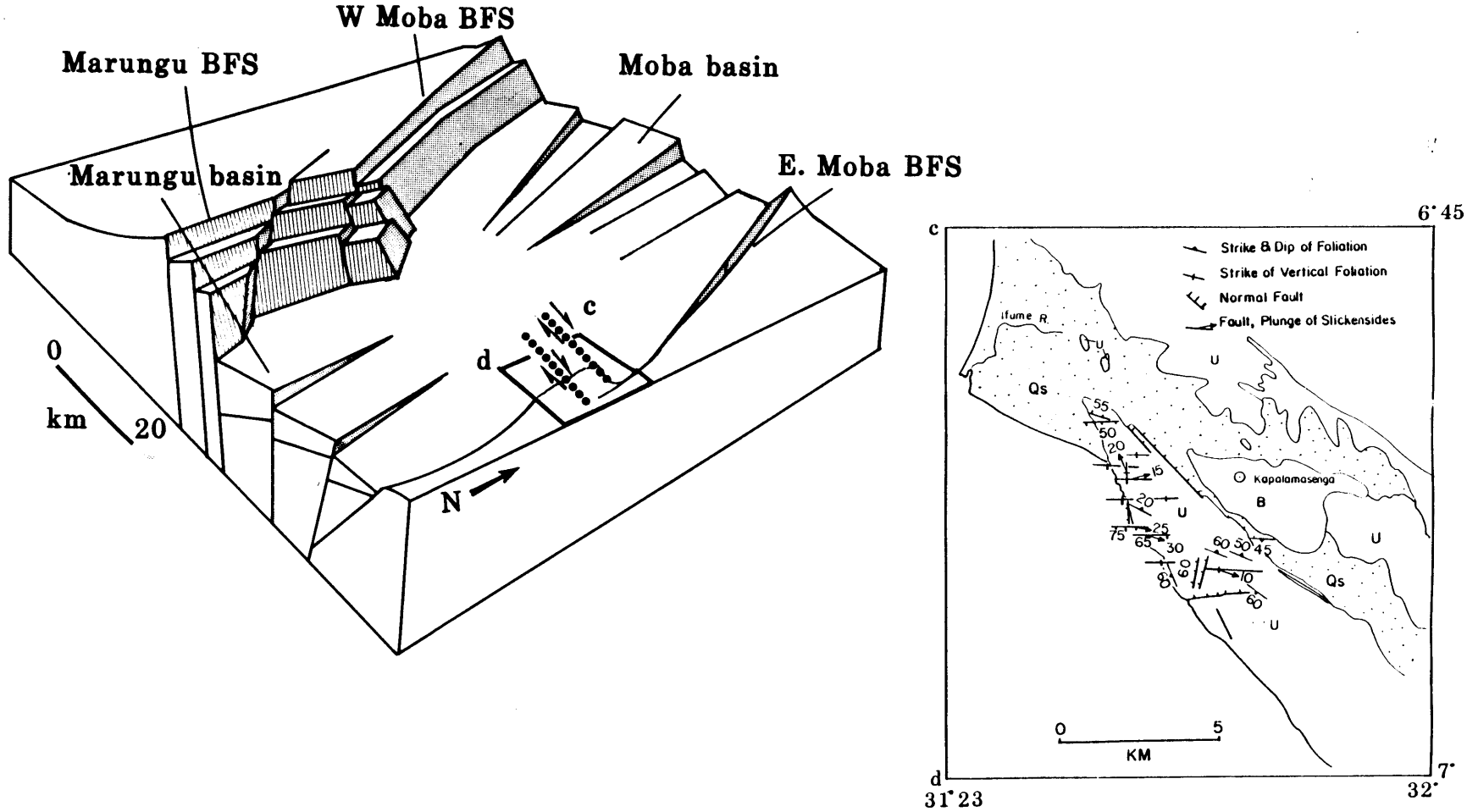

Figure 8. a) Schematic diagram of border fault segments and morphology of Moba and Marungu basins. Intersection of Moba (N30°W strike) and Marungu (N-S strike) border fault systems produces zig-zag lake outline (e.g. Figure 5). Strike-slip faults (dotted lines) interpreted from fault patterns in region shown in Figure 8b. b) Late Cenozoic faults and metamorphic foliations along eastern margin of Moba basin. Fault surfaces oriented approximately E-W commonly show subhorizontal slickensides, and Riedel shear system suggests dextral movement. Note gneissic foliation (N30-40°W) oblique to strike of strike-slip faults. Legend same as in Figure 2.

Figure 9. Slickenside surfaces plunge 15° to N80°E along surface of fault striking N85°Ealong eastern margin of Moba basin (see Figure 6). Gneissic foliation of augen gneisses N35°W/40°SW (Ubendian system).

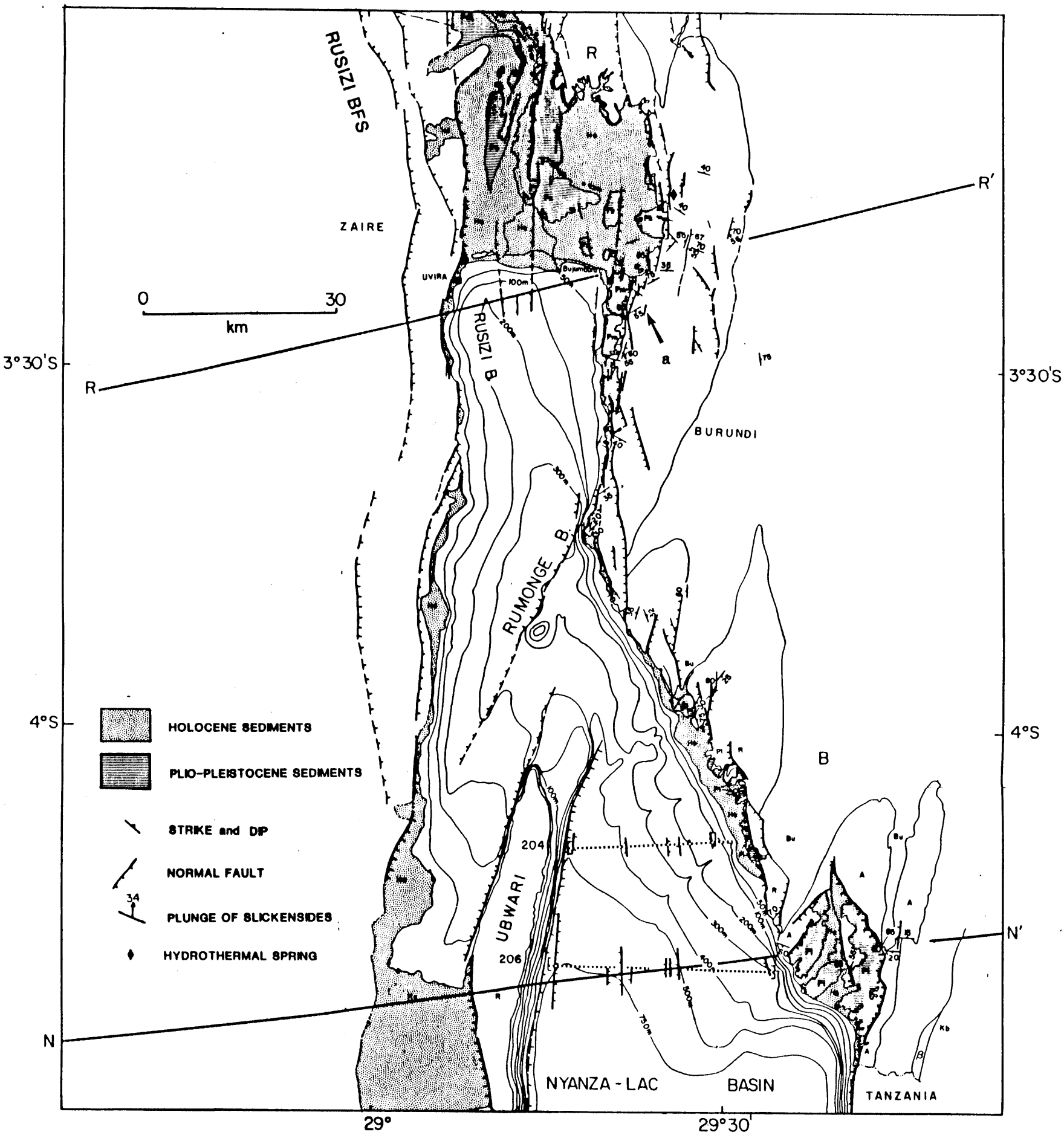

Figure 10. Fault patterns along the northern part of the Tanganyika rift; bathymetric contours beneath Lake Tanganyika in meters below lake level (774m). Fault patterns based on field mapping and interpretation of aerial photographs. Lithologic contacts and basement structures from Lepersonne (1978); Theunissen et al. (1986; in press); Ilunga (1984). Structural information beneath Lake Tanganyika from multi-channel seismic reflection profiles 204 and 206 (dotted lines) provided by B. Rosendahl (pers. comm.); single-channel data from Patterson (1983). Bold line N-N' indicates location of cross-section shown in Figure 12. Kb=Kibaran; Bu=Burundian; R=Rusizian; A=Archaean (see Figure 2).

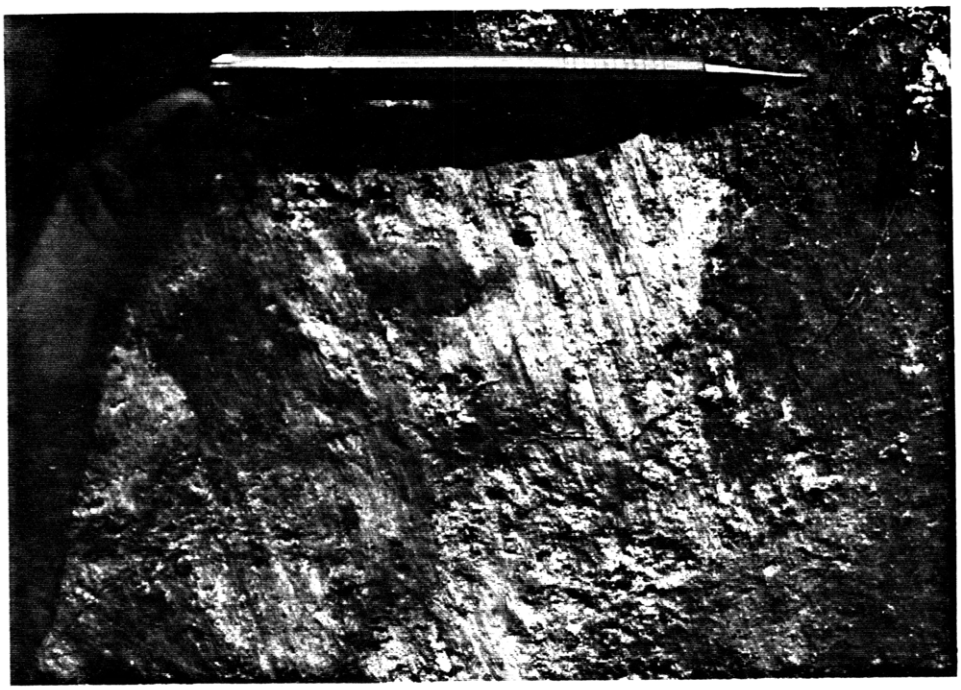

Figure 11. Subvertical slickensides along normal fault bounding eastern side of Rusizi basin (Figures 4a; 10).

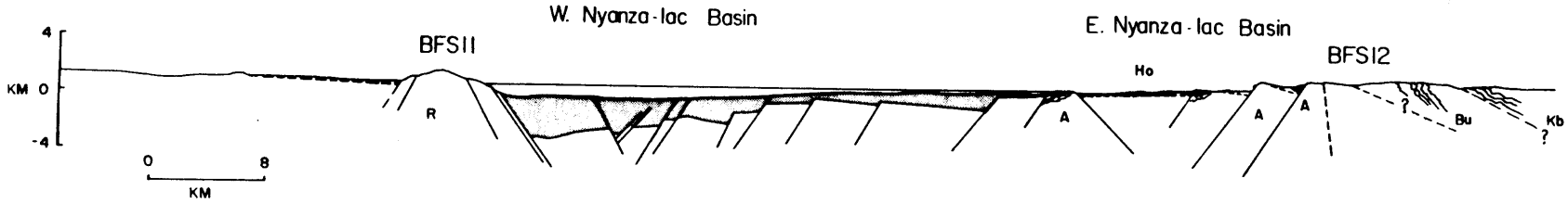

Figure 12. Geologic cross-section of Rumonge basin, including the northern part of the Nyanza-lac border fault segment (N-N'; Figure 3). BFS 11 extends along the western margin of the westward-tilted Rumonge basin. Estimate of crustal extension < 15%; depth to detachment 10-15 km.

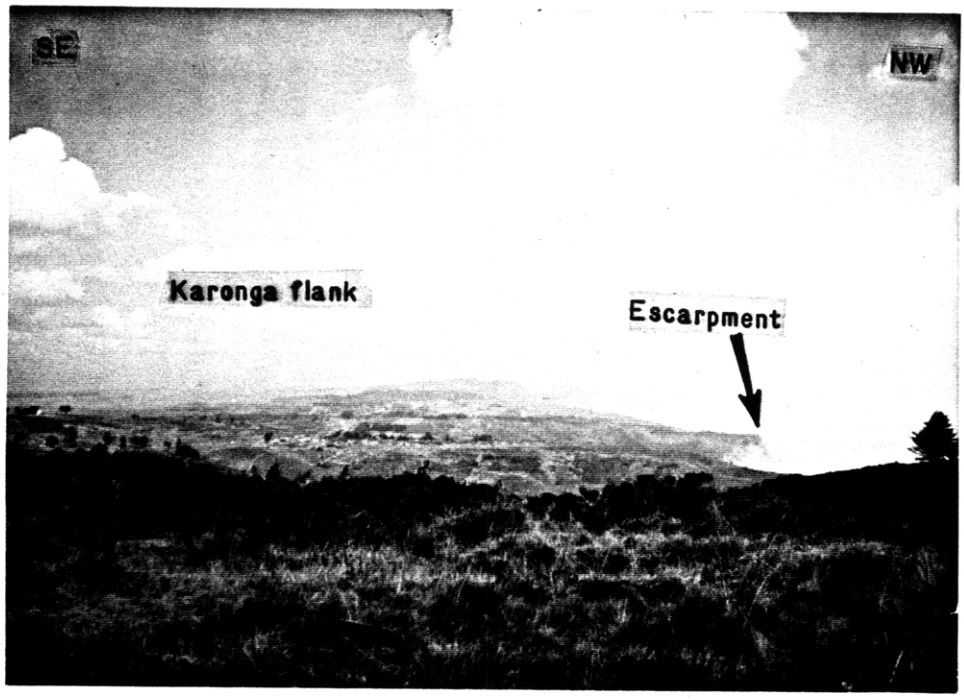

Figure 13. Active fault scarp along northeastern side of Karonga basin (BFS23), illustrating typical morphology of unfaulted rift flank that is gently tilted away from rift valley. Photo taken along strike of approximately N30°W trending fault system.

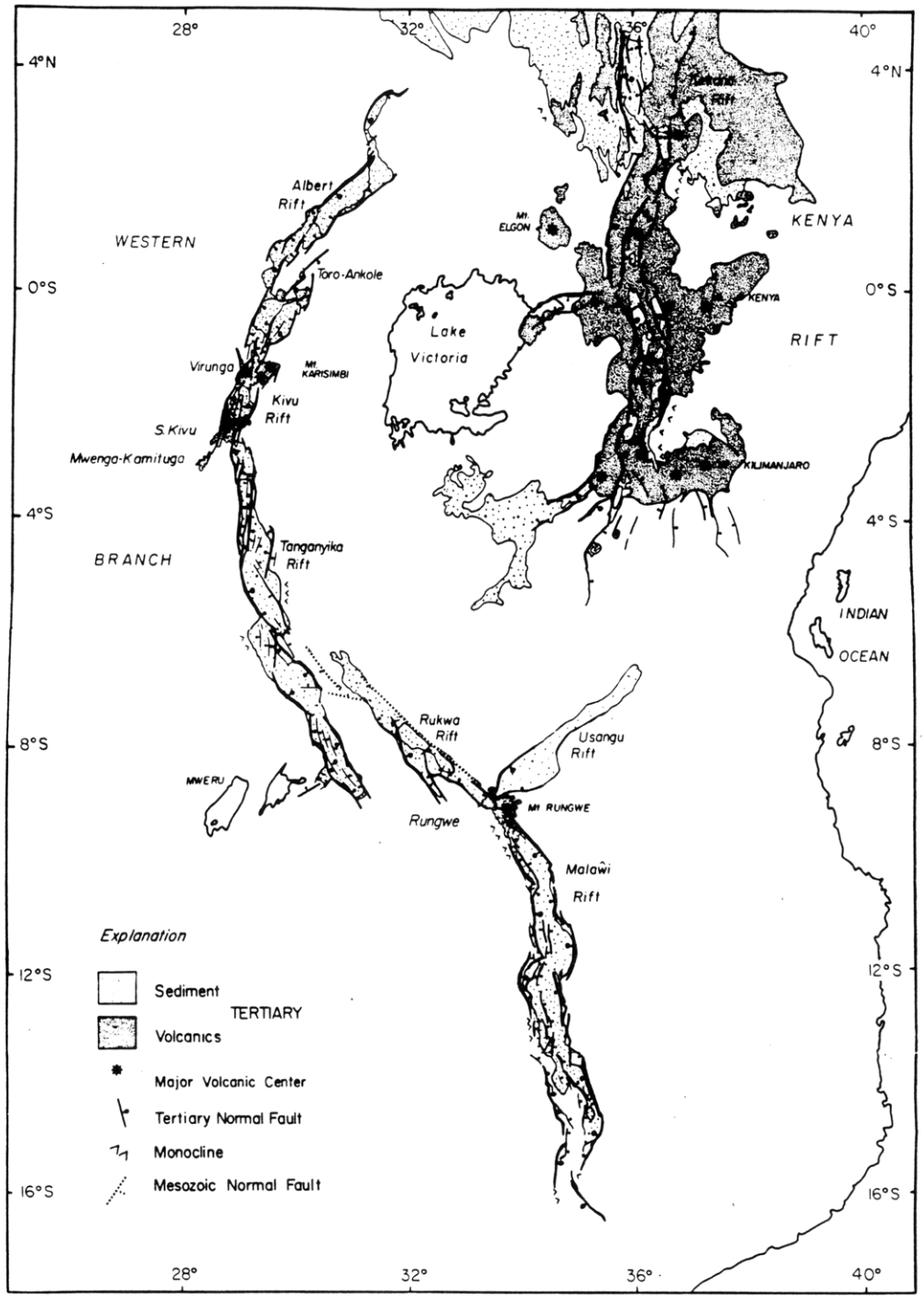

Figure 14. Major structures of the Tertiary East African rift system, summarized from Figures 3 and 4. Structural interpretation of Kenya rift from Baker et al.(1986).

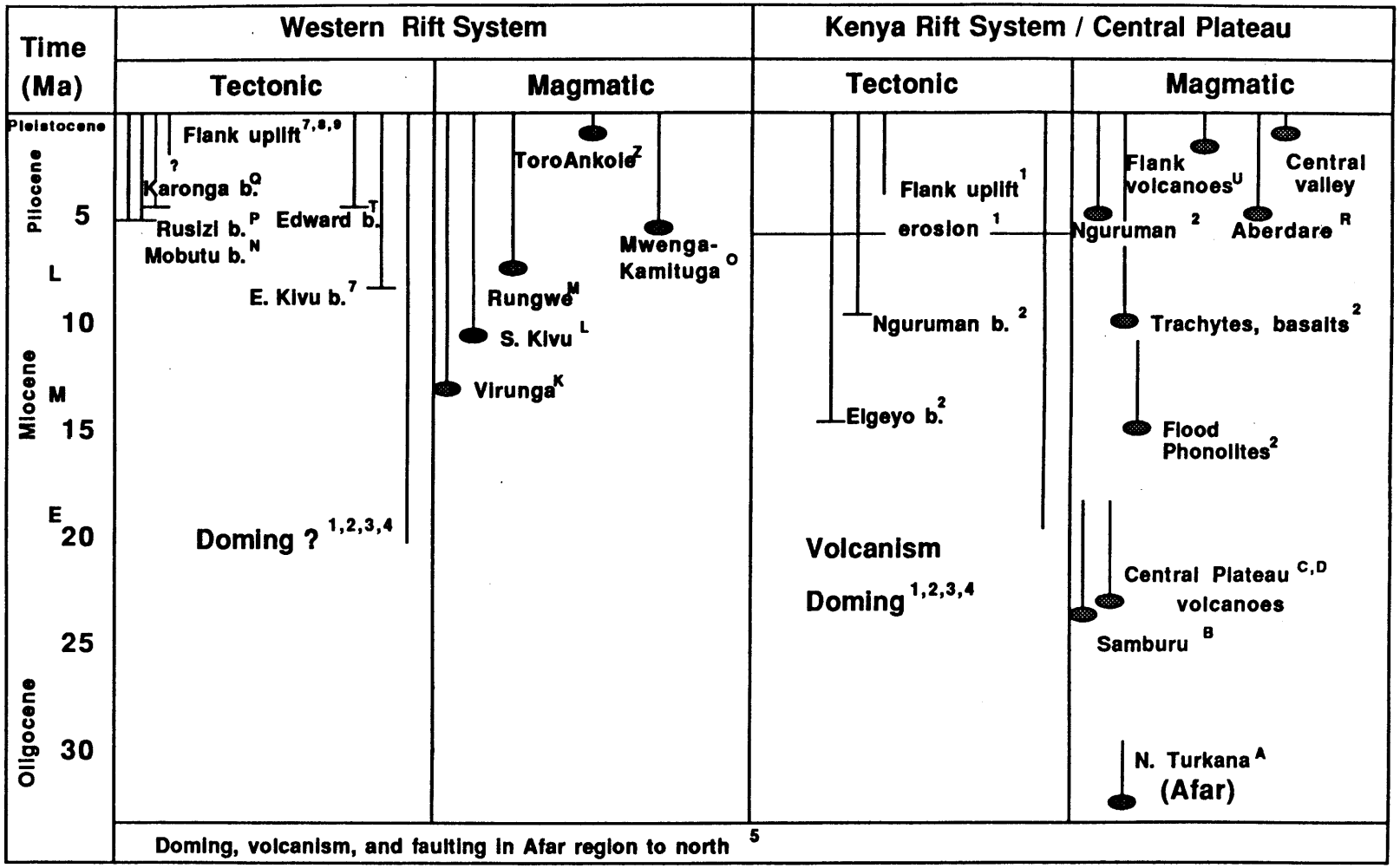

1 Saggerson and Baker, 1965
2 Baker, 1986
3 Dixey, 1956
4 Shackleton, 1978
5 Mohr, 1987
6 Baker et al, 1971
7 Ebinger
8 Bishop and Posnansky, 1960
9 Grove, 1983
10 Pouclet, 1977

Figure 15. Chronologic constraints on vertical movements, volcanic activity, and basinal subsidence within East African dome region. Letters refer to references listed in Table I.

Chapter 5

Effective elastic plate thickness beneath the East African and Afar Plateaus and Dynamic Compensation of the Uplifts

C.J. Ebinger
M.I.T./Woods Hole Joint Program in Oceanography
Department of Earth, Atmospheric, & Planetary Sciences, M.I.T.
Cambridge, MA 02139
T.D. Bechtel,
Kurz Associates, Inc.
4 First St.
Bridgewater, MA 02324
D.W. Forsyth
Department of Geological Sciences
Brown University,
Providence, RI 02912
C.O. Bowin
Department of Geology and Geophysics
Woods Hole Oceanographic Institution
Woods Hole, MA 02543

Abstract

The broad topographic domes, or plateaus, of East Africa and Afar are characterized by long-wavelength negative Bouguer gravity anomalies. Gravity and topography data from the East African and Afar plateaus and data from the stable cratonic regions to the west were subdivided into 17 smaller regions to study the variation of elastic plate thickness within part of the African continent, its relation to rifting processes within these intracontinental plateau regions, and to study compensation mechanisms for the broad uplifts. Assuming that loads at the surface, within, and beneath the base of a thin elastic plate contribute to the observed Bouguer gravity anomalies, the wavelength dependence of the coherence between gravity and topography was used to determine the effective elastic plate thickness in each of the sub-regions. Estimates of elastic plate thickness were found to be 65-180 km in the stable cratonic areas, provided that surface and subsurface loads are uncorrelated. Lower estimates (43-64 km) were obtained in the largely unfaulted regions encompassing the broad uplifted plateaus and the narrower Darfur dome to the west of the Afar plateau. Estimates of 22-55 km correspond to regions that include the severely faulted Kenya, Western, and Afar rift valleys as well as unfaulted regions adjacent to the rift valleys. We attribute the smallest estimates of elastic plate thickness (22-55 km) to averaging unfaulted topography with mechanically weakened topography within the severely faulted Kenya, Western, and Afar rift systems. The linear transfer function between gravity and topography within the uplifted East African plateau region at wavelengths longer than 1000 km can be explained by a dynamic uplift mechanism and associated heating of the thermal lithosphere above a convecting region within the asthenosphere. This interpretation is consistent with existing geological and geophysical data and with constraints on the timing of volcanism and uplift within the East African plateau region.

Introduction

Broad uplifted plateaus and narrow rift valleys characterize the topographic relief of East Africa (Figure 1). A representative cross-section through East Africa (Figure 1) illustrates the approximately 1300 km wide, 1200m high East African dome, or plateau, and the much narrower rift valley and volcanic topography of the Kenya and Western rift systems that is superimposed on the plateau. Similarly, the narrow Ethiopian rift system and Afar depression are superimposed on the Afar plateau, which lies northeast of the East African plateau, and to the southwest and southeast of the Red Sea and Gulf of Aden spreading centers (Figure 1). In contrast to the two broad plateaus, the 500 km wide Darfur dome in the north central part of the study region has no associated rift valley. Broad, negative Bouguer gravity anomalies coinciding with the topographic domes have been used to indicate that the uplifts are isostatically compensated (e.g., Bullard, 1936; Girdler and Sowerbutts, 1970; Khan and Mansfield, 1971; Makris et al., 1972; Fairhead, 1976; Bermingham et al., 1983), but there is no systematic correlation between the shorter wavelength features of the topography and Bouguer gravity anomalies (Figure 1; inset). The lack of correlation between gravity and topography at short wavelengths suggests that a regional or flexural compensation model may be appropriate, with the short wavelength surface and internal loads supported by elastic stresses within the lithosphere.

The broad domal uplifts and Tertiary to Recent volcanism of East Africa have been attributed to elevated geotherms within the lithosphere beneath these regions (Thiessen et al., 1979; Wendlandt and Morgan, 1982; Morgan, 1983; Crane and O'Connell, 1983). In earlier interpretations of gravity data from East Africa and Afar, the plateau topography is supported by buoyancy forces due to low-density material beneath the uplifted plateaus, and this low-density material produces the associated negative Bouguer gravity anomaly (Girdler and Sowerbutts, 1970; Searle and Gouin, 1971; Fairhead, 1976; Bermingham et al., 1983; Baker, 1986). In support of this thermal origin for the long-wavelength aspects of the two plateaus, both the morphology and magmatic activity of the East African and Afar plateaus are similar to oceanic midplate swells, which are attributed to hotspot activity (e.g., Burke and Dewey, 1973; Watts, 1976; Crough, 1978).

The narrow rift valley topography primarily is caused by subsidence of fault-bounded sedimentary basins and uplift of the adjacent rift flanks (e.g., Figure 1, inset). A comparison of rift structures (Figure 1) and topographic relief in the Western, Kenya, and Ethiopian rift systems (Figure 2) reveals that Tertiary volcanoes and flood basalts also contribute to the high amplitude, shorter wavelength aspects of African topography, particularly within the vicinity of the Kenya and Ethiopian rift systems, and along the crest of the Darfur dome.

Differences in timing of initial volcanism and faulting between the Afar and East African plateaus and along the length of the rift systems superimposed on the plateaus may correspond to lateral variations in crust/upper mantle structure within and between the East African and Afar plateau regions (e.g., Baker, 1986; Williams and Chapman, 1986; Ebinger, 1987). However, prior to this study no direct comparison between gravity data from the Afar and East African plateaus, and the Kenya, Western, and Ethiopian rifts had been undertaken to examine these possible differences. Previous studies of isostatic compensation for the topography of the East African and Afar plateaus using both Airy (Girdler and Sowerbutts, 1970; Fairhead, 1976; Banks and Swain, 1978) and flexural compensation models (Forsyth, 1985; Bechtel et al., 1987) have been restricted to sections of the two plateaus that may not be representative of the average lithospheric structure beneath East Africa and Afar. These regions also were too small to examine the compensation for the longest wavelength topographic elements of the East African and Afar plateau topography.

In this study we construct grids of gravity and topography data from Africa that encompass the East African and Afar plateaus, as well as the Darfur dome and the stable cratonic regions outside the uplifted regions. The objectives of this study are: 1) to determine the flexural rigidity of the African plate and its variability between and along the length of the Afar, Kenya, and Western rift systems; and 2) to examine compensation mechanisms for the long wavelength topographic plateaus.

Geologic Setting

Most of the study region has been a tectonically stable area since the end of the Pan-African cycle (~500 Ma), although some regions were affected by continental rifting during Permo-Triassic and Cretaceous times (e.g., Figure 1). The Afar and East African plateaus are separated by the Turkana depression, and faults bounding the rift basins are discontinuous along their lengths (e.g., Mohr, 1983; Baker, 1986; Chapter 4). Initial volcanism in the Ethiopian rift valley in Eocene time preceded the earliest magmatic activity in the Kenya rift system by approximately 10 My (e.g., Baker, 1986; Pasteels et al., in press). A considerable thickness of volcanic material (2-3 km) has accumulated in the Ethiopian and Kenya rifts (Mohr, 1983; Baker, 1986; Bosworth, 1987), but thin (100-300m) sequences of basalts cover isolated regions in the Western rift system (Holmes, 1940; Harkin, 1960; Ebinger, 1987). In the Ethiopian rift valley faulting began in Oligocene time (e.g., Davidson and Rex, 1980). Volcanism and regional uplift in the East African plateau region began in early Miocene time, and major fault systems in the Kenya rift valley are late Miocene and younger in age (e.g., Saggerson and Baker, 1965; King, 1978; Kent et al., 1974; Baker, 1986; Bosworth, 1987). Volcanism in the Western rift

system commenced at approximately 12 Ma, and major vertical movements began along Western border fault systems in Plio-Pleistocene time (Bellon and Pouclet, 1980; Ebinger, 1987).

The major normal fault systems that bound the roughly 70 km wide Kenya, Western, and Ethiopian rift valleys lie within zones of seismicity, although the magnitude and number of events are greater in the Western rift than in either the Ethiopian or Kenya rift systems (Wohlenberg, 1968; Fairhead and Stuart, 1982; Shudofsky, 1985). Earthquakes have been reported throughout the depth range 5-30 km beneath the East African rift valleys (e.g., Zana and Hamaguchi, 1978; Shudofsky, 1985). Tensional earthquake mechanisms in the Western and Kenya rift systems suggest that the direction of extension there is approximately east-west (Fairhead and Stuart, 1982; Shudofsky, 1985). Models of seismic velocity structure beneath the Afar and East African plateaus determined from seismic refraction and surface wave dispersion studies indicate that crustal thinning is limited to the central rift valleys of East Africa and Afar (Searle and Gouin, 1971; Griffiths et al., 1971; Lepine et al., 1972; Long et al., 1973; Bram and Schmeling, 1975; KRISP, 1987). Normal continental crustal thicknesses of 35-41 km are found beneath the uplifted rift flanks and the unfaulted plateau between the Western and Kenya rift valleys (Rykounov et al., 1972; Bram and Schmeling, 1975; Maguire and Long, 1976; Hebert and Langston, 1985; Shudofsky, 1985).

The Kenya rift valley is characterized by an average heat flow of 100 mW/m^2 that is significantly higher than the African continental mean of 50 mW/m^2 (Skinner, 1977; Morgan, 1983; Crane and O'Connell, 1983). When reported values are corrected for sedimentation effects, mean heat flow values of 67-73 mW/m^2 in the Western rift lakes also are elevated above the continental mean (Degens et al., 1971; Degens et al., 1973; Ebinger et al., 1987). Evidence for elevated temperatures in the upper mantle is found in anomalously low P_n velocities and S-wave velocities beneath the central section of the Kenya rift valley (Griffiths et al., 1971; Long et al., 1976; KRISP, 1987; Nolet and Mueller, 1982). A high conductivity region reported at 20 km depth beneath the central Kenya rift valley has been interpreted as a zone of melting within the subcrustal lithosphere (Banks and Beamish, 1979).

The 400 km wide Darfur dome rises over 800m above the surrounding elevation (Figure 2), and it is believed to mark an intracontinental hotspot (Vail, 1973; Morgan, 1981; Bermingham et al., 1983). The Darfur dome is covered by Miocene and younger basalts of the Jebel Marra province, but the rift valley topography characteristic of the East African and Afar plateaus is absent (Whiteman, 1971; Bermingham et al., 1983).

In summary, geological and geophysical data from the East African and Afar

regions indicate that lithospheric geotherms are elevated beneath the rift valleys. These data also point to Late Cenozoic crustal extension localized beneath the Western, Kenya, and Ethiopian rift valley regions. There is evidence that uplift and volcanism in Afar preceded volcanism, faulting, and uplift in the East African plateau region. Similarly, faulting and volcanism in the Kenya rift system preceded extensional basin formation within the Western rift system. The similarities in the rift valleys and the broad domal uplifts suggests a similar causal mechanism for these features, whereas the differences in the timing of faulting and volcanism suggests that they may be in different stages of development. The lack of faulting within the volcanically active Darfur dome region contrasts with the severely faulted rift valleys that have formed atop the East Africn and Afar plateaus. Therefore, these possible differences in stage of development may correspond to differences in lithospheric structure beneath the East African and Afar plateaus and the Darfur dome, and between the Ethiopian, Kenya, and Western rift systems.

Construction of Data Grids

Elevation

A compilation of continental and oceanic elevations (ETOPO5) gridded at 5' longitude and 5' latitude intervals by the National Geophysical Data Center were used as the primary data base in these analyses. Bathymetric data from Lakes Malawi (Eccles, 1974), Victoria (Beauchamp, 1964), and Tanganyika (Capart, 1949) were substituted for ETOPO5 data in these regions of the grid (Figure 1). The northeastern and eastern margins of the grids were chosen to exclude those points lying seaward of the ocean-continent boundary in order to avoid edge-effects in the spectral analyses. Latitudes and longitudes were converted to an x-y coordinate system using a Mercator projection that introduces little distortion within this equatorial region. These data were re-interpolated to a constant 20 km spacing (Figure 2) using a minimum curvature algorithm (Swain, 1978). This coarser (~10') re-sampling was chosen in order to make the elevation grid compatible with the gravity grid, in which data are much less evenly distributed and areal coverage is less dense.

Gravity

Digital free-air gravity anomaly and topographic data from the African continent (Figure 3) were converted to the same x-y coordinate system using the methods described above. Bouguer anomalies were calculated assuming a crustal density of 2670 kg/m^3. For gravity stations in Lake Tanganyika (Degens et al., 1971) where the lake floor is above sealevel, a density contrast of 1010 kg/m^3 and water depths were used to make the Bouguer correction; where water depths fall below sealevel in Lake Tanganyika, the Red Sea, and in the Indian Ocean, a density contrast of 1660 kg/m^3 and bathymetry were used.

In the Rukwa rift basin in the Western rift system sediment thicknesses exceed five kilometers, hence the low-density of these sediments contributes significantly to the observed Bouguer anomaly (Peirce and Lipkov, in press). We included the regional Bouguer gravity anomaly, or the observed minus the gravity anomaly attributed to these low-density sediments (Peirce and Lipkov, in press), to the data base prior to interpolation to a uniform 20 km spacing (Figure 4). We also digitized contoured Bouguer gravity anomalies from the Sudan region (Bermingham et al., 1983; Browne et al., 1983) and included these data prior to interpolation. Elevations used to make the Bouguer gravity correction were compared to those of the topography grid, and found to be in good agreement.

Flexural Model

The coherence technique we use to estimate the flexural rigidity of the African lithosphere takes advantage of the wavelength dependence between gravity and topography to estimate the flexural rigidity of the lithosphere, D, or, equivalently, the effective elastic plate thickness, T_e. Flexural models of isostatic compensation for continental topography assume that an elastic lithosphere overlying an inviscid asthenosphere is deflected by topographic and subsurface loads, and regional compensation occurs by plate flexure. The wavelength dependence of the relationship between topography and the gravity anomaly due to the compensating mass at depth provides an estimate of the flexural rigidity of the continental lithosphere. Airy and flexural compensation models are equivalent when the plate has no flexural rigidity, or where the wavelength of the applied load is much greater than the characteristic flexural wavelength of the lithosphere.

In the flexural model short wavelength surface and subsurface loads are supported by the strength of the lithosphere, and neither load deflects the plate to produce a corresponding topographic or density anomaly. Gravity and topography are incoherent at short wavelengths, if the surface and subsurface loads are uncorrelated. At long wavelengths, the rigidity of the lithosphere is insufficient to support the loads and the plate flexes, producing local compensation of surface topographic loads and topographic anomalies over subsurface loads. As a consequence, topography and Bouguer gravity anomalies are correlated and the coherence approaches unity at these long wavelengths. The wavelength where the transition between low and high coherence occurs corresponds to the characteristic flexural wavelength of the lithosphere.

The primary advantage of the coherence technique we use over more conventional admittance techniques is that estimates of the effective elastic plate thickness obtained using the coherence technique are not biased towards low values of flexural rigidity in the presence of subsurface loading, unlike those obtained using admittance

techniques (e.g., Dorman and Lewis, 1970; McKenzie and Bowin, 1976). The coherence technique is also less biased toward regions with high topography, such as the uplifted flanks of the East African rift valleys (Forsyth, 1985).

We may expect that variations in the relative distribution of surface and subsurface loads occur within these two parts of the African plate because differences in the amounts and timing of volcanism, subsidence, extension, erosion, and faulting are found between the Afar, Kenya, and Western rift systems, as well as along their length. We also anticipate that spatial variations in elastic plate thickness occur within the two study regions, which include stable cratons, inactive rifts, and uplifted, tectonically active plateaus (e.g., Figure 1). However, in fitting the observed coherence with theoretical models, we must assume a uniform elastic plate model, or that elastic plate thickness is invariant spatially within a study region. For this reason, we have subdivided East Africa into seventeen smaller regions, minimizing the number of active and ancient tectonic provinces averaged within any sub-region (Figure 5). In making these subdivisions, there is a trade-off between choosing regions small enough so that elastic plate thickness does not vary significantly, and choosing regions large enough to include wavelengths that will exhibit the transition from high to low coherence between gravity and topography.

Coherence Technique

We briefly describe the steps taken to calculate the observed and predicted coherence within each of the sub-regions shown in Figure 7 and listed in Table I. Because the predicted coherence depends on the relative importance of surface and subsurface loading within each sub-region, we also summarize the procedure used to solve directly for surface and subsurface loads. Data from all sub-regions of the grid were mirrored in x (east-west) and y (north-south) prior to transformation to the wavenumber domain using a fast Fourier transform algorithm. Through a comparison of the observed coherence with the predicted coherence, we then estimate the flexural rigidity of the lithosphere beneath the East African and Afar plateau regions. The reader is referred to Forsyth (1985) and (Bechtel et al., 1987) for a detailed description of the coherence technique.

Observed Coherence

Using lower case letters for the spatial domain and uppercase letters for the wavenumber domain, the observed coherence between gravity and topography is defined as:

$$\gamma_0^2 = \frac{C^2(\bar{k})}{[E_0(\bar{k})E_1(\bar{k})]} \qquad (1)$$

where $|\mathbf{k}| = (k_x^2 + k_y^2)^{1/2}$, $\lambda = 2\pi/k$, $E_0(\bar{k}) = \langle H(\mathbf{k})\, H(\mathbf{k})^* \rangle$ is the wavenumber-averaged power of the topography, $H(\mathbf{k})$, $E_1(\bar{k}) = \langle B(\mathbf{k})B(\mathbf{k})^* \rangle$ is the wavenumber-averaged power of the gravity, $B(\mathbf{k})$. In equation (1), $\langle\ \rangle$ indicates averaging over discrete wavebands, $\bar{k}$ is the average k for a particular waveband, and * indicates complex conjugation. The cross-spectrum, $C(\bar{k})$, is given by $\langle B(\mathbf{k})H^*(\mathbf{k}) \rangle$. In order to minimize biasing introduced by noise, we calculate the coherence within each sub-region as:

$$\gamma^2 = \frac{(n\gamma_0^2 - 1)}{(n-1)} \tag{2}$$

where n is the number of independent Fourier coefficients within a waveband (e.g., Munk and Cartwright, 1966). Note that for small n and near zero values of the coherence, γ^2 may be negative. For each sub-region standard errors are computed as:

$$\Delta\gamma^2 = (1-\gamma_0^2)\sqrt{\frac{2\gamma_0^2}{n}} \tag{3}$$

Using (2) to compute the coherence means that the errors are approximately symmetrical about the best estimate.

Density Model and Calculation of Surface and Subsurface Loads

In tectonically active regions such as the uplifted East African and Afar plateaus and the Darfur dome, we anticipate that a number of factors contribute to the observed Bouguer gravity anomaly, as illustrated schematically in Figure 6a. For example, volcanoes represent surface topographic loads; inactive Permo-Triassic and Cretaceous rift basins within the study region may be underlain by anomalous continental crust, based on analogy to other failed rift systems (e.g., Mooney et al., 1983). In the coherence analyses we assume for mathematical convenience that density contrasts, or loads, are distributed in the form of relief on two interfaces: the topography of the surface, h; and relief on a deep density contrast, w, taken as the base of the crust (z_m; Figure 6). In these analyses, the relative importance of surface to subsurface loading is important in the determination of the flexural rigidity, but the coherence model is insensitive to errors in the depth to the subsurface load, as shown in Figure 9 of Forsyth (1985). Although density contrasts within each of the sub-regions may occur at other levels, the inclusion of a shallow density contrast within the crust made no significant difference in the estimate of the elastic plate thickness found in an earlier study of gravity data from a part of the Kenya rift system (Bechtel et al., 1987). Thus, the simple two-layer density model that we adopt takes into account these surface topographic loads (e.g., volcanoes) and subsurface loads (e.g.,

crustal thinning, magmatic underplating, lithospheric heating) and provides a realistic measure of the elastic plate thickness beneath each sub-region. However, in a later section we also consider density contrasts at other depths, particularly those in the lower lithosphere and asthenosphere arising from thermal anomalies in order to examine compensation mechanisms for the broad uplifts of East Africa.

Relief at the density contrasts H and W has contributions from loads at both interfaces. For example, the amplitude of the surface topography, H, is:

$$H = H_t + H_b \tag{4a}$$

where H_t is the net surface relief caused by surface topographic loads, and H_b is relief due to loads on the deep density contrast. Similarly, the subsurface topographic relief is:

$$W = W_t + W_b \tag{4b}$$

By downward continuing the observed Bouguer gravity anomaly we determine the amplitude of relief on the deep density contrast. Using the generalized density model shown in Figure 6b, we solve exactly for the surface and subsurface loads, leaving no isostatic anomalies (Forsyth, 1985; Bechtel et al., 1987). Thus, the model takes into account the possible contributions to the observed topography from gravity anomalies at depth z_m (e.g., Figures 6a, b) without specifying these loads *a priori* .

Using the transformed data and the two-dimensional Fourier transform of the elastic plate equation:

$$Dk^4U(k) + \rho_m gU(k) = M(k) \tag{5}$$

where D is the flexural rigidity, U(k) is the amplitude of the plate deflection, and M(k) is the applied load on an interface, expressions are derived for each of the components of relief at the surface and subsurface density contrasts, as discussed in Forsyth (1985) and Bechtel et al. (1987). The solution of this system is unique provided $Dk^4 \neq 0$. At wavenumbers where $Dk^4 \sim 0$ we cannot discriminate between surface and subsurface loading, which corresponds to wavelengths much greater than the wavelengths where both surface and subsurface loads are locally compensated. The amplitudes of the components of topographic relief are substituted into the expression for E_0, the power of the topography given in (1). The power of the gravity, E_1, is found by upward-continuation of the relief on the subsurface density contrast. After these substitutions, the expected coherence is:

$$\gamma^2 = \frac{\langle H_t W_t + H_b W_b \rangle^2}{\langle H_t^2 + H_b^2 \rangle \langle W_t^2 + W_b^2 \rangle} \tag{6}$$

assuming that surface and subsurface loads are independent, or that cross-terms in the expressions for E_0, E_1, and C cancel in the expression for the expected coherence

(Forsyth, 1985). Thus, an important assumption in the coherence analyses is that loads on the surface and subsurface interfaces are uncorrelated, or of random relative phase. By assuming that the two loads are independent, and, therefore, minimizing the correlation between surface and subsurface loading, the flexural rigidity can be determined uniquely (Forsyth, 1985).

In the estimation of the flexural rigidity beneath each sub-region, we first assume an initial rigidity and solve for H_t, H_b, W_t, and W_b. We then estimate the predicted coherence using (6) and follow this procedure for a range of flexural rigidities. The best-fitting elastic plate thickness in each sub-region is found by minimizing in a least-squares sense the residuals between the observed and predicted coherence estimates. In order to maintain a consistent basis for comparison between sub-regions, and considering the paucity of seismic constraints on the crustal thickness beneath much of the study region, we assume a constant crustal thickness of 35 km within each of the sub-regions. A mean crustal density (ρ_c) of 2700 kg/m^3 , and a mean upper mantle density (ρ_m) of 3300 kg/m^3 also is assumed in all models (Table I; Figure 6b).

Results

The results of the coherence study provide a consistent basis for comparison of elastic plate thickness beneath sub-regions of the East African and Afar plateaus, including the Ethiopian, Kenya, and Western rift systems, as well as the Darfur dome, and the stable cratonic regions surrounding these zones of Tertiary uplift. The observed coherence from each of the seventeen sub-regions (Figure 5) computed using (2) is near zero at short wavelengths, and the coherence approaches unity at the longest wavelengths (Figure 7). In most of the sub-regions, the coherence rapidly increases uniformly from zero to unity within a narrow waveband, although values at intermediate wavelengths often have large standard errors.

We compare the observed coherence to theoretical models found using (6) and iterating through a range of flexural rigidities. Within each sub-region, coherence models are incoherent at short wavelengths where the rigidity of the plate is sufficient to support loads, and have high coherence at long wavelengths where the plate is deflected by surface and subsurface loads. For example, data from the SEBR sub-region (Figure 5) can be explained by a flexural compensation model for an elastic plate of thickness 32 km (Figure 7c). Topographic loads at wavelengths less than about 200 km are supported by the strength of the lithosphere. Surface and subsurface loads at wavelengths between about 200 and 500 km are partly compensated by plate flexure, and loads at wavelengths greater than 500 km are wholly flexurally compensated (Figure 7c). The transition from low to high coherence occurs within a narrow waveband in these flexural models; with increasing

flexural rigidity this transitional waveband is shifted to longer wavelengths. The distribution of surface and subsurface loads within each sub-region modifies the shape of the predicted curves.

Comparing predicted and observed, the steep part of the theoretical curves corresponds to wavelengths where the observed coherence shows the largest standard errors. This relation indicates that data in the transitional wavebands are most sensitive to waveband averaging as well as averaging over sub-regions where the elastic plate thickness is not uniform. We consider acceptable those models which predict coherence within the standard error of as many points in the transitional waveband as the best-fitting models shown in Figure 7, and these models are used to place minimum and maximum bounds on estimates (Table II).

A comparison of the estimates of elastic plate thickness calculated for each of the sub-regions reveals that significant variations in elastic plate thickness occur within the African plate (Table II; Figure 7). We would like to estimate elastic plate thickness in the tectonically stable regions to the west of the East African plateau and the Afar plateau to provide a reference relative to the uplifted plateau and rift valley sub-regions (Figure 7a). However, there are large gaps in gravity data coverage within parts of these regions (e.g., Figure 3). The minimum curvature interpolation algorithm used to uniformly grid these data creates predicted gravity with little relation to topography, and this interpolation may lead to an artificially low coherence at shorter wavelengths, biasing estimates of elastic plate thickness to stronger values. Therefore, we have estimated the flexural rigidity within smaller parts of these regions that have better data coverage (SUDN, ZAIR, CONGO). Data in these smaller sub-regions are fit by models for elastic plate thicknesses of 65-89 km, but residuals for the best-fitting models in these smaller areas are high (Table II). There are few points in the transitional waveband within these cratonic sub-regions, and the observed coherence can be fit by much thicker elastic plates (93-180 km). Because larger estimates of elastic plate thickness predict a fall-off from high to low coherency at longer wavelengths, these results suggest that sub-regions ZAIR, CONGO, and possibly SUDN are too small to observe the transition from low to high coherency for a stiff cratonic plate, so that these estimates of thickness provide lower bounds on the rigidity. We also have modelled regions which we regard as unreliable because of data gaps. Nevertheless, these regions yielded best estimates of 120-130 km that are comparable to estimates of elastic plate thickness of 100 km or more beneath cratonic areas of North America and Australia, regions where data coverage is more uniform (e.g., Bechtel et al., 1986; Zuber et al., 1987).

Divisional boundaries were chosen to isolate the eastern and western limbs of the East African and the Afar rift systems, the entire Afar and East African plateau regions (BIG, ETHP), and the Darfur dome (JBLM), as well as volcanic and non-volcanic sections of the two rift systems (Figures 7b, c). By separating faulted regions and areas affected by Tertiary volcanism within the uplifted areas, we can evaluate the relative contribution of these factors to the strength of the lithosphere beneath the East African and Afar plateaus. Estimates of elastic plate thickness beneath sub-regions that include the densely faulted rift valleys are much smaller than those determined within the cratonic regions, and the quality of fits within each of these sub-regions is good (Table II). An exception is sub-region ATRI, a region that encompasses both oceanic and continental crust and where the uniform elastic plate assumption may be invalid. Sub-region ATRI and, to a lesser extent, ETHR, show a broad transitional waveband characteristic of non-uniform regions, but, more likely, the shape of the observed coherence is indicative of sparse data in these regions and consequent lack of coherence. The upper bound on rigidity for ATRI is probably valid, but the actual elastic plate thickness may be much thinner than our best estimate. The elastic plate thickness found beneath the Ethiopian rift valley (ETHR; 24 km) is less than that found beneath either the Western rift system (NWBR, CWBR, SWBR; 31-42 km) or the Kenya rift system (NEBR, DOME, SEBR; 31-42 km). Comparing magmatically active parts of the rift valley to those which exclude Tertiary volcanic provinces, the elastic plate thickness estimate within the non-volcanic sub-region at the northern end of the Western rift NCNV (31 km) is the same as that determined within sub-region DOME (31 km), a region affected by volcanic activity from mid-Miocene to Recent time (e.g., King, 1978; Baker, 1986). Sub-region SCV which is located at the southern end of the Western rift includes a Late Miocene to Recent volcanic province and part of the rift valley (e.g., Figure 1), but the elastic plate thickness (55 km) is greater than estimates determined within other rift valley sub-regions (Figure 7c; Table II).

Elastic plate thicknesses within sub-regions that encompass the uplifted Afar and East African plateaus (ETHP, BIG) and the Darfur dome (JBLM) are significantly less than those estimated within the stable cratonic sub-regions CONGO, SUDN, and ZAIR. These estimates are greater than those estimated within the rift valley sub-regions (Figure 7c). However, sub-regions ETHP and BIG average uplifted regions with rift valley regions that are underlain by weaker plates. This averaging also is suggested by the observed coherence within ETHP and BIG, where the coherence within the transitional wavebands of the two rifted plateau sub-regions increases, decreases, then approaches unity. This pattern is not observed in the largely unfaulted Darfur dome region. The 43 km elastic plate thickness found beneath the Darfur dome (JBLM) is comparable to values

obtained within sub-regions encompassing the Kenya and Western rift valleys (NWBR, SCV), but there is little evidence for Tertiary faulting in the Darfur dome area (e.g., Whiteman, 1971; Browne et al., 1983). We have isolated a region of Archaean crust within the central part of the East African plateau (PLAT) which largely excludes the severely faulted rift valleys and volcanic provinces (Figure 5). Thus, averaging over regions affected by faulting and/or crustal thinning should not be an important factor affecting effective elastic plate thicknesses in PLAT. We find that the elastic plate thickness is twice that found beneath sub-regions that include the faulted rift valleys. The estimate of elastic plate thickness in sub-region PLAT (64 km) is greater than that found within BIG, which encompasses the East African plateau, but is less than values determined in sub-regions outside the uplifted domes (65-180 km). Considering that the elastic plate thickness estimates in ZAIR, CONGO, and SUDN probably represent minimum estimates of elastic plate thickness beneath these regions, and by analogy to the thinning observed within the largely unfaulted Darfur dome region (43 km), the lithosphere beneath the uplifted plateau sub-regions may be weaker than that beneath the neighboring cratonic regions. However, the extent of thinning of the mechanical lithosphere beneath the largely unfaulted central part of the uplifted East African plateau is poorly constrained given existing data coverage.

Discussion

This comparison of elastic plate thickness estimates beneath eastern and central Africa reveals three consistent relations between elastic plate thickness and tectonic provinces. Stable cratonic regions are underlain by relatively thick elastic plates (65-180 km). Because smaller sub-divisions of the cratonic regions are not large enough to observe the fall-off from high to low coherency, elastic plate thicknesses beneath these regions probably fall within the middle to upper part of this range. Elastic plate thicknesses decrease within regions encompassing the uplifted and rifted East African and Afar plateaus, both of which have formed in stable cratonic regions. The rift valley topography superimposed on the East African and Afar plateaus is absent within the Darfur dome region, but the elastic plate thickness determined within the uplifted Darfur dome region (JBLM) is significantly weaker than estimates corresponding to stable cratonic regions. Within the uplifted regions the smallest elastic plate thicknesses are found beneath the faulted rift valleys.

Considering the tectonic setting of the three rift valley regions, we anticipate that several factors influence the effective elastic plate thickness estimates within sub-regions encompassing the Western, Kenya, and Ethiopian rift valleys. The rift valley regions superimposed on the plateaus probably have been weakened by a combination of thermal

processes causing domal uplift, by faulting (e.g., NWBR, SWBR), and possibly by smaller scale thermal processes related to magmatic activity. Regions that encompass the 30-70 km wide, densely faulted rift valleys also include unfaulted regions adjacent to the rift valleys, but data coverage is insufficient to warrant further subdivisions. Because fault topography is averaged with the relief of the presumably stronger areas adjacent to the basins, we anticipate that estimates of 30-45 km within the rift valley sub-regions are biased to greater values. This averaging can be illustrated by comparing the elastic plate thickness corresponding to sub-region BIG (48 km) and sub-region PLAT (64 km). The elastic plate thickness within the central plateau (PLAT) is greater than the estimate of the elastic plate thickness averaged over the entire East African plateau (BIG), which also includes the East African rift valleys. In previous studies of data from regions that encompass the Basin and Range extensional province of North America, elastic plate thickness estimates are extremely small ($T_e < 10$ km; Bechtel et al., 1986). Thus, the lithosphere may be much weaker than 30 km beneath the East African and Ethiopian rift valleys, although earthquakes throughout the depth range 5-30 km beneath the East African rift valleys (e.g., Zana and Hamaguchi, 1978; Shudofsky, 1985) occur at greater depths than the 10-15 km range observed beneath the Basin and Range province (e.g., Smith and Sbar, 1974).

Within the rift valley sub-regions the assumption of a continuous plate may be invalid, as indicated by the distribution of surface and subsurface loads generated in the inversion for elastic plate thickness within the faulted rift valley regions. The 200-300 km wide uplifted regions flanking the rift valleys appear as surface loads in the coherence analyses. However, we know from geological information that volcanic edifices contribute little to the elevation of rift flanks in the Western rift system, and that most of the 1000-2000m of uplift along the rift flanks is due to deeper loads (i.e. at the base of the crust and within subcrustal lithosphere). However, if the rift flank uplift is caused by subsurface loads on a broken plate, this topography will be much shorter than the flexural wavelength of an unbroken lithosphere (~800 km; Figure 7), and the flanking uplifts will appear as surface loads. Thus, the distribution of surface loads suggests that the assumption of a uniform elastic plate may be invalid within the rift valley sub-regions, and that the lithosphere beneath the rift valleys behaves as a broken plate.

Estimates of elastic plate thickness within a sub-region encompassing the Afar plateau (ETHP; 52 km) are less than those found within sub-regions of the East African plateau (BIG; 48 km). Similarly, estimates of elastic plate thickness within sub-regions encompassing the Ethiopian rift system (ETHR; 24 km) are less than those found within the Kenya and Western rift systems (30-55 km). This trend is consistent with geological

and geophysical data; the Afar region has experienced a 5-10 My longer period of extensional faulting and volcanism than the East African rift system, and the crust beneath the Ethiopian rift valley is thinner than that beneath either the Kenya or Western rift systems, based on the results of seismic studies (e.g., Searle and Gouin, 1971; Lepine et al., 1972; Long et al., 1973). Within the uncertainties of the measurements reported in Table II, we cannot determine if the Kenya rift, where volcanism began 5-10 My prior to volcanism within the Western rift, is underlain by lithosphere that is significantly weaker than that beneath the Western rift system.

Considering the proposed thermal origin for the East African and Afar plateaus and the Darfur dome, we suggest that thermal processes in the upper mantle also may contribute to the observed weakening of the elastic plate beneath these zones of uplift. One could argue that faulting processes bias estimates of elastic plate thickness within the uplifted East African and Afar dome regions to weaker values, but the significantly thinner elastic plate found beneath the largely unfaulted and volcanically active Darfur dome suggests that the mechanical lithosphere beneath the uplifts has been weakened by thermal processes. By analogy to better-studied oceanic swells, several authors have suggested that thermal processes can cause uplift and weakening of the mechanical lithosphere beneath magmatically active oceanic midplate swells (e.g., Crough, 1978; Menard and McNutt, 1982). The elastic plate thickness of oceanic lithosphere is generally assumed to depend on the temperature structure within the lithosphere, and is believed to be approximately equal to the depth to the 450-600°C isotherm (Watts et al., 1980; Bodine et al., 1981; Menard and McNutt, 1982). Similarly, a thermal dependence has been proposed for the rheologically more complicated and more laterally heterogeneous continental lithosphere (Karner et al., 1983; Willett et al., 1985). In order to provide additional constraints on the thermal structure beneath the intracontinental swells of East Africa, we examine the long wavelength aspects of the gravity and topography fields from the East African dome region.

Depth of Compensation for East African Plateau

Much of the topographic relief of the broad plateaus, or intraplate domes, of East Africa, occurs at wavelengths longer than the characteristic flexural wavelength of the lithosphere beneath the plateaus (e.g., Figure 7b). Therefore, these domes cannot be supported by elastic stresses within the lithosphere, and the topographic relief of the plateaus must be supported by density variations within the mantle beneath the elastic plate. Because surface and intracrustal loads contribute little to the long wavelength gravity field, the relationship between gravity and topography at long wavelengths provides information on the density structure beneath the plateaus supporting the topographic relief. At shorter

wavelengths, where gravity and topography are incoherent, surface and internal loads are partially or wholly supported by elastic stresses within the plate. Therefore, the gravity field at short wavelengths largely is due to different processes than the dynamic processes supporting the long wavelength topography. At wavelengths where the gravity and topography signals are coherent, we use the ratio of the transformed gravity, G(k), to the transformed topography, H(k), the admittance, to estimate the depth of compensation for the broad East African plateau (e.g., Dorman and Lewis, 1970). In order to include a region large enough to examine the long wavelength aspects of the gravity field beneath the 1300 km wide East African plateau, we have computed the admittance in a sub-region encompassing the uplifted East African plateau, excluding cratonic regions outside the uplift (BIG; Figure 5).

The observed admittance from the uplifted East African plateau region shown in Figure 9 decreases fairly uniformly to values less than -1.0 g.u./m at wavelengths longer than 2000 km. Theoretical isostatic models of the admittance that assume surface and/or subsurface loading of an elastic plate are near zero at short wavelengths due to the attenuation of subsurface gravity fields by upward continuation, and values approach the Bouguer slab correction, $-2\pi\rho_c G$, at long wavelengths (e.g., Banks et al., 1977; McNutt, 1983). However, the observed admittance is more negative than the Bouguer slab effect (-1.12 gu/m) at long wavelengths, and the admittance values fall along a fairly linear trend (Figure 9). Because gravity and topography data in sub-region BIG were mirrored in x and y prior to transformation to the wavenumber domain, the admittance at the longest wavelengths may be biased by mirroring. Our transformation (through mirroring) is essentially a cosine transformation so that the largest wavelengths in the orthogonal decomposition are twice the length of the region. We neglected these wavelengths in the coherence analyses because an artificial coherence might have been introduced. The power at the longest wavelengths included in the coherence analyses gave an admittance value above the value for the Bouguer slab effect, as indicated by the point with small error bars in Figure 9. As confirmation of this observation, we also examine the admittance at the longest wavelengths, which have the greatest power of any of the Fourier components within this sub-region. The admittance at the longest wavelengths also is more negative than the Bouguer slab effect, and the value within this waveband falls along the same linear trend as the previous values (Figure 9). Because the observed admittance from the East African plateau is less than the Bouguer slab correction at wavelengths longer than the characteristic flexural wavelength of the lithosphere, the observed admittance cannot be fit by local isostatic compensation models, such as crustal underplating, nor by simple physical models involving density contrasts beneath the elastic plate and the consequent

upwarping of the plate above the low-density material at depth (e.g., Crough, 1978). Instead, these observations indicate that the East African plateau is overcompensated, or that there is an excess of low density material per unit topographic relief beneath the East African plateau.

Dynamic compensation mechanisms that can explain the overcompensated nature of these broad plateaus have been used to model gravity and bathymetry data from oceanic midplate swells (e.g., McKenzie, 1977; Parsons and Daly, 1983; Robinson and Parsons, 1988). We apply a technique described by Parsons and Daly (1983) to data from the uplifted East African plateau, which has developed within the rheologically more complicated continental lithosphere, in order to investigate possible compensation mechanisms for this broad intracontinental uplift. Our intent is to determine a general class of acceptable physical models (e.g. McKenzie, 1977) and to place some bounds on the depth of the low density material compensating the plateau topography. As described by McKenzie (1977), the gravity anomaly predicted in these theoretical models is sensitive to the choice of boundary conditions, and only a limited number of combinations of boundary conditions can explain gravity and topography data from the East African plateau region.

The observed admittance from the East African plateau is compared to theoretical admittance models predicted by a dynamic compensation mechanism that was formulated using a Green's function technique (Parsons and Daly, 1983). In the general case, we assume that convection occurs in a constant viscosity fluid layer overlain by a conducting lid, or the continental lithosphere (Figure 6b). Stresses within the fluid layer arise from density contrasts within the convecting region, and the top and bottom boundaries deform in order to ensure continuity of normal stresses across the boundaries (e.g., McKenzie, 1977). At the upper and lower interfaces of the convecting region, we impose no-slip boundary conditions, or require velocities to be zero at these interfaces. We impose a no-slip rather than 'free' boundary condition at the top of the convecting region because the lithosphere beneath the East African plateau is largely cratonic and, therefore, assumed to be cold and relatively strong. The no-slip boundary condition at the base of the convecting region represents an albeit crude physical representation of a large viscosity contrast within the upper mantle or at the base of the asthenosphere. We also consider solutions for models in which the bottom boundary cannot deform.

Using the Green's function derivations for no slip, or 'rigid', top and bottom boundary conditions described in Parsons and Daly (1983), we calculate weighting functions for the topographic relief at the top boundary of the region and gravity within the layer as functions of compensation depth and wavenumber. Conceptually, these weighting functions, or kernels, reveal the relative contributions of temperature distributions at

various depths within the convecting region to the observed topography and gravity. With 'rigid' boundary conditions imposed on both the top and bottom of the region, the bottom boundary kernel is related to the surface topography kernel by:

$$H_b(k,z) = H_t(k, 1 - z) \tag{7}$$

(Parsons and Daly, 1983). Because the convecting layer is overlain by a plate with some flexural rigidity D, we calculate a modified topography kernel, $H_t'(k, z_l)$:

$$H_t'(k,z_l) = H_t(k, z_l) \frac{\rho_m g}{(\rho_m g + Dk^4)} \tag{8}$$

[The topography kernel $H_t(k,z_l)$ in (8) is found by substituting expressions given in (A11) and (A12) into (A5) of Parsons and Daly (1983)]. The surface topography kernel, $H_t(k, z_l)$, is the Green's function response to a step in pressure at depth z_l, and is a function of wavenumber scaled by the thickness of the convecting layer. The surface topography kernel is always positive, and H_t varies from one at the top boundary to zero at the bottom boundary. The surface topography kernel changes from concave downward in the upper part of the region to concave upward in the lower part of the convecting region.

The gravity kernel, $G(k,z_l)$, modified from equation (22) of Parsons and Daly (1983) for the general case of Bouguer gravity data from a continental region, is:

$$G(k, z_l) = 2\pi G[\rho_m H_t'(k,z_l)e^{-kzt} - \rho_m e^{-kzl} + \rho_m H_b(k,z_l)e^{-kzb} - \rho_c H_t'(k, z_l)] \tag{9}$$

The gravity kernel represents the sum of contributions from the topography at the base of the conducting lid (H_t') at depth z_t, density variations within the layer, and relief on the bottom boundary (H_b) (Figure 6). Thus, the gravity kernel at any depth represents a balance between the topographic relief at the upper and lower boundaries (z_t, z_b) and the density contrasts within the fluid layer. In the case where the bottom boundary is non-deformable, the amplitude of the gravity kernel at any depth is less than or equal to models in which the bottom boundary deforms in response to stresses within the fluid layer. The topography and gravity kernels approach zero when z_l lies near the bottom boundary of the region, and the admittance equals the Bouguer slab correction when z_l lies near the upper boundary of the region.

Although the surface topography and gravity anomalies are dependent upon the temperature distributions within the convecting region, we represent the integrals over the thickness of the layer as a pressure perturbation at an equivalent depth, z_l, and examine the weighting functions due to the resulting stresses at the boundaries of the region. In this way, we place some bounds on the depth extent of the compensating material, without

specifying temperature distributions within the convecting region. We have computed the ratio of G to H_t' for a number of depths z_l, limiting acceptable models to those which fit the observed admittance in sub-region BIG at wavelengths greater than approximately 1000 km, wavelengths where gravity and topography signals are coherent (Figure 9). In all models, crustal thickness, z_m, is 40 km, and the flexural rigidity, D, is 9×10^{23} Nm, the effective elastic plate thickness that we determine within sub-region BIG (e.g., Figure 7b). We assume that the top boundary of the convecting region physically represents the depth within the continental lithosphere beneath which material deforms in a ductile manner and can be entrained in the convective flow (e.g., McKenzie, 1977; Parsons and Daly, 1983; Robinson et al., 1988). We consider models in which the depth to the top of the convecting region is as shallow as the base of the elastic plate, and place some maximum constraint on the depth to the top of the convecting region. Because the depth extent of mantle convection and the viscosity structure of the upper mantle are poorly understood, we also vary the depth to the base of the convecting layer (z_b) to determine a range of acceptable models.

The East African plateau appears overcompensated, indicating that z_l must lie within the depth range where the topography kernel is comparatively smaller than the absolute value of the gravity kernel, or near the middle to lower part of the convecting region. In all models shown in Figure 9, the rapid increase in the predicted admittance at intermediate wavelengths is due to the attenuation of the gravity signal from the temperature anomaly at a deeper depth compared to the positive gravity anomaly due to the upward deflection of the plate. For layer thicknesses greater than approximately 430 km, the predicted admittance curve for any depth z_l steepens over wavebands greater than observed due to attenuation by the upward continuation filter in (9) (e.g., Figure 9a). Because the relief on the upper boundary becomes more negative with depth within the convecting region, the predicted admittance decreases as z_l approaches the bottom boundary, z_b (e.g., Figure 9b).

The observed admittance can be fit by a limited range of combinations of compensation depth, z_l, and convecting layer thickness, z_b. For models that include the effects of deformation of the bottom boundary, we find that the greatest compensation depth that fits the observed admittance corresponds to 380 km within a 430 km convecting layer, and that the shallowest depth z_l is 180 km within a 240 km thick convecting layer. If we do not allow deformation of the bottom boundary ($H_b = 0$), acceptable models correspond to depths z_l between 100 and 150 km within convecting layers of thickness 240 km and 285 km, respectively. However, because sub-region BIG encompasses the much weaker rift valley regions, the mechanical plate thickness beneath the uplifted plateau may

be closer to the estimate we determine within the largely unfaulted central region (PLAT; 64 km). Considering the attenuation due to the upward continuation filter in (8), models shown in Figure 9 probably represent maximum compensation depths. The thickness of the conducting lid (thermal lithosphere) must be less than about 180 km in order to fit the observed admittance, and the compensating material lies in a thin zone (40 km thick) when this maximum thickness is assumed. Therefore, convecting layer thicknesses of 600 km or more, or models corresponding to upper mantle and whole mantle convection with uniform viscosity, cannot fit the observed admittance from the uplifted East African plateau region (e.g., Figure 9). Instead, we find acceptable models correspond to layer thicknesses between about 430 km and 40 km beneath conducting lids of thickness 48 and 180 km, respectively, and compensation depths lie at intermediate to deep levels within these regions.

One possible interpretation of these results is convective heating of the continental lithosphere decoupled from a deeper asthenospheric plume by a viscosity increase within the upper part of the asthenosphere. A low viscosity layer within a convecting region reduces the transmission of normal stresses within the layer, and, therefore, relief at the top of the convecting layer, resulting in shallower depths of compensation (e.g., Robinson et al., 1987). A low viscosity layer has been suggested beneath the oceanic lithosphere (e.g., Turcotte and Oxburgh, 1967; Solomon, 1972; Parmentier, 1978; Fleitout and Yuen, 1984), and a similar low viscosity layer also may occur beneath these tectonically active continental rift zones. The range of compensation depths that fit the observed admittance at long wavelengths (380-100 km) does not necessarily indicate that convection is limited to the uppermost mantle, but that density anomalies at greater depths contribute little to the maintenance of the plateau topography. Thus, the topographic relief of the East African plateau largely is supported by density variations within the upper mantle. These results also indicate that the base of the continental lithosphere has been heated, or thinned from below.

These dynamic models place some bounds on the thermal plate thickness beneath East Africa, but we cannot quantify the amount of lithospheric thinning that has occurred beneath the East African plateau based on these results alone. The large elastic plate thicknesses determined within the cratonic regions adjacent to the uplifted plateaus suggest that the original lithospheric thickness beneath the East African plateau was greater than 200 km, and continental lithospheric thicknesses greater than 200 km have been interpreted from independent observations elsewhere (e.g. Peltier, 1984; Lerner-Lam and Jordan, 1987). If we assume that the base of the conducting lid corresponds to the base of the thermal lithosphere beneath the East African plateau, these results indicate that the

lithosphere is less than 180 km thick. The African plate has been approximately stationary relative to the mantle during the past 25 My (e.g., Thiessen et al., 1978; Morgan, 1983). Hence a mantle upwelling may have thermally eroded the base of the slowly moving African plate. If we assume that the lower continental lithosphere beneath the elastic plate is mechanically weak, this region is susceptible to advection in the presence of a mantle upwelling (e.g., Yuen and Fleitout, 1986). Using a more complicated temperature-dependent viscosity structure, Yuen and Fleitout (1986) show that a combination of strong secondary convection and a rising lithospheric plume can thin a 225 km thick continental lithosphere by a factor of two in a 25 My time period. This is roughly the time interval that has elapsed since initial uplift and volcanism within the East African plateau region, and less than the time since initial volcanism within the Afar plateau region (e.g., Baker, 1986). This mantle lithospheric heating may lead to a slight reduction in the thickness of the mechanical lithosphere, although the amount of thinning of the mechanical lithosphere is dependent upon original lithospheric thickness and heat flux at the base of the plate. By analogy to the thinned elastic plate found beneath the volcanically active but unfaulted Darfur dome region, the apparent thinning of the mechanical lithosphere beneath the East African plateau may be due to thermal processes. The magnitude of thinning beneath the East African plateau appears to be small, but is poorly constrained by elastic plate thicknesses within the stable cratonic regions adjacent to the uplifted plateau.

The results of this study suggest that the gravity field and topographic relief of the broad East African plateau can be explained by convective processes within the upper mantle and associated conductive heating of the continental lithosphere. This thinning leads to a minor reduction in elastic plate thickness beneath the zones of Tertiary uplift. A dynamic uplift mechanism also is compatible with the time scales of volcanism, uplift, and rifting in East Africa, and the lack of evidence for crustal thinning outside the narrow rift valleys. Improved gravity coverage and additional constraints on thermal gradients beneath the central plateau regions, the geometry and depth extent of faulting, and the timing of vertical crustal movements in East Africa will improve our ability to discriminate amongst the various isostatic and dynamical compensation models described above.

CONCLUSIONS

Based on the results of these analyses of gravity and topography data integrated with existing geological and geophysical information from the East African and Afar plateau regions, estimates of effective elastic plate thickness are well correlated with tectonic provinces. Stable cratonic regions in Africa are underlain by strong lithosphere (effective elastic plate thickness 65-180 km). Smaller estimates are found beneath regions encompassing the 1000-1300 km wide uplifted East African and Afar plateaus (effective

elastic plate thicknesses 52-64 km) and the approximately 500 km wide Darfur dome (effective elastic plate thickness 43 km). The smallest estimates of effective elastic plate thickness are found within sub-regions that encompass the fault-bounded and volcanically active rift valleys superimposed on the broad plateaus. We attribute the smallest estimates of elastic plate thickness (22-55 km) to averaging unfaulted topography with mechanically weakened topography within the severely faulted Kenya, Western, and Afar rift systems. The distribution of surface loads within the rift valley regions suggests that the lithosphere beneath the narrow valleys bounded by steep faults may be effectively broken. However, we find little evidence that the lithosphere beneath inactive Mesozoic rift basins is weaker than that beneath the cratonic regions (e.g., SUDN; 74 km). In volcanically active parts of the Kenya, Western, and Ethiopian rift systems, thermal softening due to magmatic processes also may contribute to the reduction in effective elastic plate thickness.

The broad East African plateau appears overcompensated, and the long wavelength gravity and topography fields from the East African plateau region cannot be explained by simple isostatic compensation models, such as crustal underplating. Instead, the ratio of the power of gravity to topography at wavelengths longer than about 1000 km indicates that the plateau topography is dynamically maintained, and that the thermal lithosphere has been thinned beneath the uplifted regions. The apparent thinning of the elastic plate beneath the uplifted East African and Afar plateaus and the Darfur dome relative to the stable cratonic regions also is attributed to thermal processes within the upper mantle beneath the uplifted regions. This dynamic compensation mechanism is consistent with existing geological and geophysical data and with constraints on the timing of volcanism and uplift within the East African plateau region.

Acknowledgements

We thank L. Royden and M. McNutt for numerous discussions and comments on the text, K. Burke, R. Stein, and an anonymous reviewer for constructive comments. C.E. was supported by a Presidential Young Investigator award (EAR-8451139) granted to L. Royden and a Geological Society of America Student Research Grant. This study was supported in part by the National Science Foundation under grant EAR-8518605.

References

Baker, B.H., Tectonics and volcanism of the southern Kenya Rift Valley and its influence on rift sedimentation, in: L.E. Frostick, et al., eds., *Sedimentation in the East African Rifts*, Geol. Soc. Spec. Pub. 25, 45-57, 1986.

Banks, R.J., R.L. Parker, and S.P. Huestis, Isostatic compensation on a continental scale: local versus regional mechanisms, *Geophys. J.R. Astron.Soc., 51*, 431-452, 1977.

Banks, R.J. and D. Beamish, Melting in the crust and upper mantle beneath the Kenya rift: Evidence from geomagnetic deep sounding experiments, *J. geol. Soc. Lond., 136*, 225-233, 1979.

Banks, R.J. and C. Swain, The isostatic compensation of East Africa, *Proc. R. astr. Soc., Ser. A, 364*, 331-352, 1978.

Beauchamp, R. S., The rift valley lakes of Africa, *Verh. Internat. Verein Limnol., 15*, 91-99, 1964.

Bechtel, T.D., D.W. Forsyth, V.L. Sharpton, R.A.F. Grieve, Variations in effective elastic thickness of the North American lithosphere, *EOS, Trans. Amer. Geophys. Union, 67,* 370, 1986.

Bechtel, T., D. Forsyth, and C. Swain, Mechanisms of isostatic compensation in the vicinity of the East African rift, Kenya, *Geophys. J. R. Astr. Soc., 90,* 445-465, 1987.

Bellon, H., and A. Pouclet, Datations K-Ar de quelques laves du Rift-ouest de l'Afrique Centrale; Implications sur l'évolution magmatique et structurale, *Geologische Rundschau, 69*, 49-62, 1980.

Bermingham, P.M., J.D. Farihead, and G.W. Stuart, Gravity study of the central African rift system: A model of continental disruption, 2. The Darfur domal uplift and associated Cainozoic volcanism, *Tectonophysics, 94*, 205-222, 1983.

Bodine, J.H., M.S. Steckler, and A.B. Watts, Observations of flexure and the rheology of the oceanic lithosphere, *J. Geophys. Res., 86*, 3695-3707, 1981.

Bosworth, W., Off-axis volcanism in the Gregory rift, East Africa: Implications for models of continental rifting, *Geology, 15*, 397-400, 1987.

Bram, K., and B.D. Schmeling, Structure of crust and upper mantle beneath the Western Rift of East Africa, derived from investigations of near earthquakes, in: A.Pilger and A. Rosler, eds., *Afar Between Continental and Oceanic Rifting*, Schweizerbart, Stuttgart, 138-142, 1975.

Browne, S., J.D. Fairhead, and I.I. Mohamed, Gravity study of the White Nile rift, Sudan, and its regional tectonic setting, *Tectonophysics, 113,* 123-137, 1985.

Bullard, E.C., Gravity measurements in East Africa, *Proc. Roy astr. Soc., 235,* 445-531, 1936.

Burke, K., and J.F. Dewey, Plume-generated triple-junctions: Key indicators in applying plate tectonics to old rocks, *J. Geol., 81*, 406-433, 1973.

Capart, A., Sondages et carte bathymetrique, in: Exploration Hydrobiologique du lac Tanganyika (1946-1947), Brussels, *Inst. R. Sci. Nat. Belg.*, 1-16, 1949.

Crough, S.T., Thermal origin of mid-plate hotspot swells, *Geophys. J. Roy. Astr. Soc., 55,* 451-469, 1978.

Crane, K., and S. O'Connell, The distributions and implications of heat flow from the Gregory rift in Kenya, *Tectonophysics, 94*, 253-275, 1983.

Davidson, A., and D.C. Rex, Age of volcanism and rifting in sothwestern Ethiopia, *Nature, 283*, 657-658, 1980.

Degens, E.T., Von Herzen, R.P., Wong, H.K., Deuser, W.G., and Jannasch, H.W., Lake Kivu: Structure, chemistry, and biology of an East African rift lake, *Geol. Rund., 62*, 245-277, 1973.

Degens, E.T., Von Herzen, R.P., Wong, H-K., Lake Tanganyika: water chemistry, sediments, and geological structure, *Naturwissenschaften, 58*, 229-241, 1971.

Dorman, L., and B.T. Lewis, Experimental isostasy, I: Theory of the determination of the Earth's isostatic response to a concentrated load, *J. Geophys. Res., 75*, 3357-3365, 1970.

Ebinger, C.J., Tectonic controls on rift magmatism, East Africa, *EOS, Trans. Am. Geophys. Un., 68*, 1502, 1987.

Ebinger, C.J., B.R. Rosendahl, and D.J. Reynolds, Tectonic model of the Malawi rift, Africa, in: Z. Ben-Avraham, ed., Sedimentary Basins within the Dead Sea and Other Rift Zones, *Tectonophysics, 141*, 215-235, 1987.

Eccles, D., An outline of the physical limnology of Lake Malawi, *Limnol. Oceanogr.*, 730-742, 1974.

Fairhead, J., Structure of the lithosphere beneath the Eastern rift, East Africa, deduced from gravity studies, *Tectonophysics, 30*, 269-298, 1976.

Fairhead, J., and Stuart, G., The seismicity of the East African rift system and comparison with other continental rifts, in: G. P. Palmason, ed., *Continental and Oceanic Rifts,* Am.. Geophys. Un.: Washington, D.C., 41-61, 1982.

Fleitout, L., and D.A. Yuen, Steady state, secondary convection beneath lithospheric plates with temperature-dependent, pressure-dependent viscosity, *J. Geophys. Res., 89,* 9244-9277, 1984.

Forsyth, D.W., Subsurface loading and estimates of the flexural rigidity of the continental lithosphere,*J. Geophys. Res., 90*, 12,623-12,632, 1985.

Girdler, R., and Sowerbutts, W.T.C., Some recent geophysical studies of the rift system in E. Africa, *J. Geomag. Geoelectr., 22*, 153-163, 1970.

Griffiths, D., King, R., Khan, M., and Blundell, D., Seismic refraction line in the Gregory Rift, *Nature, 229*, 69-71, 1971.

Harkin, D., The Rungwe volcanics at the northern end of Lake Nyasa, *Geological Survey Tanganyika, Mem. II*, 172p., 1960.

Hebert, L., and C. Langston, Crustal thickness estimate at AAE (Addis-Ababa, Ethiopia) and NAI (Nairobi, Kenya) using teleseismic P-wave conversions. *Tectonophysics, 111*, 299-32, 1985.

Holmes, A., Basaltic lavas of S. Kivu, Belgian Congo, *Geol. Mag., 77*, 29-43, 1940.

Karner, G., M.S. Steckler, and J.A. Thorne, Long-term thermo-mechanical properties of the continental lithosphere, *Nature, 304*, 250-253, 1983.

Khan, M.A., and J. Mansfield, Gravity measurements in the Gregory rift, *Nature, Phys. Sci., 229*, 72-75, 1971.

King, B.C., Structural and volcanic evolution of the Gregory rift valley, in: W.W. Bishop, ed., *Geological Background to Fossil Man*, Scottish Academic Press, Edinburgh, 29-54, 1978.

KRISP, Working Group, Kenya Rift International Scientific Project: Preliminary results, *Nature*, 325, 239-242, 1987.

Lepine, J.C., J.C. Ruegg, and L. Steinmetz, Seismic profiles in the Djibouti area, in: R.W. Girdler, ed., *East African Rifts, Tectonophysics, 15*, 59-64, 1972.

Lerner-Lam, A.L., and T.H. Jordan, How thick are the continents?, *J. Geophys. Res., 92,* 14,007-14,026, 1987.

Long, R. and R. Backhouse, The structure of the western flank of the Gregory Rift (Kenya), Part II: The mantle, *Geophys. J. R. astr. Soc., 44*, 677-688, 1976.

Maguire, P., and R. Long, The structure of the western flank of the Gregory Rift (Kenya), Part I: The crust, *Geophys. J. R. astr. Soc, 44*, 661-675, 1976.

Makris, J., H. Menzel, and J. Zimmermann, A preliminary interpretation of the gravity field of Afar, northeast Ethiopia, *Tectonophysics, 15:* 31-39, 1972.

McKenzie, D.P., Surface deformation, gravity anomalies and convection, *Geophys. J.R. Astron. Soc., 48,* 211-238, 1977.

McNutt, M.K., Influence of plate subduction on isostatic compensation in northern California, *Tectonics, 2*, 399-415, 1983.

Menard, H.W., and M.K. McNutt, Evidence for and consequences of thermal rejuvenation, *J. Geophys. Res., 87*, 8570, 1982.

Mohr, P., Volcanotectonic aspects of Ethiopian rift evolution, *Bull. Centres Rech. Explor.-Prod. Elf-Aquitaine, 7,* 175-189, 1983.

Mooney, W.D., M.S. Andrews, A. Ginzburg, D.A. Peters, and R.M. Hamilton, Crustal structure of the northern Mississippi embayment and comparison with other rift zones, *Tectonophysics, 94*, 327-348, 1983.

Morgan, P., Constraints on rift thermal processes from heat flow and uplift, *Tectonophysics, 94,* 277-298, 1983.

Morgan, W.J., Hotspot tracks and the opening of the Atlantic and Indian Oceans, in: C. Emiliani, ed., *The Sea, v. 7*, New York: Wiley, 443-488, 1981.

Munk, W., and D.E. Cartwright, Tidal spectroscopy and prediction, *Phil. Trans.R. Soc. Lond. Ser. A, 259*, 533-589, 1966.

Nolet, G., and S. Mueller, A model for the deep structure of the East African rift system from the simultaneous inversion of teleseismic data, *Tectonophysics, 84*, 151-178, 1982.

Parmentier, E.M., A study of thermal convection in non-Newtonian fluids, *J. Fluid Mech., 84*, 1-19, 1978.

Parsons, B., and S. Daly, The relationship between surface topography, gravity anomalies, and temperature structure of convection, *J. Geophys. Res., 88*, 1128-1144, 1983.

Pasteels, P., P. De Paepe, M. Villeneuve, and J. Klerkx, Age of the volcanism of the southern Kivu area (Western Rift: Burundi, Rwanda, Zaire), submitted to *Earth Planet. Sci. Letts.*, 1986.

Peltier, W.R., The thickness of the continental lithosphere, *J. Geophys. Res., 89,* 11,303-11,316, 1984.

Peirce, J., and L. Lipkov, Report on the structural interpretation of the Rukwa rift, Tanzania, *Geophysics*, in press.

Robinson, E.M., B. Parsons, and S. Daly, The effect of a low-viscosity zone on the apparent compensation depth of mid-plate swells, *Earth Plan. Sci. Letts., 82*, 335-348, 1987.

Robinson, E.M. and B. Parsons, Effect of a low-viscosity zone on the formation of mid-plate swells, *J. Geophys. Res., 93*, 3144-3156, 1988.

Rykounov, L.N., V.V. Sedov, L.A. Savrina, and V.J. Bourmin, Study of microearthquakes in the rift zones of East Africa, in: R.W. Girdler, ed., *East African rifts, Tectonophysics, 15*, 123-130, 1972.

Saggerson, E.P., and B.H. Baker, Post-Jurassic erosion surfaces in eastern Kenya and their deformation in relation to rift structure, *Quart. J. geol. Soc. Lond.*, 121, 5-72, 1965.

Searle, R., and P. Gouin, An analysis of some local earthquake phases originating near the Afar Triple-Junction, *Bull. Seism. Soc. Am., 61*, 1071-1081, 1971.

Shudofsky, G.N., Source mechanisms and focal depths of East African earthquakes using Rayleigh wave dispersion and body-wave modeling, *Geophys. J. R. astr. Soc., 83,* 563-614, 1985.

Skinner, N.J., Recent geophysical studies of the Kenya rift valley, *Contemp. Physics, 18,* 455-470, 1977.

Smith, R.B., and M.L. Sbar, Contemporary tectonics and the seismicity of the western United States with emphasis on the Intermountain seismic belt, *Geol. Soc. Amer. Bull., 85,* 1205-1218, 1974.

Solomon, S.C., Seismic wave attenuation and partial melting in the upper mantle of North America, *J. Geophys. Res., 77,* 1489, 1972.

Swain, C.J., A FORTRAN IV program for interpolating irregularly spaced data using the difference equations for minimum curvature, *Computers and Geosciences, 1,* 231-240, 1978.

Thiessen, R., K. Burke, and W.S.F. Kidd, African hotspots and their relation to the underlying mantle, *Geology, 7,* 263-266, 1979.

Turcotte, D.L., and E.R. Oxburgh, Finite amplitude convection cells and continental drift, *J. Fluid Mech., 28,* 29, 1967.

Vail, J. R., Jebel Marra, a dormant volcano in Darfur Province, Western Sudan, *Bull. Volcan.*, 1973.

Watts, A.B., Gravity and bathymetry in the central Pacific Ocean, *J. Geophys. Res., 81,* 1533-1553, 1976.

Watts, A.B., J.H. Bodine, and M.S. Steckler, Observations of flexure and the state of stress in the oceanic lithosphere, *J. Geophys. Res., 85,* 6369-6376, 1980.

Wendlandt, R.F., and P. Morgan, Lithospheric thinning associated with rifting in East Africa, *Nature, 298,* 734-736, 1982.

Whiteman, A.J., The Geology of the Sudan Republic, Clarendon Press, Oxford, 290p., 1971.

Williams, L.A.J., and G.R. Chapman, Relationships between major structures, salic volcanism and sedimentation in the Kenya rift from the equator north to Lake Turkana, in: L.E. Frostick, et al., eds., *Sedimentation in the East African Rifts,* Geol. Soc. Spec. Pub., 25, 59-74, 1986.

Willett, S.D., D.S. Chapman, and H.J. Neugebauer, A thermo-mechanical model of continental lithosphere, *Nature, 314,* 520-523, 1985.

Wohlenberg, J., Seismizitat der ostafrikanischen Grabenzonen zwischen 4°N und 2°S sowie 23°E und 40°E, *Veroffentlichung der Bayerischen Kommission fur die Internationale Erdmessung, 43,* 95p., 1968.

Yuen, D.A., L. Fleitout, Thinning of the lithosphere and small-scale convective instabilities, *Nature, 313,* 125-128, 1985.

Zana, N., and N. Hamaguchi, Some characteristics of aftershock sequences in the Western rift valley of Africa, *Sci. Rep. Tôhoku Univ., Ser. 5, Geophysics, 25,* 55-72, 1978.

Zuber, M., T. Bechtel, and D. Forsyth, Elastic plate thickness variations in Australia, *EOS, Trans. Am. Geophys. Un. 68,* 1465, 1987.

Table I

Model Parameters
z_m = depth to deep density contrast = 35 km
ρ_c = average crustal density = 2700 kg/m^3
ρ_m = mantle density = 3300 kg/m^3
g = gravitational acceleration = 9.8 m/s^2
G = Gravitational Constant = 6.67 x 10^{-11}m^3/kg-s^2
D = flexural rigidity (Nm) = $E(T_e)^3/[12.(1-\nu^2)]$
E = Young's Modulus = 1.0 x 10^{11} N/m^2
ν = Poisson's ratio = 0.25
T_e = Effective elastic plate thickness (km)

Table I. Explanation of physical parameters used in coherence and admittance analyses.

Table II

REGION		T_e (km)	Tmin (km)	Tmax (km)	RMS	P/O	Npts
AFAR DOME							
ATRI	AFAR TRIANGLE	22	18	31	.335	3/9	3
ETHP	ETHIOPIAN PLATEAU	52	50	69	.274	4/6	4
ETHR	ETHIOPIAN RIFT	24	20	34	.298	3/6	2
EAST AFRICAN DOME							
BIG	EAST AFRICAN PLATEAU	48	45	56	.234	5/8	4
NEBR	N. EASTERN BRANCH	30	26	32	.287	3/5	4
DOME	KENYA DOME	31	26	32	.226	4/6	4
SEBR	S. EASTERN BRANCH	37	34	41	.172	4/5	3
NCNV	N. CENTRAL NON-VOLCANIC	31	21	32	.315	2/4	5
PLAT	E. AFRICAN PLATEAU	64	55	82	.211	6/6	2
SCV	S. CENTRAL VOLCANIC	55	50	63	.183	5/5	2
NWBR	N. WESTERN BRANCH	42	33	44	.253	2/3	5
CWBR	CENTRAL WESTERN BRANCH	32	26	47	.244	4/8	3
SWBR	S. WESTERN BRANCH	31	29	38	.431	5/7	2
STABLE CRATON							
SUDN	SUDAN	74	61	108	.168	5/7	3
ZAIR	ZAIRE	65	53	93	.254	1/4*	4
CONG	CONGO	89	46	180	.458	0/2*	3
MAGMATIC							
JBLM	JEBEL MARRA	43	39	51	.112	5/5	5

Table II. Summary of model parameters and effective elastic plate thicknesses determined in each of the sub-regions (Figures 7a, b). Column z_m is average depth to deep density contrast used in coherence analysis. **Tmin, Tmax** are the minimum and maximum elastic plate thicknesses that fit the same number of points in the fall-off waveband as the best-fitting model, **Te**. The number of points fit in the fall-off waveband are indicated in column **P/O**. **RMS** corresponds to rms residuals for best-fitting model. *See discussion in text for preferred interpretation of **Te** in these sub-regions. **Npts** is the number of points within the longest waveband.

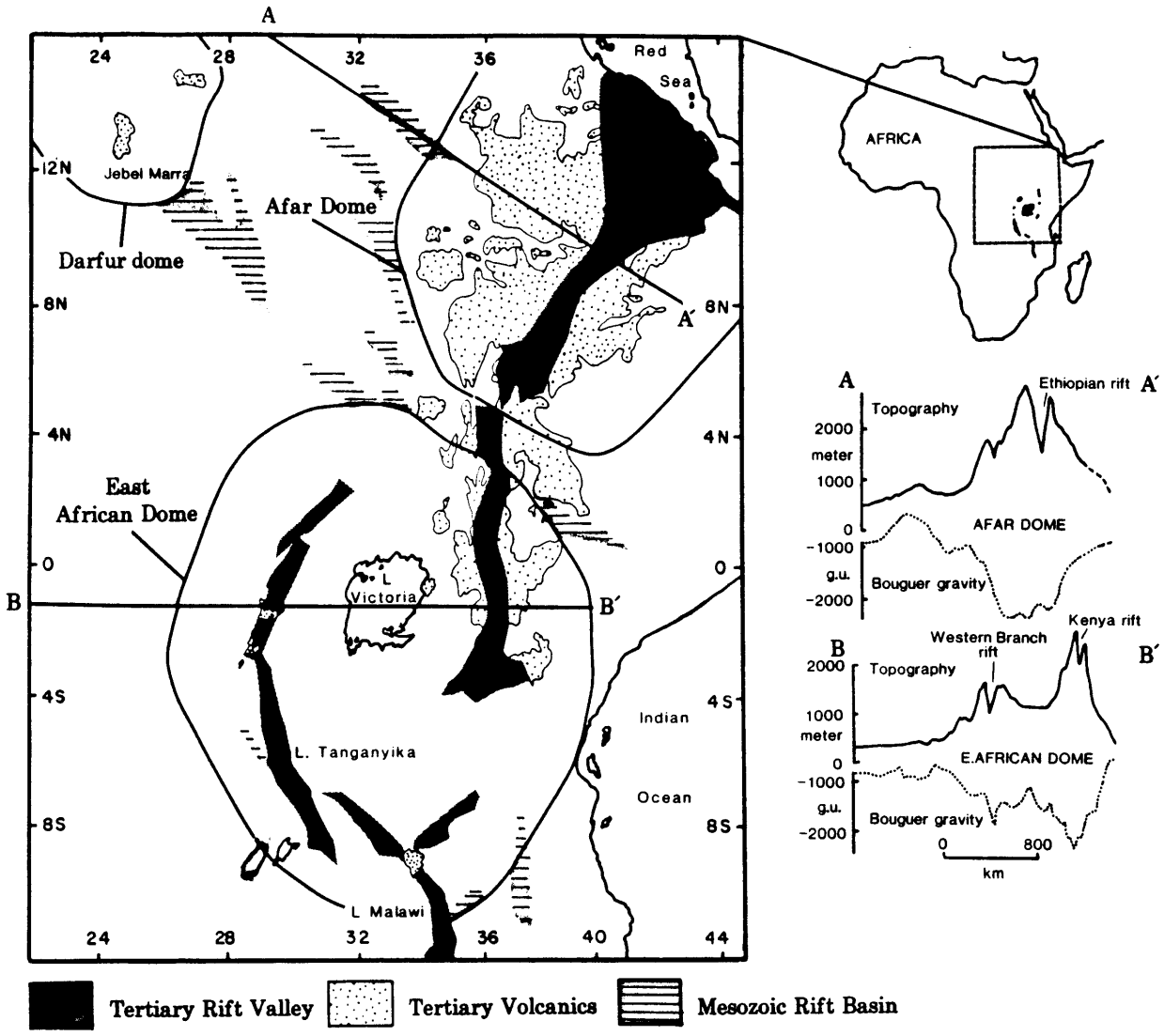

Figure 1. Study region with respect to African continent (inset) showing location of uplifted domes, or plateaus within study region. Profiles of gravity and topography across A-A' (Afar plateau) and B-B' (East African plateau) illustrate topographic relief of broad plateaus and corresponding Bouguer gravity anomalies (dotted lines). Solid lines enclose elevations greater than 800m; Tertiary rift valleys superimposed on the Afar and East African plateaus indicated by dark shading. Excluding regions affected by rifting in Mesozoic time (light shading), rift systems have formed in Precambrian basement.

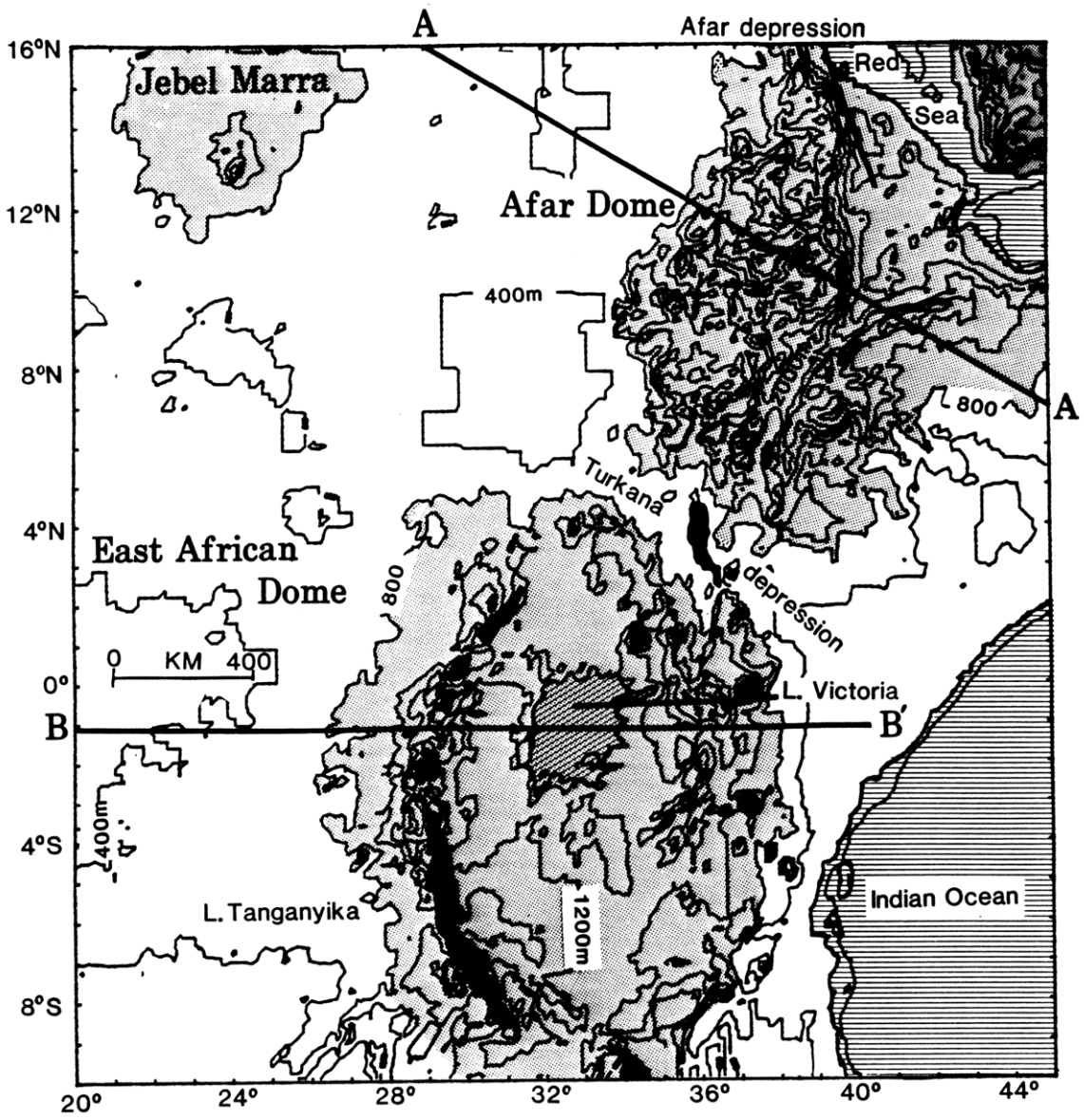

Figure 2. Contour map of topography data used in these analyses. Uplifted East African and Afar plateaus are separated by Turkana depression. Contour interval equals 400 m. Regions with elevations greater than 800m shaded. Lakes (black) filling parts of rift valley shown for geographic references in this and subsequent figures. Locations of profile A-A' and B-B' (Figure 1) indicated.

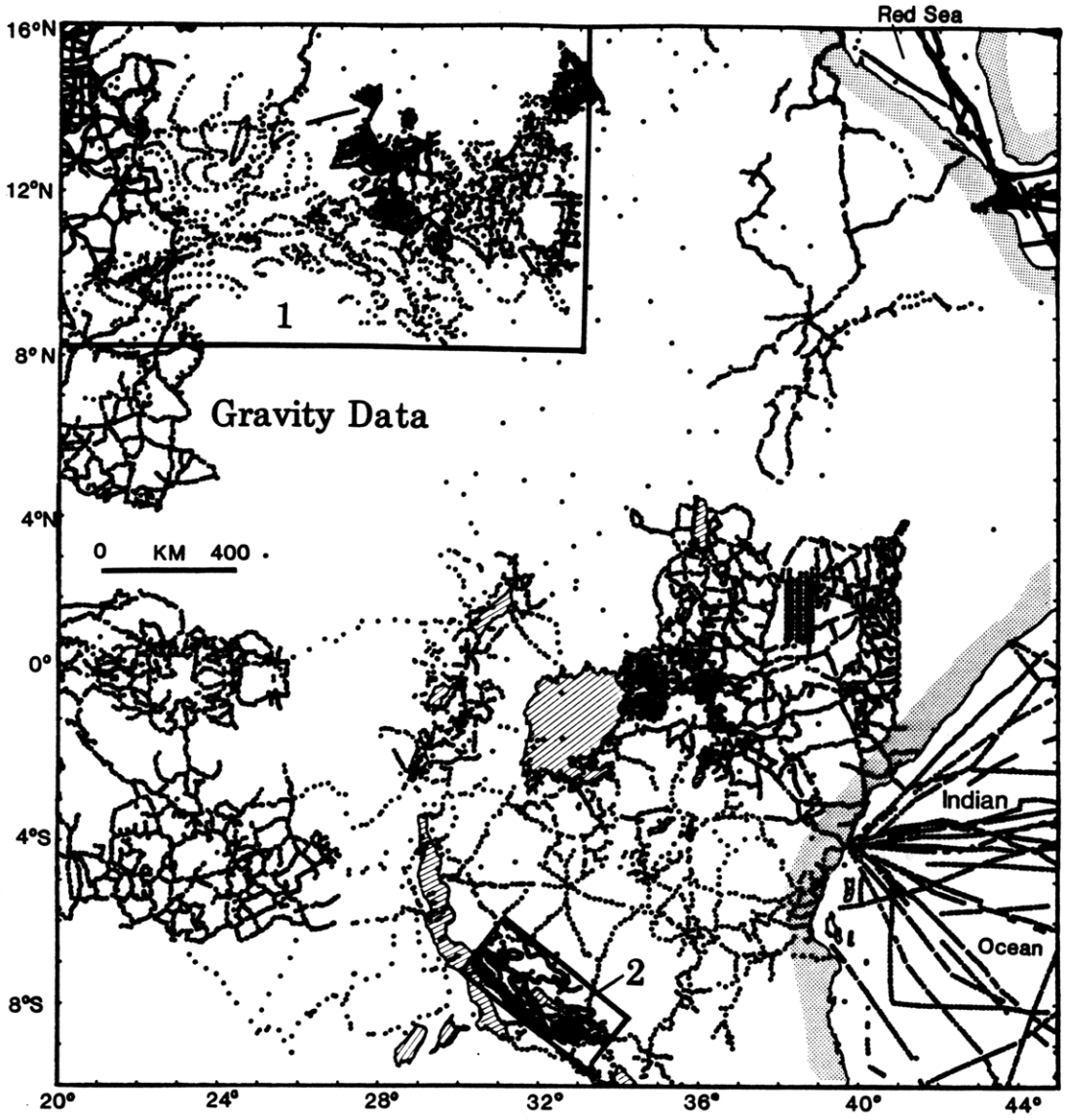

Figure 3. Gravity data coverage used in these analyses. Boxes enclose regions where coverage supplemented by data from 1) Bermingham et al. (1983) 2) Peirce and Lipkov (in press). Lake regions indicated by diagonal line pattern.

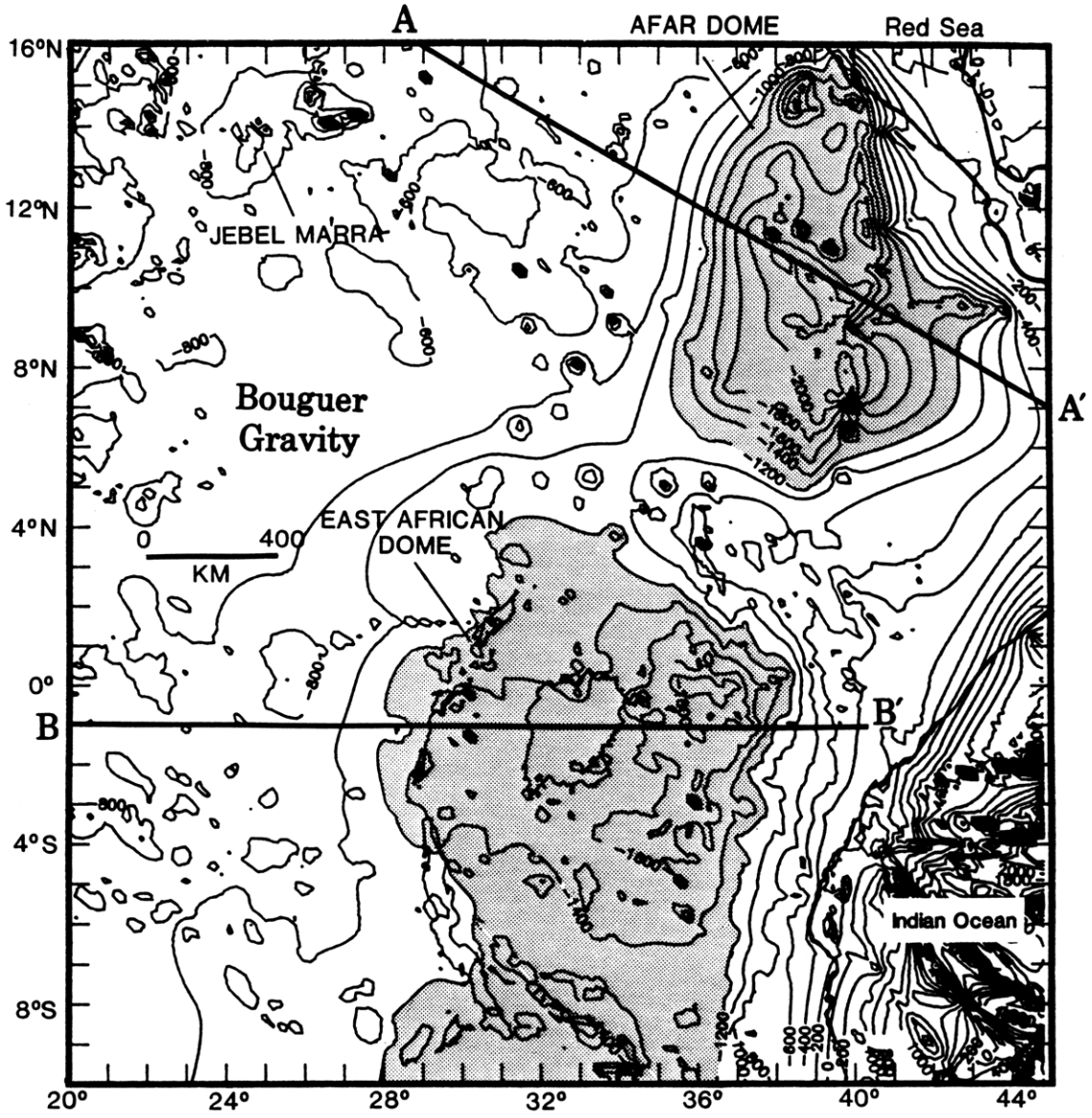

Figure 4. Contours of gridded Bouguer gravity data interpolated from data shown in Figure 3, as described in text. Contour interval equals 200 g.u (10 g.u. = 1 mgal), and anomalies less than -1400 g.u. shown shaded. Locations of profile A-A' and B-B' (Figure 1) indicated.

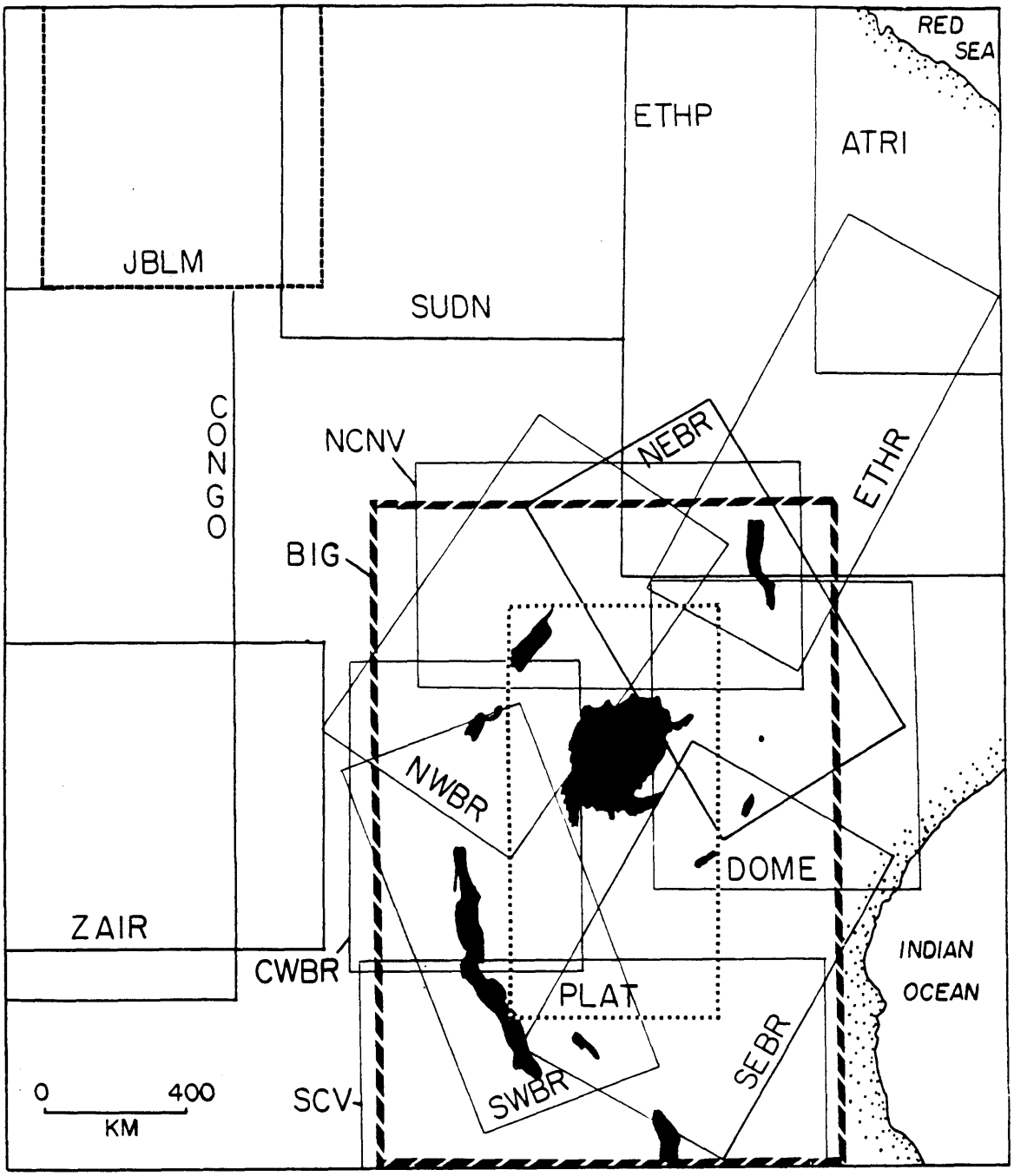

Figure 5. Locations of sub-regions in which elastic plate thicknesses have been estimated (Figure 7). Parameters used in each sub-region listed in Tables I, II. Data in tilted sub-regions re-interpolated prior to analyses. Lakes (black) indicate approximate location of East African rift valleys. N.b.: horizontal and vertical axes in kilometers.

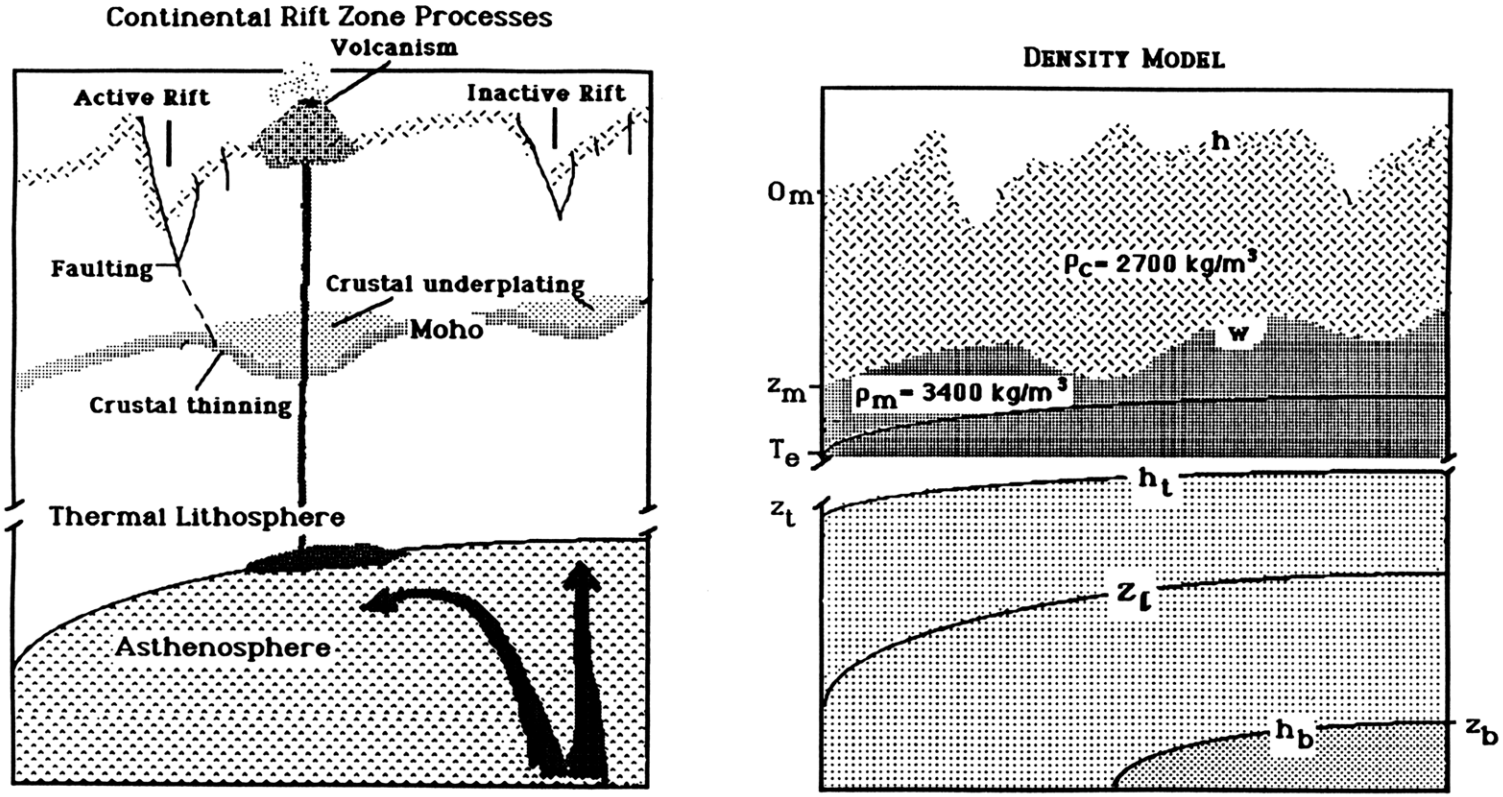

Figure 6. a) Schematic diagram illustrating possible contributions to observed Bouguer gravity anomalies within tectonically active continental rift zones. For example, variations in density due to volcanoes at surface, and crustal thinning, magmatic underplating at the base of the crust may occur. These loads can be represented as relief at the surface and at the base of the crust. Density variations within mantle (e.g. mantle upwelling) may contribute to gravity anomalies at long wavelengths. b) Top part of diagram shows density model used in inversion for best-fitting effective elastic plate thickness within each sub-region, using average layer crustal and upper mantle densities ρ_c, ρ_m indicated. Relief on the deep density contrast (w) was obtained by downward continuation of the observed gravity anomaly (see text). Lower part of diagram shows physical model used to estimate depth of dynamical compensation for broad plateaus. $\mathbf{T_e}$ is elastic plate thickness; $\mathbf{h_t}$ is relief on top boundary of convecting region at depth $\mathbf{z_t}$; $\mathbf{h_b}$ is relief on bottom boundary of region at depth $\mathbf{z_b}$; both boundaries assumed to be no-slip (velocities zero at boundaries).

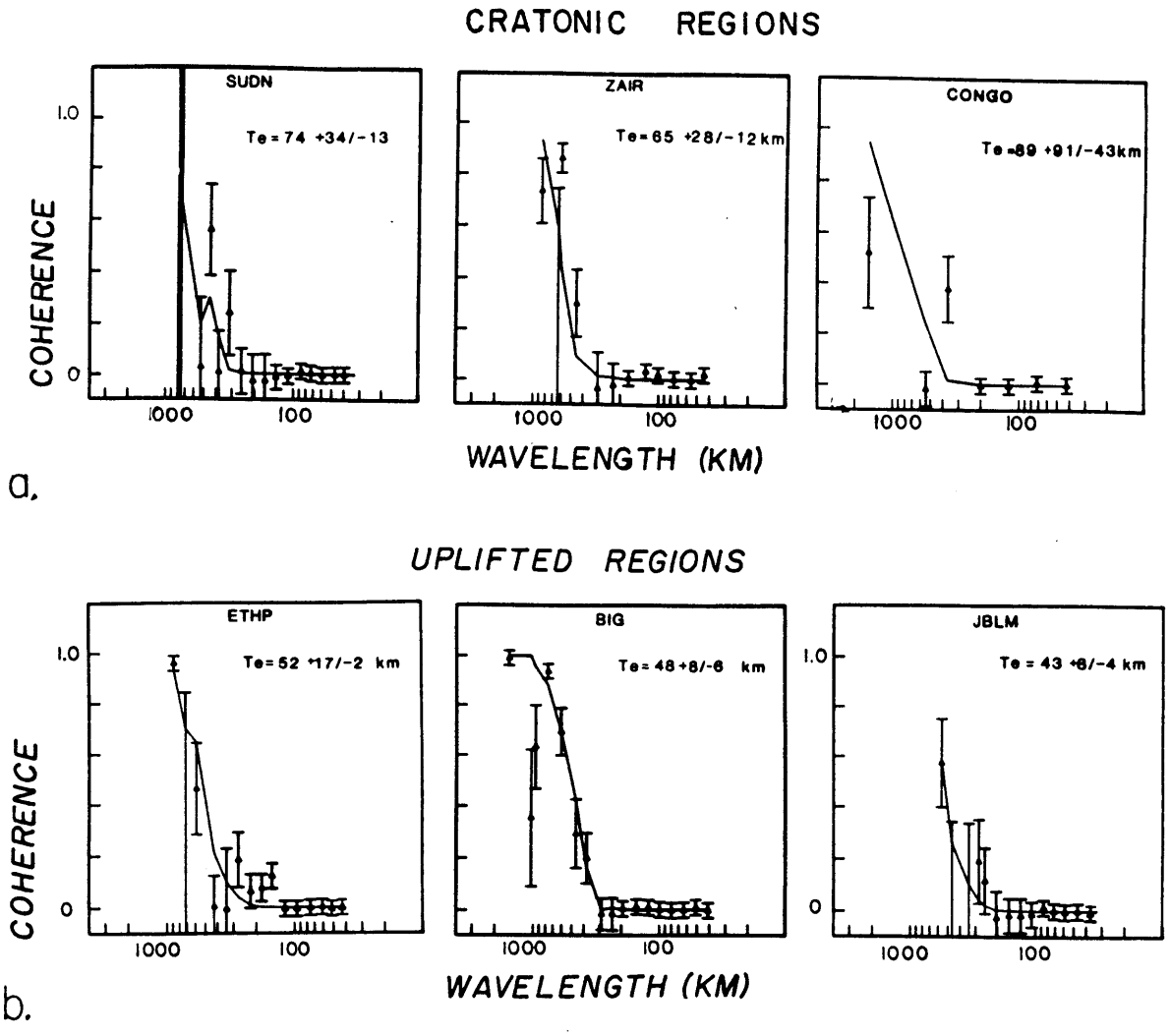

Figure 7. Comparison between observed coherence (triangles) and coherence predicted by best-fitting models in each of the sub-regions shown in Figure 6, and parameters listed in Tables I and II. Error bars on observed admittance are one standard deviation. Effective elastic plate thickness determined by best-fitting model indicated in upper right corner of each box; minimum and maximum values are models that fit same number of points in transition range from high to low coherence as model shown. At short wavelengths topography is supported by the strength of the lithosphere and the coherence between gravity and topography approaches zero; at longer wavelengths the lithosphere deflects beneath the load, and the coherence approaches unity.

a) Observed and model coherence within cratonic sub-regions of grid. Residuals for the best-fitting models are high (Table II), and points in the transitional waveband can be fit by much thicker elastic plates (93-180 km). Sub-regions ZAIR, CONGO, and possibly SUDN are too small to constrain the transition from low to high coherency. b) Observed and model coherence within sub-regions encompassing the uplifted Afar, East African plateaus and Darfur dome. c) Observed and model coherence within sub-regions encompassing the rift valleys superimposed on uplifted plateaus.

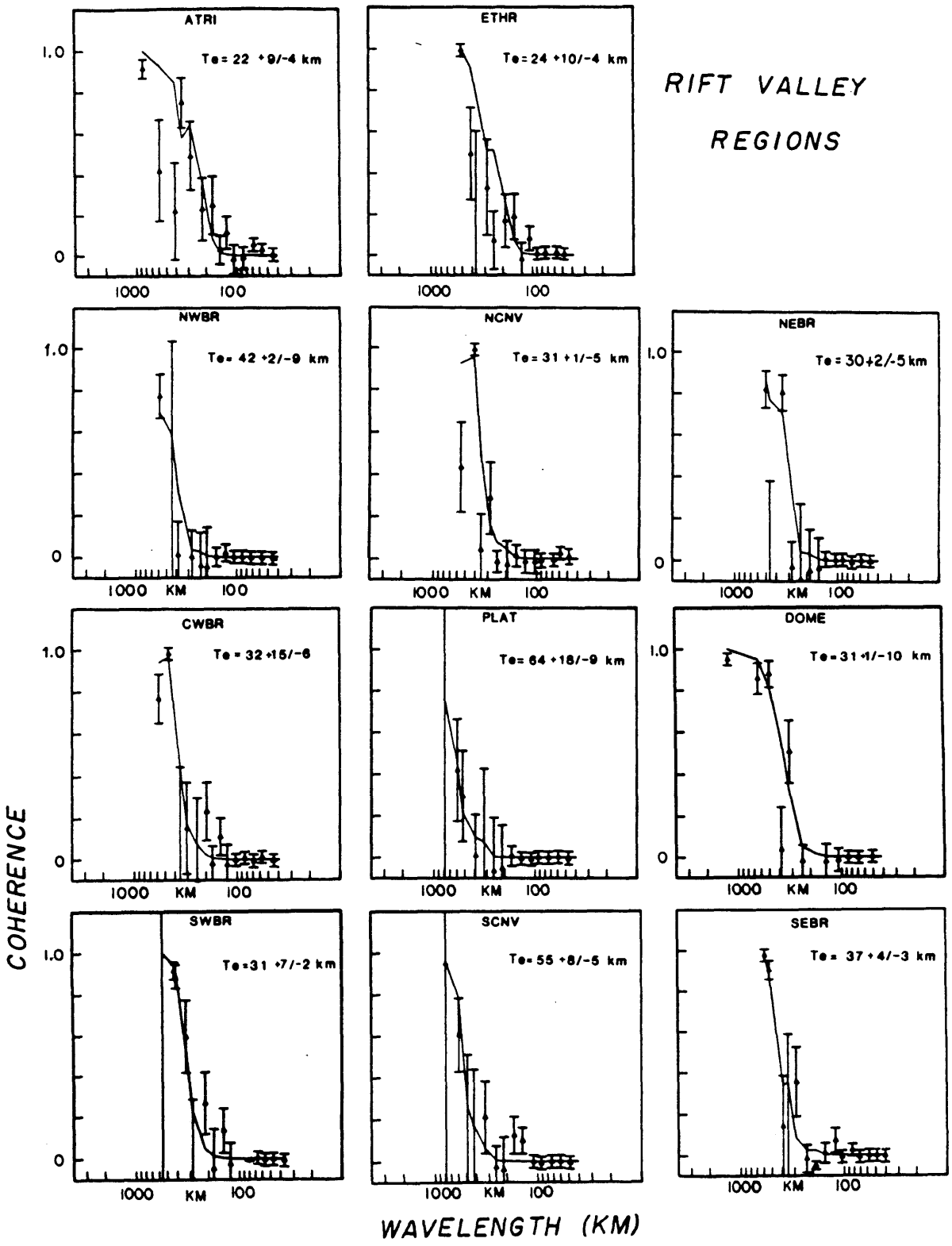
ATRI
Te= 22 +9/-4 km
ETHR
Te= 24 +10/-4 km
RIFT VALLEY
REGIONS
NWBR
Te= 42 +2/-9 km
NCNV
Te= 31 +1/-5 km
NEBR
Te= 30+2/-5km
CWBR
Te= 32+15/-6
PLAT
Te= 64 +18/-9 km
DOME
Te= 31+1/-10 km
SWBR
Te=31 +7/-2 km
SCNV
Te= 55 +8/-5 km
SEBR
Te= 37 +4/-3 km
1.0
0
1000
KM
100
COHERENCE
WAVELENGTH (KM)

7c.

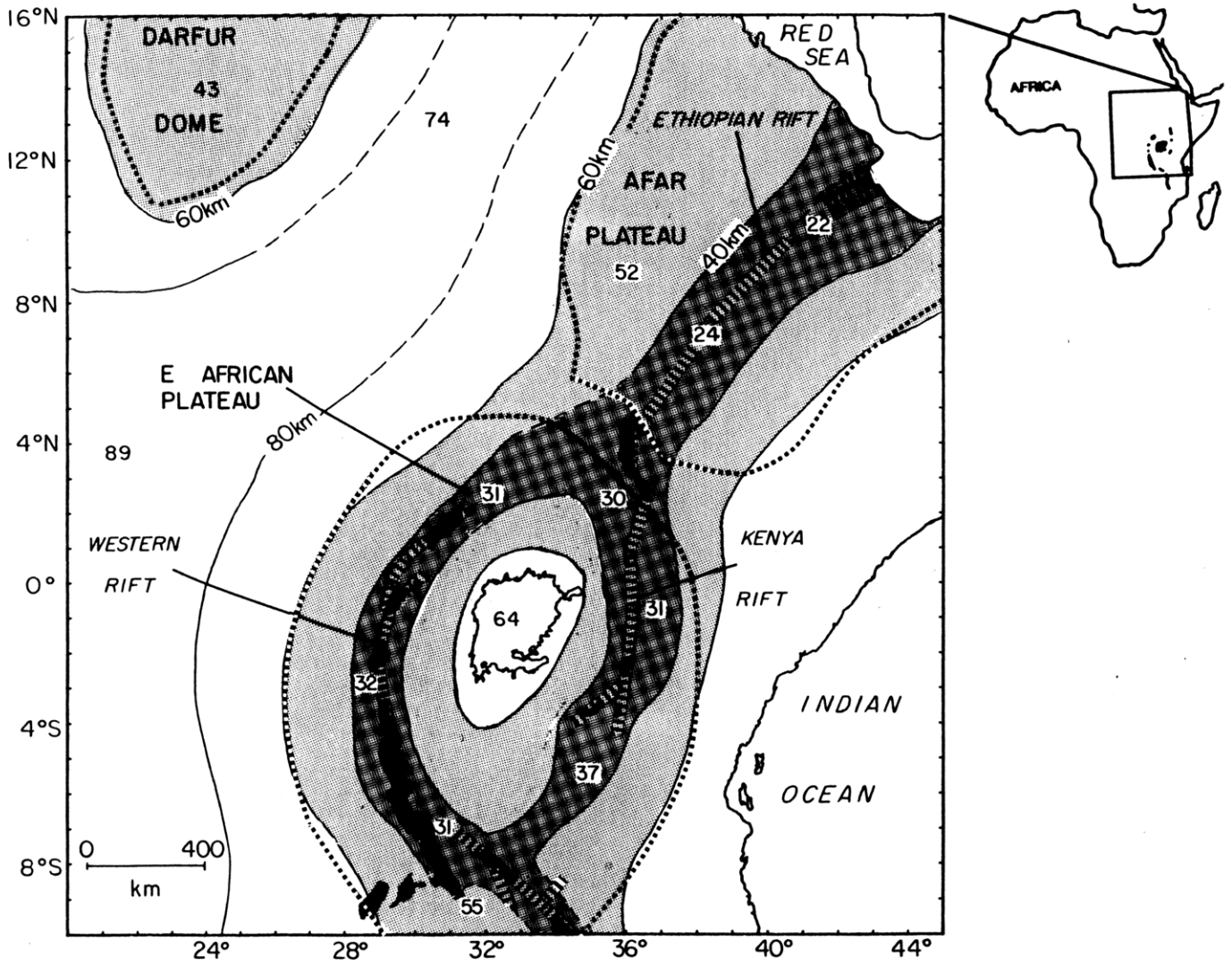

Figure 8. Contours of elastic plate thickness (km) estimated within each of the sub-regions shown in Figure 6. Contour interval 20 km. Dark shading: elastic plate thickness less than 40 km. Light shading: elastic plate thickness less than 60 km. Dotted lines enclose uplifted regions (elevation > 800m); bar pattern denotes approximate location of fault-bounded Western, Kenya, and Ethiopian rift valleys.

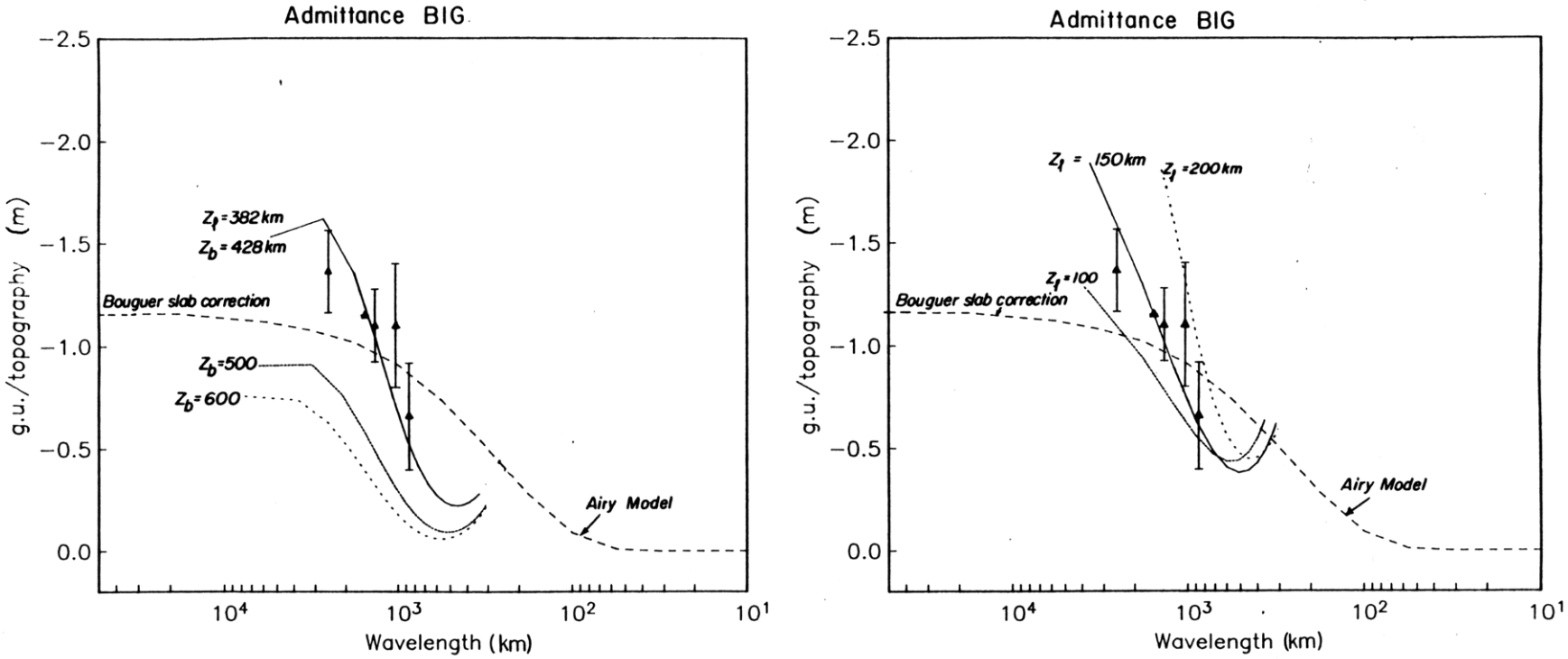

Figure 9. Observed admittance (triangles) from the uplifted East African plateau (sub-region BIG, Figure 5) calculated in wavebands where gravity and topography are coherent (see Figure 7). Note that observed admittance falls above the Bouguer slab correction at long wavelengths. In both a) and b) admittance predicted by Airy compensation model (compensation at base of crust) indicated by dashed line. Dynamical models shown by solid lines in a) and b) represent maximum depths of compensation (z_l) for the given boundary conditions within convecting region beneath 48 km thick elastic plate. a) Solid line shows admittance predicted with z_l approximately equal to 380 km below elastic plate of thickness 48 km. Dotted lines show dependence of predicted admittance on thickness of convecting layer (z_b). With increasing thickness of layer, curve is shifted to longer wavelengths. b) Solid line shows admittance predicted by dynamic compensation mechanism when bottom boundary is non-deformable. Solid line shows z_l = 150 km. Base of convecting region (z_b) is 285 km. Predicted admittance shown by short dashed line and dotted line show sensitivity of model to depth of compensation, z_l. As z_l approaches bottom boundary, the predicted admittance becomes more negative.